

The magmatic evolution of Oceanic Plateaus: a case study from the Azores

Dissertation
zur Erlangung des Doktorgrades
der Mathematisch-Naturwissenschaftlichen Fakultät
der Christian-Albrechts-Universität
zu Kiel



vorgelegt von
Christoph Beier

Kiel
2006

Ich versichere an Eides statt, daß die vorliegende Abhandlung ausschließlich unter Verwendung der angegeben Hilfsmittel entstanden ist und, abgesehen von der Beratung durch meine akademischen Lehrer, nach Inhalt und Form meine eigene Arbeit darstellt. Des weiteren habe ich weder diese noch eine ähnliche Arbeit an dieser oder einer anderen Hochschule im Rahmen eines Prüfungsverfahrens vorgelegt oder veröffentlicht.

Kiel, den

.....

Christoph Beier

Referent/in:

Koreferent/in:

Tag der mündlichen Prüfung:

Zum Druck genehmigt: Kiel,

Der Dekan

TABLE OF CONTENTS

Vorwort.....	XI
Einführung und Zusammenfassung	XIII
Introduction and Summary	XV

CHAPTER I

GEOCHEMICAL AND GEOCHRONOLOGICAL CONSTRAINTS ON THE VOLCANIC EVOLUTION OF THE AZORES PLATEAU

1.1 ABSTRACT.....	1
1.2 INTRODUCTION	2
1.3 GEOLOGICAL SETTING	2
1.4 METHODS	4
1.4.1 Sampling and sample treatment	4
1.5 RESULTS	9
1.5.1 Major elements, trace elements and isotopes	9
1.5.2 Age dating	11
1.6 DISCUSSION	11
1.6.1 Partial melting processes of the Azores Plateau magmas	11
1.6.2 Source heterogeneities	15
1.7 DYNAMICS OF THE AZORES PLATEAU.....	18
1.8 ACKNOWLEDGMENTS	20
REFERENCES.....	21

CHAPTER II**MELTING AND MANTLE SOURCE VARIATIONS ALONG AN ULTRASLOW SPREADING****RIFT: THE TERCEIRA AXIS, AZORES**

2.1 ABSTRACT	27
2.2 INTRODUCTION	28
2.3 GEOLOGICAL SETTING	28
2.4 METHODS	30
2.4.1 Sampling and sample treatment	30
2.5 RESULTS	38
2.5.1 Major and trace elements	38
2.5.2 Radiogenic isotope compositions	40
2.6 DISCUSSION	41
2.6.1 Magma generation along the Terceira axis	41
2.6.2 Mantle sources and mixing along the Terceira axis	45
2.6.3 Comparison to other ultraslow ridges	48
2.7 CONCLUSIONS	49
2.8 ACKNOWLEDGMENTS	50
REFERENCES	50

CHAPTER III**RELICS OF A SUBDUCTED SEAMOUNT: THE SÃO MIGUEL MANTLE SOURCE**

3.1 ABSTRACT	55
3.2 INTRODUCTION	56
3.3 GEOLOGICAL SETTING	56
3.4 METHODS	57
3.5 RESULTS	64
3.6 DISCUSSION	68

3.6.1 The Sete Cidades mantle source	69
3.6.2 The Nordeste mantle source	72
3.6.2.1 <i>Sediments</i>	73
3.6.2.2 <i>Subcontinental lithosphere</i>	74
3.6.2.3 <i>Melt-rock interactions</i>	75
3.6.2.4 <i>Subduction of enriched basalts and trachytes</i>	76
3.7 CONCLUSIONS	78
3.8 ACKNOWLEDGMENTS	78
REFERENCES	79

CHAPTER IV

MAGMA EVOLUTION OF THE SETE CIDADES VOLCANO, SÃO MIGUEL, AZORES

4.1 ABSTRACT	85
4.2 INTRODUCTION	86
4.3 GEOLOGICAL BACKGROUND	86
4.3.1 Geological setting of São Miguel	86
4.3.2 The stratigraphy of Sete Cidades volcano	88
4.4 SAMPLING STRATEGY AND ANALYTICAL METHODS	89
4.4.1 Sampling and sample treatment	89
4.4.2 Major and trace element analysis	98
4.4.3 Mineral chemistry	98
4.4.4 Nd-Sr isotopes	99
4.5 PETROLOGY AND MINERAL CHEMISTRY	99
4.5.1 Petrology	99
4.5.1.1 <i>Primitive rocks</i>	99
4.5.1.2 <i>Intermediate rocks</i>	99
4.5.1.3 <i>Evolved rocks (trachytes)</i>	100
4.5.2 Mineral chemistry	102
4.5.2.1 <i>Olivine</i>	102

4.5.2.2 <i>Clinopyroxene</i>	102
4.5.2.3 <i>Feldspar</i>	103
4.5.2.4 <i>Spinel and iron-titanium oxides</i>	104
4.5.2.5 <i>Amphibole</i>	104
4.5.2.6 <i>Biotite</i>	104
4.5.2.7 <i>Apatite</i>	104
4.6 GEOCHEMISTRY	105
4.6.1 Whole-rock compositions	105
4.6.2 Glasses	107
4.6.3 The caldera outflow deposit	107
4.7 DISCUSSION	107
4.7.1 Primitive magmas of Sete Cidades and their formation	107
4.7.2 Magma ascent and fractional crystallization processes of the Sete Cidades magmas	109
4.7.2.1 <i>Geothermobarometry</i>	109
4.7.2.2 <i>Oxygen fugacity</i>	111
4.7.2.3 <i>Fractional crystallization and modelling using MELTS</i>	111
4.7.2.4 <i>Effects of fractional crystallization processes on incompatible element ratios</i>	112
4.7.3 Time-scales of magma evolution and ascent beneath Sete Cidades	114
4.7.4 Temporal variations in the petrogenesis of the Sete Cidades lavas	116
4.7.5 Evidence for magma mixing?	117
4.8 CONCLUSIONS	119
4.9 ACKNOWLEDGMENTS	120
REFERENCES	120
 APPENDIX	
TABLES	A-I
CURRICULUM VITAE	A-XXIX

VORWORT

Diese Arbeit stellt in ihrer Gesamtheit eine monographische Dissertation dar, die aus vier relativ unabhängig voneinander rezipierbaren Kapiteln besteht. So enthalten die Tabellen in den einzelnen Kapiteln lediglich die Daten derjenigen Proben, an denen Messungen der Haupt-, Spurenelemente und Isotopen vorgenommen wurden. Zusätzliche Haupt- und Spurenelementdaten finden sich im Anhang. Die Analysen der Proben zu den Inseln Terceira und Graciosa befinden sich in Kapitel II, Analysen von São Miguel befinden sind in den Kapiteln III und IV.

Diese Arbeit entstand auf Anregung von Prof. Dr. Karsten Haase im Rahmen der von der Deutschen Forschungsgemeinschaft geförderten Projekte HA2568/9-1, HA2568/9-2 und HA2568/9-3. Ihm möchte ich für seine Unterstützung in jeder Hinsicht danken. Dazu zählen sein Engagement für meine Arbeit, seine Denkanstöße und viele konstruktive Diskussionen: *Jeg vil gerne sige dig mange tak for din hjælp og din støtte.*

Einen ganz wesentlichen Anteil an der Entstehung dieser Arbeit hat Prof. Dr. Albrecht Hofmann vom Max-Planck-Institut für Chemie in Mainz. Ihm gilt mein Dank für die großzügige Bereitstellung der Mainzer Labore, für hilfreiche Diskussionen und nicht zuletzt für seine Zwischenfinanzierungen.

Ich danke Herrn Prof. Dr. Peter Stoffers dafür, daß er sich als Koreferent und Prüfer zur Verfügung gestellt hat.

Von den Mainzer Kollegen gilt mein Dank insbesondere Wafa Abouchami und Steve Galer für ihre unschätzbare Hilfe bei den Isotopenanalysen und für zahlreiche konstruktive Vorschläge sowohl während der Analytik als auch während des Schreibens.

Ebenso danke ich Andreas Stracke für seine Hilfe, ohne die die Hafnium-Analysen nicht zustande gekommen wären, aber auch für die eine oder andere sehr unterhaltsame Diskussion und Situation, zu deren Höhenpunkten eine unter Wasser gesetzte Herrentoilette und der Besuch im Sushiboat zählen.

Bei Dieter Garbe-Schönberg und seinem gesamten Team, insbesondere bei Heidi Blascheck und Ulrike Westernströer, bedanke ich mich für die Unterstützung während der ICP-MS Analysen, bei Peter Appel, Barbara Mader und Astrid Weinkauff für die große Hilfe während der RFA- und Mikrosondenanalysen. Paul van den Bogaard danke ich für die Hilfe bei den Altersdatierungen, Folkmar Hauff für einen Teil der Isotopenanalysen und Susanne Fretzdorf für ihre Hilfe bei den Volatilmessungen.

Niels Jöns sei an dieser Stelle ganz besonders gedankt für die wissenschaftliche und persönliche Unterstützung als Freund, einschließlich großer mit mir konsumierter Mengen an Kaffee, Tee, Kuchen und natürlich Bier. Zuzana Fekiacova, Sylvain Pichat und Francois Nauret haben mir das Leben in vielen Situation erleichtert und mich sehr zum Lachen gebracht.

Judith Kaatz danke ich dafür, daß sie mich immer nach Kräften unterstützt und meine Launen ertragen hat. Meinen Eltern danke ich für den Rückhalt, ein offenes Ohr, ehrlichen Rat in jeder Situation und manche geduldige Korrektur.

Bei Beate Bader und Olaf Thießen bedanke ich mich für die seelische Unterstützung während der Mittagspausen und für ihre konstruktive Hilfe, gerade in den letzten Monaten der Arbeit. Schließlich danke ich meinen „Bürogenossen“ Nicole Stroncik, Mark Krienitz und Ulrike Schacht. Sie waren geduldig, hilfsbereit, haben für die nötige Ablenkung gesorgt und meinen viel zu starken Kaffee ertragen.

Viele haben mir auf ihre Weise geholfen, aber für verbliebene Unzulänglichkeiten bin ich natürlich ganz allein verantwortlich.

Kiel, im April 2006

Christoph Beier

EINFÜHRUNG UND ZUSAMMENFASSUNG

Die Entstehung und Entwicklung ozeanischer Plateaus (z. B. Ontong Java, Island) wird oftmals mit Schmelz-anomalien im oberen Erdmantel erklärt, die sich durch großräumige Eruptionen großer Magmenmengen in geolo-gisch kurzen Zeiträumen auszeichnen. Vor diesem Hintergrund untersucht die vorliegende Arbeit die Entstehung und Entwicklung des submarinen Azorenplateaus.

Das submarine Azorenplateau erstreckt sich entlang des Mittelatlantischen Rückens im zentralen Nordatlantik (37°30'N und 40°00'N) und hat eine Breite von 300 km (N–S) sowie eine Länge von 700 km (W–O). Von ihm erheben sich die neun Inseln des Azorenarchipels. Die ultralangsam spreizende Terceira-Achse begrenzt das Plateau im Norden. Sie streicht in NW–SE-Richtung und trifft auf den Mittelatlantischen Rücken. Dort befindet sich der Tripelpunkt der Eurasischen, Afrikanischen und Amerikanischen Platte. Drei der Inseln (Graciosa, Terceira und São Miguel), die sich entlang der Terceira-Achse befinden, zeigen den wichtigen Einfluß von Spreizungsbewegungen auf die Magmenbildung.

Ziel dieser Arbeit ist es, die Entstehung und Entwicklung ozeanischer Plateaus und ultralangsam spreizender Rücken zu untersuchen und deren Zusammenspiel, die involvierten Schmelzprozesse und beteiligten Mantelquellen zu charakterisieren. Dies erfolgt in den vier Kapiteln der Arbeit mit abnehmender morphologischer „Größenordnung“: vom größten System, dem submarinen Plateau (Kapitel I) über die Terceira-Achse (Kapitel II) und die Insel São Miguel (Kapitel III) bis hin zum Vulkan Sete Cidades auf der Insel São Miguel (Kapitel IV).

Das *erste Kapitel* dieser Arbeit befaßt sich mit der geochemischen und geochronologischen Entstehung des submarinen Azorenplateaus. Die beprobten Laven reichen von tholeiitischen, in den inkompatiblen Elementen leicht verarmten, bis zu alkalibasaltischen, in den inkompatiblen Elementen stark angereicherten Zusammensetzungen. Die weniger angereicherten tholeiitischen Laven befinden sich am westlichen Rand des Plateaus. Sie zeigen höhere Schmelzgrade als die alkalibasaltischen Laven, die sich auf räumlich sehr begrenzte Strukturen beschränken. Anhand der Altersdatierungen ($^{40}\text{Ar}/^{39}\text{Ar}$) lassen sich drei Phasen vulkanischer Aktivität unterscheiden: (a) Die ältesten Laven (39 Millionen Jahre) wurden im Bereich des östlichen Plateaus beprobt. Es handelt sich um angereicherte Alkalibasalte, die chemische Ähnlichkeiten zu den jüngeren Laven der Inseln aufweisen. (b) Vor 4.9 bis 6.0 Millionen Jahren kam es zu Eruptionen alkalibasaltischer und tholeiitischer Magmen mit hohen Schmelzgraden im zentralen und östlichen Plateau sowie im Bereich der Princessa Alice Bank. (c) Seit 1.5 Millionen Jahren werden alkalibasaltische Magmen mit relativ niedrigen Schmelzgraden auf dem zentralen Plateau und den Inseln eruptiert. Das regionale Auftreten von Vulkanismus im Zeitraum von 4.9 bis 6.0 Millionen Jahren ist auf eine verhältnismäßig kleine Schmelzanomalie unter der Lithosphäre zurückzuführen. Das gemeinsame Auftreten hoher Schmelzgrade und verarmter, MORB-ähnlicher Isotopenverhältnisse zeigt, daß diese Laven wahrscheinlich entlang des Mittelatlantischen Rückens eruptiert wurden. Die sehr variablen Sr-, Nd- und Pb-Isotopenverhältnisse weisen auf einen sehr heterogenen Mantel hin. Die einzelnen vulkanischen Strukturen werden dabei durch einen eigenen binären Mischungstrend definiert; Mischungen zwischen den größeren Strukturen treten jedoch nur in geringem Maße auf. Die Tatsache, daß die Azoren nicht von einer Plumequelle dominiert werden, unterscheidet sie wesentlich von anderen Plumelokalitäten (z.B. Hawaii, Tahiti). Trotzdem weist die weiträumige Verbreitung zeitgleichen Vulkanismus auf eine Schmelzanomalie hin. Dies zeigt, daß die Azoren entscheidend durch die Interaktion einer Schmelzanomalie mit der lokalen Tektonik geprägt wurden.

In *Kapitel II* werden die Schmelzvariationen und Mantelquellen der ultralangsam (2–4 mm/Jahr) spreizenden Terceira-Achse untersucht, die sich am nördlichen Rand der Azorenplattform befindet. Drei Inseln und ein submariner Vulkan, die entlang der Achse angeordnet sind, werden jeweils voneinander durch tiefe, magmatisch nicht aktive Becken getrennt. Die Haupt- und Spurenelemente und Isotopenverhältnisse variieren entlang der Achse. Die Haupt- und Spurenelemente der östlichsten Insel São Miguel zeigen, daß die Schmelzen im Granatstabilitätsfeld entstanden sind und niedrigere Schmelzgrade als die westlichen Inseln aufweisen, deren Schmelzen im Übergang zwischen Spinell- und Granatstabilitätsfeld liegen. Das Zusammenwirken einer jungen (< 6 Millionen Jahre), ultralangsam, schiefen Spreizung („oblique spreading“) mit relativ dicker Lithosphäre führt zu niedrigeren Schmelzgraden als an vergleichbaren ultralangsam spreizenden Rücken (z.B. Gakkel-Rücken, Südwest-Indischer Rücken). Trotz der niedrigeren Schmelzgrade führt eine stationäre, stabile Schmelzanomalie dazu, daß sich Inseln entlang der Achse gebildet haben. Die Sr-, Nd-, und Pb-Isotopenverhältnisse zeigen, daß jedes vulkanische System auf einem eigenen Mischungstrend liegt, was auf das Auftreten fokussierter Schmelzen hinweist. Mischungen zwischen den relativ unradiogenen Isotopenendgliedern der Insel Graciosa und den radiogenen Endgliedern des Mittelatlantischen Rückens zeigen, daß Mantelmaterial von Graciosa zum Mittelatlantischen Rücken fließt.

Kapitel III befaßt sich mit der Ursache und Entstehung der Mantelquellen unter der Insel São Miguel, die sich am östlichen Ende der Terceira Achse befindet und aus vier großen Vulkanen besteht. Der westlichste Vulkan, Sete Cidades, zeichnet sich durch Sr-, Nd-, Hf- und Pb-Isotopenverhältnisse aus, welche ähnlich denen der sogenannten FOZO-Komponente sind. Die Laven des östlichsten Vulkans, Nordeste, haben hingegen ungewöhnlich radiogene $^{208}\text{Pb}/^{204}\text{Pb}$ - und $^{87}\text{Sr}/^{86}\text{Sr}$ - sowie unradiogene $^{143}\text{Nd}/^{144}\text{Nd}$ - und $^{176}\text{Hf}/^{177}\text{Hf}$ -Isotopenverhältnisse, die bisher nicht auf der Erde bekannt sind. Beide Vulkane stellen jeweils ein Endglied der Mischungslinie der inkompatiblen Elemente und Isotopenverhältnisse dar. Die räumliche Nähe und die Ähnlichkeit der inkompatiblen Elemente weist auf eine ähnliche Entstehungsgeschichte ihrer Mantelquellen hin. Die gute Korrelation zwischen inkompatiblen Elementen und Isotopenverhältnissen zeigt, daß die Entstehung der chemischen Signaturen durch den gleichen Prozeß hervorgerufen wird. Obwohl es Ähnlichkeiten zwischen den inkompatiblen Elementen von São Miguel und den sogenannten HIMU-Inseln gibt (hohes μ = hohes $^{238}\text{U}/^{204}\text{Pb}$; z. B. St. Helena, Tubuaii), sind die inkompatiblen Elemente Rb und Ba relativ zu Th angereichert. Die geochemische Modellierung der Quelle von Sete Cidades weist auf eine durch Subduktion recycelte, alterierte, angereicherte ozeanische Kruste hin. Vermutlich handelt es sich hierbei um einen angereicherten MORB oder eine alkalibasaltische Zusammensetzung. Die höheren $^{87}\text{Sr}/^{86}\text{Sr}$ -Verhältnisse von Sete Cidades zeigen, daß die ozeanische Kruste deutlich weniger durch die Subduktion modifiziert wurde als vergleichbare HIMU-Zusammensetzungen. Die Laven des Nordeste-Vulkans sind, verglichen mit Sete Cidades, durch angereicherte inkompatible Elemente charakterisiert, zeigen aber relative Verarmungen von Sr, Eu, Ti und Rb. Dies zeigt, daß das Ausgangsgestein möglicherweise durch fraktionierte Kristallisation von Alkalifeldspäten und Fe-Ti-Oxiden beeinflusst war. Führt man der angereicherten ozeanischen Kruste von Sete Cidades noch eine entwickelte Zusammensetzung (z.B. Trachyt) zu, so ist man in der Lage, die angereicherten inkompatiblen Elemente und Isotopenverhältnisse von Nordeste zu erklären. Dies zeigt, daß die Quellen beider Vulkane im gleichen geodynamischen Milieu, jedoch durch unterschiedliche Zusammensetzungen der subduzierten ozeanischen Kruste entstanden sind.

Das *vierte Kapitel* dieser Arbeit behandelt die geochemische und petrologische Entwicklung eines ozeanischen Intraplattenvulkans. Der Vulkan Sete Cidades, der sich am westlichen Rand der Insel São Miguel befindet, zeigt

drei Entwicklungsstadien: (a) das Präcaldera- oder Schildstadium, welches hauptsächlich aus Alkalibasalten besteht, (b) das Stadium der Calderabildung, welches durch Ablagerungen mehrerer pyroklastischer Eruptionen geprägt ist, und (c) das Postcalderastadium, das sich sowohl durch höher entwickelte Laven als auch durch die synchrone Eruption trachytischer Zusammensetzungen aus der Caldera und basaltischer Laven von kleineren Eruptionszentren an den Flanken des Vulkans auszeichnet. Die basaltischen Proben des Postcalderastadiums sind primitiver als die des Präcalderastadiums, was auf längere Krustenverweilzeiten und stärkere fraktionierte Kristallisation während des Präcalderastadiums hinweist. Thermobarometrische Abschätzungen zeigen, daß die aufsteigenden primitiven Magmen in einer Tiefe von ~ 15 km erstmalig stagnieren und partiell kristallisieren. Im Bereich der Azoren entspricht diese Tiefe der Grenze zwischen Kruste und Mantel. Die entwickelteren Magmen hingegen stagnieren in einer Tiefe von lediglich ~ 3 km. Die Calderabildung wurde durch die Injektion eines heißeren basaltischen Magmas in die flache, entwickelte Magmenkammer und der daraus resultierenden Überhitzung initiiert. Die Proben von Sete Cidades liegen auf einem gut definierten Fraktionierungstrend, jedoch zeigen Unterschiede zwischen dem Prä- und Postcalderastadium (z. B. Sauerstoffugazität, Ba/Nb), daß es eine zeitliche Variation der Magmenquelle gibt. Die Magmen von Sete Cidades zeichnen sich, verglichen mit den radiogeneren Zusammensetzungen des benachbarten Vulkans Agua de Pau, durch relativ unradiogene Sr-Isotopenverhältnisse aus. Die radiogenen Sr-Isotopenverhältnisse eines kleineren Eruptionszentrums an der Flanke von Sete Cidades resultieren aus Magmenmischungsprozessen zwischen Agua de Pau und Sete Cidades, jedoch zeigen die generell unterschiedlichen Zusammensetzungen der beiden Vulkane, daß Mischungen trotz räumlicher Nähe nur sehr begrenzt auftreten.

INTRODUCTION AND SUMMARY

The formation and evolution of oceanic plateaus (e.g. Ontong Java Plateau, Iceland) have often been associated with the presence of melting anomalies in the upper mantle. These are characterised by the large spatial distribution of volcanism erupted in relatively short periods of time. Against this background, the present doctoral thesis presents an investigation of the formation and evolution of the submarine Azores Plateau.

The Azores submarine plateau in the Central Northern Atlantic Ocean straddles the Mid-Atlantic Ridge for about 300 km from $37^{\circ}30'$ and $40^{\circ}00'$ N, and extends 700 km from its eastern to its western edge. From the submarine volcanic plateau, nine islands emerge. The ultraslow spreading Terceira axis is situated at the northern plateau, striking in a NW-SE direction towards the Mid-Atlantic Ridge and forming the triple junction between the Eurasian, African, and American Plates. There are three islands (Graciosa, Terceira, and São Miguel) directly located on the Terceira axis, which indicates the importance of the spreading movement for magma generation.

The aim of this study is to investigate the processes during the formation and evolution of oceanic plateaus and ultraslow spreading axes including melting and mantle source processes and the interaction between melting anomalies and spreading axes. The four chapters contribute to this aim by following a kind of decreasing morphological scale – **from the largest system, the submarine Plateau (Chapter I), to the Terceira axis (Chapter II), the island of São Miguel (Chapter III), and finally to the volcano of Sete Cidades (Chapter IV).**

The *first chapter* focuses on the geochemical and geochronological evolution of the Azores submarine plateau. The sampled lava compositions range from slightly incompatible element depleted tholeiitic compositions to highly enriched alkali basaltic compositions. The less enriched lavas are restricted to the western plateau and imply relatively high degrees of partial melting in contrast to the highly enriched alkali basalts that occur

at distinct volcanic structures. $^{40}\text{Ar}/^{39}\text{Ar}$ age determinations suggest three different phases of volcanic activity: (a) the oldest lavas (39 Ma) occur on the easternmost plateau and are highly enriched alkali basalts with compositions similar to those from the young islands, (b) 4.9 to 6.0 Ma ago, eruptions occurred at the Central and Western Plateau and at the Princessa Alice Bank consisting of tholeiitic to alkali basaltic compositions indicating higher degrees of partial melting, (c) for 1.5 Ma, alkaline lavas with relatively small degrees of partial melting have been erupted at a few locations in the Central Plateau and on the islands. The wide spatial distribution of eruptions from 4.9 to 6.0 Ma ago is a result of the arrival of a relatively small melting anomaly beneath the lithosphere leading to the eruption of tholeiitic and alkaline lavas. Higher degrees of partial melting and the occurrence of depleted 'MORB'-like isotopic compositions suggest eruptions in the vicinity of the MAR spreading axis. The Sr-Nd-Pb isotope systematics reveals a small scale heterogeneous mantle beneath the Azores, where each volcanic structure is defined by a single isotopic range, with only very limited mixing between them. Although the absence of one prevailing plume source marks a difference between the Azores and other plume-related settings (e.g. Hawaii, Tahiti), the large spatial distribution of volcanism suggests the presence of a melting anomaly beneath the Azores. Thus, the Azores formed as a result of the interaction of an anomalous mantle and the local plate tectonics which provide ascent paths for the magmas.

The *second chapter* deals with the melting and mantle source variations along the ultraslow spreading Terceira Rift and its interaction with the mantle melting anomaly. The ultraslow spreading Terceira axis (2-4 mm/a) is situated at the northern boundary of the Azores Plateau and consists of three islands and a seamount, each separated by deep amagmatic basins. The major elements, trace elements and isotope ratios show large along-axis geochemical variations. The major and trace elements imply melting in the garnet stability field, and slightly smaller degrees of partial melting at the easternmost island of São Miguel, in contrast to slightly higher degrees of partial melting in the garnet/spinel transition zone towards the west. Although a melting anomaly is proposed for the Azores, the degrees of partial melting are smaller than those suggested for other ultraslow spreading ridges such as the Arctic Gakkel Ridge or the Southwest Indian Ridge. This may be a result of a combined interaction of highly oblique, very slow spreading and a relatively thick lithosphere in the Azores. The thickness of the lithosphere can be accounted for by the relatively young spreading movement (< 6 Ma) at the Terceira axis. The occurrence of islands along the Terceira axis suggests that, despite the smaller degrees of melting compared to other ultraslow spreading ridges, the presence of a stable melting anomaly over relatively long periods of time produces sufficient melts for the formation of islands. The Sr-Nd-Pb isotope ratios show that each volcanic system lies on a single binary mixing array with only very limited interaction, which indicates focused magmatism towards the large volcanic centres. The unradiogenic endmember composition of the Graciosa array and the most radiogenic compositions from the Mid-Atlantic Ridge imply a flux of mantle material from Graciosa towards the Mid-Atlantic Ridge.

The *third chapter* focuses on the origin and evolution of the São Miguel mantle sources. São Miguel, situated at the eastern end of the Terceira axis, comprises four large volcanic systems, where the westernmost volcano Sete Cidades has Sr-Nd-Pb-Hf isotope ratios that resemble the compositions of the so-called FOZO component. In contrast, the easternmost volcanic system of Nordeste has unusual radiogenic $^{208}\text{Pb}/^{204}\text{Pb}$ and $^{87}\text{Sr}/^{86}\text{Sr}$ combined with unradiogenic $^{143}\text{Nd}/^{144}\text{Nd}$ and $^{176}\text{Hf}/^{177}\text{Hf}$ isotope ratios, a combination which has not yet been found anywhere on Earth. The Sete Cidades and Nordeste lavas represent the end-members of a binary mixing array in the isotope and incompatible elements. Some similarities in the incompatible element compositions of the two volcanoes and the small distance between them suggest some relationship between their sources. The isotope ratios correlate with the incompatible elements, which supports the conclusion that one single process

is responsible for these signatures. While similarities are observed between the trace elements at São Miguel and the so-called HIMU-islands (high μ = high $^{238}\text{U}/^{204}\text{Pb}$; e.g. St. Helena, Tubuaii), the São Miguel lavas, in contrast to HIMU, are generally enriched in the incompatible elements Rb and Ba relative to Th. Geochemical modelling of the Sete Cidades mantle source suggests the presence of a recycled, altered enriched oceanic crust, most likely an enriched MORB or alkaline basaltic composition. The higher $^{87}\text{Sr}/^{86}\text{Sr}$ isotope ratios of Sete Cidades, as compared to HIMU, imply that the oceanic crust was less modified during subduction than HIMU. As compared to Sete Cidades, the Nordeste lavas are characterised by enriched incompatible element compositions, while Sr, Eu, Ti, and Rb at Nordeste are relatively depleted, giving evidence that the precursor rock may have been influenced by fractional crystallisation of alkali feldspar and Fe-Ti oxides. If we add an evolved (e.g. trachytic) composition to the enriched oceanic crust proposed for Sete Cidades, we are able to reproduce the Nordeste incompatible element and isotope ratios observed. Thus, we suggest that both sources have a similar geodynamic origin with slightly variable compositions for the subducted oceanic crust.

The *fourth chapter* deals with the geochemical and petrological evolution of an oceanic intraplate volcano on the Azores plateau. The Sete Cidades volcanic system, situated at the westernmost end of São Miguel, comprises three volcanic stages: (a) a mainly basaltic, pre-caldera, shield building stage, (b) pyroclastic deposits from a series of caldera forming eruptions, and (c) a more evolved post-caldera stage with the coeval eruption of trachytic compositions from the caldera and basaltic eruption from several smaller flank vents. The post-caldera flank lavas are more primitive (> 5 wt. % MgO) than the pre-caldera lavas, a fact which implies extended fractional crystallization and longer crustal residence times for the pre-caldera stage. Thermobarometric estimates show that the primitive ascending magmas stagnated and crystallized near the crust-mantle boundary at a depth of ~ 15 km, whereas the more evolved magmas resided at a shallower depth (~ 3 km). The caldera-forming eruption was initiated by a basaltic, and, hence, hotter injection into the shallow magma chamber overheating the evolved magmas. Although all lavas are situated on a single line of liquid descent in the major elements, slight geochemical differences (e.g. oxygen fugacity, Ba/Nb) between the pre- and post-caldera stages suggest a variation in magma composition over time. As compared to the more radiogenic compositions of the neighbouring Agua de Pau volcano, the lavas from Sete Cidades are generally defined by relatively unradiogenic Sr isotope ratios. The samples from one post-caldera vent on the Sete Cidades flank indicate that they are mixed with magmas that resemble the Agua de Pau isotope compositions. The different magma sources between the two volcanic systems imply that, despite their close proximity, there is only limited mixing between them.

CHAPTER I

GEOCHEMICAL AND GEOCHRONOLOGICAL CONSTRAINTS ON THE VOLCANIC EVOLUTION OF THE AZORES PLATEAU

Christoph Beier^{1,2}, Karsten M. Haase^{1,3}, Wafa Abouchami², Paul van den Bogaard⁴, and Nicole A. Stroncik^{1,5}

¹Institut für Geowissenschaften, Christian-Albrechts-Universität zu Kiel, Ludewig-Meyn-Straße 10, 24118 Kiel, Germany
Email: chb@gpi.uni-kiel.de

²Max-Planck-Institut für Chemie (Otto-Hahn-Institut), Abteilung Geochemie, Joh.-Joachim-Becher-Weg 27, 55128 Mainz, Germany

³Department of Earth Sciences, University of Aarhus, C.F. Møllers Allé 110, 8000 Aarhus C, Denmark

⁴IFM-GEOMAR, Leibniz-Institut für Meereswissenschaften, Wischhofstr. 1-3, 24148 Kiel, Germany

⁵GeoForschungsZentrum Potsdam, Telegrafenberg B124, 14473 Potsdam, Germany

1.1 ABSTRACT

Lavas sampled from the submarine part of the Azores Plateau range from slightly incompatible element-enriched tholeiites to highly enriched alkali basalts similar to those known from the Azores islands. The less enriched lavas occur in the western part of the plateau and formed by relatively high degrees of partial melting. The highly enriched alkali basalts appear to be restricted to local volcanic structures implying different phases of intraplate volcanism which could be related to the jump of the ultraslow spreading Terceira axis within the Azores Plateau. ⁴⁰Ar/³⁹Ar age determinations suggest three eruptive phases at 39 Ma (Eastern Plateau), 4.9 to 6.0 Ma (Central and Western Plateau) and 1.5 Ma to recent. The abundance and spatial distribution of volcanism with ages of 4.9 to 6.0 Ma suggests the arrival of a relatively small plume head with tholeiitic and alkali-basaltic volcanism beneath the lithosphere. The Sr-Nd-Pb isotope systematics reveals small scale heterogeneities in the Azores mantle source with each volcanic structure defined by a single isotopic range with very limited mixing. The absence of one prevailing plume source composition is different from observations made on other plume-related settings such as Hawaii or Galapagos, however, the occurrence of widespread spatiotemporal distribution of volcanism suggests the presence of a melting anomaly beneath the Azores. We suggest that the Azores Plateau represents interaction between an anomalous mantle and the local plate tectonics providing ascent paths for the generated magmas.

1.2 INTRODUCTION

Oceanic plateaus such as Iceland or the Ontong Java Plateau cover large regions of the seafloor and the thickened crust of these plateaus indicates the eruption of large volumes of lavas and anomalously high degrees of partial melting of the mantle. This increased degree of partial melting could be either due to increased mantle temperatures in a mantle plume (e.g. Iceland; White *et al.*, 1995), or a lower solidus temperature of the mantle material due to a higher fertility and/or volatile enrichment (Asimov & Langmuir, 2003). The chemical and isotopic compositions of lavas erupted on oceanic plateaus range from those of Mid-Ocean Ridge Basalts (MORB) to Oceanic Intraplate Basalts (OIB). Many oceanic plateau basalts are more enriched in incompatible elements and show more radiogenic Sr and Pb isotopic signatures than MORB resembling OIB (Schilling, 1975; Schilling *et al.*, 1983). It has also been shown that several oceanic plateaus have formed over relatively long periods of time or by a pulsing mantle plume (White *et al.*, 1995; Cushman *et al.*, 2004). Thus, the study of oceanic plateaus is important in order to define the formation processes of these large magmatic features and it also yields insights into the dynamics of the mantle. The Azores archipelago is situated on the large submarine Azores Plateau (Fig. 1.1) which may have formed either during the impact of a relatively small mantle plume head on the lithosphere close to the Mid-Atlantic Ridge (MAR) some 10 million years ago (Cannat *et al.*, 1999) or by the northward move of an accreting plate boundary, the so-called Terceira axis, recently situated on the NE-rim of the plateau (Vogt & Jung, 2004).

Here we present the first geochemical and geochronological data on lavas from the submarine part of the Azores Plateau and provide new insights into the evolution and origin of the Azores Plateau and the connection between local tectonic settings and geochemistry. We can show that much of the plateau formed between 4.9 to 6.0 Ma by higher degrees of partial melting thus supporting the arrival of a melting anomaly beneath the Azores lithosphere.

1.3 GEOLOGICAL SETTING

The Azores Plateau is situated at the triple junction between the African, Eurasian and North American Plates and reaches water depths of about 1500 m (Fig. 1.1). The MAR separates the plateau into a western and an eastern part. It has a total extension of ~ 700 km from east to west and extends approximately 300 km from the northern to the southern boundary. The recent plate boundary between the Eurasian and African plates is defined by the NW-SE trending Terceira axis, an ultraslow spreading centre with an average spreading rate of 2-4 mm/a (Vogt & Jung, 2004) consisting of the volcanic centres of Graciosa, Terceira, João de Castro Seamount and São Miguel which are separated from each other by non-volcanic basins (Chapter II; Fig. 1.1a). Whereas the islands have been the subject of several studies (Schmincke & Weibel, 1972; Moore, 1990; Widom *et al.*, 1997; Haase & Beier, 2003; Beier *et al.*, 2006) submarine samples from the Azores Plateau have not yet been investigated. The subaerial volcanoes typically erupt alkaline basaltic lavas as well as more differentiated lavas and are strongly enriched in the incompatible elements. MORB from the MAR close to the Azores are enriched in incompatible elements and have relatively high Sr, Pb, and He isotope ratios compared to normal depleted MORB (White, 1977; Kurz, 1982; Schilling *et al.*, 1983; Bourdon *et al.*, 1996; Dosso *et al.*, 1999). The occurrence of a topographic high and a positive gravity anomaly (Escartín *et al.*, 2001; Gente *et al.*, 2003) combined with the geochemical anomaly were taken as evidence for an upwelling mantle plume beneath the Azores Plateau. The unusually thick crust (14 km, Escartín *et al.*, 2001) beneath the Azores Plateau was suggested to have formed either by plume-ridge interactions (Gente *et al.*, 2003) or the NW-SE trending structures of the Princessa Alice bank (Fig. 1.1) could have been generated during a northward jump of the Terceira axis (Vogt & Jung, 2004).

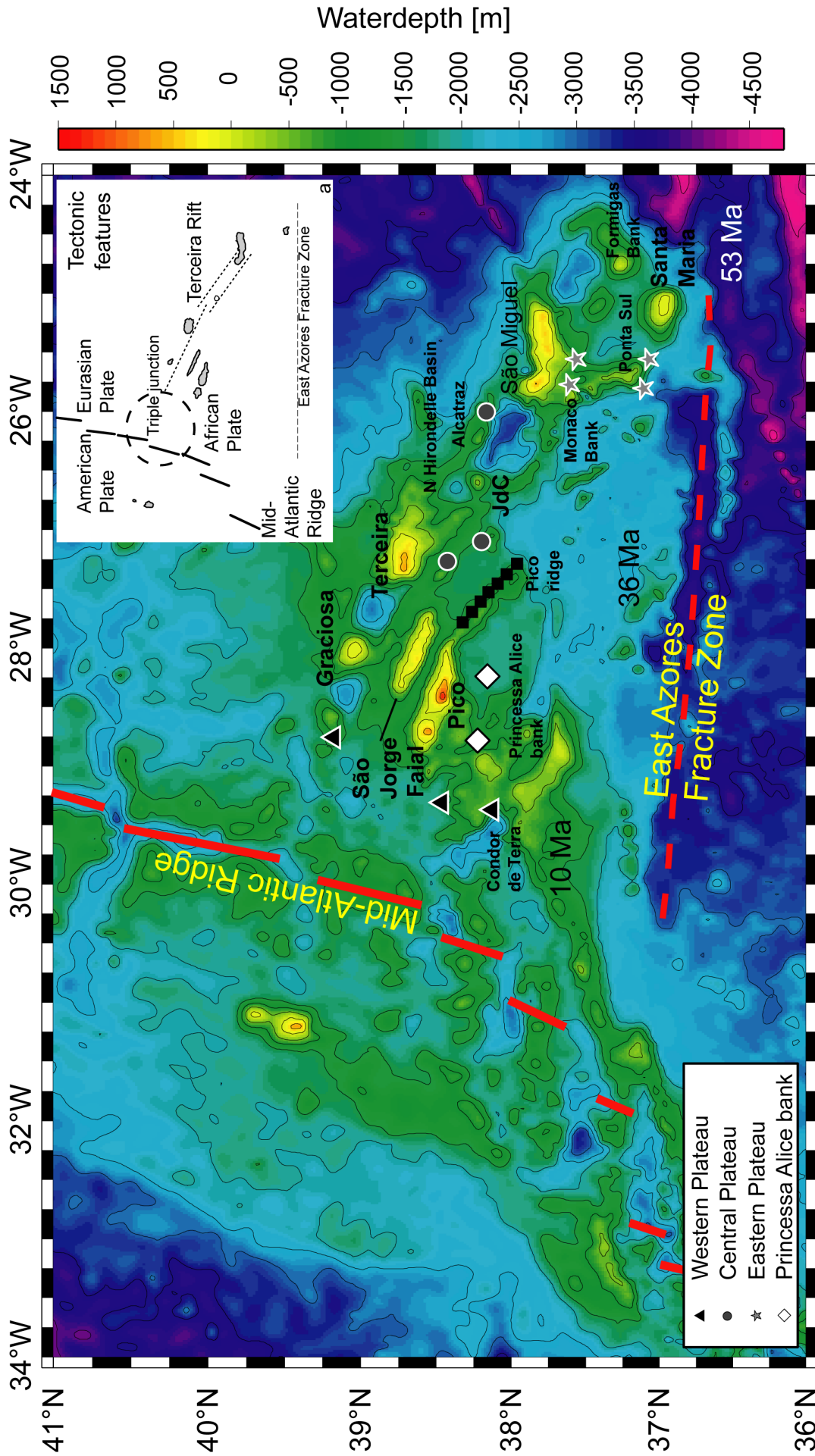


Figure 1.1: Bathymetric chart of the Azores Plateau modified after Smith & Sandwell (1997). JdC = João de Castro submarine volcanic system. Lithospheric age assumptions given by Searle (1980) and Cannat *et al.* (1999). Inset a): major tectonic structures in the Azores. The East Azores Fracture Zone (EAFZ) is the seismically inactive former plate boundary between the Eurasian and African Plates. The recent plate boundary is thought to be in the vicinity of the Terceira axis. Symbols represent dredge locations.

Whereas some islands like Faial and Graciosa only consist of one large volcano surrounded by smaller volcanic cones other islands like São Miguel and Terceira are composed of several large stratovolcanoes. In contrast, the islands of São Jorge and Pico are elongated and consist of rows of volcanoes located along a fault zone. The island of Pico is elongated in a south-eastern direction, parallel to the Terceira axis but has a 85 km long submarine continuation in the east, the so-called “Pico Ridge” with a south-easterly strike.

1.4 METHODS

1.4.1 Sampling and sample treatment

The submarine samples (Fig. 1.1) were obtained during two cruises with RV POSEIDON in 1997 (cruise Pos232) and in 2002 (cruise Pos286). Most submarine samples are fresh but a few of the samples dredged along the Terceira axis show evidence of a slight hydrothermal alteration. Samples dredged in the northeast, at Pico Ridge, and at the Princessa Alice bank are moderately to strongly altered. Many of them show a strong hydrothermal overprint with completely iddingsitised olivines, and zeolite and carbonate fillings of cracks and vesicles. However, some of the samples contain fresh glass shards which allow major element analyses. Glasses were dredged west of São Miguel, at João de Castro and west of Graciosa. On the basis of their occurrence on the Azores Plateau the samples have been separated into five groups; (1) the Western Plateau, (2) the Princessa Alice bank, (3) the Central Plateau, (4) the Eastern Plateau and (5) Pico Ridge lavas (Fig. 1.1). The samples from the Western Edge were dredged from seamounts west of the Azores Plateau, whereas the other samples were dredged on slopes or seamounts directly on the plateau (Fig. 1.1).

Representative samples have been studied petrographically and mineral compositions were determined by means of electron microprobe. Wherever possible, glass was separated, hand-picked, washed and used for the geochemical analyses and electron microprobe analyses. For whole rock analysis, fresh cores were cut, coarsely crushed, washed thoroughly in deionised water, and then fine-crushed in an agate ball mill.

For the major element analyses of the whole rocks, 0.6 grams of dried powder were mixed with lithium tetraborate and ammonium nitrate, fused to a homogeneous glass bead, and analysed using a Philips 1400 XRF spectrometer calibrated against international rock standards. Results for the samples and international rock standards analysed together with the samples are presented in Table 1.1, showing that precision was for most elements better than 0.3 wt. % and accuracy better than 1% of the measured values. The major element analyses of minerals and glasses were carried out on a JEOL JXA8900 Superprobe electron microprobe at the Institut für Geowissenschaften, University of Kiel. The major elements SiO_2 , TiO_2 , Al_2O_3 , FeO^T , MnO , MgO , CaO , Na_2O , K_2O , P_2O_5 , Cr_2O_3 and, in glasses, also F, Cl, and NiO, were measured. The electron microprobe was operated for minerals at an accelerating voltage of 15 kV, a probe current of 12 nA and a beam diameter of 1 μm . Counting times were set to 15 and 7 seconds for mineral peaks and single backgrounds, respectively. For glasses the beam was defocused and counting times of 20 and 10 seconds were used.

The trace element analyses were carried out using an Agilent 7500c/s Quadrupole Inductively Coupled Plasma Mass Spectrometer (ICP-MS) at the Institut für Geowissenschaften, University of Kiel. The samples were prepared following the pressurised HF-HClO₄-aqua regia acid digestion procedure described by Garbe-Schönberg (1993). Trace element analyses of the samples and of international rock standards are shown in Table 1.1 indicating a standard deviation of the precision and accuracy of < 5 % and < 8 % (2 σ), respectively.

Table 1.1: Selected major element, trace element and Sr-Nd-Pb isotope data of whole rocks and glasses from the submarine Azores Plateau and international rock standards. Major element, trace element and isotopic data from São Miguel are presented in Chapters III and IV, Terceira data are shown Chapter II. Additional major element and trace element data are available in the Appendix. The whole-rock (WR) major element data were determined by XRF and the trace element data were determined by ICP-MS. The major element glass data were determined by electron microbeam and the trace element data were analysed by XRF. Melting pressure was calculated using fractionation-corrected SiO₂ contents and the equation of Haase (1996).

Sample	188DS-1	494DS-1	497DS-1	513DS-1	515DS-1	516DS-2	529DS-4	532DS-1
Location	Ponta Sul, S of São Miguel	Monaco Bank, S of São Miguel	Monaco Bank, S of São Miguel	W slope of São Miguel	W slope of São Miguel	Alcatraz, Terceira axis	E of Terceira	Seamount S of Terceira
Latitude [°N]	37°10.861	37°38.084	37°36.559	37°51.933	37°51.874	38°08.008	38°32.614	38°23.373
Longitude [°W]	25°42.318	25°54.076	25°54.109	25°56.277	25°59.887	26°00.687	26°52.509	27°15.461
	Submarine	Submarine	Submarine	Submarine	Submarine	Submarine	Submarine	Submarine
TAS classification	Basalt	Basalt	Basalt	Basalt	Trachyandesite	Basanite	Basalt	Basalt
Age [Ma]	5.90 ± 0.12	39.00 ± 0.22				5.43 ± 0.17		
Melting pressure [GPa]	4.28	4.34	3.83	2.65		4.04	2.81	
WR/GL	WR	WR	WR	WR	WR	WR	WR	WR
[wt.%]								
SiO ₂	43.22	43.08	44.26	46.95	59.29	43.78	46.57	47.55
TiO ₂	2.72	4.34	4.28	2.74	1.28	4.24	1.90	2.97
Al ₂ O ₃	12.84	14.20	15.78	12.33	18.69	15.84	14.54	16.42
Fe ₂ O ₃	13.17	13.95	14.45	11.06	5.93	14.51	9.62	12.18
FeO								
MnO	0.18	0.20	0.19	0.17	0.19	0.19	0.15	0.20
MgO	11.71	6.61	5.83	12.13	1.58	4.90	10.55	4.77
CaO	10.15	10.27	9.35	10.97	3.53	9.67	10.23	8.92
Na ₂ O	2.43	2.59	3.19	2.56	5.99	2.99	2.90	3.41
K ₂ O	0.99	1.42	1.12	1.38	4.32	1.44	1.10	1.82
P ₂ O ₅	0.46	1.47	0.86	0.48	0.38	0.78	0.38	0.76
SO ₃								
Cl								
LOI	1.43	0.00	0.00	0.00	0.00	0.00	0.00	0.00
Total	99.30	98.13	99.31	100.77	101.18	98.34	97.94	99.00
[ppm]								
Sc	29.3	18.0	54.2	24.1	3.16		26.2	
Cr	533	137	16.4	996	2.25	121	539	201
Co	61.9	30.5	31.1	44.6	4.95		35.1	
Ni	273	57.0	24.0	319	1.75	184	205	86.0
Cu	37.5	15.5	26.8	70.5	3.29		48.0	
Zn	114	110	129	90.0	92.1	123	77.0	124
Mo		0.82	1.85	1.90	0.97		4.21	
Rb	21.8	23.0	18.3	28.5	1090	17.0	22.2	49.0
Sr	611	1123	598	622	543	770	414	644
Y	24.8	28.8	33.4	19.3	33.7		18.1	
Zr	223	166	219	259	607	336	136	360
Nb	43.0	33.7	38.7	48.0	130		27.0	
Cs	0.22	0.48	0.27	0.32	0.26		0.25	
Ba	323	540	241	404			324	
La	30.2	48.4	36.4	36.6	89.5		21.5	
Ce	63.1	107	68.5	75.5	173		44.4	
Pr	8.20	14.5	9.90	9.51	19.4		5.62	
Nd	33.1	62.6	42.7	38.3	68.0		22.7	
Sm	7.01	13.1	9.96	7.93	11.8		5.07	
Eu	2.23	4.74	3.19	2.43	3.32		1.64	
Gd	6.35	11.2	9.54	6.70	9.65		4.80	
Tb	0.94	1.53	1.41	0.96	1.44		0.74	
Dy	5.06	8.03	7.99	5.16	7.76		4.43	
Ho	0.90	1.41	1.50	0.93	1.44		0.86	
Er	2.22	3.30	3.78	2.28	3.81		2.24	
Tm	0.29	0.39	0.48	0.29	0.54		0.30	
Yb	1.79	2.22	2.92	1.76	3.49		1.87	
Lu	0.25	0.31	0.42	0.24	0.50		0.27	
Hf	5.13	5.07	6.94	5.98	15.1		4.21	
Ta	2.47	2.28	2.86	3.34	8.73		1.85	
Pb	1.79	1.42	1.49	2.05	6.13		2.08	
Th	3.04	3.10	3.09	3.82	13.5		2.35	
U	0.76	1.00	1.47	1.14	1.76		0.68	
	Pb triple spike	Pb triple spike	Pb triple spike				Pb triple spike	
⁸⁷ Sr/ ⁸⁶ Sr	0.703557	0.703657	0.703649	0.703273	0.703553	0.704093	0.703519	0.704124
¹⁴³ Nd/ ¹⁴⁴ Nd	0.51287	0.51290	0.51296	0.51299	0.51289	0.51280	0.51287	0.51290
ε Nd	4.43	5.11	6.22	6.83	4.88	3.25	4.45	5.18
²⁰⁶ Pb/ ²⁰⁴ Pb	19.39	19.30	19.29	19.33	19.50		19.51	19.24
²⁰⁷ Pb/ ²⁰⁴ Pb	15.60	15.60	15.60	15.56	15.61		15.55	15.54
²⁰⁸ Pb/ ²⁰⁴ Pb	39.21	39.27	39.26	39.05	39.37		39.07	38.85
²⁰⁸ Pb/ ²⁰⁶ Pb	2.022	2.035	2.035	2.020	2.018		2.003	2.019

Table 1.1: continued

Sample	535DS-7	543DS-1	198DS-6	201DS-2	203DS-5	206DS-2	212DS-2	215DS-1	548DS-1	
Location	W flank of Terceira	WNW of Graciosa	Pico Ridge	Pico Ridge	Pico Ridge	Pico Ridge	Pico Ridge	Pico Ridge	SW of Faial	
Latitude [°N]	38°42.446	39°12.881	37°58.736	38°03.552	38°07.886	38°09.771	38°18.273	38°22.216	38°31.755	
Longitude [°W]	27°28.720	28°52.096	27°21.057	27°28.401	27°34.223	27°38.940	27°51.681	27°56.993	29°02.998	
	Submarine	Submarine	Submarine	Submarine	Submarine	Submarine	Submarine	Submarine	Submarine	
TAS classification	Basalt	Basalt	Trachyandesite						Basalt	Basalt
Age [Ma]										
Melting pressure [GPa]	2.95	2.37						2.67	2.31	
WR/GL	WR	WR	WR	WR	WR	WR	WR	WR	WR	
[wt.%]										
SiO ₂	46.27	47.59	53.79					46.89	47.72	
TiO ₂	3.86	1.56	1.69					2.94	2.01	
Al ₂ O ₃	14.96	14.62	17.82					14.26	16.16	
Fe ₂ O ₃	13.31	12.16	8.20					11.09	9.96	
FeO										
MnO	0.18	0.18	0.20					0.16	0.15	
MgO	6.15	6.77	1.52					8.21	7.38	
CaO	10.58	10.80	4.24					10.27	11.59	
Na ₂ O	3.22	2.99	5.61					3.21	2.72	
K ₂ O	0.85	0.49	3.28					1.19	0.38	
P ₂ O ₅	0.46	0.21	0.62					0.52	0.28	
SO ₃										
Cl										
LOI	0.00	0.00	2.38					0.07	0.00	
Total	99.84	97.37	99.35					98.81	98.35	
[ppm]										
Sc		33.8	4.26					27.3	27.8	
Cr	92.0	36.0	0.61					338	274	
Co		36.1	5.71					43.1	39.7	
Ni	72.0	36.0	16.7					152	115	
Cu		28.5	2.65					39.1	34.1	
Zn	109	106	127					107	84.0	
Mo		0.68							0.77	
Rb	24.0	9.98	67.8					26.8	5.82	
Sr	593	168	492					614	335	
Y		28.2	52.4					29.9	22.1	
Zr	272	81.9	460					254	107	
Nb		6.92	119					48.0	13.7	
Cs		0.73	0.36					0.25		
Ba		57.0	779					309	104	
La		6.81	76.6					35.6	11.9	
Ce		16.9	143					74.7	27.2	
Pr		2.60	17.1					9.64	3.83	
Nd		12.9	61.8					38.3	17.5	
Sm		4.18	11.6					7.88	4.81	
Eu		1.48	3.22					2.48	1.70	
Gd		5.16	10.4					7.12	5.26	
Tb		0.94	1.63					1.06	0.87	
Dy		6.24	9.38					5.83	5.33	
Ho		1.33	1.80					1.05	1.06	
Er		3.76	4.92					2.66	2.80	
Tm		0.54	0.71					0.35	0.38	
Yb		3.47	4.64					2.21	2.37	
Lu		0.52	0.67					0.31	0.35	
Hf		3.01	9.64					5.65	3.57	
Ta		0.48	6.11					2.71	1.02	
Pb		1.14	4.81					2.64	0.73	
Th		0.68	10.4					3.48	1.11	
U		0.65	2.63					1.16	1.59	
	Pb triple spike	Pb triple spike	Pb triple spike	Pb triple spike	Pb triple spike	Pb triple spike				
⁸⁷ Sr/ ⁸⁶ Sr	0.703580	0.703757	0.703525	0.704337	0.704392	0.704004	0.703788	0.703687	0.703562	
¹⁴³ Nd/ ¹⁴⁴ Nd	0.51297	0.51302	0.51293	0.51280	0.51287	0.51293	0.51297	0.51290	0.51299	
ε Nd	6.46	7.41	5.67	3.13	4.51	5.61	6.46	5.17	6.83	
²⁰⁶ Pb/ ²⁰⁴ Pb	19.92	18.42	20.22	18.56	18.63	19.03				
²⁰⁷ Pb/ ²⁰⁴ Pb	15.62	15.53	15.64	15.44	15.46	15.52				
²⁰⁸ Pb/ ²⁰⁴ Pb	39.23	38.22	39.69	38.02	38.28	38.59				
²⁰⁸ Pb/ ²⁰⁶ Pb	1.969	2.075	1.963	2.061	2.055	2.027				

Table 1.1: continued

Sample	550DS-5	220DS-1	220DS-2	224DS-1	236DS-1	BHVO-1	BHVO-1
Location	SE of São Jorge	Princesa Alice Bank	Princesa Alice Bank	Princesa Alice Bank	Condor de Terra	XRF	n=23 ICP-MS n=12
Latitude [°N]	38°28.174	37°44.293	37°44.293	37°52.926	38°32.232		
Longitude [°W]	27°50.280	29°12.136	29°12.136	29°53.008	29°03.828		
	Submarine	Submarine	Submarine	Submarine	Submarine	Standard	standard deviation Standard standard deviation
TAS classification	Basalt	Trachybasalt	Trachybasalt		Trachybasalt	Basalt	Basalt
Age [Ma]	4.89 ± 0.48	6.01 ± 0.14	5.51 ± 0.13		1.10 ± 0.80		
Melting pressure [GPa]	2.74	2.92	2.80		2.59		
WR/GL	GL	WR	WR	WR	WR	WR	WR
[wt.%]							
SiO ₂	46.74	46.32	46.61		47.08	49.94 ± 0.14	
TiO ₂	4.74	3.28	3.22		1.84	2.76 ± 0.01	
Al ₂ O ₃	14.09	14.69	15.06		15.37	13.57 ± 0.07	
Fe ₂ O ₃		13.23	12.32		10.35	12.22 ± 0.04	
FeO	11.77						
MnO	0.22	0.23	0.19		0.23	0.17 ± 0.00	
MgO	4.33	4.90	3.82		6.93	7.18 ± 0.06	
CaO	9.46	7.10	9.71		11.39	11.46 ± 0.04	
Na ₂ O	3.23	4.43	4.01		2.79	2.40 ± 0.07	
K ₂ O	1.53	1.39	1.29		0.27	0.53 ± 0.01	
P ₂ O ₅	0.61	0.72	0.61		0.45	0.28 ± 0.00	
SO ₃							
Cl							
LOI	0.00	2.93	2.50		3.11		
Total	96.72	99.22	99.34		99.81	100.52	
[ppm]							
Sc	33.6	17.9	26.4		32.2		32.9 ± 1.54
Cr	6.46	0.40	9.87		382	282 ± 4.85	291 ± 9.84
Co	34.1	27.4	49.2		41.4		45.5 ± 1.95
Ni		16.7	22.3		188	107 ± 7.30	120 ± 4.54
Cu	28.0	8.23	56.2		23.0		135 ± 9.81
Zn		150	132		113	106 ± 4.04	104 ± 4.22
Mo	1.77						1.06 ± 0.09
Rb	18.8	18.3	21.7		2.86	9.91 ± 1.85	9.36 ± 0.30
Sr	491	564	458		358	398 ± 2.52	394 ± 12.7
Y	31.9	47.6	40.6		27.7		26.4 ± 1.29
Zr	222	297	267		101	188 ± 2.38	175 ± 6.47
Nb	39.6	52.6	47.8		12.1	17.6 ± 1.34	17.5 ± 0.46
Cs	0.26	0.10	0.08		0.09		0.10 ± 0.00
Ba	222	344	315		71.1	160	131 ± 2.54
La	33.7	37.7	33.9		9.30		15.2 ± 0.38
Ce	67.5	79.7	72.6		21.2	10.2 ± 3.66	37.8 ± 0.58
Pr	9.49	10.8	9.55		3.10		5.50 ± 0.07
Nd	40.7	44.8	39.5		14.4		24.9 ± 0.31
Sm	9.60	10.2	8.79		4.11		6.20 ± 0.13
Eu	3.08	3.24	2.74		1.57		2.13 ± 0.06
Gd	9.05	9.94	8.48		4.84		6.20 ± 0.20
Tb	1.35	1.55	1.32		0.81		0.96 ± 0.03
Dy	7.66	8.90	7.55		4.93		5.39 ± 0.15
Ho	1.43	1.66	1.40		0.96		0.98 ± 0.04
Er	3.58	4.34	3.66		2.54		2.47 ± 0.08
Tm	0.47	0.60	0.51		0.36		0.33 ± 0.01
Yb	2.82	3.79	3.20		2.25		2.02 ± 0.07
Lu	0.40	0.54	0.46		0.33		0.28 ± 0.01
Hf	6.88	6.87	6.05		2.66		4.40 ± 0.08
Ta	2.88	2.87	2.55		0.66		1.08 ± 0.04
Pb	1.50	2.76	2.45		1.28		1.94 ± 0.23
Th	3.07	3.78	3.44		0.82		1.21 ± 0.09
U	1.29	0.58	1.45		0.74		0.42 ± 0.02
		Pb triple spike					
⁸⁷ Sr/ ⁸⁶ Sr	0.703622	0.703464	0.703366	0.704052	0.703426		
¹⁴³ Nd/ ¹⁴⁴ Nd	0.51300	0.51299	0.51299	0.51302	0.51303		
ε Nd	6.97	6.83	6.88	7.41	7.69		
²⁰⁶ Pb/ ²⁰⁴ Pb		19.97	19.95				
²⁰⁷ Pb/ ²⁰⁴ Pb		15.64	15.63				
²⁰⁸ Pb/ ²⁰⁴ Pb		39.32	39.29				
²⁰⁸ Pb/ ²⁰⁶ Pb		1.969	1.972				

Table 1.2: $^{40}\text{Ar}/^{39}\text{Ar}$ age determinations of the Azores submarine and subaerial lavas. Analytical details are described in the main text.

Matrix step-heating analyses								
Sample	Location	Age	\pm	1σ	^{39}Ar	MSWD	Probability	n (N)
			[Ma]		%			
188 DS-1	Ponta Sul (Western Plateau)	5.90	\pm	0.12	49.10	1.50	0.20	5(20)
236 DS-1	Condor de Terra (Western Plateau)	1.10	\pm	0.80	55.40	0.68	0.75	11(20)
220 DS-1	Princessa Alice Bank	6.01	\pm	0.14	68.20	1.80	0.08	9(20)
220 DS-2	Princessa Alice Bank	5.51	\pm	0.13	70.20	1.80	0.04	15(20)
550DS-5	North of Pico Ridge (Central Plateau)	4.89	\pm	0.48	84.70	1.70	0.10	9(20)
494DS-1	Monaco Bank (Eastern Plateau)	39.00	\pm	0.22	73.00	1.80	0.12	5(20)
201DS-1	Pico Ridge	1.49	\pm	0.12	80.00	0.46	0.95	13(20)
516DS-2	Alcatraz (Central Plateau)	5.43	\pm	0.17	59.70	0.68	0.77	12(20)
AZT03-66	Terceira	0.75	\pm	0.11	70.00	1.60	0.09	13(20)
AZT03-80	Terceira	0.01	\pm	0.09	69.30	0.59	0.76	8(20)

For isotopic determinations, 150-200 mg of hand picked grains and standard ion exchange techniques were used to separate Sr, Nd and Pb from the matrix. Because several samples show signs of significant alteration they were leached in 6N HCl for two hours on a hotplate, ultrasonicated 30 minutes and then dissolved using the standard digestion procedure described by Eisele *et al.* (2002) and Abouchami *et al.* (2000).

The Sr isotopic ratios of most samples were determined using a TRITON thermal ionization mass spectrometer at IFM-GEOMAR in Kiel. Some Sr isotopic ratios were determined with a Finnigan MAT261 thermal ionization mass spectrometer at the Max-Planck-Institut für Chemie (MPI) in Mainz. The Nd isotopic ratios were measured by means of Multi-Collector Inductively Coupled Plasma Mass Spectrometry (MC-ICP-MS, Nu Plasma HR) at the MPI. The Pb triple spike analyses were measured on a TRITON thermal ionization mass spectrometer at the MPI in Mainz.

Sr and Nd isotope ratios were analysed in static mode and isotope fractionation corrections are relative to $^{86}\text{Sr}/^{88}\text{Sr} = 0.1194$ and $^{146}\text{Nd}/^{144}\text{Nd} = 0.7219$, respectively. In Mainz, standard runs for Sr isotopes gave NBS 987 (n = 8): 0.710182 (2SD = 0.000010) and all Sr isotope analyses were normalised to NBS 987 = 0.710250. Standard runs for $^{143}\text{Nd}/^{144}\text{Nd}$ gave La Jolla (n = 11): 0.511827 (2SD = 0.000025). In Kiel, the NBS987 (n = 8) gave 0.710273 (2SD = 0.000005) and all Sr isotope analyses were normalised to NBS987 = 0.710250. Standard runs for $^{143}\text{Nd}/^{144}\text{Nd}$ gave 0.511710 (2SD = 0.000005) for the Nd Spex standard (n = 5) corresponding to a La Jolla value of 0.511828. Procedural blanks in both laboratories were generally better than 0.2 ng and 0.1 ng for Sr and Nd.

Following the elution of Pb, the samples were split and a sample aliquot was mixed with an amount of triple spike that was estimated to be optimal (spike/sample ratio between 0.6 – 1.6). Loaded onto “Good fellow” Re-filaments with silica-gel H_3PO_4 activator both unspiked and spiked sample aliquots were measured on a TRITON mass spectrometer in static multicollection mode. The bias-correction estimated from the two runs has been done following the method of Galer (1999). Based on duplicate analyses, the external reproducibility is ~150 ppm for $^{206}\text{Pb}/^{204}\text{Pb}$, $^{207}\text{Pb}/^{204}\text{Pb}$, and $^{208}\text{Pb}/^{204}\text{Pb}$. Standard runs for the NBS-981 Pb standard (n = 8) give average values of 16.9431 ± 0.0034 , 15.5008 ± 0.0029 , and 36.7300 ± 0.0074 for $^{206}\text{Pb}/^{204}\text{Pb}$, $^{207}\text{Pb}/^{204}\text{Pb}$, and $^{208}\text{Pb}/^{204}\text{Pb}$, respectively.

The $^{40}\text{Ar}/^{39}\text{Ar}$ age determinations were done at the IFM-GEOMAR, Leibniz-Institut für Meereswissenschaften, Kiel (Table 1.2). Matrix samples were carefully selected based on thin sections and K_2O contents. The particles

were handpicked from crushed and sieved splits (250-500 μm) and cleaned in ultrapure H_2O with an ultrasonic disintegrator. The samples were neutron irradiated in aluminum trays and irradiation cans for seven days with a Cd-liner at the 5-MW reactor at the GKSS Reactor Center (Geesthacht). Age determinations were done with laser-step heating analyses; the purified gas samples were analysed with a MAP 216 series noble gas mass spectrometer. Raw mass spectrometer peaks were corrected for mass discrimination, background and blank values determined every fifth analyses. The neutron flux was monitored using the TCR sanidine (Taylor Creek Rhyolite, 27.92 Ma, Duffield & Dalrymple, 1990). Vertical variations in J-values ($\sim 0.12\%$) were quantified by a cosine function fit. Corrections for the interfering neutron reactions on Ca and K are based on high purity CaF_2 and K_2SO_4 salt crystal analyses that were irradiated with the samples. Mean squared weighted deviates ($\text{MSWD} = \text{Sum of Squares} / \text{N}-2$) were used to determine the scatter of the single fusion data. Acceptable plateau ages are more than three consecutive steps and ages within uncertainties of $> 49 \text{ Vol. } \% \text{ } ^{39}\text{Ar}$.

1.5 RESULTS

1.5.1 Major elements, trace elements and isotopes

The submarine lavas of the Azores Plateau generally belong to the alkaline volcanic series similar to those from the islands and form a trend from alkali basalts to trachytes (Fig. 1.2). However, few samples from the Central and Eastern Plateau also have tephritic compositions. Generally, the submarine lavas from the Eastern and Central Groups resemble the lava series from São Miguel which contain higher $\text{Na}_2\text{O} + \text{K}_2\text{O}$ contents than the Terceira lavas. In contrast, the primitive submarine lavas from the Princesa Alice Bank resemble the less alkaline Terceira island series, whereas samples from the Western Group have tholeiitic compositions. The samples from Pico Ridge are situated between the Terceira and São Miguel fields.

One sample (543DS-1) of the Western Group contains low La and Nb but high K and U concentrations and has, as a consequence, unusually high K/La and low Nb/U ratios compared to the other Azorean samples. The combined high K and U contents are most likely the product of alteration. However, the REE systematics are not influenced by alteration and can therefore be used for the investigation of variations in degree of partial melting. Most of the plateau lavas do not give any evidence for a significant major or trace element mobility by alteration processes and have, for example, Nb/U ratios in the range of 47 ± 10 suggested for fresh oceanic lavas (Hofmann, 1988).

Most Azores Plateau samples show light REE-enriched patterns similar to lavas from the islands. Thus, the trace element variations (Fig. 1.3) correspond to the alkali element compositions, where the samples from Pico Ridge, Pico, and São Miguel have $(\text{La}/\text{Sm})_{\text{N}} > 2.2$, whereas the lavas from Terceira, the Princesa Alice bank, the Western and Eastern Groups have lower $(\text{La}/\text{Sm})_{\text{N}}$ ratios. The three samples from the Western Plateau Edge reveal relatively flat REE patterns that result in $(\text{La}/\text{Sm})_{\text{N}}$ ratios between 1.1 to 1.6, resembling MORB from the neighbouring MAR (Fig. 1.4). The Ba/La, Nb/Zr and $(\text{La}/\text{Sm})_{\text{N}}$ show that the three samples from the Western Plateau and one sample from the Princesa Alice bank have much lower Nb/Zr and $(\text{La}/\text{Sm})_{\text{N}}$ but comparable Ba/La ratios compared to the lavas from Princesa Alice bank, Pico Ridge, and São Miguel suggesting both different degrees of partial melting ($(\text{La}/\text{Sm})_{\text{N}}$) and different mantle source signatures (Nb/Zr; Fig. 1.4).

The Sr-Nd-Pb isotope ratios are not influenced by different degrees of partial melting or by fractional crystallization and, thus, represent different mantle source compositions (Fig. 1.5). Lavas from the Western

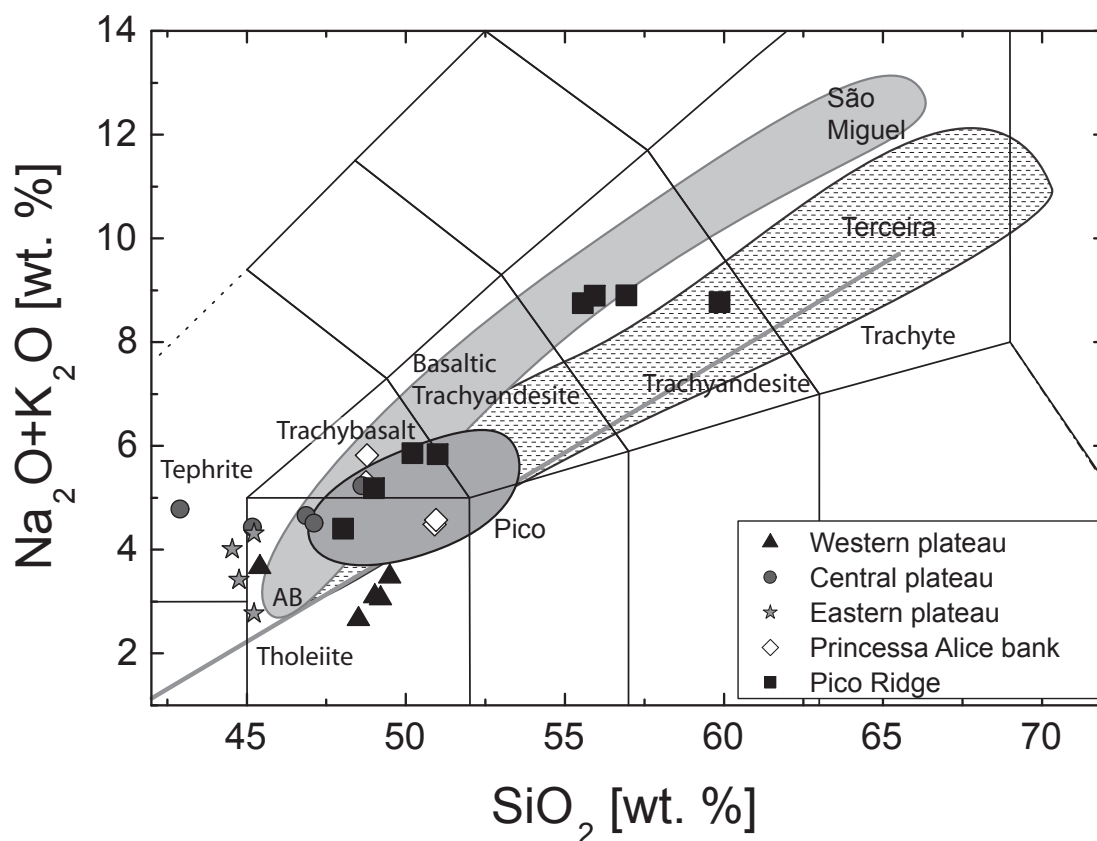


Figure 1.2: Total alkalis ($\text{Na}_2\text{O}+\text{K}_2\text{O}$) versus SiO_2 on a volatile-free basis according to Le Maitre (1989). The separation line between alkaline (AB) and tholeiitic compositions was taken from Macdonald (1968). The fields of São Miguel and Terceira include subaerial and submarine samples. Subaerial Pico samples are literature data (Berthois, 1953; Flower *et al.*, 1976; White *et al.*, 1979; Féraud *et al.*, 1980; Hofmann *et al.*, 1986; Turner *et al.*, 1997; Claude-Ivanaj *et al.*, 2001).

Group and Princessa Alice Bank have relatively high Nd isotope ratios comparable to MORB from the neighbouring MAR but variable $^{87}\text{Sr}/^{86}\text{Sr}$ most likely due to seawater alteration. The three samples from the Eastern Plateau, those from the Central Plateau and from Pico Ridge resemble the São Miguel lavas in terms of Sr and Nd isotope compositions (Fig. 1.5a). However, most Pico Ridge samples as well as the one analysed sample from the Western Plateau have ‘MORB’-like Pb isotope compositions (Fig. 1.5 b-d), whereas the samples from the Princessa Alice Bank and one sample from Pico Ridge have elevated $^{206}\text{Pb}/^{204}\text{Pb}$ and $^{208}\text{Pb}/^{204}\text{Pb}$ isotope ratios comparable to the radiogenic Terceira and Pico lavas (Fig. 1.5 b-d). Thus, only this one sample (198DS-6) from Pico Ridge which is situated at the end most distant from Pico island has a composition similar to the lavas from Pico island, whereas all other Pico Ridge lavas differ significantly suggesting a distinct mantle source for the Pico Ridge magmas. The samples from the Princessa Alice Bank have relatively low Sr isotope ratios comparable to those found on Terceira at higher $^{206}\text{Pb}/^{204}\text{Pb}$ ratios. The Eastern Plateau samples lie at the intersection of the trends of the different Azores volcanic systems and close to the so-called FOZO component (cf. Hart *et al.*, 1992). Combining the Sr, Nd and Pb isotope data (Fig. 1.5), we can distinguish four different groups with similar mantle sources: 1) Princessa Alice, Terceira, and Pico samples with radiogenic Pb and less radiogenic Sr isotope ratios, 2) the Eastern and Central Group samples with compositions comparable to the western São Miguel lavas with relatively low Sr and Pb isotope compositions, 3) the generally ‘MORB’-like depleted lavas from the Western Plateau, and 4) the Pico Ridge samples trending towards more enriched mantle compositions.

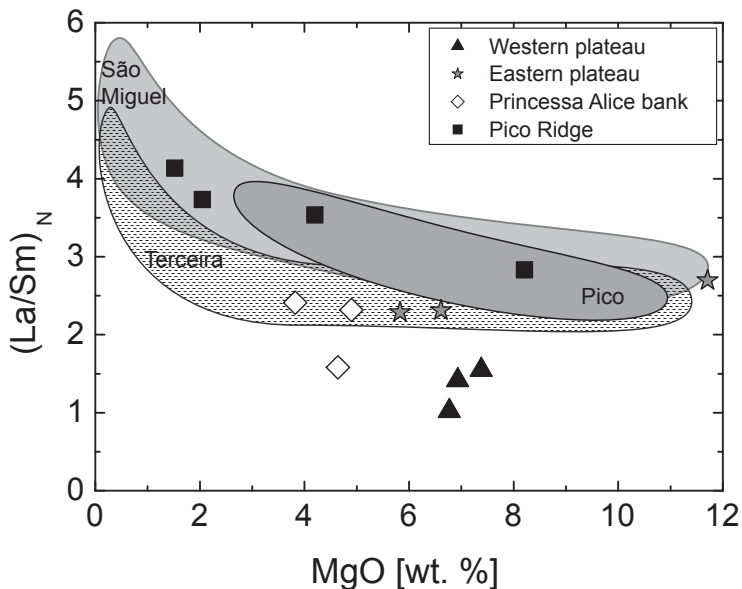


Figure 1.3: Chondrite-normalised La/Sm trace element ratios versus MgO [wt. %]. Pico data as in Figure 1.2. Chondrite composition from Sun & McDonough (1989).

Monaco Bank south of São Miguel (Fig. 1.1). Several rocks from the Princessa Alice Bank, the Central Group and also one from the Eastern Group reveal ages between 4.9 and 6.0 Ma (Fig. 1.6) which is roughly the age range of the lavas of the island Santa Maria and the Formigas Bank (Fig. 1.1, Abdel Monem *et al.*, 1975; Féraud *et al.*, 1980). The Western Group samples are situated on seafloor between magnetic anomalies 4 and 4 A, i.e. 7.0 to 8.7 Ma old (Luis *et al.*, 1994) implying that the Western Group lavas erupted off-axis on lithosphere older than 1 Ma. Samples from Pico Ridge and one seamount from the Western Group give ages of 1.49 ± 0.12 and 1.10 ± 0.80 Ma, respectively, in agreement with K-Ar ages from most of the islands (Fig. 1.6). Consequently, two major volcanic phases can be distinguished which affected most of the plateau, i.e. one between 4.9 and 6.0 Ma and the other from about 1.49 Ma to recent times. Interestingly, these two phases approximately correspond to phases, when significant changes in both spreading direction and rate occurred on the MAR (Luis *et al.*, 1994). However, the first eruptions that may be associated with the plateau appear to be much older and occurred at 39 Ma on the eastern part of the Azores Plateau.

1.6 DISCUSSION

1.6.1 Partial melting processes of the Azores Plateau magmas

The major and trace elements were used to investigate the influence of partial melting processes to the compositions of the Azorean lavas. The SiO_2 , Al_2O_3 and FeO^T concentrations in the primitive magmas mainly depend on the pressure of melting and seem to be independent of source composition and extent of melting, whereas the Na_2O and TiO_2 are varying with the average degree of partial melting. Although the FeO^T and Na_2O contents are sensitive to varying volatile contents in the mantle source (Asimow *et al.*, 1995; Asimow *et al.*, 2004) we find a broad negative correlation between FeO^T and SiO_2 among the Azorean rocks (Fig. 1.7) indicating that different pressures of melting affected the Azores Plateau magmas. The variations in fractionation-corrected Na and Fe could also be a result of melting in the presence of garnet pyroxenite (Hirschmann & Stolper, 1996). This would also lead to higher heavy REE ratios (e.g. Dy/Yb) correlated with lower fractionation-corrected

1.5.2 Age dating

Although only few samples were suitable for $^{40}\text{Ar}/^{39}\text{Ar}$ age dating analysis, the results give important insights into the evolution of the Azores Plateau (Table 1.2, Fig. 1.6). Most subaerial samples from Terceira and Faial yield zero ages within the error of the method (± 0.60 Ma). Only one sample from Terceira gives an age of 0.75 ± 0.11 Ma which is significantly older than previously dated samples from Terceira (< 0.3 Ma; Féraud *et al.*, 1980). However, this age is comparable to the oldest Ar-Ar ages known from the easternmost and oldest volcanic system on São Miguel (0.8 Ma; Johnson *et al.*, 1998). The oldest submarine samples yield ages of 39 ± 0.22 Ma and occur on the

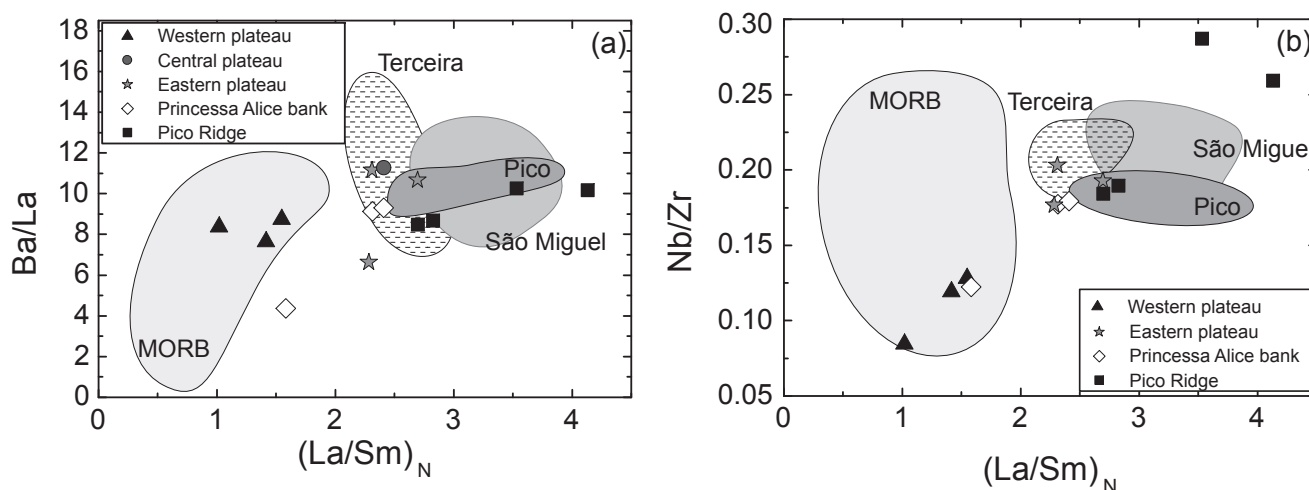


Figure 1.4: Trace element ratios of primitive Azorean lavas (> 4.6 wt. % MgO for submarine lavas and > 5 wt. % MgO for subaerial lavas). a) Ba/La versus Chondrite-normalised La/Sm ratios indicating both higher degrees of partial melting with decreasing La/Sm and mantle source signatures with varying Ba/La (e.g. Hémond *et al.*, 1994). b) Nb/Zr versus Chondrite-normalised La/Sm ratios giving evidence for less enriched mantle sources signatures at the Western Plateau and Princessa Alice compared to the other locations. Pico data as in Figure 1.2. Chondrite composition from Sun & McDonough (1989).

Fe contents (Fig. 1.8, Shen & Forsyth, 1995). However, the broad positive correlation between the heavy REE ratios and the fractionation-corrected Fe contents in the Azorean lavas (Fig. 1.8a), suggests that a pyroxenite component, if present, is of minor importance during melt generation in the Azores Plateau. Instead, the positive correlation of the Azores lavas suggests the presence of enriched peridotite mantle sources with varying amounts of garnet (Fig. 1.8a). We estimated the pressures of melting by applying the equation ($P(\text{GPa}) = 23.217 - 0.4381 \times \text{SiO}_2$) published by Haase (1996) and give the results together with the fractionation-corrected Na_2O contents (10 wt. % MgO), which are sensitive to different degrees of partial melting (Fig. 1.7). A broad range in melting pressures is observed among the submarine lavas ranging from average melting depths of about 70 km in samples from the Western Group, Terceira and Pico to melting depth of about 90 to 120 km for the Central and Eastern Groups and for São Miguel. However, a systematic correlation between melting depth and degree of partial melting has not been observed in the major elements of the submarine lavas.

The Western Plateau and Princessa Alice lavas are less incompatible element enriched compared to the other Azores Plateau lavas (Figs. 1.3, 1.4, and 1.8). These compositions probably indicate relatively large degrees of partial melting as is shown by our melting model (Fig. 1.8) and/or mixing of enriched melts with depleted ‘MORB’-like magmas. The Princessa Alice lavas generally, with the notable exception of one sample situated within the Western Group lavas, resemble the Terceira basalts in terms of incompatible element ratios ($(La/Sm)_N$, Nb/Zr) but they are situated at the lower end of the Terceira field (Fig. 1.4). It is unlikely that the lower $(Ce/Yb)_N$ of the Princessa Alice lavas compared to Terceira are a result of a depleted source composition because both have similar Nb/Zr (Fig. 1.4) and isotopic compositions (Fig. 1.5). Rather, the slightly lower $(Ce/Yb)_N$ reflect higher degrees of partial melting for the Princessa Alice bank than for most of the Terceira basaltic magmas but similar mantle source compositions (Fig. 1.8).

In order to distinguish between different degrees of partial melting and source compositions we model the partial melting of the REE using the batch melting equation (Shaw, 1970) and re-enriched mantle compositions based on a depleted primitive mantle source (Hofmann, 1988). The majority of the submarine lavas can be modelled

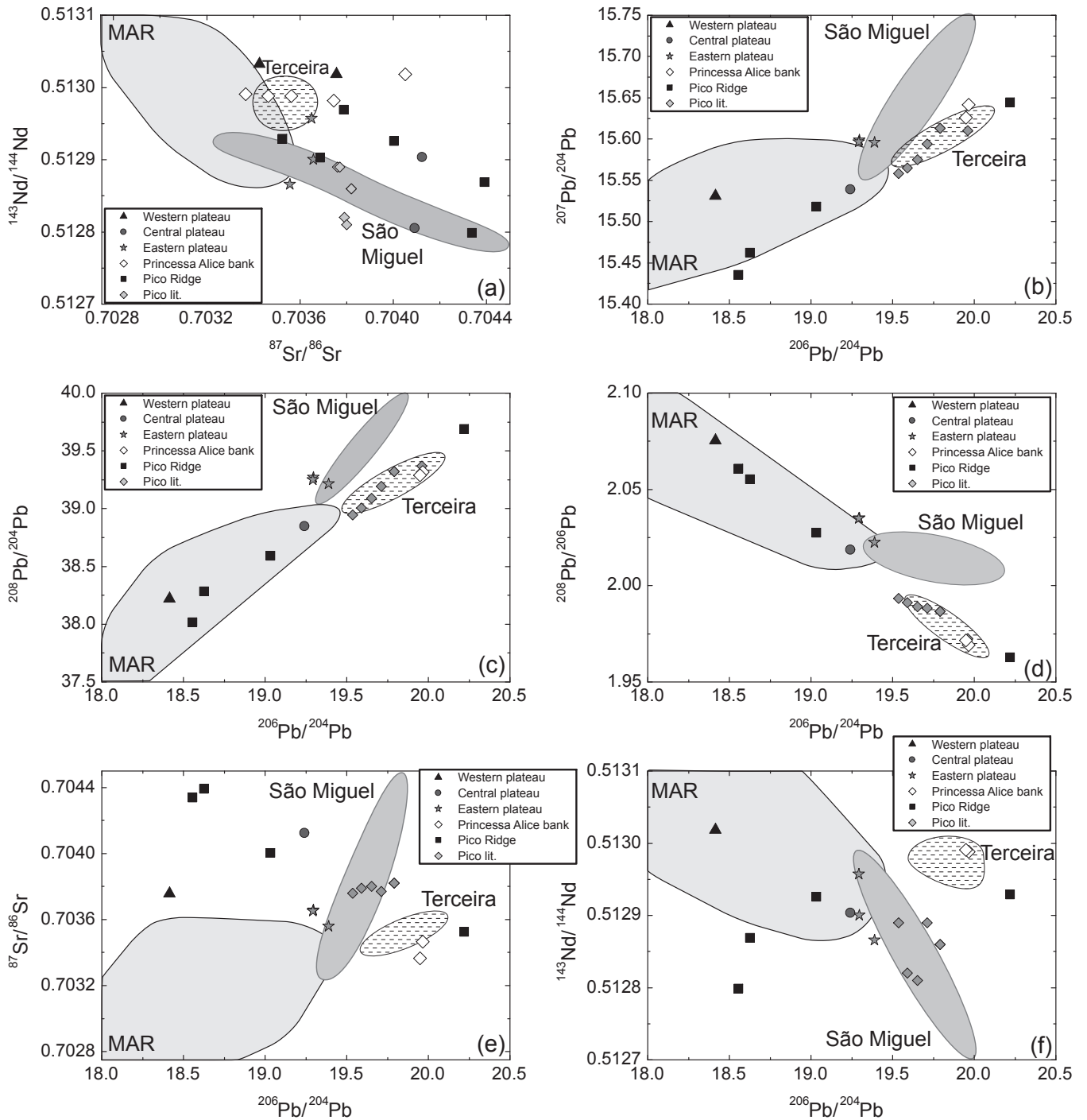


Figure 1.5: Sr-Nd-Pb isotope ratios of São Miguel, Terceira and the submarine basement lavas. Conventional Pb isotope data were measured in the São Miguel samples and in duplicate measurements from Princessa Alice bank, however, all samples are situated at same values within the error of the triple spike measurements. Pico data as in Figure 1.2.

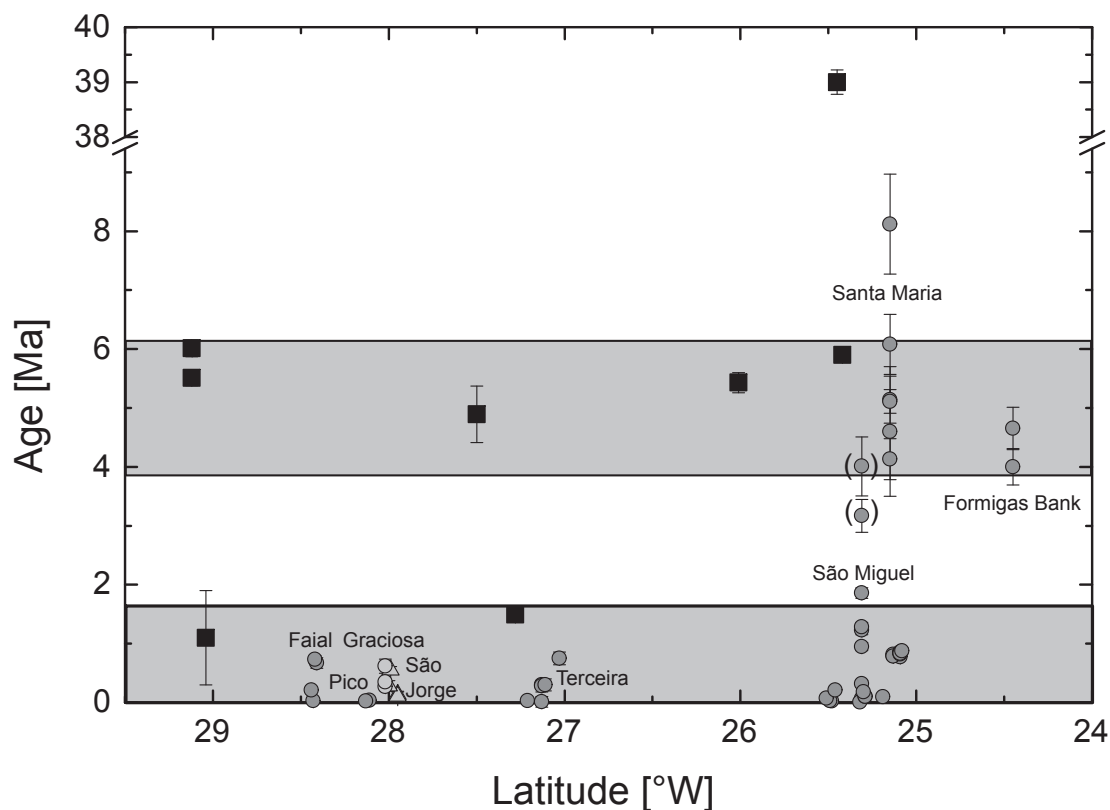


Figure 1.6: Age in Ma versus Latitude of the western Azorean samples. Black squares indicate $^{40}\text{Ar}/^{39}\text{Ar}$ ages of this work. Three distinct age groups are found in the submarine lavas: 39 Ma, 4.9 to 6.0 Ma, and 1.49 to 1.10 Ma. Subaerial data from the islands are literature data (Abdel Monem *et al.*, 1975; Féraud *et al.*, 1980; Moore & Rubin, 1991; Johnson *et al.*, 1998). Brackets indicate questionable samples from the Nordeste volcano at São Miguel from Abdel Monem *et al.* (1975) remeasured by Johnson *et al.* (1998).

assuming enriched garnet-peridotite sources (Fig. 1.8). The source composition resembles a previously depleted (0.5 % and 0.05 % melt depleted) primitive mantle (Hofmann, 1988) that has been re-enriched by varying amounts (1 % and 1.5 %) of depleted mantle melts (0.5 % and 2 % degree of partial melting). The melting degrees of these samples roughly coincide with the degrees calculated by means of Na_2O (Fig. 1.7) giving average melting degrees between 4-10 % partial melting of this mantle source. The chemical enrichment of the São Miguel mantle source can be modelled by assuming mixing of a previously depleted primitive mantle with 1.5% melt from a depleted mantle (Model details in Fig. 1.8). The compositions from Terceira are slightly less enriched than at São Miguel, whereas the samples from Pico Ridge spread the whole range of modelled compositions from São Miguel to Terceira. Figure 1.8 also shows that one sample from the Western Group can be reproduced by 15-20 % partial melting of a typical depleted mantle source (McDonough & Sun, 1995) in the spinel stability field whereas the other two samples originated from high melting degrees (~ 15 % partial melting) of the re-enriched sources. This also confirms the observed REE ratios (Figs. 1.3, 1.4) that roughly represents similar melting degrees among the lavas from the Western Group.

Based on the REE systematics we conclude that the degrees of partial melting of the early plateau-forming eruptions (Western Group, Princessa Alice bank) were different from the later formation of alkali basalts with significant fractionation of the heavy REE. Larger degrees of melting for the plateau-forming magmas compared to later stage magmas have also been observed at other volcanic plateaus such as Ontong Java and Iceland (Neal *et al.*, 1997). The shallower melting during the early phase implies that this may have occurred close to the spreading axis in agreement with geophysical data and reconstructions (Cannat *et al.*, 1999). The increased

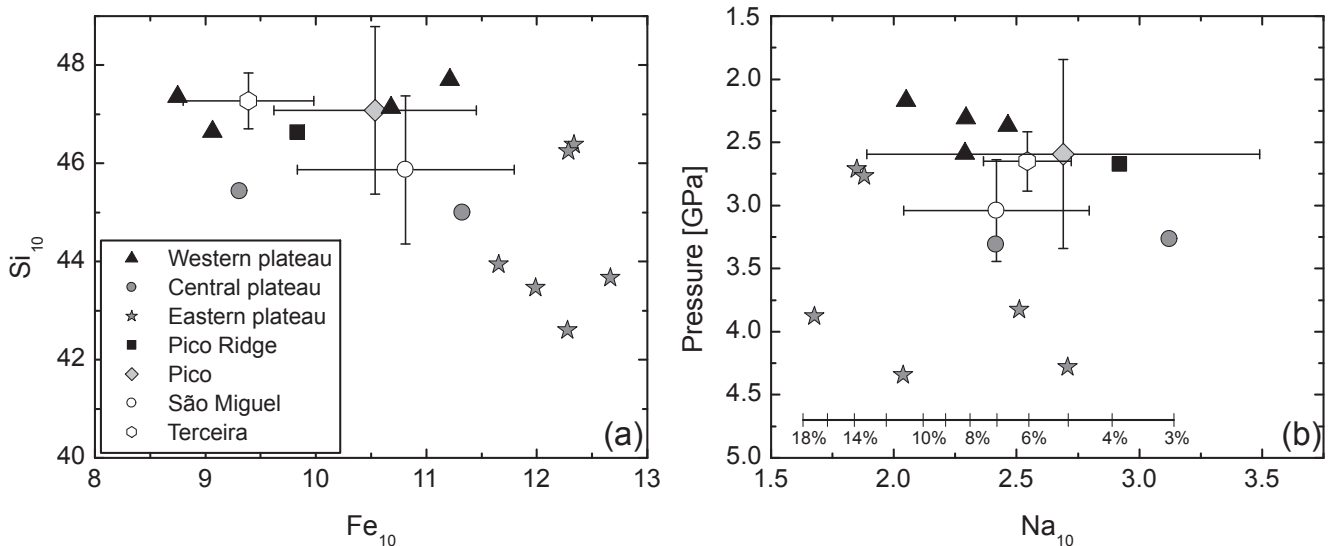


Figure 1.7: Fractionation-corrected major element and depth variations in the Azores lavas. Error bars reflect standard deviation from average values. All primitive lavas (> 5 wt. % MgO) were calculated to 10 wt. % MgO. a) Si_{10} versus Fe_{10} contents, where increasing Si_{10} correlates with decreasing Fe_{10} and, hence, indicates lower melting pressures. b) Calculated melting depth (Haase, 1996) versus fractionation-corrected Na_{10} . Melting degrees of Na_{10} were calculated using a power fit of a fertile mantle peridotite (Kushiro, 1996).

melting was probably due to the presence of a melting anomaly underneath the Azores Plateau although the relatively small size and only slightly thickened crust (14 km, Escartín *et al.*, 2001) compared to other oceanic plateaus (e.g. 30 km at the Ontong Java Plateau, Miura *et al.*, 2004) suggests only a small excess temperature of this plume.

1.6.2 Source heterogeneities

Both the incompatible element ratios (Fig. 1.4) and isotopes (Fig. 1.5) suggest some heterogeneity of the mantle beneath the Azores. The Ba/La and Nb/Zr ratios of the primitive (> 5 wt. % MgO) Azorean lavas show positive correlations with $(La/Sm)_N$ (Fig. 1.4). The lower LREE enrichment of the Western Plateau and Princessa Alice lavas has been discussed to be a result of larger degrees of partial melting (Fig. 1.8) compared to the REE ratios at São Miguel and Terceira. The $(La/Sm)_N$ ratios at São Miguel are generally higher than at the Central and Western Plateau and at Terceira with the exception of the Pico lavas which cover a large range in $(La/Sm)_N$ compositions. Although both the Ba/La and $(La/Sm)_N$ ratios are sensitive to different degrees of partial melting, where higher degrees of partial melting lower the ratios, we suggest that the $(La/Sm)_N$ ratios, with the exception of the Western Group and Princessa Alice lavas, can also be used as an indicator for mantle fertility. The correlated behaviour of $(La/Sm)_N$ and Nb/Zr (Fig. 1.4b), and the small variations in degree of partial melting as modelled from the REE ratios (Fig. 1.8), suggest differences in mantle source compositions in the São Miguel, Terceira, Pico, and Pico Ridge lavas rather than different degrees of partial melting. It has been suggested that Ba/La could be used as an indicator for the presence of a recycled ancient oceanic crust (Weaver, 1991), however, the variations in Ba/La may also be attributed to several processes, such as melting degree, source composition, and alteration. In contrast the higher $(La/Sm)_N$ suggest some sort of a fertile mantle component beneath the western part of São Miguel and Pico. A primitive, deeper mantle component was suggested by Moreira *et al.* (1999) by means of relatively high $^3He/^4He$ ratios found at Terceira ($R/R_a = 11.3$). Thus, the trace element systematics suggests that both degrees of partial melting and mantle source compositions vary in the Azores lavas.

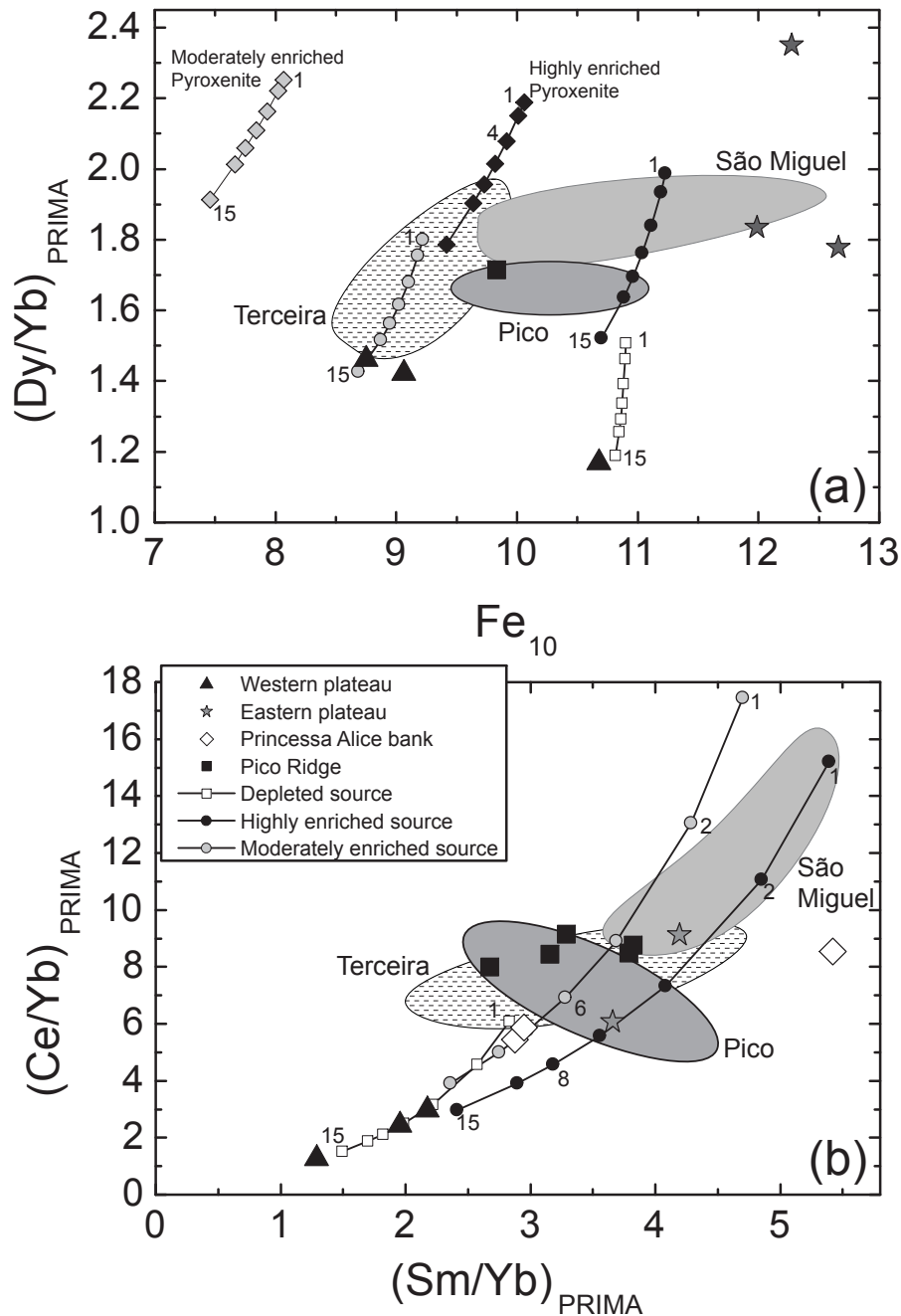


Figure 1.8: a) PRIMA-normalised Dy/Yb ratios versus fractionation-corrected Fe_{10} contents, and b) PRIMA-normalised Ce/Yb versus Sm/Yb ratios of the Azorean lavas. Three distinct sources were modelled using the batch melting equation of Shaw (1970). The depleted source composition consists of a depleted mantle (0.5 % melt depleted primitive mantle, Hofmann, 1988) source in the spinel peridotite stability field (55 % Ol, 20 % Opx, 21 % Cpx, 4 % Spl; 0.39 ppm Sm, 1.32 ppm Ce, 0.65 ppm Dy, 0.44 ppm Yb, 8.00 wt. % Fe). The moderately enriched source consists of a previously depleted primitive mantle source (0.5 % melt depleted) that has been re-enriched by 1 % of melt of the depleted mantle (2 % degree of partial melting) in the garnet peridotite stability field (52 % Ol, 20 % Opx, 21 % Cpx, 7 % Grt; 0.42 ppm Sm, 1.66 ppm Ce, 0.66 ppm Dy, 0.44 ppm Y, 10.00 wt. % Fe). The highly enriched source consists of a depleted primitive mantle source (0.05 % melt depleted) that has been re-enriched by 1.5 % melt (0.5 % degree of partial melting) of the depleted mantle (55 % Ol, 20 % Opx, 21 % Cpx, 4 % Grt; 0.47 ppm Sm, 2.46 ppm Ce, 0.68 ppm Dy, 0.45 ppm Yb, 10.90 wt. % Fe). Pyroxenite calculations for the enriched mantle sources are shown in a) assuming a mixture between garnet peridotite and pyroxenite (30 % Ol, 25 % Opx, 30 % Cpx, 15 % Grt) for the two re-enriched source compositions, respectively. The partition coefficients are taken from Kelemen *et al.* (1993) for Olivine, Ortho- and Clinopyroxene and Spinel. The garnet partition coefficients are from Johnson (1994). Fe partition coefficients are from Gaetani & Grove (1997) for Ol, Okamoto (1979) for Opx, Bougault & Hekinian (1974) for Cpx, Ohtani *et al.* (1989) for Grt, and Sisson (1991) for Spl. Tick marks represent 15, 10, 8, 6, 4, 2, and 1 % degree of partial melting, respectively.

Lavas from most plateau localities only cover a small range in isotopic compositions (Fig. 1.5) in contrast to the Pico and Pico Ridge lavas which range from relatively radiogenic Pb isotope compositions comparable to the Terceira lavas to less radiogenic Pb isotopes but radiogenic Sr and Nd isotopes. Although the samples from São Miguel, Terceira, Pico and Pico Ridge suggest binary mixing within each locality, there seems to be no coherent mixing trend in the Azores lavas. Instead each volcanic structure is situated upon a single mixing line suggesting very limited interaction between them. Thus, there appears to be not a single plume component, but several distinct radiogenic (São Miguel, Terceira; Princesa Alice, Pico, Pico Ridge) and unradiogenic endmembers (Western Plateau, Pico Ridge) that suggest small scale heterogeneity in the mantle. The very fine-scale heterogeneity and the large compositional span of the Azores as a whole compared to other plume-related settings such as Hawaii (Abouchami *et al.*, 2000; Regelous *et al.*, 2003) and Galapagos (White *et al.*, 1993; Geist *et al.*, 2002) and the very localised and distinct occurrence of mixing arrays makes the occurrence of a large “typical” mantle plume (e.g. Hawaii or Galapagos) to appear unlikely, however, the presence of a large plateau and the coeval, widespread occurrence of volcanism suggests the presence of an anomalous mantle beneath the Azores.

Most likely the largest eruptive event which formed the Azores Plateau occurred 4.9 to 6.0 Ma ago. Although one dated sample from the Western Group reveals an age of 1.10 Ma (Table 1.2), we suggest that the similarities in degrees of partial melting between the Princesa Alice bank and the Western Group lavas imply a similar eruption period, which, most likely, has an age of 4.9 to 6.0 Ma. The younger age of this sample may be a result of a later eruption from a residual melt pocket. Samples from the main eruption period from the Western Group and also most of the Pico Ridge lavas appear to have mixed with a mantle source with relatively low Pb isotope ratios, most likely MORB mantle. On the other hand, some of these lavas from the Princesa Alice bank have compositions similar to the Terceira lavas which have been suggested to reflect the mantle plume composition because of their high $^3\text{He}/^4\text{He}$ (Moreira *et al.*, 1999). Consequently, much of the plateau formed from plume mantle, most likely a small plume head that arrived beneath the lithosphere about 4.9 to 6.0 Ma ago. This may reflect mixing processes between melts from the Azores plume mantle as represented by Terceira and Princesa Alice lavas and magmas from the upper mantle represented by the Western Group lavas. The fact that the samples from the main eruption period not only show the highest degree of partial melting but have also either plume-like isotopic compositions or resemble MORB in terms of radiogenic isotopes, supports a situation close to the spreading axis. The eruption of relatively radiogenic isotopic compositions at Monaco Bank 39 Ma ago that resemble the western São Miguel lavas (Fig. 1.5) indicate that a relatively radiogenic component must have been present before the main plateau forming stage occurred.

The Pico Ridge lavas were erupted 1.49 Ma ago, the lavas from Terceira and Pico are younger than 0.8 Ma giving evidence for the relatively coeval eruption of both depleted and radiogenic isotopic compositions. However, generally neither trace elements nor isotope ratios of the main stage magmas give evidence for a systematic temporal evolution of the Azores mantle sources like it has been observed on other intraplate settings (e.g. Hawaii; Reiners, 2002), i.e. the younger lavas on the islands and at Pico Ridge are neither systematically enriched nor depleted relative to the main stage eruptions 4.9 to 6.0 Ma ago, but give evidence for simultaneous eruptions of both depleted and enriched mantle source compositions.

To sum up, we suggest that the combined REE and isotope systematics shows that the degrees of partial melting and the mantle source compositions of the main plateau forming phase were different from the earlier (Monaco Bank) and later eruptions (e.g. Terceira, São Miguel). The Western Group lavas not only resemble depleted

'MORB'-like mantle compositions as indicated by lower $(\text{La}/\text{Sm})_N$, Nb/Zr and less radiogenic Pb isotope ratios, but also reflect higher degrees of partial melting indicated by lower REE ratios compared to the other Azores lavas. A depleted 'MORB'-like composition and higher degrees of melting may be a result of eruption in the vicinity of a spreading axis as suggested from geophysical models (Cannat *et al.*, 1999; Gente *et al.*, 2003). Higher degrees of partial melting have also been observed in the Princessa Alice Bank lavas but the radiogenic Nd and Pb isotope ratios resemble the source compositions of Terceira reflecting influence of a more radiogenic, possibly a mantle plume component. The coeval eruption and small spatial distribution of relatively depleted and radiogenic compositions from the plateau forming eruptions 4.9 to 6.0 Ma ago until recent suggests a small scale heterogeneous mantle beneath the Azores. The relatively similar degrees of partial melting suggest that the younger eruptions formed from different sources but with similar degrees of partial melting.

1.7 DYNAMICS OF THE AZORES PLATEAU

Combining the age determinations with the melting and mantle source systematics provides the possibility to develop a geodynamic model of the evolution of the Azores Plateau (Figure 1.9). Our $^{40}\text{Ar}/^{39}\text{Ar}$ age determinations give evidence for three distinct volcanic stages that are characterised by different melting and mantle source signatures. The Western Group and Princessa Alice lavas are defined by larger degrees of partial melting but the Western Group gives evidence for a 'MORB'-like depleted mantle source compositions compared to enriched source compositions of Princessa Alice bank resembling the Terceira lavas.

Based on magnetic anomalies and spreading velocities Searle (1980) suggested a lithospheric age of about 53 Ma for the easternmost part of the Azores Plateau. Our $^{40}\text{Ar}/^{39}\text{Ar}$ ages of this area give 39 Ma indicating that some 15 Ma after formation of the lithosphere the first intraplate magmas formed. These samples have alkaline compositions that resemble the rocks from the young islands suggesting an early start of volcanism on the Azores Plateau (Fig. 1.9). The fact that these lavas have the same composition as the volcanic rocks from the presently active volcanoes on São Miguel indicates that the mantle source of these magmas has been present for a long time beneath the Azores Plateau.

Further to the west, the age of the Princessa Alice Bank was determined to be about 10 Ma based on magnetic lineations (Cannat *et al.*, 1999) whereas our age dates reveal younger ages of 5.5 to 6 Ma. Abundant volcanism occurred in a time span between 4.9 and 6.0 Ma and the tholeiitic to slightly alkaline composition of the Western Plateau lavas implies relatively large degrees of partial melting at that time at shallower depth. Although the Western Plateau and Princessa Alice have distinct mantle source compositions both reveal relatively high degrees of partial melting compared to the younger eruptions. Consequently, the age range from 4.9 to 6.0 Ma probably reflects the arrival of a melting anomaly beneath the region which led to the formation of most of the Azores Plateau in agreement with the model of Cannat *et al.* (1999)(Fig. 1.9). This melting anomaly led to abundant melting of the mantle generally comparable to other oceanic plateaus although the Azores Plateau is much smaller in size than, for example, the Pacific Plateaus (e.g. Ontong Java). The widespread occurrence of volcanism is contrary to the age progression expected when assuming a stable mantle plume beneath the lithosphere (e.g. Hawaiian-Emperor Chain).

Following the abundant melting and eruption of large volumes of basaltic magmas which formed the plateau, volcanic activity apparently decreased. Some 1.5 Ma ago, abundant volcanism then formed the islands and

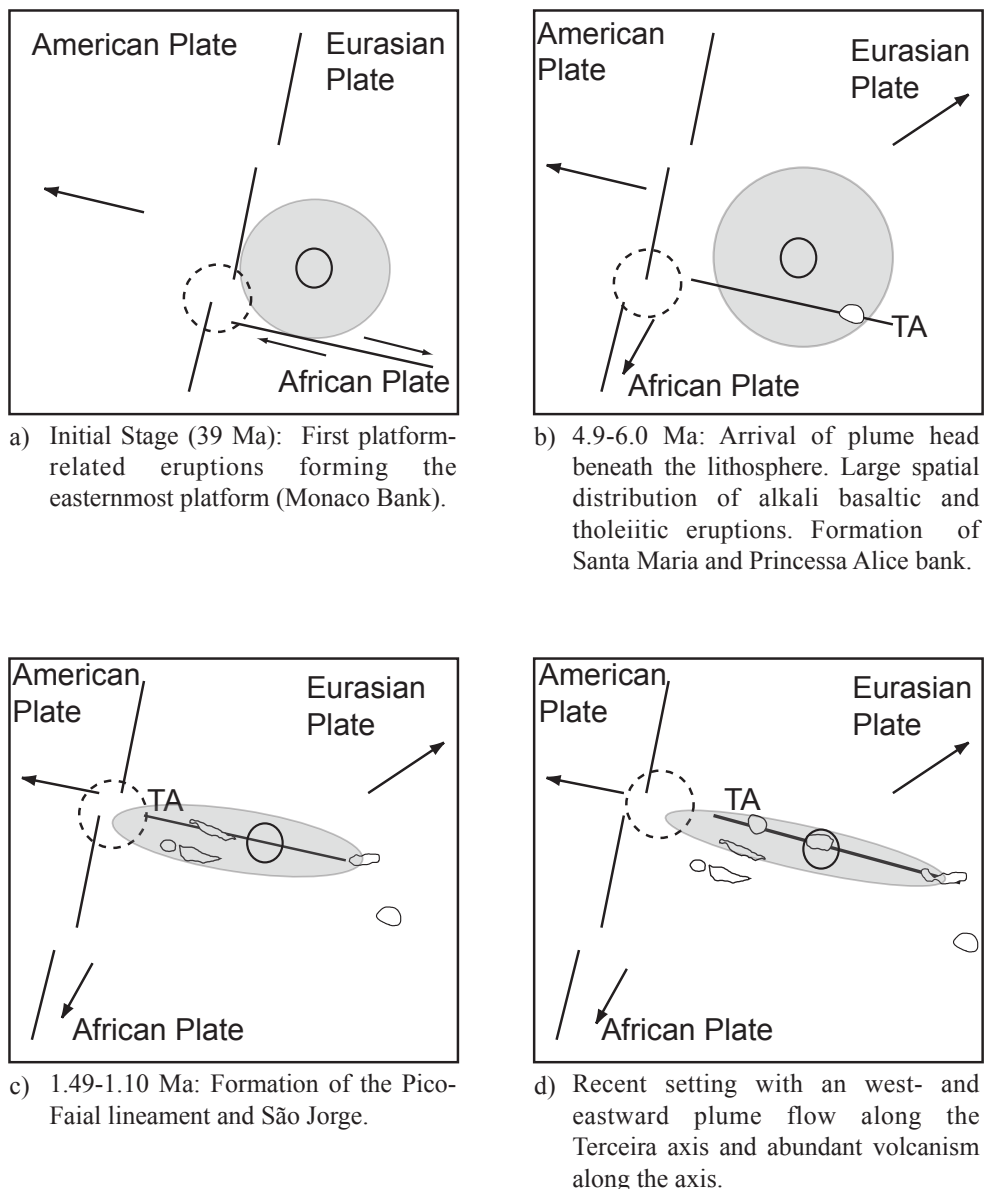


Figure 1.9: Evolution of the Azores Plateau since 39 Ma. Grey field mark the Azorean plume and black circle marks the assumed plume centre. Dotted circle shows position of the triple junction between the three bordering plates stepping northward with the northward move of the Terceira axis (TA). Ages based on $^{40}\text{Ar}/^{39}\text{Ar}$ determinations.

numerous seamounts on the Azores mostly situated along the Terceira axis, and along the Faial-Pico lineament (Fig. 1.1). While the western Terceira axis does another step further north, the islands of Pico and Faial and São Jorge are formed and the plume influence narrows into a broad band ranging along the Terceira axis. The elongated shape of recent volcanism along the Faial-Pico lineament and the Terceira axis most likely is a result of the tectonic ascent paths provided by faults along the axis.

The presence of the unradiogenic He isotope ratios at Terceira and its similarity to the lavas from Princessa Alice bank suggests a primitive source component in these lavas (Moreira *et al.*, 1999), which gives evidence for a connection into the deeper mantle similar to the situation which has been proposed for other mantle plumes (e.g. Hawaii, Galapagos). In the Azores, the connection to a deeper mantle component possibly was separated during the ascent leading to the lower seismic velocity anomaly being restricted to the upper mantle (Ritsema & Allen, 2003). The isotopic heterogeneities in the mantle beneath the Azores suggest that each volcanic structure

samples a different source composition implying small scale heterogeneities rather than one homogeneous plume source. Thus, there was no large melting anomaly in which magmas were homogenised by mixing, which would lead to a relatively uniform distribution of isotopic signatures, but rather small heterogeneities survived during the melting. The mantle heterogeneities found in other plume-related localities such as Hawaii or Iceland (e.g. Hémond *et al.*, 1993; Abouchami *et al.*, 1999; Abouchami *et al.*, 2000) are in general larger than in the Azores. However, at Hawaii comparable small-scale heterogeneities have also been found (Abouchami *et al.*, 2000). The survival of the small-scale heterogeneities in the Azores could possibly be a result of the relatively lower excess temperatures compared to other mantle plume settings, because with increasing temperatures, the viscosity of melts generally decreases, which, in turn, leads to more homogenised melts at higher temperatures. Therefore one could speculate that if the excess temperature and, hence, the viscosity in the Azores mantle sources are lower compared to other mantle plumes, this would also lead to less efficient mixing of melts.

We conclude that several features of the Azores submarine plateau differ from the observations made at other mantle plume settings (e.g. Hawaii, Galapagos) such as a lack of age progression, the small scale spatial and/or temporal heterogeneity of the Azorean mantle sources with very limited mixing, and the absence of a common abundant plume source component. In contrast, the occurrence of widespread, coeval volcanic activity, relatively unradiogenic He isotope ratios and a bathymetric high as well as a chemical or thermal anomaly confirmed by geophysical methods (Ito & Lin, 1995; Cannat *et al.*, 1999) can only be explained by an anomalous mantle beneath the Azores. The relatively small size and only slightly thickened oceanic crust (14 km, Escartín *et al.*, 2001) in the Azores vicinity suggests only very small excess temperatures relative to the surrounding mantle. The generated magmas were apparently erupted by ascent paths provided by the Terceira axis and the Mid-Atlantic Ridge. This also explains the NW-SE trending volcanic structures observed at the plateau (Vogt & Jung, 2004). As the Terceira axis jumped further north, volcanism in the south slowly decreased. The recent structure of the Azores archipelago therefore is a result of both the influence of an anomalous mantle and the local plate tectonics at the triple junction between the three plates enhancing partial melting and providing ascent paths for the generated magmas.

1.8 ACKNOWLEDGEMENTS

We gratefully acknowledge the help of F. Hauff with the isotope analyses in Kiel and S. J. Galer and P. Jaeckel in Mainz. We are also very grateful to D. Garbe-Schönberg and H. Blaschek with the ICP-MS analyses and P. Appel and A. Weinkauff with XRF analyses. We also thank the captains and crews of RV Poseidon for their help with the work onboard. This study has been funded by the Deutsche Forschungsgemeinschaft through grants HA2568/9-2, and HA2568/9-3.

REFERENCES

- Abdel Monem, A.A., Fernandez, L.A. and Boone, G.M. (1975) K-Ar-Ages from the eastern Azores group (Santa Maria, Sao Miguel and the Formigas islands). *Lithos* **8**, 247-254.
- Abouchami, W., Galer, S.J.G. and Hofmann, A.W. (2000) High precision lead isotope systematics of lavas from the Hawaiian Scientific Drilling Project. *Chemical Geology* **169**, 187-209.
- Abouchami, W., Hofmann, A.W. and Galer, S.J.G. (1999) Lead isotope anatomy of the Hawaiian Plume. In: *AGU 1999 fall meeting*. pp. 1183. American Geophysical Union: Washington, DC, United States.
- Asimow, P.D. and Langmuir, C.H. (2003) The importance of water to oceanic mantle melting regimes. *Nature* **421**, 815-820.
- Asimow, P.D., Dixon, J.E. and Langmuir, C.H. (2004) A hydrous melting and fractionation model for mid-ocean ridge basalts: Application to the Mid-Atlantic Ridge near the Azores. *Geochemistry, Geophysics, Geosystems* **5**, DOI: 10.1029/2003GC000568.
- Asimow, P.D., Hirschmann, M.M., Ghiorso, M.S., O'Hara, M.J. and Stolper, E.M. (1995) The effect of pressure-induced solid-solid phase transitions on decompression melting of the mantle. *Geochimica et Cosmochimica Acta* **59**, 4489-4506.
- Beier, C., Haase, K.M. and Hansteen, T.H. (2006) Magma evolution of the Sete Cidades volcano, São Miguel, Azores. *Journal of Petrology*, DOI: 10.1093/petrology/egl014.
- Berthois, L. (1953) Contribution to the lithological study of the Azores archipelago. *Comincaoes Serv. Geol. Portugal* **24**, 29-198.
- Bougault, H. and Hekinian, R. (1974) Rift valley in the Atlantic Ocean near 36 degrees 50'N; petrology and geochemistry of basalt rocks. *Earth and Planetary Science Letters* **24**, 249-261.
- Bourdon, B., Langmuir, C.H. and Zindler, A. (1996) Ridge-hotspot interaction along the Mid-Atlantic Ridge between 37°30' and 40°30'N: the U-Th disequilibrium evidence. *Earth and Planetary Science Letters* **142**, 175-189.
- Cannat, M., *et al.* (1999) Mid-Atlantic Ridge - Azores hotspot interactions: along-axis migration of a hotspot-derived event of enhanced magmatism 10 to 4 Ma ago. *Earth and Planetary Science Letters* **173**, 257-269.
- Claude-Ivanaj, C., Joron, J.-L. and Allègre, C.-J. (2001) ²³⁸U-²³⁰Th-²²⁶Ra fractionation in historical lavas from the Azores: long-lived source heterogeneity vs. metasomatism fingerprint. *Chemical Geology* **176**, 295-310.
- Cushman, B., Sinton, J., Ito, G. and Dixon, J.E. (2004) Glass compositions, plume-ridge interaction, and hydrous melting along the Galápagos Spreading Center, 90.5°W to 98°W. *Geochemistry, Geophysics, Geosystems* **5**, DOI: 10.1029/2004GC000709.

- Dosso, L., Bougault, H., Langmuir, C., Bollinger, C., Bonnier, O. and Etoubleau, J. (1999) The age and distribution of mantle heterogeneity along the Mid-Atlantic Ridge (31-41°N) *Earth and Planetary Science Letters*. pp. 269-286.
- Duffield, W.A. and Dalrymple, G.B. (1990) The Taylor Creek Rhyolite of New Mexico; a rapidly emplaced field of lava domes and flows. *Bulletin of Volcanology* **52**, 475-487.
- Eisele, J., Sharma, M., Galer, S.J.G., Blichert-Toft, J., Devey, C.W. and Hofmann, A.W. (2002) The role of sediment recycling in EM-1 inferred from Os, Pb, Hf, Nd, Sr isotope and trace element systematics of the Pitcairn hotspot. *Earth and Planetary Science Letters* **196**, 197-212.
- Escartín, J., Cannat, M., Pouliquen, G. and Rabain, A. (2001) Crustal thickness of V-shaped ridges south of the Azores: Interaction of the Mid-Atlantic Ridge (36°-39°N) and the Azores hot spot. *Journal of Geophysical Research* **106**, 21,719-21,735.
- Féraud, G., Kaneoka, I. and Allègre, C.J. (1980) K/Ar Ages and Stress Pattern in the Azores: Geodynamic Implications. *Earth and Planetary Science Letters* **46**, 275-286.
- Flower, M.F.J., Schmincke, H.U. and Bowman, H. (1976) Rare earth and other trace elements in historic Azorean lavas. *Journal of Volcanology and Geothermal Research* **1**, 127-147.
- Gaetani, G.A. and Grove, T.L. (1997) Partitioning of moderately siderophile elements among olivine, silicate melt, and sulfide melt; constraints on core formation in the Earth and Mars. *Geochimica et Cosmochimica Acta* **61**, 1829-1846.
- Galer, S.J.G. (1999) Optimal double and triple spiking for high precision lead isotopic measurement. *Chemical Geology* **157**, 255-274.
- Garbe-Schönberg, C.-D. (1993) Simultaneous determination of thirty-seven trace elements in twenty-eight international rock standards by ICP-MS. *Geostandards Newsletters* **17**, 81-97.
- Geist, D., White, W.M., Albarede, F., Harpp, K., Reynolds, R., Blichert, T.J. and Kurz, M.D. (2002) Volcanic evolution in the Galapagos; the dissected shield of Volcan Ecuador. *Geochemistry, Geophysics, Geosystems* **3**, DOI: 10.1029/2002GC000355.
- Gente, P., Dymant, J., Maia, M. and Goslin, J. (2003) Interaction between the Mid-Atlantic Ridge and the Azores hotspot during the last 85 Myr: Emplacement and rifting of the hot spot-derived plateaus. *Geochemistry, Geophysics, Geosystems* **4**, DOI: 10.1029/2003GC000527.
- Haase, K.M. (1996) The relationship between the age of the lithosphere and the composition of oceanic magmas: Constraints on partial melting, mantle sources and the thermal structure of the plates. *Earth and Planetary Science Letters* **144**, 75-92.

- Haase, K.M. and Beier, C. (2003) Tectonic control of ocean island basalt sources on Sao Miguel, Azores? *Geophysical Research Letters* **30**, 1856.
- Hart, S.R., Hauri, E.H., Oschmann, L.A. and Whitehead, J.A. (1992) Mantle plumes and entrainment; isotopic evidence. *Science* **256**, 517-520.
- Hémond, C., Arndt, N.T., Lichtenstein, U., Hofmann, A.W., Oskarsson, N. and Steinthorsson, S. (1993) The heterogeneous Iceland Plume: Nd-Sr-O isotopes and trace element constraints. *Journal of Geophysical Research* **98**, 15833-15850.
- Hémond, C., Devey, C.W. and Chauvel, C. (1994) Source compositions and melting processes in the Society and Austral plumes (South Pacific Ocean); element and isotope (Sr, Nd, Pb, Th) geochemistry. *Chemical Geology* **115**, 7-45.
- Hirschmann, M.M. and Stolper, E.M. (1996) A possible role for garnet pyroxenite in the origin of the “garnet signature” in MORB. *Contributions to Mineralogy and Petrology* **124**, 185-208.
- Hofmann, A.W. (1988) Chemical differentiation of the Earth: the relationship between mantle, continental crust, and oceanic crust. *Earth and Planetary Science Letters* **90**, 297-314.
- Hofmann, A.W., Jochum, K.P., Seufert, M. and White, W.M. (1986) Nb and Pb in oceanic basalts: new constraints on mantle evolution. *Earth and Planetary Science Letters* **79**, 33-45.
- Ito, G. and Lin, J. (1995) Oceanic spreading center-hotspot interactions; constraints from along-isochron bathymetric and gravity anomalies. *Geology* **23**, 657-660.
- Johnson, C.L., Wijbrans, J.R., Constable, C.G., Gee, J., Staudigel, H., Tauxe, L., Forjaz, V.-H. and Salgueiro, M. (1998) $^{40}\text{Ar}/^{39}\text{Ar}$ ages and paleomagnetism of Sao Miguel lavas, Azores. *Earth and Planetary Science Letters* **1160**, 637-649.
- Johnson, K.T.M. (1994) Experimental cpx/ and garnet/ melt partitioning of REE and other trace elements at high pressures; petrogenetic implications. In: *V M Goldschmidt Conference; extended abstracts*. pp. 454-455. Mineralogical Society: London, United Kingdom.
- Kelemen, P.B., Shimizu, N. and Dunn, T. (1993) Relative depletion of niobium in some arc magmas and the continental crust: partitioning of K, Nb, La and Ce during melt/rock reaction in the upper mantle. *Earth and Planetary Science Letters* **120**, 111-134.
- Kurz, M.D. (1982) *Helium isotope geochemistry of oceanic volcanic rocks; implications for mantle heterogeneity and degassing*. Doctoral thesis: Woods Hole Oceanographic Institution, United States.
- Kushiro, I. (1996) Partial melting of a fertile mantle peridotite at high pressures: An experimental study using aggregates of diamond. In: *Earth Processes: Reading the isotopic code*. pp. 109-122. Am. Geophys. Union, Geophys. Monograph.

- Le Maitre, R. (ed.) (1989) *A classification of igneous rocks and glossary of terms, recommendations of the International union of geological sciences, subcommission on the systematics of igneous rocks*. Blackwell: Oxford, London.
- Luis, J.F., Miranda, J.M., Galdeano, A., Patriat, P., Rossignol, J.C. and Mendes Victor, L.A. (1994) The Azores triple junction evolution since 10 Ma from aeromagnetic survey of the Mid-Atlantic Ridge. *Earth and Planetary Science Letters* **125**, 439-459.
- Macdonald, G.A. (1968) Composition and origin of Hawaiian lavas. In: *Studies in volcanology--A memoir in honor of Howel Williams*. pp. 477-522. Geological Society of America (GSA): Boulder, CO, United States.
- McDonough, W.F. and Sun, S.-S. (1995) The composition of the Earth. *Chemical Geology* **120**, 223-253.
- Miura, S., Suyehiro, K., Shinohara, M., Takahashi, N., Araki, E. and Taira, A. (2004) Seismological structure and implications of collision between the Ontong Java Plateau and Solomon Island Arc from ocean bottom seismometer-airgun data. *Tectonophysics* **389**, 191-220.
- Moore, R.B. (1990) Volcanic geology and eruption frequency, Sao Miguel, Azores. *Bulletin of Volcanology* **52**, 602-614.
- Moore, R.B. and Rubin, M. (1991) Radiocarbon dates for Lava flows and pyroclastic deposits on Sao Miguel, Azores. *Radiocarbon* **33**, 151-164.
- Moreira, M., Doucelance, R., Kurz, M.D., Dupre, B. and Allegre, C.J. (1999) Helium and lead isotope geochemistry of the Azores Archipelago. *Earth and Planetary Science Letters* **169**, 189-205.
- Neal, C.R., Mahoney, J.J., Kroenke, L.W., Duncan, R.A. and Petterson, M.G. (1997) The Ontong Java Plateau. In: *Large igneous provinces; continental, oceanic, and planetary flood volcanism*. pp. 183-216. American Geophysical Union: Washington, DC, United States.
- Ohtani, E., Kawabe, I., Moriyama, J. and Nagata, Y. (1989) Partitioning of elements between majorite garnet and melt and implications for petrogenesis of komatiite. *Contributions to Mineralogy and Petrology* **103**, 263-269.
- Okamoto, K. (1979) Geochemical study on magmatic differentiation of Asama Volcano, central Japan. *Chishit-sugaku Zasshi = Journal of the Geological Society of Japan* **85**, 525-535.
- Regelous, M., Hofmann, A.W., Abouchami, W. and Galer, S.J.G. (2003) Geochemistry of Lavas from the Emperor Seamounts, and the Geochemical Evolution of Hawaiian Magmatism from 85 to 42 Ma. *J. Petrology* **44**, 113-140.
- Reiners, P.W. (2002) Temporal -compositional trends in intraplate basalt eruptions: Implications for mantle heterogeneity and melting processes. *Geochemistry, Geophysics, Geosystems* **3**, DOI: 10.1029/2001GC000250.
- Ritsema, J. and Allen, R.M. (2003) The elusive mantle plume. *Earth and Planetary Science Letters* **207**, 1-12.

- Schilling, J.-G. (1975) Azores mantle blob: rare-earth evidence. *Earth and Planetary Science Letters* **25**, 103-115.
- Schilling, J.-G., Zajac, M., Evans, R., Johnston, T., White, W., Devine, J.D. and Kingsley, R. (1983) Petrologic and geochemical variations along the Mid-Atlantic Ridge from 29°N to 73°N. *American Journal of Science* **283**, 510-586.
- Schmincke, H.-U. and Weibel, M. (1972) Chemical study of rocks from Madeira, Porto Santo, and Sao Miguel, Terceira (Azores). *Neues Jahrbuch Mineralogische Abhandlungen*. **117**, 253-281.
- Searle, R.C. (1980) Tectonic pattern of the Azores spreading center and triple junction. *Earth and Planetary Science Letters* **51**.
- Shaw, D.M. (1970) Trace element fractionation during anatexis. *Geochimica et Cosmochimica Acta* **34**, 237-243.
- Shen, Y. and Forsyth, D.W. (1995) Geochemical constraints on initial and final depths of melting beneath mid-ocean ridges. *Journal of Geophysical Research, B, Solid Earth and Planets* **100**, 2211-2237.
- Sisson, T.W. (1991) Pyroxene-high silica rhyolite trace element partition coefficients measured by ion microprobe. *Geochimica et Cosmochimica Acta* **55**, 1575-1585.
- Smith, W. and Sandwell, D. (1997) Measured and estimated seafloor topography (version 4.2). World Data Center A for Marine Geology and Geophysics research publication RP-1.
- Sun, S.-s. and McDonough, W.F. (1989) Chemical and isotopic systematics of oceanic basalts: implications for mantle composition and processes. In: Saunders, A. D. and Norry, M. J. (eds.) *Magmatism in the ocean basins*. pp. 313-345. Geol. Soc. Spec. Publ.: London.
- Turner, S., Hawkesworth, C., Rogers, N. and King, P. (1997) U-Th isotope disequilibria and ocean island basalt generation in the Azores. In: Hawkesworth, C. and Arndt, N. T. (eds.) *Highlights of the Goldschmidt meeting, in honor of A. W. Hofmann*. pp. 145-164. Elsevier: Amsterdam, Netherlands.
- Vogt, P.R. and Jung, W.Y. (2004) The Terceira Rift as hyper-slow, hotspot-dominated oblique spreading axis: A comparison with other slow-spreading plate boundaries. *Earth and Planetary Science Letters* **218**, 77-90.
- Weaver, B.L. (1991) The origin of ocean island basalt end-member compositions; trace element and isotopic constraints. *Earth and Planetary Science Letters* **104**, 381-397.
- White, R.S., Bown, J.W. and Smallwood, J.R. (1995) The temperature of the Iceland plume and origin of outward-propagating V-shaped ridges. In: *The Iceland plume and its influence on the evolution of the NE Atlantic*. pp. 1039-1045. Geological Society of London: London, United Kingdom.
- White, W.M. (1977) *Geochemistry of igneous rocks from the central North Atlantic; the Azores and the Mid-Atlantic Ridge*. Doctoral thesis: University of Rhode Island, United States.

White, W.M., McBirney, A.R. and Duncan, R.A. (1993) Petrology and geochemistry of the Galapagos Islands; portrait of a pathological mantle plume. *Journal of Geophysical Research, B, Solid Earth and Planets* **98**, 19,533-19,563.

White, W.M., Tapia, M.D.M. and Schilling, J.-G. (1979) The Petrology and Geochemistry of the Azores Islands. *Contributions to Mineralogy and Petrology*. **69**, 201-213.

Widom, E., Carlson, R.W., Gill, J.B. and Schmincke, H.U. (1997) Th-Sr-Nd-Pb isotope and trace element evidence for the origin of the Sao Miguel, Azores, enriched mantle source. *Chemical Geology* **140**, 49-68.

CHAPTER II

MELTING AND MANTLE SOURCE VARIATIONS ALONG AN ULTRASLOW SPREADING RIFT: THE TERCEIRA AXIS, AZORES

Christoph Beier^{1,2}, Karsten M. Haase^{1,3}, Wafa Abouchami², Mark-S. Krienitz^{1,4}, and Folkmar Hauff⁵

¹Institut für Geowissenschaften, Christian-Albrechts-Universität zu Kiel, Ludewig-Meyn-Straße 10, 24118 Kiel, Germany, Email: chb@gpi.uni-kiel.de

²Max-Planck-Institut für Chemie (Otto-Hahn-Institut), Abteilung Geochemie, Joh.-Joachim-Becher-Weg 27, 55128 Mainz, Germany

³Department of Earth Sciences, University of Aarhus, C.F. Møllers Allé 110, 8000 Aarhus C, Denmark

⁴GeoForschungsZentrum Potsdam, Telegrafenberg B124, 14473 Potsdam, Germany

⁵IFM-GEOMAR, Leibniz-Institut für Meereswissenschaften, Wischhofstr. 1-3, 24148 Kiel, Germany

2.1 ABSTRACT

The ultraslow spreading Terceira axis situated along the northern boundary of the Azores platform forms a Ridge-Ridge-Ridge triple junction with the Mid-Atlantic Ridge separating the Eurasian, African and American Plates. Four volcanic systems, three of which are islands are distinguished along the axis and are separated by deep amagmatic basins similar to other ultraslow spreading centres. The major element, trace element and isotope geochemistry of submarine and subaerial lavas along the axis show large lateral geochemical variations. Modelling by means of major and trace elements suggests melting in the garnet stability field with slightly smaller degrees of partial melting at the easternmost volcanic system, compared to the central and western volcanoes giving evidence for melting in the spinel/garnet transition zone with slightly higher degrees of partial melting. The degrees of partial melting at the Terceira axis are slightly smaller or equal to those observed on other ultraslow spreading axes (Southwest Indian Ridge, Gakkel Ridge) despite the fact that an anomalous mantle is proposed. A combined interaction of a high obliquity, very slow spreading rates and a thick lithosphere along the axis avoid the formation and eruption of large amounts of melt along the Terceira axis. However, the presence of a stable melting anomaly over relatively long time periods is obviously able to produce enough melts for the formation of islands. The trace element and Sr-Nd-Pb isotopes show that every volcanic system along the axis lies on a single binary mixing array with no interaction in between them, giving evidence for focused magmatism. The westernmost mantle sources beneath Graciosa and the most radiogenic lavas from the neighbouring MAR suggest mantle flux from Graciosa towards the Mid-Atlantic Ridge.

2.2 INTRODUCTION

The model of sea-floor spreading explains a large variety of geochemical and geophysical observations made on Mid-Ocean Ridge systems worldwide. Several parameters are important to know concerning sea-floor spreading structures. One important factor that influences the ridge's structure is the spreading rate varying from 160 mm/a (full spreading) in the vicinity of the East Pacific Rise down to 20-30 mm/a at the Mid-Atlantic Ridge (MAR). A few locations have very much slower spreading rates such as at the Southwest Indian Ridge (12-16 mm/a, Dick *et al.*, 2003) or the Arctic Gakkel Ridge (8-13 mm/a, Cochran *et al.*, 2003). Direct measurements using GPS and laser systems as well as plate motion models revealed, that the Terceira axis also belongs to the ultraslow spreading ridges (Miranda *et al.*, 1998; Vogt & Jung, 2004; Fernandes *et al.*, accepted). Spreading systems with intermediate spreading rates such as the MAR have distinct morphological features such as an axial high with a deep rift valley and transform faults (Macdonald, 1982). In contrast the ultraslow or hyperslow spreading ridges do not contain a clear rift valley and lack transform faults but contain either a set of overlapping en echelon structures or they are connected by small non-transform discontinuities. Investigations on ultraslow spreading rifts have shown that their ridge morphology is not only generated by different spreading rates, but that there is also an interaction between local tectonics, melting processes, and mantle compositions (Dick *et al.*, 2003). Both, the Southwest Indian Ridge (SWIR) and the Gakkel Ridge are defined by large amagmatic segments (e.g. Sauter *et al.*, 2004a). The oblique spreading Terceira axis (2-4mm/a) located along the northern Azores platform (Fig. 2.1) runs from its junction with the lateral Gloria Fault in a NW-SE direction towards the MAR. In contrast to other ultraslow spreading centres the Terceira axis consists of large subaerial volcanic centres separated by smaller amagmatic basins. The investigation of such slow spreading rifts is important for the understanding of mantle processes and their influence on the generation of accreting plate boundaries. Three Azorean islands lie on the axis allowing precise sampling along the axis. This also gives the opportunity to study the temporal variations in each volcanic system which has been shown to be an important factor in the evolution of the Azorean volcanoes (Beier *et al.*, 2006). In contrast to the examples from the SWIR and from Gakkel Ridge, the Terceira axis has been sampled at its whole length including both, subaerial and submarine samples. These samples provide the unique opportunity to investigate melting, melt extraction and mantle source variations along the axis and also allow investigations concerning the formation and evolution of an ultraslow spreading axis.

2.3 GEOLOGICAL SETTING

The Azores archipelago is situated on a large volcanic plateau cut by the MAR and is separated asymmetrically into a western and eastern half where the latter has seven of the nine Azorean islands emerging from the submarine plateau. This eastern platform is divided into an eastern area including the islands of Santa Maria and São Miguel and the central part with the islands of Faial, Pico, Terceira and Graciosa. The submarine plateau probably formed by a melting anomaly either due to a small plume head (Cannat *et al.*, 1999), or a wetspot (Schilling *et al.*, 1980; Bonatti, 1990). Seismic tomography studies reveal the presence of mantle with anomalously slow seismic velocities beneath the Azores but a connection to the lower mantle is disputed (Ritsema & Allen, 2003). The islands of São Miguel, Terceira, and Graciosa are situated upon the so-called Terceira axis, each island bordered by deep amagmatic basins (Fig. 2.1). The seamount João de Castro lies between the islands of Terceira and São Miguel and reached subaerial stages in 1638 and 1720 but was eroded again soon after (Nunes *et al.*, 2003). GPS and laser measurements show that the islands lie in an extensional regime (Miranda *et al.*, 1998; Vogt & Jung, 2004; Fernandes *et al.*, accepted) and based on relative plate motions using the NUVEL-1A model, Vogt & Jung (2004) determined spreading rates of 2-4mm/a for the recent plate boundary between the Eurasian

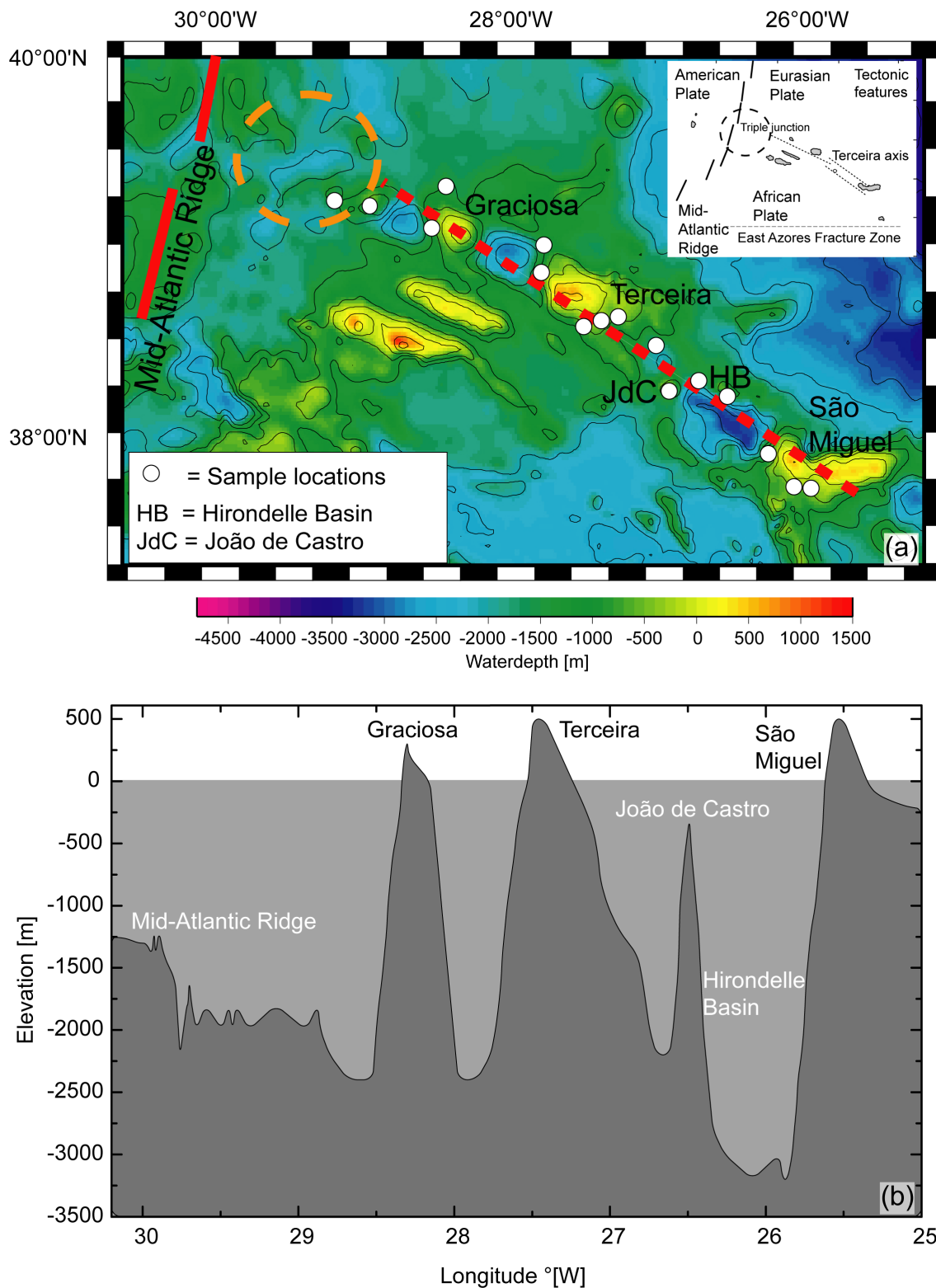


Figure 2.1: a) Bathymetric chart of the northern Azores platform and the Terceira axis according to Smith & Sandwell (1997). Dotted circle marks the assumed position of the Ridge-Ridge-Ridge triple junction and the dotted line is the estimated general trend of the Terceira axis. Subaerial samples were taken on each of the three islands (for detailed sample locations contact the corresponding author). Inset shows the major tectonic features in the Azores. The East Azores Fracture Zone (EAFZ) is the seismically inactive former plate boundary between the Eurasian and African Plates. The recent plate boundary is thought to be in the vicinity of the Terceira axis. b) Depth profile along the Terceira axis showing a segmentation pattern as also observed on other slow spreading ridges (Michael *et al.*, 2003).

and African Plates. Extensional tectonics is also revealed by “horst-and-graben” structures found at the Sete Cidades volcano at the western end of São Miguel (Beier *et al.*, 2006).

The conjunction between the Terceira axis and the MAR forms the Ridge-Ridge-Ridge triple junction between the three bordering plates. Although this triple junction cannot be defined exactly it is supposed to be located W of Faial and/or Graciosa determined by focal earthquake mechanisms (Udias *et al.*, 1976; Grimison & Chen, 1986; Grimison & Chen, 1988). Suggesting that the triple junction is formed by the Terceira axis, Luis *et al.* (1994; 1998) concluded that the axis itself and therefore the triple junction, too, made several ‘jumps’ northward since its location at the East Azores Fracture Zone more than 10 Ma ago (Fig. 2.1). Therefore, several southerly situated tectonic lineaments parallel to the Terceira axis have been interpreted as extinct spreading axes. One of those tectonic lineaments comprises the islands of Faial and Pico and the submarine Pico Ridge in the south-western platform. The recent location of the Terceira axis at the northern platform rim explains its asymmetrical structure with the large volcanic plateau in the south and a small northern counterpart (Fig. 2.1). The slow spreading rate and young age (< 6 Ma from $^{40}\text{Ar}/^{39}\text{Ar}$ ages, Chapter I) give only a limited volume (~ 20-40 km) of oceanic crust generated by spreading suggesting that several submarine structures represent the rifted shoulders of the axis.

2.4 METHODS

2.4.1 Sampling and sample treatment

The submarine samples were obtained during two cruises with the German research vessel RV POSEIDON in 1997 (POS 232) and in 2002 (POS 286). The island of São Miguel has been sampled during two fieldtrips in 2001 and 2002 and the islands of Terceira and Graciosa have been investigated in 2003.

Most submarine samples dredged along the Terceira axis are fresh and only few are slightly hydrothermally altered. Glasses were dredged west of São Miguel, at João de Castro and west of Graciosa. Representative samples have been studied petrographically and mineral compositions were determined with the electron microprobe (EPMA). Wherever possible glass was separated, hand-picked, washed and used for the geochemical analyses. Fresh cores were cut from samples without glass, coarse crushed, washed thoroughly in deionised water, and then fine crushed in an agate ball mill.

For whole rocks, 0.6 grams of dried powder were mixed with lithium tetraborate and ammonium nitrate, fused to a homogeneous glass bead, and analysed using a Philips 1400 XRF spectrometer calibrated with international rock standards. Results for the samples and international rock standards analysed together with the samples are presented in Table 2.1, showing that precision for most elements is better than 0.8 % and that accuracy is better than 1 % of the measured values. The major element analyses of glasses were carried out on a JEOL JXA8900 Superprobe electron microprobe at the Institut für Geowissenschaften, University of Kiel (Table 2.2). The major elements SiO_2 , TiO_2 , Al_2O_3 , FeO^T , MnO , MgO , CaO , Na_2O , K_2O , P_2O_5 , Cr_2O_3 and, in some cases, also F, Cl, and NiO were measured. The electron microprobe was operated at an accelerating voltage of 15 kV, a probe current of 12 nA and a defocused beam (12 μm). Counting times were set to 20 and 10 seconds for peaks and single backgrounds, respectively.

Table 2.1: Selected major element, trace element and Sr-Nd-Pb isotope data of whole rocks from the Terceira axis. Major element, trace element and isotopic data from São Miguel are presented in Chapter III. Additional major element and trace element data are available in the Appendix. The whole-rock (WR) major element data were determined by XRF and the trace element data were determined by ICP-MS. Melting pressure was calculated using fractionation-corrected SiO₂ contents and the equation of Haase (1996). The ²³²Th/²³⁸U ratios have been calculated from the trace element concentrations.

Sample	188 DS-1	494DS-1	497DS-1	513DS-1	515DS-1	SM0128	SM0129	SM9714	SM9716	SM9718
Location	Ponta Sul, S of São Miguel	Monaco Bank S of São Miguel	Monaco Bank S of São Miguel	W slope of São Miguel	W slope of São Miguel	Nordeste volcano, São Miguel	Nordeste volcano, São Miguel	Pico Longo, Nordeste volcano, São Miguel	Agua Retorta, Nordeste volcano, São Miguel	Agua Retorta, Nordeste volcano, São Miguel
Latitude [°N]	37°10.861	37°38.084	37°36.559	37°51.933	37°51.874	37°77.400	37°85.100	37°77.134	37°45.900	37°45.900
Longitude [°W]	25°42.318	25°54.076	25°54.109	25°56.277	25°59.887	25°14.700	25°22.400	25°21.150	25°09.800	25°09.800
	Submarine	Submarine	Submarine	Submarine	Submarine	Subaerial	Subaerial	Subaerial	Subaerial	Subaerial
TAS classification	Basanite	Basanite	Basanite	Basalt	Trachyandesite	Basalt	Basalt	basaltic Trachyandesite	Trachybasalt	Trachybasalt
Melting pressure [GPa]	4.28	4.34	3.83	2.65					2.04	
[wt. %]										
SiO ₂	43.22	43.08	44.26	46.95	59.29	48.8	46.9	52.70	48.33	49.68
TiO ₂	2.72	4.34	4.28	2.74	1.28	3.55	3.95	2.27	3.92	3.21
Al ₂ O ₃	12.84	14.20	15.78	12.33	18.69	15.31	14.52	17.61	14.69	17.08
Fe ₂ O ₃	13.93	13.95	14.45	11.06	5.93	11.76	13.36	8.07	13.06	11.37
MnO	0.18	0.20	0.19	0.17	0.19	0.16	0.17	0.17	0.16	0.16
MgO	11.71	6.61	5.83	12.13	1.58	4.03	4.85	3.28	5.52	3.32
CaO	10.15	10.27	9.35	10.97	3.53	8.11	8.18	6.00	8.80	7.39
Na ₂ O	2.43	2.59	3.19	2.56	5.99	3.44	3.08	3.97	2.98	3.74
K ₂ O	0.99	1.42	1.12	1.38	4.32	2.25	1.91	3.82	2.08	2.56
P ₂ O ₅	0.46	1.47	0.86	0.48	0.38	0.69	0.58	0.72	0.54	0.75
LOI	1.43	0.00	0.00	0.00	0.00	0.00	1.15	0.00	0.00	0.00
Total	100.06	98.13	99.31	100.77	101.18	96.89	97.29	97.80	98.77	98.12
[ppm]										
Sc	29.3	18.0	54.2	24.1	3.16	13.7	18.8	8.81	19.2	12.4
Cr	533	137	16.4	996	2.25	1.61	134	86.3	152	7.00
Co	61.9	30.5	31.1	44.6	4.95	29.3	37.0	11.8	40.0	24.9
Ni	273	57.0	24.0	319	1.75	21.4	53.1	25.4	95.0	39.0
Cu	37.5	15.5	26.8	70.5	3.29	41.8	51.4	12.1	28.1	13.8
Zn	114	110	129	90.0	92.1	107	122	95.4	99.5	103
Mo		0.82	1.85	1.90	0.97	2.78	2.28	1.66	2.41	2.55
Rb	21.8	23.0	18.3	28.5	1090	54.7	78.3	106	55.3	64.8
Sr	611	1123	598	622	543	744	660	847	624	698
Y	24.8	28.8	33.4	19.3	33.7	38.3	42.9	48.4	38.8	42.4
Zr	223	166	219	259	607	404	367	572	389	441
Nb	43.0	33.7	38.7	48.0	130	71.8	66.8	111	62.4	77.6
Cs	0.22	0.48	0.27	0.32	0.26	0.16	4.40	0.49	0.16	0.05
Ba	323	540	241	404		773	798	968	487	633
La	30.2	48.4	36.4	36.6	89.5	60.8	61.1	107	59.1	62.5
Ce	63.1	107	68.5	75.5	173	126	121	185	112	129
Pr	8.20	14.5	9.90	9.51	19.4	15.7	15.9	25.1	13.6	15.1
Nd	33.1	62.6	42.7	38.3	68.0	62.3	63.3	94.6	53.0	59.6
Sm	7.01	13.1	9.96	7.93	11.8	12.9	13.0	17.0	10.5	12.0
Eu	2.23	4.74	3.19	2.43	3.32	3.76	3.85	4.86	3.04	3.53
Gd	6.35	11.2	9.54	6.70	9.65	11.5	11.8	14.6	9.75	10.9
Tb	0.94	1.53	1.41	0.96	1.44	1.68	1.75	2.05	1.34	1.54
Dy	5.06	8.03	7.99	5.16	7.76	8.96	9.43	10.6	7.67	8.42
Ho	0.90	1.41	1.50	0.93	1.44	1.61	1.72	1.92	1.43	1.54
Er	2.22	3.30	3.78	2.28	3.81	4.07	4.39	4.92	3.69	3.91
Tm	0.29	0.39	0.48	0.29	0.54	0.54	0.58	0.65	0.50	0.52
Yb	1.79	2.22	2.92	1.76	3.49	3.31	3.58	3.94	3.06	3.21
Lu	0.25	0.31	0.42	0.24	0.50	0.46	0.51	0.56	0.44	0.45
Hf	5.13	5.07	6.94	5.98	15.1	10.6	10.0	14.7	8.99	9.69
Ta	2.47	2.28	2.86	3.34	8.73	4.85	4.55	7.32	4.18	4.95
Pb	1.79	1.42	1.49	2.05	6.13	3.85	3.68	6.54	3.46	3.84
Th	3.04	3.10	3.09	3.82	13.5	7.25	7.28	14.1	6.98	8.15
U	0.76	1.00	1.47	1.14	1.76	1.79	1.78	3.31	1.59	1.71
⁸⁷ Sr/ ⁸⁶ Sr	Pb triple spike	Pb triple spike	Pb triple spike							
	0.703557	0.703657	0.703649	0.703273	0.703553	0.705167	0.705338		0.706210	
¹⁴³ Nd/ ¹⁴⁴ Nd	0.51287	0.51290	0.51296	0.51299	0.51289	0.51274	0.51270		0.51268	
²⁰⁶ Pb/ ²⁰⁴ Pb	19.39	19.30	19.29	19.33	19.50	19.90	20.01	20.00	20.16	19.97
²⁰⁷ Pb/ ²⁰⁴ Pb	15.60	15.60	15.60	15.56	15.61	15.73	15.75	15.75	15.80	15.77
²⁰⁸ Pb/ ²⁰⁴ Pb	39.21	39.27	39.26	39.05	39.37	40.09	40.24	40.34	40.43	40.20
²⁰⁸ Pb/ ²⁰⁶ Pb	2.022	2.035	2.035	2.020	2.018	2.014	2.011	2.017	2.005	2.013
²³² Th/ ²³⁸ U	4.15	3.21	2.17	3.46	7.91	4.17	4.22	4.39	4.54	4.93

Table 2.1: continued

Sample	SM9719	SM0169	SM0170	SM0171	SM0145	SM0204	SM0202	18-8-97-3	SM0101	SM0102
Location	Água Retorta, Nordeste vulcano, São Miguel	Queimadas, Furnas vulcano, São Miguel	Fogo vulcano, São Miguel	Fogo vulcano, São Miguel	Ribeira Grande, Waist Zone, São Miguel	Pico de Lima, Waist Zone, São Miguel	Pico do Cedro, Waist Zone, São Miguel	Mosteiros, Sete Cidades, São Miguel	Beira Mar de Beixo, Sete Cidades, São Miguel	Ponta dos Mosteiros, Sete Cidades, São Miguel
Latitude [°N]	37°45.900	37°45.700	37°46.250	37°46.250	37°48.550	37°47.356	37°45.460	37°53.910	37°53.910	37°53.910
Longitude [°W]	25°09.800	25°19.075	25°28.890	25°28.890	25°32.120	25°38.850	25°42.200	25°49.130	25°49.130	25°49.162
	Subaeral	Subaeral	Subaeral	Subaeral	Subaeral	Subaeral	Subaeral	Subaeral	Subaeral	Subaeral
TAS classification	Basanite	Basalt	Trachybasalt	Basalt	Basalt	Basalt	Basalt	Basalt	Basalt	Basalt
Melting pressure [GPa]	4.40	2.90		3.33	2.60	3.66	3.40	3.01	3.56	3.30
[wt. %]										
SiO ₂	42.95	46.38	48.70	45.40	47.06	44.63	45.24	46.13	44.87	45.47
TiO ₂	3.45	3.01	3.10	3.83	3.53	3.54	2.68	2.51	3.08	2.74
Al ₂ O ₃	9.73	12.90	16.57	14.16	13.92	11.84	11.39	9.57	10.96	10.25
Fe ₂ O ₃	13.57	11.83	10.95	13.09	12.12	13.14	11.66	11.63	11.96	11.34
MnO	0.17	0.17	0.18	0.18	0.17	0.17	0.16	0.17	0.17	0.16
MgO	12.58	8.84	4.41	7.68	8.47	10.41	13.04	16.58	12.26	14.09
CaO	10.12	8.93	7.79	9.30	9.26	11.9	11.27	10.39	11.62	10.52
Na ₂ O	1.50	2.93	4.16	2.85	3.05	1.92	2.18	1.74	2.11	2.01
K ₂ O	1.44	2.32	2.60	1.86	1.87	1.24	1.04	1.25	1.19	1.40
P ₂ O ₅	0.45	0.44	0.84	0.66	0.61	0.41	0.44	0.39	0.52	0.45
LOI	0.00	0.00	0.09	1.63	0.00	0.21	0.1	0.00	0.00	0.00
Total	94.60	96.56	98.29	99.33	98.85	98.09	98.03	99.19	97.54	97.29
[ppm]										
Sc	24.5	17.7	10.8	22.4		35.3	30.9	29.6	30.9	29.0
Cr	597	321	26.2	183	439	578	1107	1369	654	705
Co	52.3	44.8	23.8	47.4		57.5	57.6	53.4	55.8	59.7
Ni	315	141	17.6	123	145	114	329	428	225	311
Cu	81.2	55.3	18.4	46.6		27.1	63.6	54.7	83.5	74.9
Zn	91.6	91.0	110	118	113	99.2	92.8	91.0	85.0	84.3
Mo	1.01	3.31	3.14	2.13		1.82	1.52	1.45	1.68	1.84
Rb	38.7	60.7	65.7	46.1	45.0	35.5	26.9	24.7	27.1	32.3
Sr	410	551	995	844	714	550	550	409	589	534
Y	30.2	27.2	36.5	34.0		25.8	24.6	16.0	20.4	19.5
Zr	265	350	444	360	346	253	176	180	200	226
Nb	50.7	61.9	89.6	65.0		42.9	39.7	35.0	43.6	44.8
Cs	0.32	0.61	0.61	0.41		0.36	0.27	0.25	0.25	0.28
Ba	385	379	767	541	732	373	379	307	347	348
La	50.1	50.5	73.4	50.9		32.2	30.0	29.6	32.5	33.5
Ce	91.5	104	153	118		67.7	60.8	62.5	69.3	71.4
Pr	12.9	12.7	18.9	13.4		8.59	7.84	8.00	8.71	8.85
Nd	51.6	49.0	73.9	53.6		35.1	32.1	32.6	35.5	35.5
Sm	10.1	9.76	14.2	10.7		7.44	6.83	6.80	7.37	7.17
Eu	2.89	2.71	4.19	3.18		2.30	2.13	1.98	2.25	2.13
Gd	9.13	8.49	11.9	8.93		6.65	6.15	5.57	6.40	6.04
Tb	1.29	1.25	1.70	1.28		0.97	0.89	0.80	0.91	0.86
Dy	6.81	6.66	8.84	6.61		5.12	4.76	4.31	4.75	4.51
Ho	1.23	1.19	1.57	1.16		0.90	0.84	0.77	0.84	0.80
Er	3.04	3.00	3.95	2.90		2.23	2.10	1.89	2.09	1.97
Tm	0.39	0.40	0.52	0.37		0.29	0.27	0.24	0.27	0.26
Yb	2.33	2.46	3.16	2.24		1.74	1.67	1.45	1.62	1.57
Lu	0.33	0.34	0.45	0.31		0.24	0.23	0.20	0.21	0.22
Hf	7.79	9.48	11.7	7.55		5.68	4.39	5.52	5.43	5.95
Ta	3.54	4.30	6.08	3.92		2.72	2.46	2.53	2.86	2.94
Pb	3.01	3.82	3.96	2.80		1.42	1.92	1.80	1.59	1.84
Th	5.99	7.43		5.25		3.95	3.34	3.28	3.33	3.73
U	1.02	1.94		1.35		1.03	0.85	1.00	0.89	1.00
⁸⁷ Sr/ ⁸⁶ Sr		0.704673	0.704368	0.704497	0.704364	0.704264	0.703640		0.703731	0.704143
¹⁴³ Nd/ ¹⁴⁴ Nd		0.51275	0.51279	0.51278	0.51280	0.51281	0.51289		0.51289	0.51280
²⁰⁶ Pb/ ²⁰⁴ Pb	19.98		19.81			19.69	19.53	19.57		19.62
²⁰⁷ Pb/ ²⁰⁴ Pb	15.77		15.70			15.68	15.61	15.64		15.64
²⁰⁸ Pb/ ²⁰⁴ Pb	40.38		39.95			39.75	39.35	39.55		39.61
²⁰⁸ Pb/ ²⁰⁶ Pb	2.021		2.017			2.019	2.014	2.021		2.019
²³² Th/ ²³⁸ U	6.05	3.97		4.02		3.97	4.07	3.40	3.89	3.84

Table 2.1: continued

Sample	SM0104	SM0106	SM0114	SM0116	SM0120	SM0133	SM0134	SM0136	SM0144	SM0161
Location	NNW-flank - rim, Sete Cidades, São Miguel	N - flank - rim, Sete Cidades, São Miguel	Caldeira Secca, Sete Cidades, São Miguel	Ponta da Ferraria, Sete Cidades, São Miguel	Ponta da Ferraria, Sete Cidades, São Miguel	Ponta da Ferraria, Sete Cidades, São Miguel	Ponta da Ferraria, Sete Cidades, São Miguel	Ponta da Ferraria, Sete Cidades, São Miguel	Calhetas, Waist Zone, São Miguel	Mafra, Sete Cidades, São Miguel
Latitude [°N]	37°52.500	37°52.630	37°51.820	37°51.620	37°51.490	37°51.652	37°51.652	37°51.652	37°49.590	37°53.360
Longitude [°W]	25°47.400	25°46.840	25°48.140	25°51.570	25°51.310	25°51.150	25°51.150	25°51.150	25°36.050	25°48.510
TAS classification	Subaeral	Subaeral	Subaeral	Subaeral	Subaeral	Subaeral	Subaeral	Subaeral	Subaeral	Subaeral
TAS classification	Basalt	Trachyte	Trachyte	Basalt	basaltic Trachyandesite	Basalt	basaltic Trachyandesite	Basalt	Basalt	Basalt
Melting pressure [GPa]	2.75			3.02		2.59		2.69		3.34
[wt. %]										
SiO ₂	46.71	61.23	63.28	46.09	58.16	47.09	54.56	46.85		45.36
TiO ₂	2.98	0.72	0.49	3.55	1.27	3.40	1.92	3.17		3.59
Al ₂ O ₃	14.05	17.64	15.56	14.74	17.99	13.33	17.35	11.89		13.05
Fe ₂ O ₃	10.94	3.02	3.16	11.81	4.87	11.60	7.33	11.47		12.44
MnO	0.18	0.17	0.24	0.18	0.17	0.17	0.19	0.17		0.18
MgO	7.51	0.48	0.23	6.85	1.24	8.60	2.41	10.63		9.14
CaO	9.96	1.46	0.50	9.92	3.23	11.03	4.86	11.96		10.81
Na ₂ O	2.95	6.85	7.72	3.08	5.81	2.83	5.63	2.48		2.76
K ₂ O	1.80	5.17	5.10	1.80	4.31	1.58	3.61	1.38		1.26
P ₂ O ₅	0.69	0.09	0.05	0.59	0.31	0.57	0.62	0.52		0.69
LOI	0.51	0.15	2.30	0.00	0.47	0.00	0.03	0.11		0.00
Total	97.18	96.68	98.31	97.43	97.34	99.04	97.78	99.48		98.03
[ppm]										
Sc	20.2	1.91	2.20	22.4	2.76	28.1	5.63	28.4	30.2	24.4
Cr	344	1.07	1.39	162	2.87	449	1.38	662	188	405
Co	35.8	0.58	6.06	40.8	3.43	44.9	8.28	47.4	50.1	47.1
Ni	117	0.26	0.30	57.4	0.72	122	0.39	198	95.6	139
Cu	54.8	1.53	0.99	43.8	2.28	67.8	3.42	87.7	64.2	36.7
Zn	101	92.1	154	104	97.7	98.7	113	88.4	103	99.0
Mo	2.24	2.06	11.2	2.44	3.76	2.02	2.57	1.56	1.54	1.99
Rb	39.8	133	177	40.9	102	39.0	86.1	31.6	32.1	33.1
Sr	786	313	4.14	833	743	715	814	638	694	797
Y	28.7	39.7	64.0	26.3	36.8	28.2	41.8	21.7	29.6	25.4
Zr	321	808	1214	336	646	305	572	238	187	248
Nb	73.5	166	272	74.1	148	60.7	130	56.5	43.5	57.4
Cs	0.36	0.29	1.78	0.29	0.51	0.23	0.62	0.25	0.28	0.32
Ba	571	1398	6.84	502	1301	518	1008	381	429	494
La	50.5	98.8	137	48.8	87.6	42.5	81.3	37.0	30.9	40.9
Ce	106	190	265	102	170	88.3	164	78.9	67.1	86.5
Pr	12.9	19.0	28.6	12.5	19.3	11.0	19.1	9.74	8.73	10.8
Nd	51.2	63.4	95.0	49.2	69.8	44.1	71.6	39.1	36.6	44.3
Sm	10.2	10.3	16.4	9.65	12.2	8.82	13.4	7.88	7.97	8.97
Eu	3.04	2.88	2.47	2.89	3.60	2.67	3.98	2.36	2.54	2.77
Gd	8.64	7.92	13.1	8.06	9.82	7.54	11.2	6.63	7.24	7.59
Tb	1.23	1.23	2.11	1.13	1.41	1.08	1.62	0.94	1.07	1.07
Dy	6.44	6.65	12.2	5.94	7.66	5.57	8.81	4.83	5.71	5.60
Ho	1.16	1.26	2.41	1.05	1.44	0.98	1.62	0.86	1.02	1.00
Er	2.91	3.52	6.73	2.62	3.83	2.45	4.23	2.10	2.55	2.47
Tm	0.38	0.51	0.98	0.33	0.53	0.31	0.57	0.27	0.33	0.31
Yb	2.30	3.42	6.43	2.07	3.42	1.93	3.54	1.62	1.98	1.90
Lu	0.32	0.50	0.93	0.28	0.50	0.27	0.50	0.23	0.27	0.26
Hf	7.59	14.4	26.8	7.71	13.9	6.33	12.4	6.01	4.76	5.94
Ta	4.67	8.28	15.5	4.72	8.32	3.64	7.62	3.58	2.67	3.65
Pb	2.46	7.13	10.6	2.22	6.61	2.04	4.44	1.64	1.70	1.80
Th	5.81	15.3	23.8	5.33	12.8	4.57	11.0	3.87	3.18	4.06
U	1.38	3.49	6.53	1.53	2.99	1.24	2.84	1.14	0.82	1.06
⁸⁷ Sr/ ⁸⁶ Sr	0.703534	0.703594	0.704176	0.703336	0.703653	0.703274	0.703483	0.703397	0.703764	0.703604
¹⁴³ Nd/ ¹⁴⁴ Nd	0.51290	0.51291	0.51291	0.51292	0.51290	0.51292	0.51290	0.51292	0.51286	0.51291
²⁰⁶ Pb/ ²⁰⁴ Pb		19.51				19.45	19.43		19.65	
²⁰⁷ Pb/ ²⁰⁴ Pb		15.60				15.58	15.58		15.63	
²⁰⁸ Pb/ ²⁰⁴ Pb		39.35				39.24	39.23		39.50	
²⁰⁸ Pb/ ²⁰⁶ Pb		2.017				2.017	2.019		2.010	
²³² Th/ ²³⁸ U	4.35	4.51	3.77	3.61	4.44	3.81	3.99	3.52	4.01	3.96

Table 2.1: continued

Sample	SM0176	SM0203	SM160501-4	SM220501-1	SM9704-a	516DS-2	523DS-1	525DS-2	529DS-4	532DS-1
Location	Cliffs in Mosteiros, Sete Cidades, São Miguel	Pico da Pintona, Waist Zone, São Miguel	Inner northern caldera wall, Sete Cidades, São Miguel	North of Ginetes, Sete Cidades, São Miguel	S of Relva, Aeroporto, São Miguel	Alcatraz	Banco João de Castro	Banco João de Castro	E of Terceira	Seamount S of Terceira
Latitude [°N]	37°53.180	37°47.850	37°52.850	37°51.300	37°45.310	38°08.008	38°10.455	38°11.746	38°32.614	38°23.373
Longitude [°W]	25°49.290	25°41.605	25°46.800	25°52.459	25°42.430	26°00.687	26°37.895	26°35.852	26°52.509	27°15.461
	Subaeral	Subaeral	Subaeral	Subaeral	Subaeral	Submarine	Submarine	Submarine	Submarine	Submarine
TAS classification	Trachybasalt	Basalt	Basalt	Trachyte	Basalt	Basanite	Trachyandesite	Basalt	Basalt	Basalt
Melting pressure [GPa]		2.82	2.99		3.19	4.04		2.67	2.81	
[wt. %]										
SiO ₂	50.08	46.56	46.17	61.98	45.71	43.78	55.58	46.89	46.57	47.55
TiO ₂	2.61	2.43	3.49	0.78	3.44	4.24	1.87	2.01	1.90	2.97
Al ₂ O ₃	16.87	12.52	14.18	16.88	12.76	15.84	17.64	10.45	14.54	16.42
Fe ₂ O ₃	9.16	11.18	12.01	3.42	12.75	14.51	6.90	10.55	9.62	12.18
MnO	0.18	0.16	0.17	0.19	0.17	0.19	0.18	0.15	0.15	0.20
MgO	3.75	10.42	6.38	0.64	9.81	4.90	2.24	15.78	10.55	4.77
CaO	7.35	11.58	10.76	1.16	11.14	9.67	4.64	11.73	10.23	8.92
Na ₂ O	3.73	2.67	3.02	6.94	2.55	2.99	6.22	2.10	2.90	3.41
K ₂ O	2.65	1.15	1.47	5.21	1.06	1.44	3.93	1.09	1.10	1.82
P ₂ O ₅	0.92	0.4	0.52	0.15	0.52	0.78	0.59	0.33	0.38	0.76
LOI	2.34	0.23	0.71	1.13	0.00	0.00	0.00	0.00	0.00	0.00
Total	98.72	98.18	97.68	98.14	98.63	98.34	99.79	101.08	97.94	99.00
[ppm]										
Sc	9.77	31.2	22.2	29.8	19.9		7.53	38.6	26.2	
Cr	12.0	788	211	6.78	670	121	1.49	845	539	201
Co	17.5	50.3	41.9	7.34	48.6		7.85	59.4	35.1	
Ni	7.27	212	77.1	2.47	185	184		376	205	86.0
Cu	10.9	86.2	95.3	2.53	25.9		5.37	162	48.0	
Zn	105	89.7	110	115	82.6	123	103	84.8	77.0	124
Mo	1.55	1.71	2.22	6.37	1.86		4.63	1.29	4.21	
Rb	56.7	33.3	20.6	95.0	22.6	17.0	101	27.2	22.2	49.0
Sr	893	527	733	110	615	770	593	391	414	644
Y	33.5	25.8	26.6	37.1	23.2		41.8	18.2	18.1	
Zr	414	177	305	698	207	336	447	146	136	360
Nb	98.3	40.9	68.1	168	45.7		96.8	31.8	27.0	
Cs	0.20	0.40	0.28	0.95	0.05		0.82	0.23	0.25	
Ba	752	411	484	730	359		976	290	324	
La	68.4	28.0	45.5	76.4	30.5		72.5	24.1	21.5	
Ce	138	57.8	91.0	152	64.6		137	49.2	44.4	
Pr	16.1	7.26	11.1	17.0	8.04		15.9	5.98	5.62	
Nd	61.2	29.5	43.8	59.9	33.5		58.5	24.1	22.7	
Sm	11.6	6.44	8.74	10.5	7.13		11.2	5.13	5.07	
Eu	3.40	2.04	2.65	2.69	2.22		3.17	1.53	1.64	
Gd	9.56	5.92	7.52	8.41	6.61		9.39	4.61	4.80	
Tb	1.35	0.90	1.08	1.31	0.92		1.36	0.65	0.74	
Dy	7.20	4.92	5.71	7.38	4.97		7.75	3.61	4.43	
Ho	1.29	0.89	1.02	1.41	0.89		1.46	0.66	0.86	
Er	3.28	2.23	2.58	3.85	2.19		3.92	1.68	2.24	
Tm	0.43	0.29	0.33	0.55	0.28		0.56	0.23	0.30	
Yb	2.67	1.84	2.03	3.55	1.70		3.58	1.41	1.87	
Lu	0.38	0.26	0.29	0.50	0.24		0.52	0.20	0.27	
Hf	9.03	4.37	6.98	14.5	5.36		10.8	3.89	4.21	
Ta	5.94	2.47	4.23	9.08	3.04		5.14	1.45	1.85	
Pb	3.51	1.85	2.30	6.26	1.93		5.28	1.62	2.08	
Th	8.00	3.33	5.80	11.9	3.67		8.79	2.51	2.35	
U	2.15	0.89	1.63	3.19	1.08		2.56	0.72	0.68	
⁸⁷ Sr/ ⁸⁶ Sr	0.703511		0.703627	0.703594	0.703743	0.704093		Pb triple spike	Pb triple spike	Pb triple spike
¹⁴³ Nd/ ¹⁴⁴ Nd	0.51291	0.51292	0.51291	0.51290	0.51289	0.51280	0.703498	0.703361	0.703519	0.704124
²⁰⁶ Pb/ ²⁰⁴ Pb		19.50			19.65		19.31	19.19	19.51	19.24
²⁰⁷ Pb/ ²⁰⁴ Pb		15.59			15.63		15.52	15.52	15.55	15.54
²⁰⁸ Pb/ ²⁰⁴ Pb		39.23			39.51		38.95	38.89	39.07	38.85
²⁰⁸ Pb/ ²⁰⁶ Pb		2.011			2.011		2.017	2.027	2.003	2.019
²³² Th/ ²³⁸ U	3.85	3.87	3.69	3.84	3.51		3.55	3.59	3.59	

Table 2.1: continued

Sample	535DS-7	AZT-03-11	AZT-03-12	AZT-03-16	AZT-03-18	AZT-03-116	AZT-03-138	AZT-03-142	542DS-1	245 DS-4
Location	W flank of Terceira	Coastline at Cais dos Biscoitos, Terceira	Road Junction between Road 3-2 and 502, East of Pico Gordo, Terceira	East of Road 502, scoria cone Pico do Gaspar, Terceira	West of Road 502, E of Misterios Negors, Terceira	Cal Pedra, N flank of Santa Barbara, Terceira	Meadow at Malha Grande, 800m NW of Pico Vermelho, Terceira	At Road 3-1 (Altares-Angra), 250m NW of wastewater treatment plant, Terceira	SW of Graciosa	W of Graciosa
Latitude [°N]	38°42.446	38°47.960	38°44.466	38°53.830	38°44.001	38°46.333	38°45.033	38°45.916	39°05.966	39°08.184
Longitude [°W]	27°28.720	27°15.830	27°15.866	28°16.333	27°16.516	27°17.750	27°15.266	27°16.983	28°16.412	28°14.311
	Submarine	Subaeral	Subaeral	Subaeral	Subaeral	Subaeral	Subaeral	Subaeral	Submarine	Submarine
TAS classification	Basalt	Basalt	Basalt	Basalt	Trachybasalt	Basalt	Basalt	Basalt	Basalt	Basanite
Melting pressure [GPa]	2.95	2.65	2.65	2.78		2.74	2.83		3.17	3.57
[wt. %]										
SiO ₂	46.27	46.95	46.95	46.66	53.45	46.75	46.54	50.57	45.76	44.85
TiO ₂	3.86	3.02	3.88	3.00	2.54	3.68	3.02	2.68	2.73	2.73
Al ₂ O ₃	14.96	13.81	13.92	15.64	15.00	13.84	14.26	18.32	15.10	15.07
Fe ₂ O ₃	13.31	11.95	13.79	12.06	11.10	13.45	5.98	9.44	10.54	10.74
MnO	0.18	0.17	0.21	0.18	0.24	0.21	0.17	0.15	0.16	0.17
MgO	6.15	8.25	5.45	5.67	3.18	6.09	7.55	3.05	9.67	9.67
CaO	10.58	10.51	9.48	10.59	6.29	9.69	12.08	8.98	11.09	10.11
Na ₂ O	3.22	3.21	3.65	3.55	3.32	3.33	2.46	4.34	2.85	2.90
K ₂ O	0.85	0.93	1.29	1.00	1.87	1.20	0.75	1.34	0.91	0.95
P ₂ O ₅	0.46	0.85	1.31	0.45	1.15	1.17	0.39	0.65	0.39	0.49
LOI	0.00	0.00	0.00	0.45	0.42	0.00	0.00	0.00	0.00	1.87
Total	99.84	98.45	98.55	98.04	99.45	98.06	98.07	98.57	99.20	99.55
[ppm]										
Sc		27.6	23.3	24.3	13.9	14.9	34.3	13.8	28.2	29.5
Cr	92.0	301	64.0	51.3	0.59	8.58	101	7.39	465	433
Co		40.9	31.4	41.3	9.15	20.6	47.3	19.0	38.9	45.4
Ni	72.0	116	27.8	31.2	0.47	11.0	59.0	10.2	182	183
Cu		35.5	22.6	31.3	3.40	20.4	41.2	14.6	42.2	46.1
Zn	109	95.1	118	101	152	115	94.9	102	103	91.9
Mo		1.30	1.39	0.45	3.76	2.03	1.29	2.54	1.39	
Rb	24.0	19.0	27.2	20.1	39.2	27.0	13.8	25.7	15.4	20.1
Sr	593	529	536	569	729	782	527	812	491	521
Y		32.0	42.7	28.5	58.4	38.8	28.0	36.0	20.3	26.4
Zr	272	178	216	190	429	328	196	302	172	222
Nb		37.0	48.4	36.9	92.3	61.6	37.6	57.2	33.7	45.6
Cs		0.16	0.24	0.15	0.36	0.12	0.07	0.11	0.19	0.26
Ba		496	756	305	745	390	232	364	280	263
La		34.9	49.0	29.1	79.4	49.3	28.9	46.6	25.6	31.4
Ce		79.0	112	60.4	166	105	60.5	98.4	55.1	67.5
Pr		10.2	14.2	7.99	20.2	12.9	7.98	12.1	7.24	8.64
Nd		44.2	61.3	33.1	84.3	52.2	33.3	49.2	30.0	34.2
Sm		10.1	13.6	7.69	18.7	11.5	7.74	10.8	6.59	6.90
Eu		3.82	4.79	2.53	6.56	3.70	2.58	3.53	2.10	2.17
Gd		9.71	12.9	7.59	17.5	10.7	7.50	10.1	5.90	6.18
Tb		1.37	1.80	1.14	2.54	1.57	1.12	1.46	0.89	0.92
Dy		7.49	9.79	6.58	13.9	8.62	6.23	8.14	5.09	5.05
Ho		1.34	1.74	1.21	2.50	1.55	1.13	1.47	0.97	0.92
Er		3.33	4.29	3.13	6.33	3.96	2.85	3.73	2.49	2.40
Tm		0.43	0.54	0.42	0.83	0.53	0.38	0.49	0.33	0.33
Yb		2.59	3.31	2.67	5.13	3.30	2.35	3.10	2.03	2.10
Lu		0.35	0.45	0.37	0.71	0.46	0.32	0.43	0.29	0.30
Hf		4.59	5.40	5.06	10.9	7.91	5.02	7.50	5.32	4.98
Ta		2.52	3.15	2.48	5.57	3.89	2.39	3.68	2.47	2.54
Pb		1.15	1.59	3.10	2.97	2.45	1.31	2.03	1.78	2.19
Th		2.16	3.03	2.32	5.95	4.70	2.46	4.48	2.69	3.37
U		0.71	0.92	0.68	2.05	1.58	0.77	1.52	0.71	1.10
⁸⁷ Sr/ ⁸⁶ Sr	Pb triple spike	Pb triple spike	Pb triple spike	Pb triple spike	Pb triple spike	Pb triple spike		Pb triple spike	Pb triple spike	Pb triple spike
	0.703580	0.703455	0.703420	0.703492	0.703556	0.703591	0.703510	0.703593	0.703470	0.703452
¹⁴³ Nd/ ¹⁴⁴ Nd	0.51297	0.51298	0.51298	0.51299	0.51301	0.51300	0.51295	0.51295	0.51292	0.51294
²⁰⁶ Pb/ ²⁰⁴ Pb	19.92	19.62	19.65	20.03	19.90	19.98		19.99	19.71	19.43
²⁰⁷ Pb/ ²⁰⁴ Pb	15.62	15.59	15.60	15.63	15.62	15.62		15.62	15.63	15.62
²⁰⁸ Pb/ ²⁰⁴ Pb	39.23	39.08	39.13	39.32	39.23	39.25		39.27	39.36	39.20
²⁰⁸ Pb/ ²⁰⁶ Pb	1.969	1.992	1.992	1.963	1.972	1.964		1.964	1.997	2.018
²³² Th/ ²³⁸ U		3.14	3.40	3.52	3.00	3.07	3.31	3.05	3.94	3.15

Table 2.1: continued

Sample	248 DS-1	249 DS-1	AZG-03-04	AZG-03-07	AZG-03-08	AZG-03-28	BHVO-1	BHVO-1		
Location	W of Graciosa	W of Graciosa	Coastal outcrop at Negro Lighthouse, scoria and lavaflows, Graciosa	South of Redondo at Porto Afonso, Graciosa	At Road 1010 after Ribeirinha, direction to Pico da Brásleira, ~1 km behind village, Graciosa	Road to Caldeira, before Tunnelentrance, road outcrop of lavaflow (2m thick), Graciosa	XRF	n=23 ICP-MS	n=12	
Latitude [°N]	39°05.749	39°06.356	39°05.600	39°04.210	39°03.512	39°01.950				
Longitude [°W]	28°10.084	28°10.581	28°02.800	28°04.250	28°02.350	27°58.911				
TAS classification	Submarine	Submarine	Subaeral	Subaeral	Subaeral	Subaeral	Standard	standard deviation	Standard	standard deviation
Melting pressure [GPa]	3.01	1.91	2.88	3.43	3.22	2.96				
[wt. %]										
SiO ₂	46.13	48.63	46.43	45.17	45.64	46.24	49.94 ± 0.14			
TiO ₂	2.85	3.33	3.04	3.10	3.19	3.27	2.76 ± 0.01			
Al ₂ O ₃	14.88	14.73	15.86	15.80	16.49	16.89	13.57 ± 0.07			
Fe ₂ O ₃	10.73	12.76	10.76	11.48	11.02	10.55	4.56 ± 5.95			
MnO	0.15	0.21	0.15	0.16	0.17	0.15	7.83 ± 5.93			
MgO	8.57	4.27	7.94	8.17	7.84	7.02	7.18 ± 0.06			
CaO	10.07	8.24	10.24	10.70	9.17	10.50	11.46 ± 0.04			
Na ₂ O	3.04	4.08	2.84	2.42	2.55	2.86	2.40 ± 0.07			
K ₂ O	1.09	1.25	0.96	0.82	1.26	1.08	0.53 ± 0.01			
P ₂ O ₅	0.58	1.01	0.44	0.45	0.54	0.46	0.28 ± 0.00			
LOI	0.65	0.32	0.49	1.13	1.88	0.00				
Total	98.74	98.83	99.15	99.40	99.75	99.02	100.52			
[ppm]										
Sc		19.9	30.9	33.0	32.4	27.2			32.9 ± 1.54	
Cr		19.0	327	334	413	222	282 ± 4.85		291 ± 9.84	
Co		26.6	46.8	48.5	45.9	42.2			45.5 ± 1.95	
Ni		13.0	149	137	167	108	107 ± 7.30		120 ± 4.54	
Cu		9.44	40.3	39.3	44.4	28.3			135 ± 9.81	
Zn		147	98.1	89.7	95.1	89.2	106 ± 4.04		104 ± 4.22	
Mo			2.09	1.27	1.39	1.33			1.06 ± 0.09	
Rb		26.0	22.4	9.24	23.6	23.0	9.91 ± 1.85		9.36 ± 0.30	
Sr		717	618	590	520	639	398 ± 2.52		394 ± 12.7	
Y		46.4	27.6	25.9	29.4	25.6			26.4 ± 1.29	
Zr		309	245	237	269	224	188 ± 2.38		175 ± 6.47	
Nb		63.6	43.2	42.4	50.0	40.7	17.64 ± 1.34		17.5 ± 0.46	
Cs		0.24	0.23	0.02	0.16	0.18			0.10 ± 0.00	
Ba		368	287	335	339	303	160	18.4	131 ± 2.54	
La		49.1	28.1	32.1	35.2	26.5			15.2 ± 0.38	
Ce		104	61.7	69.0	75.4	58.2	10.21 ± 3.66		37.8 ± 0.58	
Pr		14.1	8.09	8.62	9.70	7.53			5.50 ± 0.07	
Nd		57.7	32.4	33.7	38.7	30.3			24.9 ± 0.31	
Sm		12.5	6.97	6.68	7.74	6.45			6.20 ± 0.13	
Eu		4.05	2.28	2.13	2.45	2.13			2.13 ± 0.06	
Gd		11.6	6.46	6.20	7.03	6.05			6.20 ± 0.20	
Tb		1.71	0.92	0.87	0.99	0.86			0.96 ± 0.03	
Dy		9.26	4.99	4.73	5.38	4.67			5.39 ± 0.15	
Ho		1.66	0.90	0.86	0.98	0.84			0.98 ± 0.04	
Er		4.12	2.32	2.25	2.55	2.16			2.47 ± 0.08	
Tm		0.54	0.31	0.30	0.34	0.29			0.33 ± 0.01	
Yb		3.32	1.95	1.90	2.15	1.80			2.02 ± 0.07	
Lu		0.45	0.27	0.27	0.31	0.25			0.28 ± 0.01	
Hf		7.14	5.48	4.49	6.09	5.02			4.40 ± 0.08	
Ta		3.53	2.49	2.47	2.99	2.39			1.08 ± 0.04	
Pb		2.36	1.54	1.66	1.76	1.46			1.94 ± 0.23	
Th		4.52	2.86	2.86	3.23	2.47			1.21 ± 0.09	
U		1.55	0.86	0.77	0.88	0.77			0.42 ± 0.02	
⁸⁷ Sr/ ⁸⁶ Sr	0.703564	0.703583	0.703388	0.703647		0.703373				
¹⁴³ Nd/ ¹⁴⁴ Nd	0.51291	0.51298	0.51296	0.51290	0.51293	0.51296				
²⁰⁶ Pb/ ²⁰⁴ Pb		20.05		19.30	19.56	19.89				
²⁰⁷ Pb/ ²⁰⁴ Pb		15.63		15.61	15.60	15.62				
²⁰⁸ Pb/ ²⁰⁴ Pb		39.30		39.15	39.18	39.30				
²⁰⁸ Pb/ ²⁰⁶ Pb		1.960		2.030	2.005	1.978				
²³² Th/ ²³⁸ U		3.01	3.43	3.81	3.78	3.31				

Table 2.2: Selected major element, trace element and Sr-Nd-Pb isotope data of glasses from the Terceira axis. The major element glass data were determined by electron microprobe and the trace element data were analysed by ICP-MS. Melting depth were calculated using fractionation-corrected SiO₂ contents and the equation of Haase (1996). The ²³²Th/²³⁸U ratios have been calculated from the trace element concentrations.

Sample	524DS-2	556DS-3	558DS-1	558DS-8	244 DS-1
Location	Banco João de Castro	Banco João de Castro	Banco João de Castro	Banco João de Castro	W of Graciosa
Latitude [°N]	38°11.287	38°14.777	38°13.725	38°13.725	39°10.026
Longitude [°W]	26°36.761	26°36.657	26°39.068	26°39.068	28°17.959
	Submarine	Submarine	Submarine	Submarine	Submarine
TAS classification	Trachybasalt	Trachybasalt	Trachyandesite	Trachybasalt	Basalt
Melting pressure [GPa]		1.52		1.57	3.08
[wt. %]					
SiO ₂	52.39	49.52	56.70	49.42	45.98
TiO ₂	2.56	3.24	1.56	3.29	4.66
Al ₂ O ₃	17.67	15.93	17.75	16.33	14.60
FeO ^T	6.85	8.46	5.99	8.32	11.11
MnO	0.20	0.21	0.25	0.19	0.15
MgO	3.39	3.30	1.95	3.73	5.88
CaO	6.91	7.39	3.50	7.82	11.62
Na ₂ O	4.07	4.34	5.16	4.10	2.95
K ₂ O	3.25	3.43	4.78	3.12	2.14
P ₂ O ₅	0.76	0.88	0.40	0.90	0.82
SO ₃					0.07
Cl					0.06
Total	98.06	96.70	98.04	97.22	100.05
[ppm]					
Sc	11.2	20.0	2.97	3.41	30.2
Cr	5.01	16.1	6.57	1.82	132
Co	16.3	18.8	6.67	6.77	48.8
Ni	5.94	12.3	0.10		100
Cu	16.3	30.3	4.40	3.95	45.9
Zn	112	96.3	111	107	114
Mo	3.65	2.98	5.42	4.93	
Rb	77.8	67.9	118	108	22.3
Sr	776	675	847	766	684
Y	36.8	34.4	38.2	36.6	26.1
Zr	296	244	376	476	279
Nb	81.0	59.8	99.2	87.4	57.5
Cs	0.61	0.51	0.92	0.86	0.21
Ba	792	690	1442	1165	275
La	67.4	59.4	86.6	80.4	34.2
Ce	131	118	159	151	83.8
Pr	15.7	14.3	18.0	17.0	10.0
Nd	60.8	55.8	64.3	60.8	39.5
Sm	11.5	10.8	11.1	10.8	7.87
Eu	3.27	3.05	3.29	3.12	2.48
Gd	9.29	9.01	8.80	8.63	6.74
Tb	1.31	1.27	1.27	1.21	0.99
Dy	7.20	6.72	6.96	6.79	5.31
Ho	1.30	1.20	1.31	1.27	0.95
Er	3.41	3.12	3.57	3.44	2.42
Tm	0.46	0.41	0.50	0.49	0.32
Yb	2.88	2.59	3.29	3.14	2.03
Lu	0.41	0.36	0.48	0.47	0.28
Hf	7.48	5.80	9.59	11.3	6.35
Ta	3.00	2.78	4.35	4.39	3.38
Pb	3.92	3.21	5.41	4.94	1.96
Th	7.32	5.98	10.4	9.58	3.48
U	2.15	1.71	3.04	2.84	1.04
⁸⁷ Sr/ ⁸⁶ Sr	Pb triple spike	0.703594	Pb triple spike	Pb triple spike	Pb triple spike
¹⁴³ Nd/ ¹⁴⁴ Nd	0.51285	0.703563	0.703566	0.703565	0.703543
²⁰⁶ Pb/ ²⁰⁴ Pb	18.82		0.51283	0.51285	0.51288
²⁰⁷ Pb/ ²⁰⁴ Pb	15.48		18.86	18.85	19.53
²⁰⁸ Pb/ ²⁰⁴ Pb	15.48		15.49	15.48	15.63
²⁰⁸ Pb/ ²⁰⁶ Pb	38.64		38.70	38.66	39.33
²⁰⁸ Pb/ ²⁰⁶ Pb	2.053		2.052	2.051	2.014
²³² Th/ ²³⁸ U	3.52	3.62	3.54	3.49	3.46

The trace element analyses were carried out using an Agilent 7500c/s Quadrupole Inductively Coupled Plasma Mass Spectrometer (ICP-MS) at the Institut für Geowissenschaften, University of Kiel. The samples were prepared following the pressurised HF-HClO₄-aqua regia acid digestion procedure described by Garbe-Schönberg (1993). Trace element analyses of the samples and of international rock standards are shown in Table 2.1 indicating a standard deviation of the precision and accuracy of < 5 % and < 8 % (2σ), respectively, from multiple standard measurements.

The Sr, Nd, and Pb isotopic solutions of most samples were prepared at the Max-Planck-Institut für Chemie in Mainz (MPI) and at the IFM-GEOMAR in Kiel. Sr and Nd in Mainz were measured using a Finnigan MAT 261 and a Nu Plasma HR MC-ICP-MS, respectively. At IFM-GEOMAR, Sr and Nd were measured using a Triton thermal ionization mass spectrometer. The samples were leached in hot 6N HCl for two hours, ultrasonicated 30 minutes and then dissolved using the standard digestion procedure described by Eisele *et al.* (2002) and Abouchami *et al.* (2000). For isotopic determinations, 150-200 mg of grains and standard ion exchange techniques were used to separate Sr, Nd and Pb from the matrix. Sr and Nd isotope ratios were analysed in static mode and isotope fractionation corrections are ⁸⁶Sr/⁸⁸Sr = 0.1194 and ¹⁴⁶Nd/¹⁴⁴Nd = 0.7219, respectively. In Mainz, standard runs for Sr isotopes gave NBS 987 (n = 16): 0.710299 (2SD = 0.000026) compared to NBS987 (n=8) of 0.710273 (2SD = 0.000005) in Kiel. All Sr isotope analyses were normalised to NBS 987 = 0.710250. Standard runs for ¹⁴³Nd/¹⁴⁴Nd gave La Jolla (n = 14): 0.511862 (2SD = 0.000024). Standard runs for ¹⁴³Nd/¹⁴⁴Nd gave 0.511710 (2SD = 0.000005) for the Nd Spex standard (n = 5) corresponding to a La Jolla value of 0.511828. Procedural blanks in both laboratories were generally better than 0.2 ng and 0.1 ng for Sr and Nd, respectively.

In Kiel, the Pb isotopes were determined using a Finnigan MAT 262 mass spectrometer in static mode. For Pb, the analyses were fractionation corrected using repeated measurement of NBS-981 (n = 6; errors are 2σ values; ²⁰⁶Pb/²⁰⁴Pb = 16.899 ± 0.007, ²⁰⁷Pb/²⁰⁴Pb = 15.437 ± 0.007; ²⁰⁸Pb/²⁰⁴Pb = 36.525 ± 0.022) normalised to the values of Todt *et al.* (1996). Following the elution of Pb during the triple spike analyses at the MPI, the samples were split and a sample aliquot was mixed with an amount of triple spike that was estimated to be optimal (Spike/Sample ratio between 0.6 – 1.6). Loaded onto “Good fellow” Re filaments with silica-gel H₃PO₄ activator both, unspiked and spiked sample aliquots were measured on a TRITON mass spectrometer in static multicollection mode. The bias-correction estimated from the two runs has been done following the method of Galer (1999). Based on some duplicate analyses, the external reproducibility is ~150 ppm for ²⁰⁶Pb/²⁰⁴Pb, ²⁰⁷Pb/²⁰⁴Pb, and ²⁰⁸Pb/²⁰⁴Pb. Standard runs for the NBS-981 standard (n=8) give average values of 16.9431 ± 0.0034, 15.5008 ± 0.0029, and 36.7300 ± 0.0074 for ²⁰⁶Pb/²⁰⁴Pb, ²⁰⁷Pb/²⁰⁴Pb, and ²⁰⁸Pb/²⁰⁴Pb, respectively. Pb blanks in both laboratories were negligible (< 70 pg).

2.5 RESULTS

2.5.1 Major and trace elements

The Azorean samples generally cover a range from alkali basalts to trachytes and the two major islands of São Miguel and Terceira show different trends with the São Miguel lavas being more alkaline (Fig. 2.2). A few samples also plot in the basanite and phonotephrite fields. Samples from the João de Castro seamount are generally situated in the field of the São Miguel lavas whereas the Graciosa samples are relatively primitive plotting into the region where the trends of the two major islands overlap. The Terceira axis flank lavas, that are supposed to represent the oldest rocks in the vicinity of the axis, tend towards lower silica concentrations.

Lavas from all volcanic systems of the Terceira axis show similarities in CaO and Na₂O contents (Fig. 2.3) but slight differences occur in FeO^T, where the primitive Graciosa, Terceira and João de Castro samples (MgO > 8 wt. %) have lower FeO^T contents for a given MgO than lavas from São Miguel. The TiO₂ concentrations are lowest at Graciosa, João de Castro and in the submarine Terceira samples. The highest concentrations were observed at São Miguel, the Terceira axis flank and also in the João de Castro samples. High Al₂O₃ contents of Graciosa are conspicuous in contrast to lower values at the Hirondele Basin and João de Castro. The most significant differences among the Terceira axis lavas occur in the K₂O contents with the São Miguel and João de Castro lavas having higher K₂O contents for a given MgO than lavas from the other volcanic systems along the axis (Fig. 2.3).

The differences observed in the K₂O contents are also obvious in the La/Sm ratios (Fig. 2.4) where the lavas from the two eastern volcanic systems São Miguel and João de Castro are significantly more enriched in the light REE than lavas from Terceira, Graciosa, the Hirondele Basin and the Terceira axis flank. The lavas from the João de Castro volcanic system have elevated Rb-concentrations reflected in higher Rb/Nb (Fig. 2.4). Systematic correlations are also observed in the heavy rare earth elements (HREE), where São Miguel lavas show the highest HREE ratios (e.g. Dy/Yb; Fig. 2.4) in contrast to lower values found in the João de Castro and Graciosa samples and in most of the Terceira lavas. The Terceira and Graciosa lavas also have lower Nb/Zr and Th/U (Fig. 2.4) than the eastern lavas from São Miguel and João de Castro implying different mantle sources along the Terceira axis.

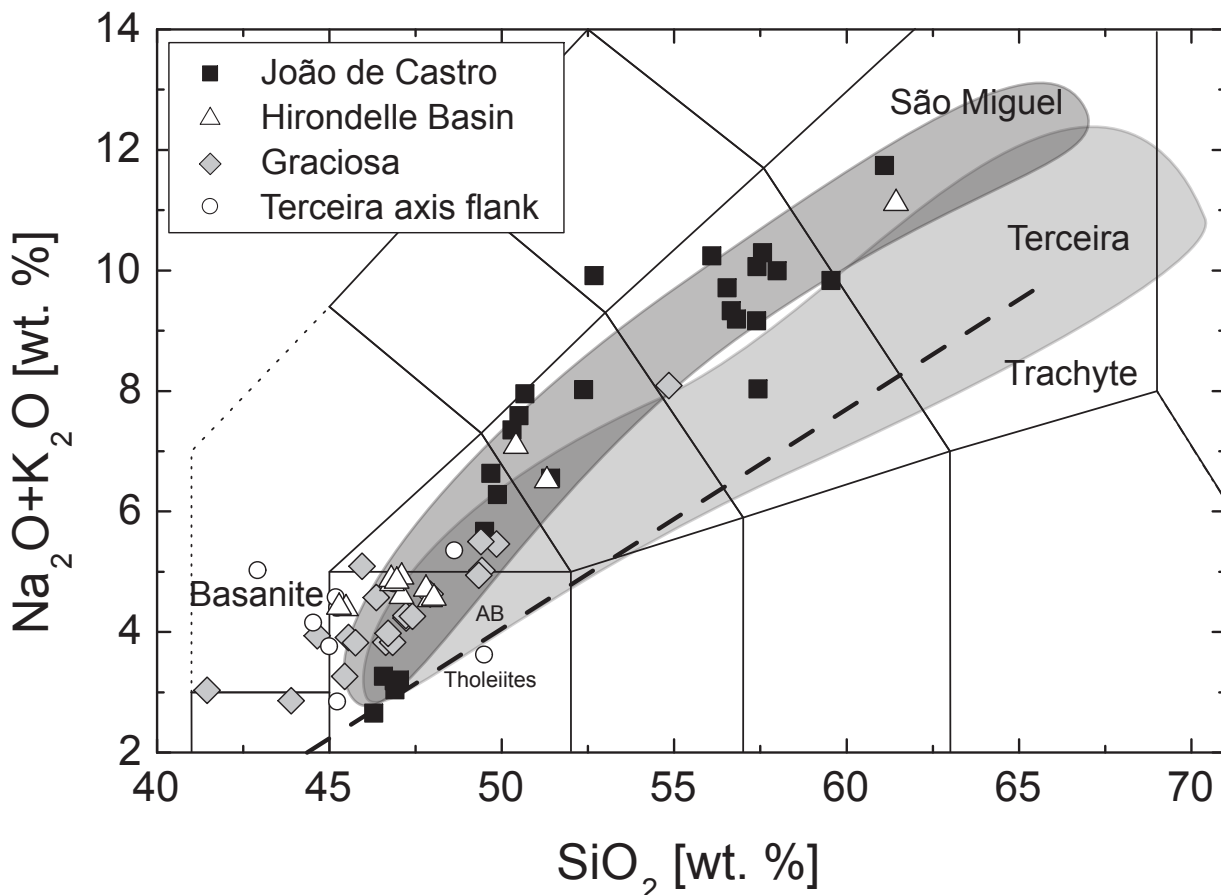


Figure 2.2: Total alkalis (Na₂O+K₂O) versus SiO₂ on a volatile-free basis according to Le Maitre (1989). The separation line between alkaline (AB) and tholeiitic compositions was taken from Macdonald (1968). The fields of São Miguel and Terceira include subaerial and submarine samples.

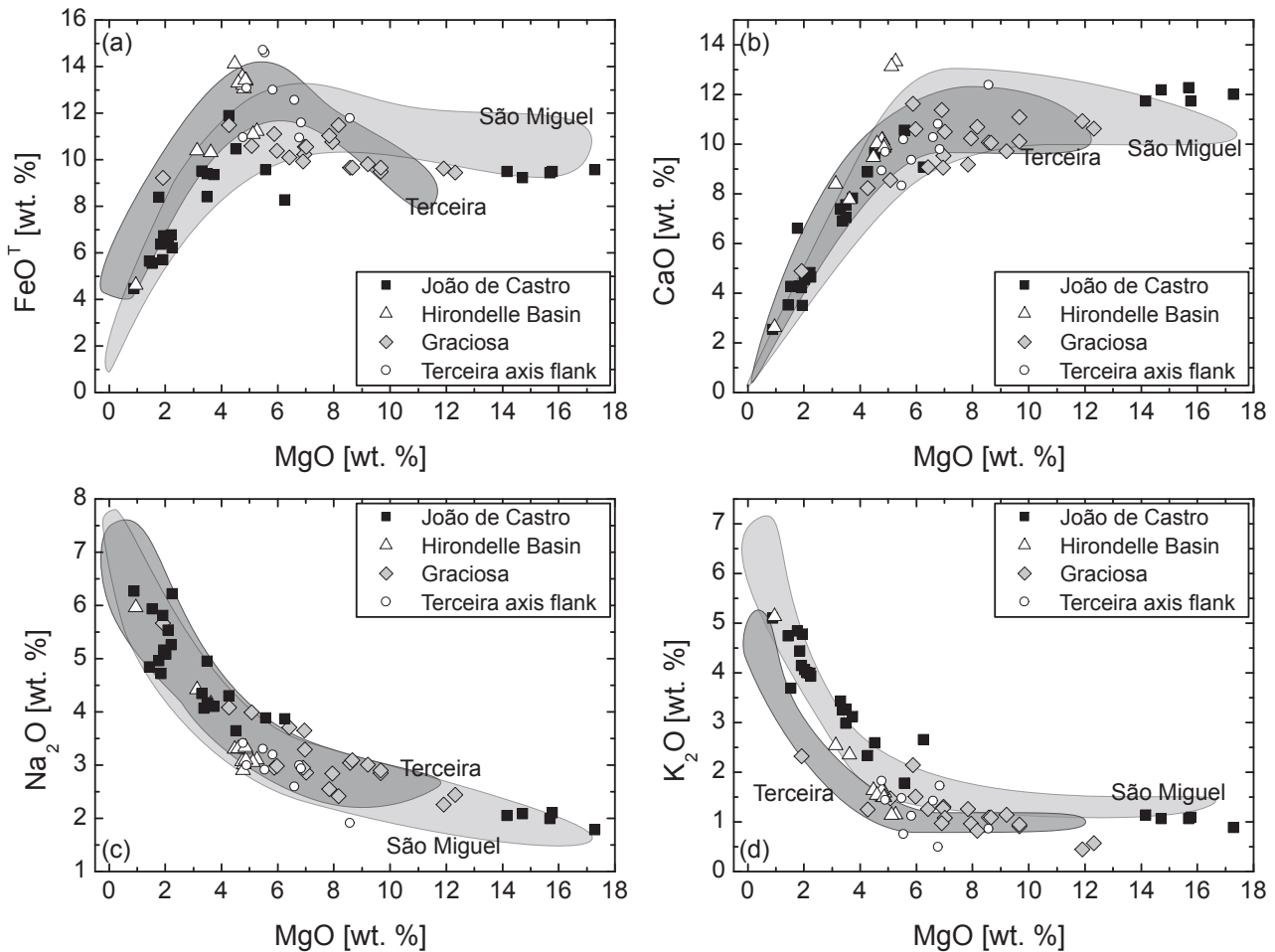


Figure 2.3: a-d) Major element data versus MgO of the Terceira axis samples. Grey fields show trend of the São Miguel and Terceira data. The most notable differences are observed in the FeO^T and K₂O contents (Fig. 2.3 a & d).

2.5.2 Radiogenic isotope compositions

With the exception of the lavas from the eastern volcanoes of São Miguel island the variation in $^{87}\text{Sr}/^{86}\text{Sr}$ is relatively small compared to that of the $^{143}\text{Nd}/^{144}\text{Nd}$ ratios (Fig. 2.5). At comparable Sr isotope ratios each volcanic system has distinct $^{143}\text{Nd}/^{144}\text{Nd}$. The lowest $^{143}\text{Nd}/^{144}\text{Nd}$ occur at João de Castro, slightly higher $^{143}\text{Nd}/^{144}\text{Nd}$ at São Miguel and the highest Nd isotope ratios are found in Terceira and some Graciosa lavas. The Pb isotope systematics also reveals a complex variation with each volcanic system forming a distinct trend with different slopes (Fig. 2.5). The São Miguel lavas lie on a relatively steep slope ranging from high $^{207}\text{Pb}/^{204}\text{Pb}$ and $^{208}\text{Pb}/^{204}\text{Pb}$ at high $^{206}\text{Pb}/^{204}\text{Pb}$ to lower ratios resembling those of the Terceira axis flank samples. The Pb isotope ratios of lavas from João de Castro, Terceira and Graciosa show that each volcanic system lies on a separate slope in the $^{207}\text{Pb}/^{204}\text{Pb}$ and $^{208}\text{Pb}/^{204}\text{Pb}$ versus $^{206}\text{Pb}/^{204}\text{Pb}$ isotope spaces (Fig. 2.5). Lavas from João de Castro have lower Pb isotopic ratios than the other Terceira axis volcanoes and could represent the unradiogenic endmember for the São Miguel trend. The samples from Graciosa have slightly more radiogenic $^{208}\text{Pb}/^{204}\text{Pb}$ and $^{207}\text{Pb}/^{204}\text{Pb}$ ratios at a $^{206}\text{Pb}/^{204}\text{Pb}$ range comparable to Terceira but converge at the highest $^{206}\text{Pb}/^{204}\text{Pb}$. The $^{143}\text{Nd}/^{144}\text{Nd}$ and $^{206}\text{Pb}/^{204}\text{Pb}$ ratios of the Terceira axis samples are situated along a broad negative correlation (Fig. 2.5f) whereas the São Miguel samples lie on a trend orthogonal to the other Terceira axis lavas ranging towards low $^{143}\text{Nd}/^{144}\text{Nd}$ and high $^{206}\text{Pb}/^{204}\text{Pb}$ ratios. Importantly, the trends of the different volcanic systems of the Terceira axis as well as the MAR converge at a composition with $^{87}\text{Sr}/^{86}\text{Sr} \sim 0.7035$, $^{143}\text{Nd}/^{144}\text{Nd} \sim 0.5129$

and $^{206}\text{Pb}/^{204}\text{Pb}$ of 19.5. This composition may thus represent a common endmember inherent in all Terceira axis magmas and is tapped relatively undiluted by some lavas from Graciosa, Terceira and the western end of São Miguel. This, endmember also affects the adjoining MAR. The João de Castro lavas have the lowest $^{143}\text{Nd}/^{144}\text{Nd}$ and highest $^{208}\text{Pb}/^{206}\text{Pb}$ ratios (with the exception of the eastern São Miguel lavas) forming the other end-member of the Terceira axis.

2.6 DISCUSSION

2.6.1 Magma generation along the Terceira axis

The variations in degree of partial melting and melting depth can be modelled using both, the major elements and trace element ratios. The major elements SiO_2 , Al_2O_3 , and FeO^T yield information about variations in melting depth (e.g. Hirose & Kushiro, 1998). Whereas the SiO_2 contents in all Terceira axis lavas are comparable, we find that lavas from São Miguel show higher FeO^T and Dy/Yb ratios than the other volcanic systems (Figs. 2.3 and 2.4) implying a higher melting pressure with more residual garnet beneath São Miguel than beneath the other Terceira axis volcanoes. In order to study these variations in more detail the lava compositions were fractionation-corrected to 10 wt. % MgO . The Terceira axis lavas cover a broad negative trend with the highest

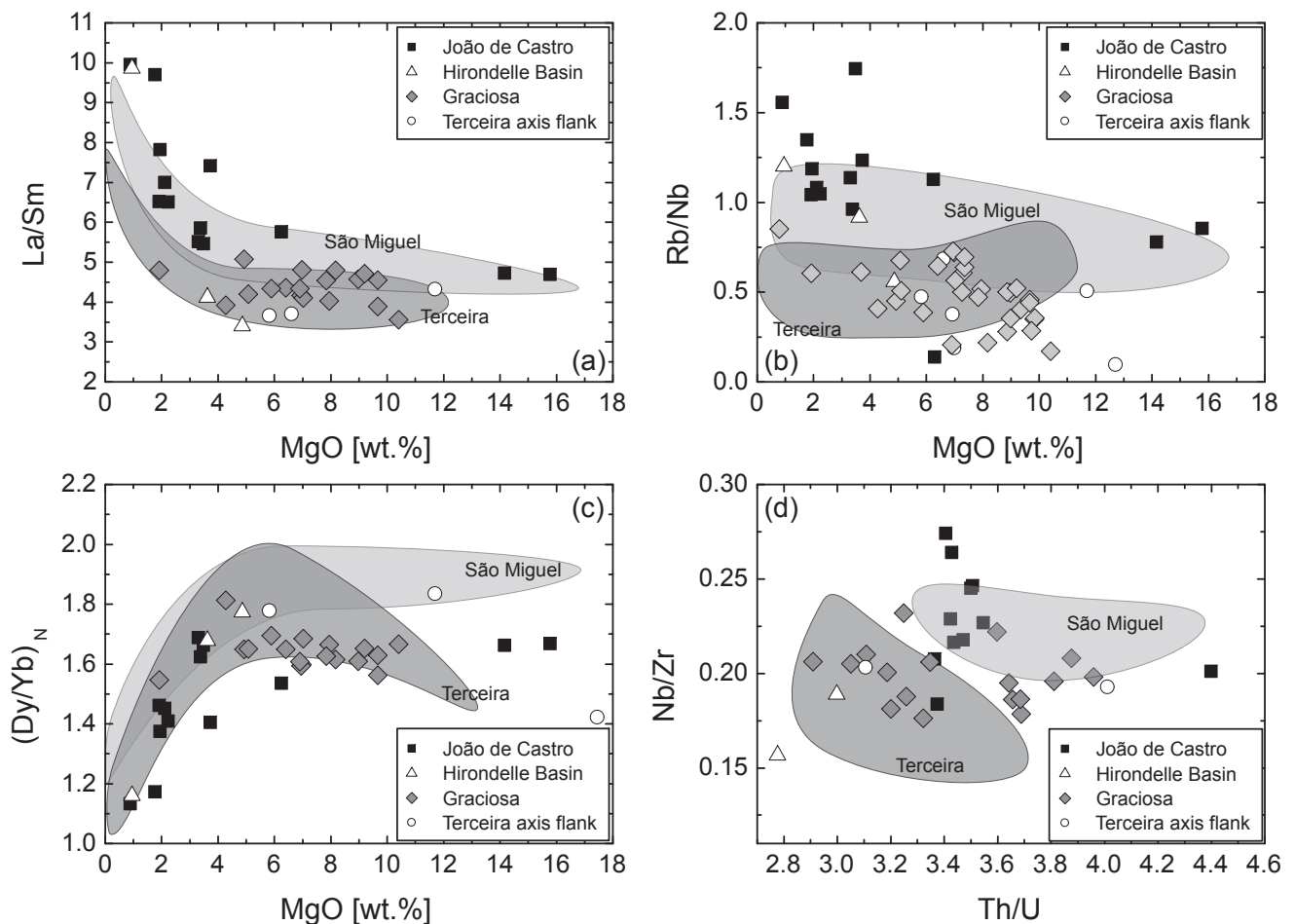


Figure 2.4: Trace element (a) La/Sm , (b) Rb/Nb and (c) PRIMA-normalised Dy/Yb ratios versus wt. % MgO of the Terceira axis lavas, and (d) Nb/Zr versus Th/U ratios of the Terceira axis lavas. Primitive mantle composition (PRIMA) from McDonough & Sun (1995).

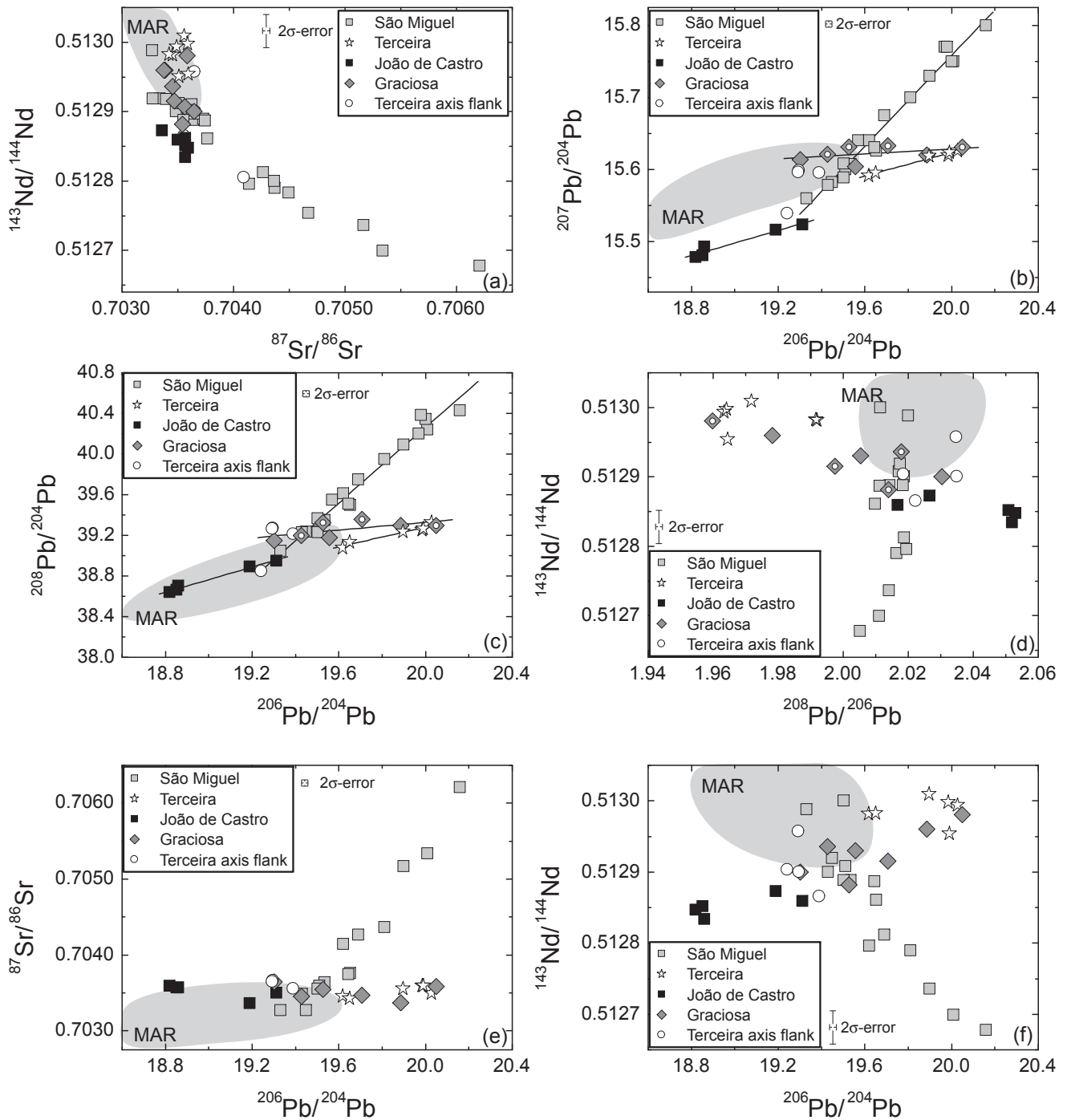


Figure 2.5: Isotope systematics of the Terceira axis. MAR indicates samples from the Mid-Atlantic Ridge from Dosso *et al.* (1999). Lines in (b) and (c) indicate linear arrays of São Miguel, Terceira, Graciosa, and João de Castro, respectively. All samples from João de Castro and Terceira are triple spike analyses. Triple spike analyses from Graciosa are marked with a white circle inside.

FeO^T and lowest Al_2O_3 at São Miguel and lowest FeO^T and highest Al_2O_3 in samples from Graciosa and Terceira (Fig. 2.6a). Lavas from the João de Castro volcanic system have Al_2O_3 comparable to São Miguel but as low FeO^T contents as the basalts from Graciosa. The presence of residual garnet during partial melting reduces the concentration of Al in the melt and thus the composition of the São Miguel basalts implies deeper melting than that of the western Terceira axis magmas in agreement with the high Fe concentrations and Dy/Yb ratios. Thus, the HREE ratios such as Dy/Yb of Graciosa, Terceira and São Miguel are correlated with the Al_2O_3 and FeO^T contents (Fig. 2.6b) suggesting that the pressure dependence of the major elements is reflected by increasing

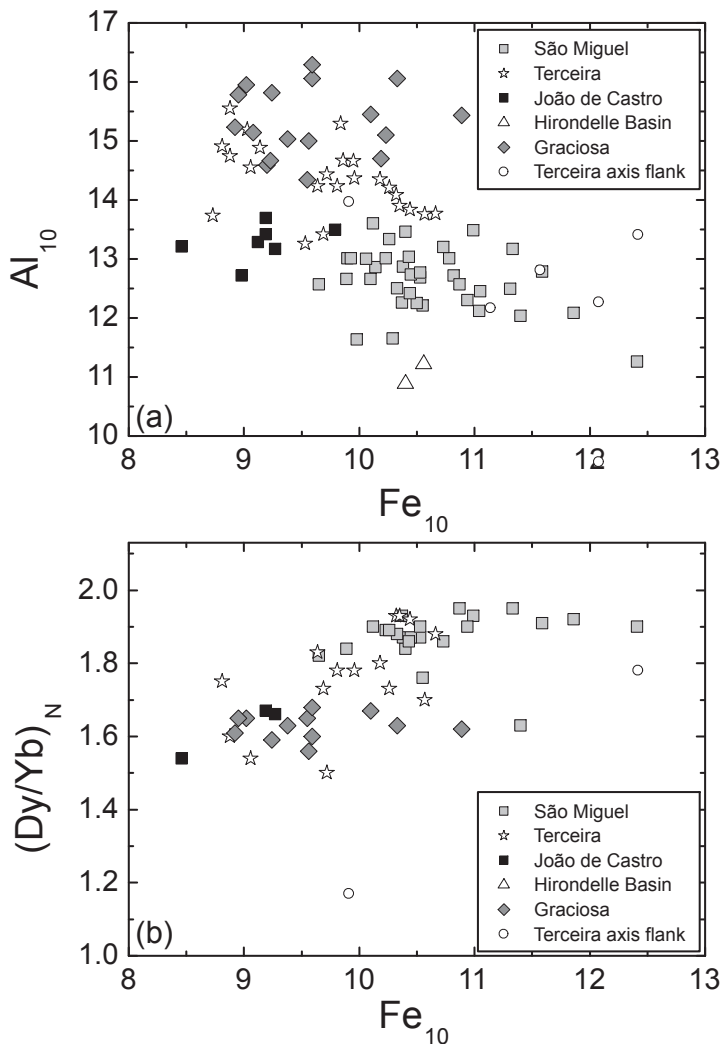


Figure 2.6: (a) Fractionation-corrected Al_2O_3 and FeO^T contents (10 wt.% MgO), and (b) PRIMA-normalised Dy/Yb ratios versus fractionation-corrected FeO^T . PRIMA composition from McDonough & Sun (1995).

amounts of garnet with increasing depth, and, hence, by varying HREE ratios. The Graciosa and some of the Terceira magmas have formed at lower pressures possibly ranging into the spinel peridotite stability field.

It has been shown that Na_2O and TiO_2 are incompatible elements and thus are sensitive to varying degrees of partial melting under anhydrous conditions (e.g. Hirschmann *et al.*, 1998; Hirschmann *et al.*, 1999). However, the fractionation-corrected Na_2O versus TiO_2 contents (Fig. 2.7a) show a broad negative correlation from highest TiO_2 and lower Na_2O for the São Miguel samples to lowered TiO_2 and slightly higher Na_2O concentrations at Terceira (Fig. 2.7a) contrary to the expected positive correlation. As the variations of Na_2O between the eastern and western islands are quite small (Fig. 2.3) compared to the TiO_2 contents (Fig. 2.4) it appears reasonable to assume that a variable TiO_2 rather than a varying Na_2O content is responsible for the observed pattern. Although the behaviour of Ti is complicated during partial melting, the Ti concentrations should increase with

decreasing degree of partial melting at degrees of partial melting below $\sim 10\%$ (Hirschmann *et al.*, 1999). The relatively enriched Ti contents at slightly lower Na contents of the São Miguel lavas compared to the Terceira lavas might therefore be either explained by an increased Ti concentration in the mantle source relative to Na or by an increased modal abundance of clinopyroxene during melting. If an increased Ti content in the mantle source would be responsible for this signature, Ti has to be enriched at least twice the amount of the Na concentration to produce the observed trend assuming the same modal composition for all Terceira axis mantle sources; i.e. the presence of a Ti enriched source seems unlikely as Ti is generally depleted or equal relative to Na in the mantle (e.g. McDonough & Sun, 1995; Salters & Stracke, 2004). Clinopyroxene is thought to be the major host of Ti in the Earth's mantle and also has the largest partition coefficient for TiO_2 in a peridotite mantle, which significantly increases at very small melt fractions (Baker *et al.*, 1995). Experimental phase constraints (Walter, 1998) have shown that the modal percentage of clinopyroxene increases at smaller melting intervals, hence, at smaller degrees of partial melting, which is consistent with the LREE ratios indicating slightly smaller degrees of partial melting at São Miguel. Modelling the Na and Ti contents and REE contents of the Terceira axis lavas (Fig. 2.7) using the batch-melting equation (Shaw, 1970) shows that the chemical mantle composition seems of minor importance compared to the modal mineral composition of the mantle. An increased amount of residual clinopyroxene at São Miguel leads to increased Ti concentrations but leaves the incompatible trace elements and

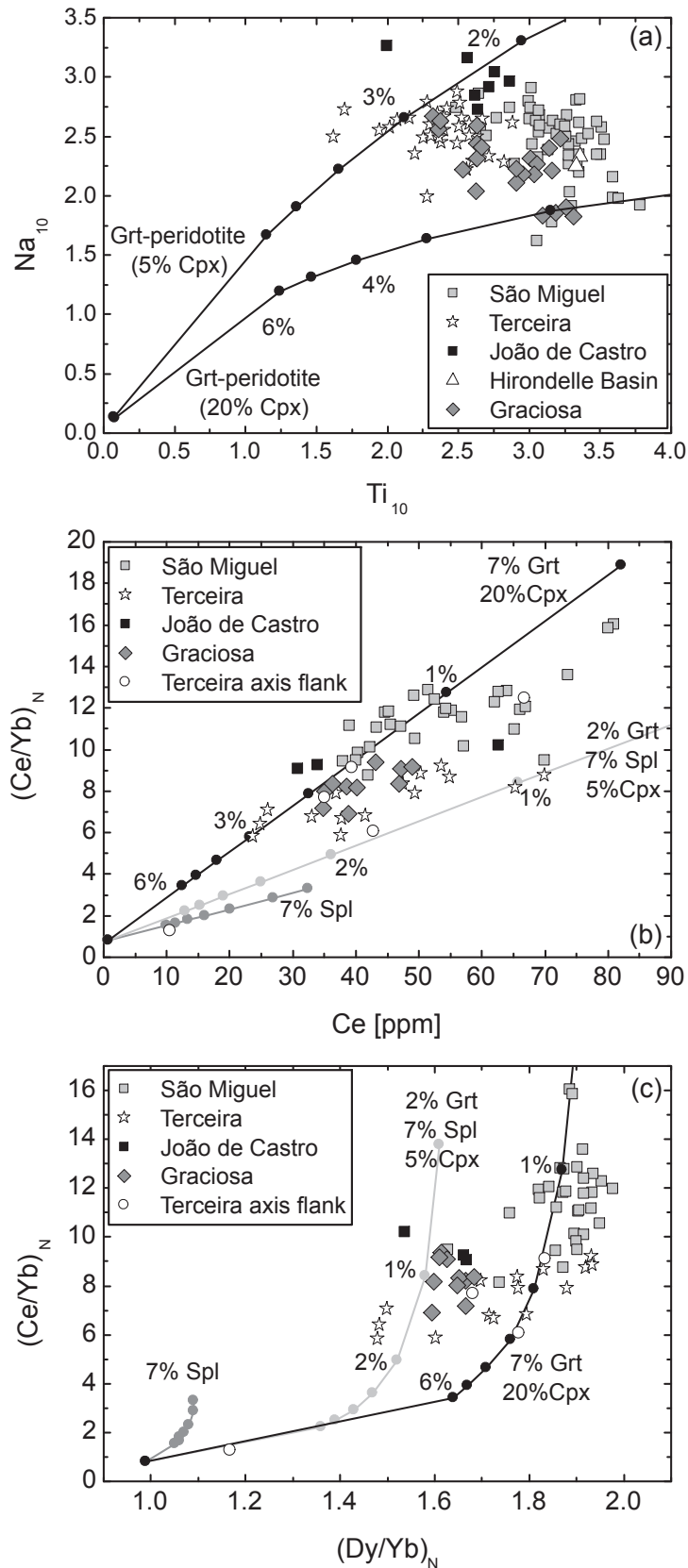


Figure 2.7: (a) Fractionation-corrected (10 wt. % MgO) Ti₁₀ versus Na₁₀ concentrations. The negative correlation of the Terceira axis samples can best be explained by varying amounts of clinopyroxene during melting. Degrees of partial melting correspond to the melting degrees inferred from the trace element ratios. (b & c) PRIMA-normalised trace element ratios of (b) Ce/Yb versus Ce and (c) PRIMA-normalised Dy/Yb. Tick marks of melting curves represent 0.5 %, 1 %, 2 %, 3 %, 5 %, and 6 % partial melting of a depleted mantle source after 1% melting of a pyrolite composition (McDonough & Sun, 1995). Different estimates have been modelled for a garnet peridotite (7 % Grt), a transitional garnet/spinel peridotite (2 % Grt, 7 % Spl) and a spinel peridotite (7 % Spl), respectively. PRIMA composition from McDonough & Sun (1995).

REE concentrations relatively unaffected (Fig. 2.7). Therefore, we suggest that a varying modal abundance of clinopyroxene seems to be a reasonable explanation for the Na-Ti systematics along the Terceira axis.

Modelling the REE ratios suggest comparable degrees of partial melting; the Ce/Yb versus Ce systematics are positively correlated in the Terceira axis samples indicating a slightly increasing degree of partial melting from São Miguel (lowest) over Graciosa (intermediate) to highest degrees of partial melting beneath Terceira with the lowest Ce/Yb ratio (Fig. 2.7b) as already inferred from the variations in La/Sm ratios (Fig. 2.4). Because the MREE and HREE are mostly sensitive to varying amounts of garnet, we will also use the even more incompatible trace elements to confirm the observations made by the La/Sm ratios. Our model suggests that the elevated Dy/Yb of the São Miguel and Terceira lavas formed by partial melting of garnet peridotite whereas the lower Dy/Yb of the western islands of Graciosa and Terceira (Fig. 2.7c) formed by melting of mantle containing ~ 2-3 % residual garnet and 7 % spinel, i.e. at the transition from garnet to spinel peridotite. If the source compositions are similar then the magmas from São Miguel and João de Castro have formed by slightly smaller degrees of partial melting (0.5 - 1 %) than the melts beneath the western Terceira axis ranging from 1 to 4 %. One sample from the Terceira axis flank is only slightly enriched in the light REE suggesting a higher degree of partial melting. We suggest that this sample formed some 5 Ma earlier during the impact of a plume head yielding the Azores oceanic plateau (Chapter I). Consequently, this sample cannot be taken into consideration for recent processes on the ultraslow spreading rift. We conclude that the magmas generated beneath Graciosa, Terceira and João de Castro have been generated in the garnet/spinel transition zone in contrast to the magmas beneath São Miguel which formed in the garnet peridotite stability field only. The degrees of partial melting along the axis indicate that, in general, the eastern volcanoes (João de Castro and São Miguel) have slightly lower degrees of partial melting than the western islands (Terceira and Graciosa).

The lack of a generally increasing depth of melting along the Terceira axis is consistent with magma generation beneath a spreading axis rather than beneath increasing lithospheric thickness with distance from the MAR (e.g. Cazenave, 1984). However, the formation of alkali basaltic melts beneath the Terceira axis implies relatively higher pressures and lower degrees of melting than on other ultraslow spreading axes such as the SWIR (~ 6 %, Hellebrand *et al.*, 2002) or the Arctic Gakkel Ridge (~ 5 %, Hellebrand & Snow, 2003). Thus, although a mantle plume may contribute relatively hot mantle to the region beneath the Azores the cooling from the surface leads to the creation of a thick lithospheric lid above the melting zone. Alternatively, the lithosphere formed at the MAR may be still largely intact and not yet thinned by the extension as a result of the relatively young spreading movement (< 6 Ma) of the Terceira axis. The large degrees of partial melting which possibly occurred in the plume head may have led to a significant depletion of the residual mantle which then may have had an increased rheological strength.

2.6.2 Mantle sources and mixing along the Terceira axis

Two different magma groups along the Terceira axis can be distinguished based on their K₂O contents where the Terceira and Graciosa lavas are lower than lavas from São Miguel and João de Castro (Fig. 2.3). These two groups can also be distinguished in terms of their Nb/Zr and Th/U ratios (Fig. 2.4) suggesting that the eastern volcanoes have more enriched mantle sources than the western volcanoes of the Terceira axis. A broad negative correlation between the ¹⁴³Nd/¹⁴⁴Nd isotope ratios and the K concentrations (and ratios such as K/Ti, K/U) confirm that these variations are mainly a result of mantle source signatures (Fig. 2.8). The isotope ratios of Sr and

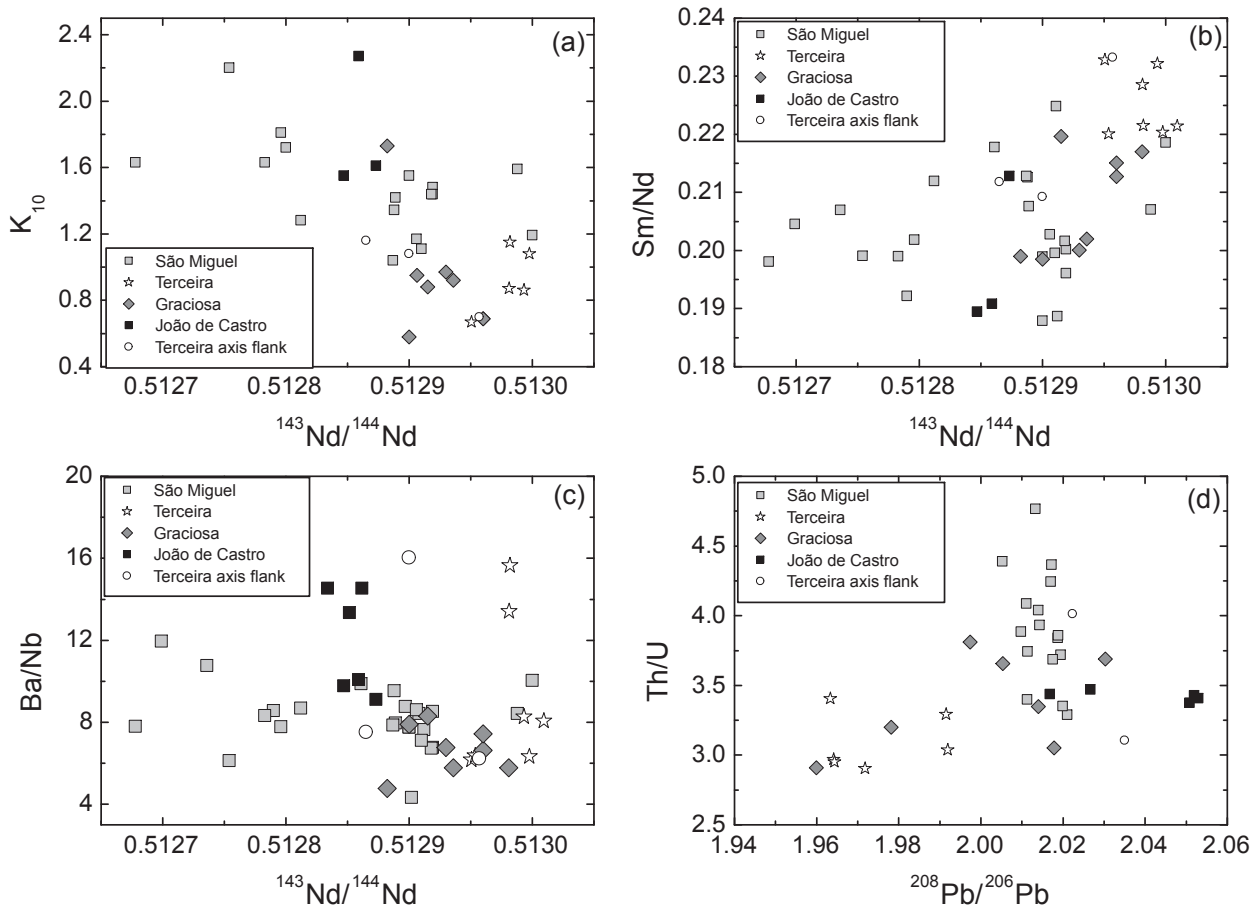


Figure 2.8: Mantle source systematics along the Terceira axis showing variations in (a) fractionation-corrected (10 wt. % MgO) K-contents, (b) Sm/Nd and (c) Ba/Nb ratios versus Nd isotope ratios and Th/U versus $^{208}\text{Pb}/^{206}\text{Pb}$ ratios.

Nd are also correlated to La/Sm, Rb/Nb, Ba/Rb, Th/Nb and Th/U. The lavas with the highest $^{143}\text{Nd}/^{144}\text{Nd}$ from Terceira also have the highest Sm/Nd but lavas from São Miguel have both, variable Sm/Nd and $^{143}\text{Nd}/^{144}\text{Nd}$ (Fig. 2.8) suggesting that partial melting processes probably affected the Sm/Nd.

The linear Pb isotope arrays of Graciosa, João de Castro and Terceira either reflect true isochrons or binary mixing lines. The results from reduced chi-squared regression lines of the triple spike data indicate a slope of 0.08733 ± 0.00547 for the João de Castro lavas which is comparable to the slope at Terceira (0.08418 ± 0.00355) in the $^{207}\text{Pb}/^{204}\text{Pb}$ versus $^{206}\text{Pb}/^{204}\text{Pb}$ space. If these slopes represent isochrons the corresponded ages would be 1.37 ± 0.12 and 1.31 ± 0.09 Ga, respectively. A calculated regression line from Graciosa gives a slope of 0.00943 ± 0.00657 , which is situated far outside the calculated isochron slopes giving evidence that the Graciosa samples most likely represent binary mixing rather than an isochron. If the $^{207}\text{Pb}/^{204}\text{Pb}$ - $^{206}\text{Pb}/^{204}\text{Pb}$ regression lines of João de Castro and Terceira are mantle isochrons this should also be the case for the linear arrays in the $^{208}\text{Pb}/^{204}\text{Pb}$ versus $^{206}\text{Pb}/^{204}\text{Pb}$ space. Hence, the inferred source K ($^{232}\text{Th}/^{238}\text{U}$) values from the measured Th and U (K_{TE}) concentrations and from the $^{208}\text{Pb}/^{206}\text{Pb}$ ratios (K_{ISO}) should be correlated, i.e. the K_{TE} should be equal or higher than the K_{ISO} if formed by melting as a result of the fractionation of Th and U during melting (Beattie, 1993). In contrast to the prediction the K_{TE} values of João de Castro and Terceira are considerably lower than the K_{ISO} which is inconsistent with the expected Th/U fractionation during melting (Abouchami *et al.*, 2000). Therefore we suggest that the linear arrays in the $^{207}\text{Pb}/^{204}\text{Pb}$ - $^{206}\text{Pb}/^{204}\text{Pb}$ and $^{208}\text{Pb}/^{204}\text{Pb}$ - $^{206}\text{Pb}/^{204}\text{Pb}$ systematics do not represent mantle isochrons but more likely reflect mixing lines between two distinct mantle sources on

each array.

The lavas from Terceira and Graciosa resemble each other in $^{206}\text{Pb}/^{204}\text{Pb}$ compositions but significant differences exist in $^{207}\text{Pb}/^{204}\text{Pb}$, $^{208}\text{Pb}/^{204}\text{Pb}$ and $^{143}\text{Nd}/^{144}\text{Nd}$ ratios. Thus, the Terceira lavas have too high $^{143}\text{Nd}/^{144}\text{Nd}$, and too low $^{207}\text{Pb}/^{204}\text{Pb}$ and $^{208}\text{Pb}/^{206}\text{Pb}$ to represent the mixing end-member for Mid-Ocean Ridge Basalts (MORB) from the adjoining MAR (Fig. 2.5) and rather, the material influencing the spreading axis has a composition similar to the Graciosa mantle source. In fact, the unradiogenic Graciosa lavas lie close to the point of convergence of the trends of all Terceira axis and MAR lavas which may suggest that they represent a mantle end-member inherent in all Terceira axis magmas as well as MORB close to the Azores. Relatively primitive He isotope ratios beneath Terceira (Moreira *et al.*, 1999a) and at the MAR have been interpreted to be the result of plume-ridge interactions between the plume centre at Terceira and the MAR. The $^{143}\text{Nd}/^{144}\text{Nd}$ and $^{206}\text{Pb}/^{204}\text{Pb}$ similarities between the MAR and Graciosa suggest mixing of the common Graciosa mantle source into the MAR mantle, and, thus, gives evidence for a mantle flux from Graciosa towards the MAR. Although the primitive He isotopes found at the MAR and Terceira suggest mixing of material from Terceira into the MAR, the Nd isotope ratios of Terceira are too high to account for the enrichment of the MAR. As no He isotope measurements are known from Graciosa and the origin of primitive He isotopic composition are still a matter of debate, we suggest that the enriched MAR signature is a result of mantle flux from Graciosa to the MAR.

Our new data reveal that rather than the three end-members suggested by previous authors (e.g. Moreira *et al.*, 1999b) four end-members are required to explain the isotopic variation of the Azores lavas. The three end-members were believed to be MORB, a plume component represented by Terceira lavas, and an enriched mantle component represented by lavas from eastern São Miguel. We suggest that the mantle plume component is rather represented by the common end-member observed in the Graciosa lavas with low Sr and Pb isotope ratios because this component appears to be most widely distributed in the mantle beneath the Azores and also represents the component influencing the MAR. Because it mixes with the enriched São Miguel end-member which has very high $^{207}\text{Pb}/^{204}\text{Pb}$ and $^{208}\text{Pb}/^{204}\text{Pb}$ ratios (Fig. 2.5) this plume component occurs as far east as São Miguel.

Each of the mixing arrays in the Sr-Nd-Pb isotope ratios therefore gives evidence of mixing between two mantle end-members although they converge on one composition roughly reflected by the unradiogenic Graciosa samples (Fig. 2.5). The common source of the João de Castro seamount apparently mixes with a relatively unradiogenic mantle source different from MORB as indicated by the lower Nd isotope ratios. At Graciosa and Terceira the common end-member mixes with a source having radiogenic Pb isotope ratios but high Nd and relatively low Sr isotopes, in that sense comparable to the HIMU ocean island lavas (high μ = high $^{238}\text{U}/^{204}\text{Pb}$) such as St. Helena (e.g. Zindler & Hart, 1986). The linear array at Graciosa covers a comparable $^{206}\text{Pb}/^{204}\text{Pb}$ range but the much shallower linear array at Graciosa is due to more radiogenic $^{208}\text{Pb}/^{204}\text{Pb}$ and $^{207}\text{Pb}/^{204}\text{Pb}$ ratios and is also reflected in higher $^{208}\text{Pb}/^{206}\text{Pb}$ ratios at Graciosa than at Terceira (Fig. 2.5). The radiogenic Pb end-member compositions of Terceira and Graciosa suggest interaction between the two systems but their relatively unradiogenic Pb end-member compositions give evidence that the two relatively unradiogenic mantle sources are slightly distinct, i.e. the common end-member shows some variation. Although the linear arrays of the Graciosa, Terceira and western São Miguel samples meet at similar ratios in the isotope spaces, the combined trace element (K, Th/U, Nb/Zr, La/Sm) and Sr-Nd-Pb isotope systematics shows that each volcano along the axis contains its own isolated mantle source implying significant heterogeneity in the mantle beneath the Azores on a scale of about 100 km. The limited mixing between different sources has also been observed on a much

smaller scale of about 20 km between the western and eastern volcanoes at São Miguel (Haase & Beier, 2003). Although the Pb isotopes ratios of the Terceira axis volcanoes suggest a slightly variable common component that resembles the lavas from western São Miguel and Graciosa, the trace element and Nd isotope ratios give evidence that each volcanic system is apparently fed by a different mantle source.

2.6.3 Comparison to other ultraslow ridges

The Terceira axis is characterised by an amagmatic - magmatic segmentation pattern that has also been observed along the Southwest Indian Ridge (SWIR; Sauter *et al.*, 2004a) and the Arctic Gakkel Ridge (Michael *et al.*, 2003). These ridges are defined by large magmatic segments with a thicker lithosphere bordered by deeper amagmatic basins with a relatively thin lithosphere. The amagmatic segments at the SWIR are also characterised by either the presence of sediments or peridotitic rocks, a feature that we can only suspect in the Azores from bathymetric maps (e.g. Smith & Sandwell, 1997). The magmatic segments of both ridges typically consist of large volcanic structures, which, in the case of the Terceira axis, form islands. As Vogt & Jung (2004) pointed out, the extreme topographic variation at the Terceira axis may be a result of the presence of anomalous mantle beneath the Azores which led to the formation of a shallow oceanic plateau which is then divided by the Terceira axis.

On the other hand, the degree of melting beneath the Terceira axis is comparable or lower than beneath the other ultraslow ridges because the magmas are alkaline in the Azores and tholeiitic for the Gakkel Ridge and the SWIR (e.g. Michael *et al.*, 2003). The process of conductive cooling becomes important at ultraslow spreading rates (<20 mm/a) leading to a decrease of melting at greater depth and lower degrees of partial melting (Reid & Jackson, 1981). The smaller degrees of partial melting at the Terceira axis are probably a result of the thicker surrounding lithosphere at the Terceira axis and the relatively recent onset of spreading (< 6 Ma from $^{40}\text{Ar}/^{39}\text{Ar}$ age determinations; Chapter I) which leads to a thick lithospheric lid and deep melting beneath the Terceira axis. In contrast, spreading has been established for a long time at the Gakkel Ridge and SWIR leading to a thin lithosphere and shallow melting. The obliquity of ultraslow spreading rifts also has an important impact onto melting processes; i.e. an increasing obliquity leads to decreasing effective spreading rates, lower upwelling velocities and smaller melt fractions (Okino *et al.*, 2002). The spreading rate along the Terceira axis increases from the east (3.7 mm/a) to the western edge (4.5 mm/a) and obliquity decreases from São Miguel (61°) to Graciosa (40°, Vogt & Jung, 2004). We suggest that the smaller degrees of partial melting at the Terceira axis compared to other ultraslow spreading rifts are a result of a combination of a thicker, relatively older lithosphere with a very slow spreading rate and a higher obliquity. The formation of islands along the axis, despite the smaller degrees of partial melting, may be a result of a relatively stable mantle plume beneath the axis generating melts over relatively long time periods. The distinct variations of melting degrees between the Terceira axis volcanoes gives either evidence for a limited melt production beneath the bathymetric basins or a highly focused magmatism along the axis like it has been proposed from the SWIR (Sauter *et al.*, 2004b).

The presence of well defined, distinct mantle sources beneath each island/seamount inferred from trace element and Nd and Pb isotope systematics suggests that focused magmatism occurs along the Terceira axis as it has been proposed from geophysical observations along the SWIR. The focusing most likely occurs in distinct mantle diapirs which underlie each volcanic system but lack beneath the amagmatic basins. Within the diapirs the melts are focussed to the surface and may mix within each diapir but not among different diapiric structures (Crane, 1985; Okino *et al.*, 2002). The diapiric melts that have lower densities and viscosities than the surround-

ing mantle move towards regularly-spaced established gravitational instabilities of the partially molten mantle by porous flow avoiding mixing between the segments (Whitehead *et al.*, 1984; Schouten *et al.*, 1985; Lin *et al.*, 1990). The initial establishment of gravitational melt instabilities is mainly controlled by the continuity and thickness of the underlying melt layer (Crane, 1985; Michael *et al.*, 2003), whereas the spacing of magmatic centres is mainly controlled by the effective spreading rate (Schouten *et al.*, 1985). Slower spreading rates are correlated to smaller distances between the magmatic segments consistent with the relatively small scale segmentation pattern (10-30 km) observed along the Terceira axis and other slow spreading rifts (e.g. Gakkel Ridge, SWIR) compared to faster spreading ridges such as the MAR (50-80 km).

2.7 CONCLUSIONS

We conclude that the melting depth along the Terceira axis does not vary systematically beneath Graciosa, Terceira and João de Castro, where melts are generated in the spinel/garnet transition zone (Fig. 2.9). However, deeper melting in the garnet stability field is observed at São Miguel, the island most distant from the MAR and possibly with the thickest lithosphere. The degrees of partial melting are smaller at São Miguel and João de

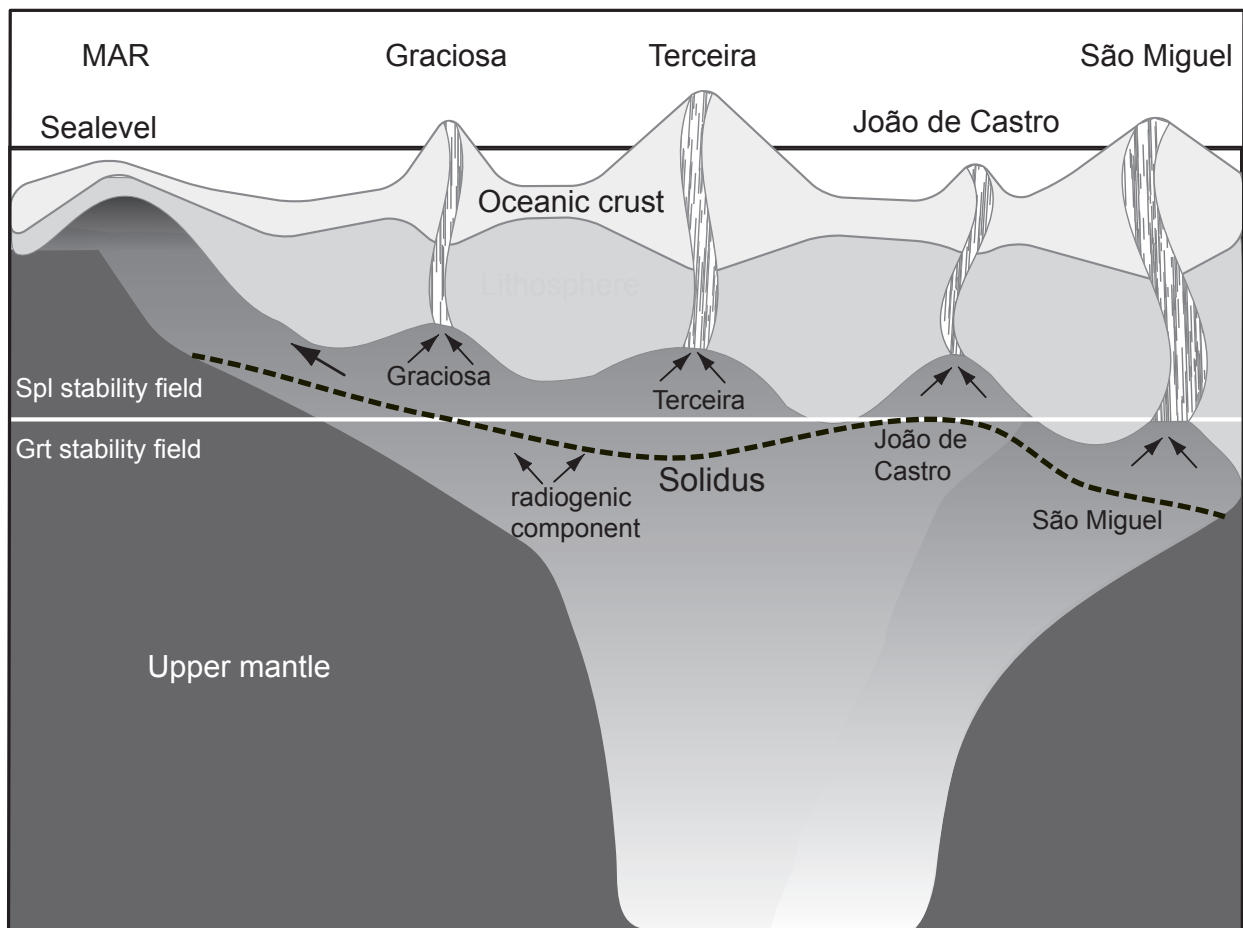


Figure 2.9: Sketch illustrating the processes dominating the Terceira axis evolution. The melting regions of Graciosa, João de Castro and Terceira are situated within the spinel/garnet transition zone at approximately 80 km depth. The São Miguel melts are generated within the garnet stability field, only. The mixing relationships described in the main text suggest only very limited mixing between each islands source. The occurrence a of a typical amagmatic – magmatic segmentation pattern has its origin in focused magmatism comparable to the SWIR. The isotope systematics suggest a mantle flux from Graciosa towards the adjoining MAR. Not to scale.

Castro compared to the other volcanic systems along the axis. Compared to other very slow spreading axes the generally low degrees of partial melting at the Terceira axis result from a combination of a thick lithospheric lid and a relatively young (< 6 Ma) and ultraslow spreading movement combined with a high obliquity (40° to 61°). Although the Terceira axis has lower degrees of partial melting compared to the SWIR or Gakkel Ridge, the presence of a stable anomalous upper mantle generates enough melts over relatively long time periods to enable subaerial volcanism. The incompatible trace element ratios (e.g. Th/U, Nb/Zr) and combined Sr-Nd-Pb isotopes suggest that every volcanic system along the Terceira axis is situated on a single binary mixing trend without evidence of mixing in between (Fig. 2.9). The limited mixing is attributed to both, the presence of geochemical boundaries and the occurrence of focused magmatism as it has been also observed on other ultraslow spreading rifts. The amagmatic – magmatic segmentation pattern along the Terceira axis is comparable to the structures observed along the SWIR. This gives evidence that these segmentation patterns belongs to characteristic features of ultraslow spreading rifts with spreading rates < 14 mm/a. The trace element and isotope similarities between Graciosa and the MAR suggest a mantle flux from Graciosa towards the MAR. This leads to the observed enriched MORB compositions along the MAR. However, the occurrence of primitive He isotope signatures at Terceira and the MAR may not be of similar origin as the Nd and Pb isotope ratios of Terceira give evidence that the Graciosa mantle source may be responsible for the MAR enrichment rather than mantle material from Terceira.

2.8 ACKNOWLEDGMENTS

We gratefully acknowledge the help of captain and crew of RV Poseidon for their help during the recovery of the samples. D. Garbe-Schönberg is thanked for the ICP-MS analyses. This study has been funded by the Deutsche Forschungsgemeinschaft through grants Ha 2568/6-1, Ha 2568/9-2, and Ha 2100/7-1.

REFERENCES

- Abouchami, W., Galer, S.J.G. and Hofmann, A.W. (2000) High precision lead isotope systematics of lavas from the Hawaiian Scientific Drilling Project. *Chemical Geology* **169**, 187-209.
- Baker, M.B., Hirschmann, M.M., Ghiorso, M.S. and Stolper, E.M. (1995) Compositions of near-solidus peridotite melts from experiments and thermodynamic calculation. *Nature* **375**, 308-311.
- Beattie, P. (1993) Uranium-thorium disequilibria and partitioning on melting of garnet peridotite. *Nature (London)* **363**, 63-65.
- Beier, C., Haase, K.M. and Hansteen, T.H. (2006) Magma evolution of the Sete Cidades volcano, São Miguel, Azores. *Journal of Petrology*, DOI: 10.1093/petrology/egl014.
- Bonatti, E. (1990) Not so hot “hot spots” in the oceanic mantle. *Science* **250**, 107-111.
- Cannat, M., *et al.* (1999) Mid-Atlantic Ridge - Azores hotspot interactions: along-axis migration of a hotspot-derived event of enhanced magmatism 10 to 4 Ma ago. *Earth and Planetary Science Letters* **173**, 257-269.
- Cazenave, A. (1984) Thermal cooling of the oceanic lithosphere; new constraints from geoid height data. *Earth and Planetary Science Letters* **70**, 395-406.

- Cochran, J.R., Kurras, G.J., Edwards, M.H. and Coakley, B.J. (2003) The Gakkel Ridge; bathymetry, gravity anomalies, and crustal accretion at extremely slow spreading rates. *Journal of Geophysical Research, B, Solid Earth and Planets* **108**, DOI: 10.1029/2002JB001830
- Crane, K. (1985) The spacing of rift axis highs; dependence upon diapiric processes in the underlying asthenosphere? *Earth and Planetary Science Letters* **72**, 405-414.
- Dick, H.J.B., Lin, J. and Schouten, H. (2003) An ultraslow-spreading class of ocean ridge. *Nature* **426**, 405-412.
- Dosso, L., Bougault, H., Langmuir, C., Bollinger, C., Bonnier, O. and Etoubleau, J. (1999) The age and distribution of mantle heterogeneity along the Mid-Atlantic Ridge (31-41°N) *Earth and Planetary Science Letters*. 269-286.
- Eisele, J., Sharma, M., Galer, S.J.G., Blichert-Toft, J., Devey, C.W. and Hofmann, A.W. (2002) The role of sediment recycling in EM-1 inferred from Os, Pb, Hf, Nd, Sr isotope and trace element systematics of the Pitcairn hotspot. *Earth and Planetary Science Letters* **196**, 197-212.
- Fernandes, R.M.S., Bastos, L., Miranda, J.M., Lourenço, N., Ambrosius, B.A.C., Noomen, R. and Simons, W. (accepted) Defining the Plate Boundaries in the Azores Region. *Journal of Volcanology and Geothermal Research*.
- Galer, S.J.G. (1999) Optimal double and triple spiking for high precision lead isotopic measurement. *Chemical Geology* **157**, 255-274.
- Garbe-Schönberg, C.-D. (1993) Simultaneous determination of thirty-seven trace elements in twenty-eight international rock standards by ICP-MS. *Geostandards Newsletters* **17**, 81-97.
- Grimison, N.L. and Chen, W.P. (1986) The Azores-Gibraltar plate boundary; focal mechanisms, depths of earthquakes, and their tectonic implications. *Journal of Geophysical Research*. **B. 91**, 2029-2047.
- Grimison, N.L. and Chen, W.P. (1988) Source mechanisms of four Recent earthquakes along the Azores-Gibraltar plate boundary. *Geophysical Journal of the Royal Astronomical Society* **92**, 391-401.
- Haase, K.M. (1996) The relationship between the age of the lithosphere and the composition of oceanic magmas: Constraints on partial melting, mantle sources and the thermal structure of the plates. *Earth and Planetary Science Letters* **144**, 75-92.
- Haase, K.M. and Beier, C. (2003) Tectonic control of ocean island basalt sources on Sao Miguel, Azores? *Geophysical Research Letters* **30**, 1856.
- Hellebrand, E. and Snow, J.E. (2003) Deep melting and sodic metasomatism underneath the highly oblique-spreading Lena Trough (Arctic Ocean). *Earth and Planetary Science Letters* **216**, 283-299.
- Hellebrand, E., Snow, J.E., Hoppe, P. and Hofmann, A.W. (2002) Garnet-field Melting and Late-stage Refertilization in 'Residual' Abyssal Peridotites from the Central Indian Ridge. *Journal of Petrology* **43**, 2305-2338.
- Hirose, K. and Kushiro, I. (1998) The effect of melt segregation on polybaric mantle melting; estimation from the incremental melting experiments. In: *Magmatology; the role of magmas in the evolution of the Earth*. 111-118. Elsevier: Amsterdam, Netherlands.
- Hirschmann, M.M., Ghiorso, M.S. and Stolper, E.M. (1999) Calculation of peridotite partial melting from thermodynamic models of minerals and melts; II, Isobaric variations in melts near the solidus and owing to variable source composition. *Journal of Petrology* **40**, 297-313.

- Hirschmann, M.M., Ghiorso, M.S., Wasylenki, L.E., Asimow, P.D. and Stolper, E.M. (1998) Calculation of Peridotite Partial Melting from Thermodynamic Models of Minerals and Melts. I. Review of Methods and Comparison with Experiments. *Journal of Petrology* **39**, 1091-1115.
- Le Maitre, R. (ed.) (1989) *A classification of igneous rocks and glossary of terms, recommendations of the International union of geological sciences, subcommission on the systematics of igneous rocks*. Blackwell: Oxford, London.
- Lin, J., Purdy, G.M., Schouten, H., Sempere, J.C. and Zervas, C. (1990) Evidence from gravity data for focused magmatic accretion along the Mid-Atlantic Ridge. *Nature (London)* **344**, 627-632.
- Luis, J.F., Miranda, J.M., Galdeano, A. and Patriat, P. (1998) Constraints on the structure of the Azores spreading center from gravity data. *Marine Geophysical Researches* **20**, 157-170
- Luis, J.F., Miranda, J.M., Galdeano, A., Patriat, P., Rossignol, J.C. and Mendes Victor, L.A. (1994) The Azores triple junction evolution since 10 Ma from aeromagnetic survey of the Mid-Atlantic Ridge. *Earth and Planetary Science Letters* **125**, 439-459.
- Macdonald, G.A. (1968) Composition and origin of Hawaiian lavas. In: *Studies in volcanology--A memoir in honor of Howel Williams*. 477-522. Geological Society of America (GSA): Boulder, CO, United States.
- Macdonald, K.C. (1982) Mid-ocean ridges; fine scale tectonic, volcanic and hydrothermal processes within the plate boundary zone. *Annual Review of Earth and Planetary Sciences* **10**, 155-190.
- McDonough, W.F. and Sun, S.-S. (1995) The composition of the Earth. *Chemical Geology* **120**, 223-253.
- Michael, P.J., *et al.* (2003) Magmatic and amagmatic seafloor generation at the ultraslow-spreading Gakkel ridge, Arctic Ocean. *Nature* **423**, 956-962.
- Miranda, J.M., *et al.* (1998) Tectonic Setting of the Azores Plateau deduced from a OBS survey. *Marine Geophysical Researches* **20**, 171-182.
- Moreira, M., Doucelance, R., Dupre, B., Kurz, M. and Allegre, C.J. (1999a) Helium and lead isotope geochemistry in the Azores Archipelago. In: *European Union of Geosciences conference abstracts; EUG 10*. pp. 814. Cambridge Publications: Cambridge, United Kingdom.
- Moreira, M., Doucelance, R., Kurz, M.D., Dupre, B. and Allegre, C.J. (1999b) Helium and lead isotope geochemistry of the Azores Archipelago. *Earth and Planetary Science Letters* **169**, 189-205.
- Nunes, J.C., Forjaz, V.H., Alves, J.L. and Bernardes, A.C. (2003) Caracterização vulcanológica do Banco D. João de Castro (Açores): novos dados. *Ciências da Terra (UNL)* **V**, D55-D58.
- Okino, K., Curewitz, D., Asada, M., Tamaki, K., Vogt, P. and Crane, K. (2002) Preliminary analysis of the Knipovich Ridge segmentation; influence of focused magmatism and ridge obliquity on an ultraslow spreading system. *Earth and Planetary Science Letters* **202**, 275-288.
- Reid, I. and Jackson, H.R. (1981) Oceanic spreading rate and crustal thickness. *Marine Geophysical Researches* **5**, 165-172.
- Ritsema, J. and Allen, R.M. (2003) The elusive mantle plume. *Earth and Planetary Science Letters* **207**, 1-12.
- Salters, V.J.M. and Stracke, A. (2004) Composition of the depleted mantle. *Geochemistry, Geophysics, Geosystems* **5**, DOI: 10.1029/2003GC000597.

- Sauter, D., Carton, H., Mendel, V., Munsch, M., Rommevaux, J.C., Schott, J.J. and Whitechurch, H. (2004a) Ridge segmentation and magnetic structure of the Southwest Indian Ridge (at 50 degrees 30'E, 55 degrees 30'E and 66 degrees 20'E); implications for magmatic processes at ultraslow-spreading centers. *Geochemistry, Geophysics, Geosystems* **5**, Doi:10.1029/2003GC000581
- Sauter, D., Mendel, V., Rommevaux-Jestin, C., Parson, L.M., Fujimoto, H., Mével, C., Cannat, M. and Tamaki, K. (2004b) Focused magmatism versus amagmatic spreading along the ultra-slow spreading Southwest Indian Ridge: Evidence from TOBI side scan imagery. *Geochemistry, Geophysics, Geosystems* **5**, DOI: 10.1029/2004GC000738.
- Schilling, J.-G., Bergeron, M.B. and Evans, R. (1980) Halogens in the mantle beneath the North Atlantic. *Philosophical Transactions of the Royal Society of London* **A297**, 147-178.
- Schouten, H., Klitgord, K.D. and Whitehead, J.A. (1985) Segmentation of mid-ocean ridges. *Nature (London)* **317**, 225-229.
- Shaw, D.M. (1970) Trace element fractionation during anatexis. *Geochimica et Cosmochimica Acta* **34**, 237-243.
- Smith, W. and Sandwell, D. (1997) Measured and estimated seafloor topography (version 4.2). World Data Center A for Marine Geology and Geophysics research publication RP-1.
- Todt, W., Cliff, R.A., Hanser, A. and Hofmann, A.W. (1996) Evaluation of a ^{202}Pb - ^{205}Pb double spike for high-precision lead isotope analyses. In: AGU (ed.) *Earth-Processes: Reading the isotopic code*. pp. 429-437.
- Udias, A., Lopez, A.A. and Mezcuca, J. (1976) Seismotectonic of the Azores-Alboran region. *Tectonophysics* **31**, 259-289.
- Vogt, P.R. and Jung, W.Y. (2004) The Terceira Rift as hyper-slow, hotspot-dominated oblique spreading axis: A comparison with other slow-spreading plate boundaries. *Earth and Planetary Science Letters* **218**, 77-90.
- Walter, M.J. (1998) Melting of garnet peridotite and the origin of komatiite and depleted lithosphere. *Journal of Petrology* **39**, 29-60.
- Whitehead, J.A., Jr., Dick, H.J.B. and Schouten, H. (1984) A mechanism for magmatic accretion under spreading centres. *Nature (London)* **312**, 146-148.
- Zindler, A. and Hart, S. (1986) Chemical Geodynamics. *Annual Review of Earth and Planetary Science Letters* **14**, 493-571.

CHAPTER III

RELICS OF A SUBDUCTED SEAMOUNT: THE SÃO MIGUEL MANTLE SOURCE

Christoph Beier^{1,2}, Andreas Stracke², Karsten M. Haase^{1,3}

¹Institut für Geowissenschaften, Christian-Albrechts-Universität zu Kiel, Ludewig-Meyn-Straße 10, 24118 Kiel, Germany, Email: chb@gpi.uni-kiel.de

²Max-Planck-Institut für Chemie (Otto-Hahn-Institut), Abteilung Geochemie, Joh.-Joachim-Becher-Weg 27, 55128 Mainz, Germany

³Department of Earth Sciences, University of Aarhus, C.F. Møllers Allé 110, 8000 Aarhus C, Denmark

3.1 ABSTRACT

The island of São Miguel in the Azores consists of three large volcanic systems and two overlapping zones with smaller scoria cones. The westernmost volcano Sete Cidades has Sr-Nd-Hf-Pb isotope ratios and trace element compositions that resemble the compositions commonly associated with the so-called FOZO compositions. The easternmost volcano Nordeste comprises an isotopic signature that is unusual upon the Earth's known isotopic compositions, i.e. the Nordeste isotope ratios point towards higher $^{208}\text{Pb}/^{204}\text{Pb}$ and $^{87}\text{Sr}/^{86}\text{Sr}$ isotope ratios and lower $^{143}\text{Nd}/^{144}\text{Nd}$ and $^{176}\text{Hf}/^{177}\text{Hf}$ isotope ratios at $^{206}\text{Pb}/^{204}\text{Pb}$ ratios comparable to Sete Cidades. Both volcanoes are situated along a linear mixing array in the Sr-Nd-Pb-Hf isotope spaces. The LREE concentrations and the according trace element ratios suggest relatively constant degrees of partial melting along the island, although the HREE indicate slightly lower amounts of garnet in the Nordeste mantle source. The incompatible elements of Nordeste are enriched compared to Sete Cidades. The Sr, Eu, Ti, and Ba concentrations are relatively depleted at Nordeste and Th is enriched relative to U. The incompatible trace element ratios such as U/Pb, Th/Pb, Rb/Sr, Nb/Zr, and Nb/La are correlated to the isotopic variations indicating that one single process is responsible for the unusual Nordeste trace element and isotopic signature. The trace element concentrations of both volcanoes show similarities to the HIMU incompatible element compositions, however, both islands do not perfectly cover the HIMU pattern, because the highly incompatible elements Rb and Ba are enriched relative to Th. The similarities between the two volcanic system suggest that they share a common source component. Geochemical models at Sete Cidades suggest that this can mainly be explained by the occurrence of a subducted, recycled, slightly altered enriched oceanic crust, which has been less influenced by subduction modification compared to the HIMU sources. A variety of models have been proposed for the evolution of the Nordeste mantle source, e.g. the presence of sediments, delamination of subcontinental lithosphere, and melting processes. Our new model is able to explain both, trace element and isotope variations of Nordeste with a recycled enriched oceanic crust combined with the presence of altered and recycled trachyte from a subducted seamount. The geodynamic implications of the model suggest that both endmember mantle sources on São Miguel originated from recycling of oceanic crust, but with an additional enriched component present at Nordeste.

3.2 INTRODUCTION

The chemical and isotopic variability observed in ocean island lavas is a key factor for deciphering the composition and evolution of the Earth's upper mantle. Despite the ever-increasing amount of data, the origin of the isotopically different mantle materials identified remains a matter of active debate (e.g. Stracke *et al.*, 2003; Workman *et al.*, 2004). The probably most-often invoked mechanism to produce enriched mantle signatures has been recycling of oceanic and continental crustal material (e.g. Weaver *et al.*, 1986; Zindler & Hart, 1986), but melt-rock interaction scenarios have recently gained renewed interest (e.g. Niu & O'Hara, 2003; Donnelly *et al.*, 2004). The geological, physical, and chemical processes involved in creation and recycling of continental and oceanic crust and/or melt rock reaction processes are manifold and complex and current models allow constraints for a large variability in quantitative estimates of the chemical and isotopic composition of recycled or metasomatised materials (Hart & Zindler, 1989; Stracke *et al.*, 2003; Workman *et al.*, 2004; Kelley *et al.*, 2005).

Among the global ocean island lavas, the rocks erupted on the island of São Miguel in the Azores are in many respects geochemically unusual. The observed variability of the trace element and isotope compositions (e.g. Hawkesworth *et al.*, 1979; Allegre *et al.*, 1987; Hart, 1988; Turner *et al.*, 1997; Widom *et al.*, 1997; Haase & Beier, 2003) is large compared to other lavas from single ocean islands. The isotopic composition of the isotopically most extreme lavas on São Miguel is unique, as São Miguel is the only island where one end-member has both highly radiogenic Pb and Sr isotope compositions. Several models have been invoked to explain this unique isotopic signature, for example, by the presence of ancient subducted sediment, delaminated continental lithosphere, or a re-enrichment by ancient modest-degree melts in the São Miguel source (Hawkesworth *et al.*, 1979; Davies *et al.*, 1989; Turner *et al.*, 1997; Widom *et al.*, 1997; Elliott *et al.*, resubmitted). It has been proven difficult, however, to find models that can explain both the incompatible element and isotopic composition of the whole range of the São Miguel lavas. Here we present new major element, trace element, and Sr, Nd, Pb, and Hf isotope data on basalts from a suite of volcanic rocks from São Miguel, which offer new constraints on the nature and origin of their mantle sources. While the unusual isotopic composition of the São Miguel mantle sources can, in principle, be explained in a number of different ways, the failure to account for the observed incompatible element compositions of the São Miguel rocks of some models poses a major difficulty. Our model calculations suggest that, overall, melting of an ancient recycled seamount is quantitatively most compatible with the chemical and isotopic variations observed in the enriched São Miguel lavas.

3.3 GEOLOGICAL SETTING

The Azores Plateau in the North Atlantic is situated in the vicinity of the Ridge-Ridge-Ridge (RRR) triple junction formed by the two adjacent arms of the Mid-Atlantic Ridge (MAR) and the oblique ultraslow spreading Terceira axis (2-4 mm/a, Vogt & Jung, 2004) and consists of nine volcanic islands, eight of which have been historically active. The MAR separates the westernmost islands Corvo and Flores from the central island group (Graciosa, Terceira, Pico, Faial, São Jorge) and Santa Maria and São Miguel in the East (Fig. 3.1a). São Miguel is formed by four large volcanoes separated by two transitional zones consisting of rows of small scoria cones. The base of the extinct easternmost volcano Nordeste is about 800,000 years old and the oldest shield stage rocks from the westernmost Sete Cidades volcano are about 210,000 years old (Abdel Monem *et al.*, 1975). The volcanic system of Sete Cidades (Haase & Beier, 2003) is situated on the Terceira axis striking in a NW-SE direction whereas the eastern volcanoes are aligned on an E-W trend (Fig. 3.1b). Only two E-W striking tectonic

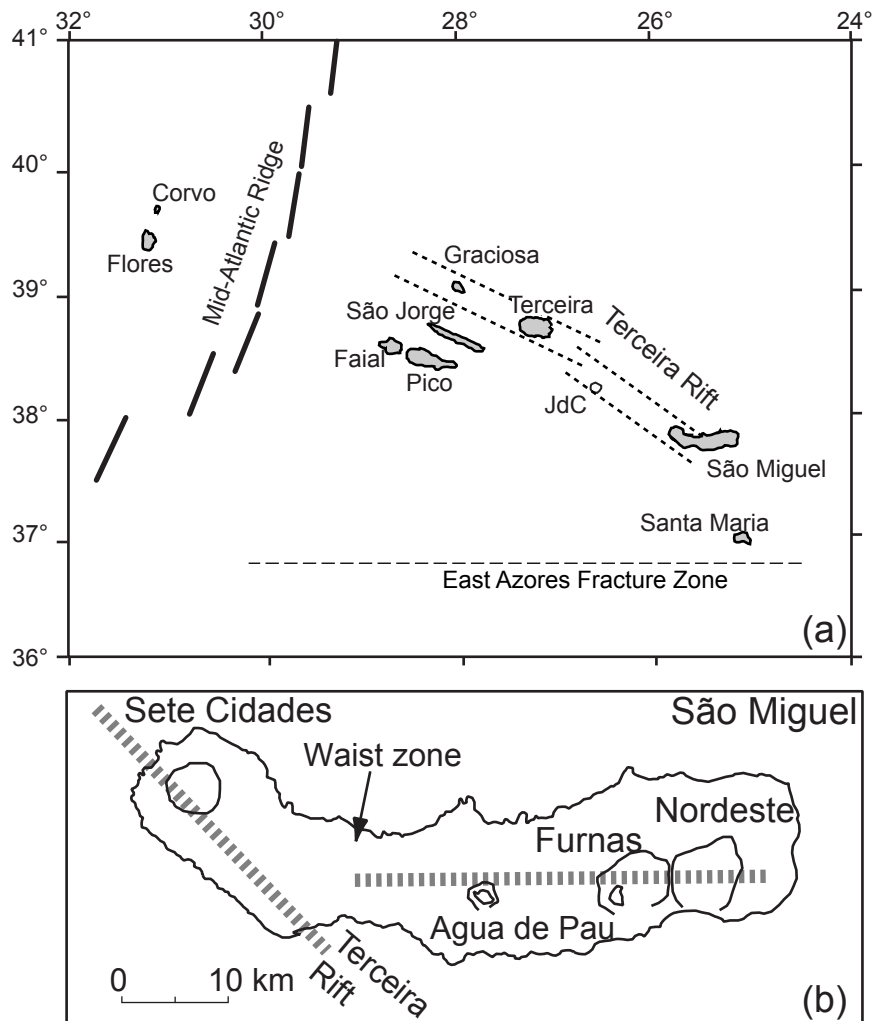


Figure 3.1: a) Schematic map of the Azores Plateau. JdC = João de Castro bank b) Map of São Miguel with main tectonic features (grey dotted lines). Sample locations are given in Table 3.1.

structures are known in the Azores: the eastern part of São Miguel, and the seismically inactive East Azores Fracture Zone (EAFZ) south of the island (Fig. 3.1a). All other tectonic structures in the Azores run parallel to the Terceira axis in a NW-SE direction. Three of the four large volcanoes on São Miguel have a large caldera and younger post-caldera flank eruptions (Sete Cidades, Agua de Pau, Furnas) with the youngest eruptions occurring in historic times. They developed through three different stages of volcanic activity with a mainly basaltic pre-caldera/shield forming stage followed by an evolved caldera-related eruptive stage and a final post-caldera stage erupting mostly evolved rocks intercalated by less evolved basaltic flank eruptions. The Nordeste volcano most likely became extinct during the shield forming stage before a caldera-forming eruption occurred.

3.4 METHODS

The western part of the island of São Miguel, i.e. the Sete Cidades volcano was sampled stratigraphically in May 2001 based on our own and previous investigations of the volcanic history on São Miguel (Booth *et al.*, 1978; Moore, 1990; Moore, 1991; Beier *et al.*, 2006). Samples from different stratigraphic units of the Agua de Pau and Nordeste volcanoes were also recovered. Most samples are optically fresh and lack alteration of olivine crystals and vesicle fillings. Glass was present in a few lavas and pyroclastic samples, and, wherever possible,

Table 3.1: Selected major element, trace element and Sr-Nd-Pb-Hf isotope data from the São Miguel whole rock (WR) and glass (GL) analyses. The major elements were determined by XRF (WR) and electron microprobe (GL), respectively. The trace elements were determined by ICP-MS. Samples marked with a star refer to Sr and Nd measurements made at the Zentrallaboratorium für Geochronologie in Münster. The melting pressure was determined using the equation of Haase (1996).

Sample	513DS-1	515DS-1	18-8-97-3	SM0101*	SM0102*	SM0104*	SM0106	SM0116
Location	W slope of São Miguel	W slope of São Miguel	Mosteiros, Sete Cidades, São Miguel	Beira Mar de Beixo, Sete Cidades, São Miguel	Ponta dos Mosteiros, Sete Cidades, São Miguel	NNW-flank-rim, Sete Cidades, São Miguel	N-flank-rim, Sete Cidades, São Miguel	Ponta da Ferraria, Sete Cidades, São Miguel
Latitude [°N]	37°51.933	37°51.874	37°53.910	37°53.910	37°53.910	37°52.500	37°52.630	37°51.620
Longitude [°W]	25°56.277	25°59.887	25°49.130	25°49.130	25°49.162	25°47.400	25°46.840	25°51.570
	Submarine	Submarine	Subaeral	Subaeral	Subaeral	Subaeral	Subaeral	Subaeral
TAS classification	Basalt	Trachyandesite	Basalt	Basalt	Basalt	Basalt	Trachyte	Basalt
Age [Ma]							0.210	
Melting pressure [GPa]	2.65		3.01	3.56	3.30	2.75		3.02
WR/GL	WR	WR	WR	WR	WR	WR	WR	WR
[wt.%]								
SiO ₂	46.95	59.29	46.13	44.87	45.47	46.71	61.23	46.09
TiO ₂	2.74	1.28	2.51	3.08	2.74	2.98	0.72	3.55
Al ₂ O ₃	12.33	18.69	9.57	10.96	10.25	14.05	17.64	14.74
Fe ₂ O ₃	11.06	5.93	11.63	11.96	11.34	10.94	3.02	11.81
FeO								
MnO	0.17	0.19	0.17	0.17	0.16	0.18	0.17	0.18
MgO	12.13	1.58	16.58	12.26	14.09	7.51	0.48	6.85
CaO	10.97	3.53	10.39	11.62	10.52	9.96	1.46	9.92
Na ₂ O	2.56	5.99	1.74	2.11	2.01	2.95	6.85	3.08
K ₂ O	1.38	4.32	1.25	1.19	1.40	1.80	5.17	1.80
P ₂ O ₅	0.48	0.38	0.39	0.52	0.45	0.69	0.09	0.59
SO ₃								
Cl								
LOI	0.00	0.00	0.00	0.00	0.00	0.51	0.15	0.00
Total	100.77	101.18	100.36	98.74	98.43	98.28	96.98	98.61
[ppm]								
Sc	24.1	3.16	29.6	30.9	29.0	20.2	1.91	22.4
Cr	996	2.25	1369	654	705	344	1.07	162
Co	44.6	4.95	53.4	55.8	59.7	35.8	0.58	40.8
Ni	319	1.75	428	225	311	117	0.26	57.4
Cu	70.5	3.29	54.7	83.5	74.9	54.8	1.53	43.8
Zn	90.0	92.1	91.0	85.0	84.3	101	92.1	104
Mo	1.90	0.97	1.45	1.68	1.84	2.24	2.06	2.44
Rb	28.5	1090	24.7	27.1	32.3	39.8	133	40.9
Sr	622	543	409	589	534	786	313	833
Y	19.3	33.7	16.0	20.4	19.5	28.7	39.7	26.3
Zr	259	607	180	200	226	321	808	336
Nb	48.0	130	35.0	43.6	44.8	73.5	166	74.1
Cs	0.32	0.26	0.25	0.25	0.28	0.36	0.29	0.29
Ba	404		307	347	348	571	1398	502
La	36.6	89.5	29.6	32.5	33.5	50.5	98.8	48.8
Ce	75.5	173	62.5	69.3	71.4	106	190	102
Pr	9.51	19.4	8.00	8.71	8.85	12.9	19.0	12.5
Nd	38.3	68.0	32.6	35.5	35.5	51.2	63.4	49.2
Sm	7.93	11.8	6.80	7.37	7.17	10.2	10.3	9.65
Eu	2.43	3.32	1.98	2.25	2.13	3.04	2.88	2.89
Gd	6.70	9.65	5.57	6.40	6.04	8.64	7.92	8.06
Tb	0.96	1.44	0.80	0.91	0.86	1.23	1.23	1.13
Dy	5.16	7.76	4.31	4.75	4.51	6.44	6.65	5.94
Ho	0.93	1.44	0.77	0.84	0.80	1.16	1.26	1.05
Er	2.28	3.81	1.89	2.09	1.97	2.91	3.52	2.62
Tm	0.29	0.54	0.24	0.27	0.26	0.38	0.51	0.33
Yb	1.76	3.49	1.45	1.62	1.57	2.30	3.42	2.07
Lu	0.24	0.50	0.20	0.21	0.22	0.32	0.50	0.28
Hf	5.98	15.1	5.52	5.43	5.95	7.59	14.4	7.71
Ta	3.34	8.73	2.53	2.86	2.94	4.67	8.28	4.72
Pb	2.05	6.13	1.80	1.59	1.84	2.46	7.13	2.22
Th	3.82	13.5	3.28	3.33	3.73	5.81	15.3	5.33
U	1.14	1.76	1.00	0.89	1.00	1.38	3.49	1.53
⁸⁷ Sr/ ⁸⁶ Sr	0.703273	0.703553		0.703731	0.704143	0.703534	0.703594	0.703336
¹⁴³ Nd/ ¹⁴⁴ Nd	0.51299	0.51289		0.51289	0.51280	0.51290	0.51291	0.51292
ε Nd	6.83	4.88		4.90	3.08	5.11	5.27	5.48
²⁰⁶ Pb/ ²⁰⁴ Pb	19.33	19.50	19.57		19.62		19.51	
²⁰⁷ Pb/ ²⁰⁴ Pb	15.56	15.61	15.64		15.64		15.60	
²⁰⁸ Pb/ ²⁰⁴ Pb	39.05	39.37	39.55		39.61		39.35	
²⁰⁸ Pb/ ²⁰⁶ Pb	2.020	2.018	2.021		2.019		2.017	
²⁰⁸ Pb*/ ²⁰⁶ Pb*	0.955	0.970	0.982		0.984		0.968	
¹⁷⁶ Hf/ ¹⁷⁷ Hf				0.282948	0.282876	0.282987	0.282976	0.282996
ε Hf				5.23	2.69	6.61	6.22	6.93

Table 3.1: continued

Sample	SM0120*	SM0121	SM0125	SM0128*	SM0129*	SM0133	SM0134	SM0136*	SM0140
Location	Ponta da Ferraria, Sete Cidades, São Miguel	Ponta da Ferraria, Sete Cidades, São Miguel	Caminho Velho, Sete Cidades, São Miguel	Nordeste vulcano, São Miguel	Nordeste vulcano, São Miguel	Ponta da Ferraria, Sete Cidades, São Miguel	Ponta da Ferraria, Sete Cidades, São Miguel	Ponta da Ferraria, Sete Cidades, São Miguel	Eguas, Sete Cidades, São Miguel
Latitude [°N]	37°51.490	37°51.490	37°53.220	37°77.400	37°85.100	37°51.652	37°51.652	37°51.652	37°49.600
Longitude [°W]	25°51.310	25°51.310	25°49.03	25°14.700	25°22.400	25°51.150	25°51.150	25°51.150	25°45.180
	Subaeral	Subaeral	Subaeral	Subaeral	Subaeral	Subaeral	Subaeral	Subaeral	Subaeral
TAS classification	basaltic Trachyandesite	Basalt	basaltic Trachyandesite	Trachybasalt	Basalt	Basalt	basaltic Trachyandesite	Basalt	Basalt
Age [Ma]									
Melting pressure [GPa]		3.34				2.59		2.69	3.20
WR/GL	WR	WR	WR	WR	WR	WR	WR	WR	WR
[wt.%]									
SiO ₂	58.16	45.36	54.92	48.77	46.88	47.09	54.56	46.85	45.68
TiO ₂	1.27	3.10	1.89	3.55	3.95	3.40	1.92	3.17	2.70
Al ₂ O ₃	17.99	12.60	17.80	15.31	14.52	13.33	17.35	11.89	10.83
Fe ₂ O ₃	4.87	11.53	7.03	11.76	13.36	11.60	7.33	11.47	11.37
FeO									
MnO	0.17	0.17	0.18	0.16	0.17	0.17	0.19	0.17	0.16
MgO	1.24	10.72	2.31	4.03	4.85	8.60	2.41	10.63	12.67
CaO	3.23	11.01	4.95	8.11	8.18	11.03	4.86	11.96	12.00
Na ₂ O	5.81	2.40	5.32	3.44	3.08	2.83	5.63	2.48	2.20
K ₂ O	4.31	1.45	3.74	2.25	1.91	1.58	3.61	1.38	1.02
P ₂ O ₅	0.31	0.47	0.58	0.69	0.58	0.57	0.62	0.52	0.43
SO ₃									
Cl									
LOI	0.47	0.00	0.97	0.00	1.15	0.00	0.03	0.11	0.00
Total	97.83	98.81	99.69	98.07	98.63	100.20	98.51	100.63	99.06
[ppm]									
Sc	2.76	30.0		13.7	18.8	28.1	5.63	28.4	
Cr	2.87	671	3.00	1.61	134	449	1.38	662	1056
Co	3.43	53.2		29.3	37.0	44.9	8.28	47.4	
Ni	0.72	247		21.4	53.1	122	0.39	198	365
Cu	2.28	96.8		41.8	51.4	67.8	3.42	87.7	
Zn	97.7	90.1	103	107	122	98.7	113	88.4	84.0
Mo	3.76	1.69		2.78	2.28	2.02	2.57	1.56	
Rb	102	35.3	91.0	54.7	78.3	39.0	86.1	31.6	24.0
Sr	743	666	773	744	660	715	814	638	505
Y	36.8	24.6		38.3	42.9	28.2	41.8	21.7	
Zr	646	215	539	404	367	305	572	238	204
Nb	148	49.6		71.8	66.8	60.7	130	56.5	
Cs	0.51	0.30		0.16	4.40	0.23	0.62	0.25	
Ba	1301	456	1025	773	798	518	1008	381	544
La	87.6	35.4		60.8	61.1	42.5	81.3	37.0	
Ce	170	72.9		126	121	88.3	164	78.9	
Pr	19.3	9.05		15.7	15.9	11.0	19.1	9.74	
Nd	69.8	36.5		62.3	63.3	44.1	71.6	39.1	
Sm	12.2	7.47		12.9	13.0	8.82	13.4	7.88	
Eu	3.60	2.30		3.76	3.85	2.67	3.98	2.36	
Gd	9.82	6.43		11.5	11.8	7.54	11.2	6.63	
Tb	1.41	0.92		1.68	1.75	1.08	1.62	0.94	
Dy	7.66	4.81		8.96	9.43	5.57	8.81	4.83	
Ho	1.44	0.85		1.61	1.72	0.98	1.62	0.86	
Er	3.83	2.15		4.07	4.39	2.45	4.23	2.10	
Tm	0.53	0.28		0.54	0.58	0.31	0.57	0.27	
Yb	3.42	1.68		3.31	3.58	1.93	3.54	1.62	
Lu	0.50	0.23		0.46	0.51	0.27	0.50	0.23	
Hf	13.9	5.22		10.6	10.0	6.33	12.4	6.01	
Ta	8.32	2.99		4.85	4.55	3.64	7.62	3.58	
Pb	6.61	1.92		3.85	3.68	2.04	4.44	1.64	
Th	12.8	3.85		7.25	7.28	4.57	11.0	3.87	
U	2.99	1.00		1.79	1.78	1.24	2.84	1.14	
⁸⁷ Sr/ ⁸⁶ Sr	0.703653			0.705167	0.705338	0.703274	0.703483	0.703397	
¹⁴³ Nd/ ¹⁴⁴ Nd	0.51290			0.51274	0.51270	0.51292	0.51290	0.51292	
ε Nd	5.05			1.91	1.19	5.48	5.11	5.46	
²⁰⁶ Pb/ ²⁰⁴ Pb				19.90	20.01	19.45	19.43		
²⁰⁷ Pb/ ²⁰⁴ Pb				15.73	15.75	15.58	15.58		
²⁰⁸ Pb/ ²⁰⁴ Pb				40.09	40.24	39.24	39.23		
²⁰⁸ Pb/ ²⁰⁶ Pb				2.014	2.011	2.017	2.019		
²⁰⁸ Pb*/ ²⁰⁶ Pb*				1.001	1.006	0.963	0.963		
¹⁷⁶ Hf/ ¹⁷⁷ Hf	0.282990	0.282990	0.282987			0.283008		0.283004	0.282995
ε Hf	6.72	6.72	6.61			7.36		7.21	6.90

Table 3.1: continued

Sample	SM0144	SM0145*	SM0146	SM0155	SM0161*	SM0169*	SM0170*	SM0171*	SM0176*
Location	Calhetas, Waist Zone, São Miguel,	Ribeira Grande, Waist Zone, São Miguel	Inner calderawall, Sete Cidades, São Miguel	Ponta da Escavaldo, Sete Cidades, São Miguel	Mafra, Sete Cidades, São Miguel	Queimadas, São Miguel	Fogo volcano, São Miguel	Fogo volcano, São Miguel	Mosteiros coast, Sete Cidades, São Miguel
Latitude [°N]	37°49.590	37°48.550	37°52.330	37°52.380	37°53.360	37°45.700	37°46.250	37°46.250	37°53.180
Longitude [°W]	25°36.050	25°32.120	25°48.630	25°50.210	25°48.510	25°19.075	25°28.890	25°28.890	25°49.290
	Subaeral	Subaeral	Subaeral	Subaeral	Subaeral	Subaeral	Subaeral	Subaeral	Subaeral
TAS classification	Basalt	Basalt	basaltic Trachyandesite	Basalt	Basalt	Basalt	Trachybasalt	Basalt	Trachybasalt
Age [Ma]									
Melting pressure [GPa]		2.60		3.41	3.34	2.90		3.33	
WR/GL	WR	WR	WR	WR	WR	WR	WR	WR	WR
[wt.%]									
SiO ₂		47.06	53.26	45.20	45.36	46.38	48.70	45.40	50.08
TiO ₂		3.53	2.02	3.14	3.59	3.01	3.10	3.83	2.61
Al ₂ O ₃		13.92	17.14	12.00	13.05	12.90	16.57	14.16	16.87
Fe ₂ O ₃		12.12	7.48	11.98	12.44	11.83	10.95	13.09	9.16
FeO									
MnO		0.17	0.18	0.17	0.18	0.17	0.18	0.18	0.18
MgO		8.47	2.55	11.11	9.14	8.84	4.41	7.68	3.75
CaO		9.26	5.12	11.36	10.81	8.93	7.79	9.30	7.35
Na ₂ O		3.05	4.72	1.85	2.76	2.93	4.16	2.85	3.73
K ₂ O		1.87	3.62	1.15	1.26	2.32	2.60	1.86	2.65
P ₂ O ₅		0.61	0.67	0.47	0.69	0.44	0.84	0.66	0.92
SO ₃									
Cl									
LOI		0.00	0.56	0.23	0.00	0.00	0.09	1.63	2.34
Total		100.06	97.32	98.66	99.28	97.75	99.39	100.64	99.64
[ppm]									
Sc	30.2			30.5	24.4	17.7	10.8	22.4	9.77
Cr	188	439	9.00	483	405	321	26.2	183	12.0
Co	50.1			59.7	47.1	44.8	23.8	47.4	17.5
Ni	95.6	145	3.00	228	139	141	17.6	123	7.27
Cu	64.2			85.4	36.7	55.3	18.4	46.6	10.9
Zn	103	113	109	93.0	99.0	91.0	110	118	105
Mo	1.54			1.73	1.99	3.31	3.14	2.13	1.55
Rb	32.1	45.0	85.0	28.1	33.1	60.7	65.7	46.1	56.7
Sr	694	714	786	640	797	551	995	844	893
Y	29.6			23.8	25.4	27.2	36.5	34.0	33.5
Zr	187	346	548	237	248	350	444	360	414
Nb	43.5			48.6	57.4	61.9	89.6	65.0	98.3
Cs	0.28			0.29	0.32	0.61	0.61	0.41	0.20
Ba	429	732	939	394	494	379	767	541	752
La	30.9			34.5	40.9	50.5	73.4	50.9	68.4
Ce	67.1			72.4	86.5	104	153	118	138
Pr	8.73			9.07	10.8	12.7	18.9	13.4	16.1
Nd	36.6			36.6	44.3	49.0	73.9	53.6	61.2
Sm	7.97			7.37	8.97	9.76	14.2	10.7	11.6
Eu	2.54			2.27	2.77	2.71	4.19	3.18	3.40
Gd	7.24			6.37	7.59	8.49	11.9	8.93	9.56
Tb	1.07			0.92	1.07	1.25	1.70	1.28	1.35
Dy	5.71			4.71	5.60	6.66	8.84	6.61	7.20
Ho	1.02			0.83	1.00	1.19	1.57	1.16	1.29
Er	2.55			2.05	2.47	3.00	3.95	2.90	3.28
Tm	0.33			0.26	0.31	0.40	0.52	0.37	0.43
Yb	1.98			1.58	1.90	2.46	3.16	2.24	2.67
Lu	0.27			0.22	0.26	0.34	0.45	0.31	0.38
Hf	4.76			5.09	5.94	9.48	11.7	7.55	9.03
Ta	2.67			3.01	3.65	4.30	6.08	3.92	5.94
Pb	1.70			1.40	1.80	3.82	3.96	2.80	3.51
Th	3.18			3.79	4.06	7.43		5.25	8.00
U	0.82			1.01	1.06	1.94		1.35	2.15
⁸⁷ Sr/ ⁸⁶ Sr	0.703764	0.704364			0.703604	0.704673	0.704368	0.704497	0.703511
¹⁴³ Nd/ ¹⁴⁴ Nd	0.51286	0.51280			0.51291	0.51275	0.51279	0.51278	0.51291
ε Nd	4.35	3.16			5.23	2.26	2.97	2.83	5.34
²⁰⁶ Pb/ ²⁰⁴ Pb	19.65						19.81		
²⁰⁷ Pb/ ²⁰⁴ Pb	15.63						15.70		
²⁰⁸ Pb/ ²⁰⁴ Pb	39.50						39.95		
²⁰⁸ Pb/ ²⁰⁶ Pb	2.010						2.017		
²⁰⁸ Pb*/ ²⁰⁶ Pb*	0.969						0.997		
¹⁷⁶ Hf/ ¹⁷⁷ Hf		0.282872	0.282973	0.282979	0.282965	0.282825	0.282865	0.282867	0.282998
ε Hf		2.55	6.12	6.33	5.83	0.88	2.30	2.37	7.00

Table 3.1: continued

Sample	SM0202	SM0203	SM0204	SM160501-4*	SM220501-1*	SM9704-a	SM9707	SM9710
Location	Pico do Cedro, Waist Zone, São Miguel	Pico da Pintona, Waist Zone, São Miguel	Pico de Lima, Waist Zone, São Miguel	N inner caldera wall, Sete Cidades, São Miguel	N of Ginetes, Sete Cidades, São Miguel	S of Relva, Aeroporto, São Miguel	Lagoa do Peixe, São Miguel	Serra Gorda, Waist Zone, São Miguel
Latitude [°N]	37°45.460	37°47.850	37°47.356	37°52.850	37°51.300	37°45.310	37°47.150	37°47.380
Longitude [°W]	25°42.200	25°41.605	25°38.850	25°46.800	25°52.459	25°42.430	25°44.100	25°41.050
	Subaeral	Subaeral	Subaeral	Subaeral	Subaeral	Subaeral	Subaeral	Subaeral
TAS classification	Basalt	Basalt	Basalt	Basalt	Trachyte	Basalt	Basalt	Basalt
Age [Ma]				0.210				
Melting pressure [GPa]	3.40	2.82	3.66	2.99		3.19	2.95	2.89
WR/GL	WR	WR	WR	WR	WR	WR	WR	WR
[wt.%]								
SiO ₂	45.24	46.56	44.63	46.17	61.98	45.71	46.27	46.39
TiO ₂	2.68	2.43	3.54	3.49	0.78	3.44	3.53	3.00
Al ₂ O ₃	11.39	12.52	11.84	14.18	16.88	12.76	14.10	12.64
Fe ₂ O ₃	11.66	11.18	13.14	12.01	3.42	12.75	12.73	11.91
FeO								
MnO	0.16	0.16	0.17	0.17	0.19	0.17	0.18	0.17
MgO	13.04	10.42	10.41	6.38	0.64	9.81	8.44	10.55
CaO	11.27	11.58	11.90	10.76	1.16	11.14	11.64	11.27
Na ₂ O	2.18	2.67	1.92	3.02	6.94	2.55	2.71	2.45
K ₂ O	1.04	1.15	1.24	1.47	5.21	1.06	1.40	1.22
P ₂ O ₅	0.44	0.40	0.41	0.52	0.15	0.52	0.54	0.48
SO ₃								
Cl								
LOI	0.10	0.23	0.21	0.71	1.13	0.00	0.00	0.00
Total	99.20	99.30	99.41	98.88	98.48	99.91	101.54	100.08
[ppm]								
Sc	30.9	31.2	35.3	22.2	29.8	19.9	27.6	26.1
Cr	1107	788	578	211	6.78	670	384	784
Co	57.6	50.3	57.5	41.9	7.34	48.6	42.5	41.1
Ni	329	212	114	77.1	2.47	185	219	289
Cu	63.6	86.2	27.1	95.3	2.53	25.9	116	99.4
Zn	92.8	89.7	99.2	110	115	82.6	102	95.0
Mo	1.52	1.71	1.82	2.22	6.37	1.86	2.01	1.63
Rb	26.9	33.3	35.5	20.6	95.0	22.6	29.4	24.3
Sr	550	527	550	733	110	615	732	594
Y	24.6	25.8	25.8	26.6	37.1	23.2	21.6	19.1
Zr	176	177	253	305	698	207	207	168
Nb	39.7	40.9	42.9	68.1	168	45.7	49.5	39.7
Cs	0.27	0.40	0.36	0.28	0.95	0.05	0.35	0.30
Ba	379	411	373	484	730	359	433	364
La	30.0	28.0	32.2	45.5	76.4	30.5	37.8	30.5
Ce	60.8	57.8	67.7	91.0	152	64.6	79.0	64.1
Pr	7.84	7.26	8.59	11.1	17.0	8.04	10.0	8.12
Nd	32.1	29.5	35.1	43.8	59.9	33.5	41.2	33.4
Sm	6.83	6.44	7.44	8.74	10.5	7.13	8.72	7.32
Eu	2.13	2.04	2.30	2.65	2.69	2.22	2.71	2.27
Gd	6.15	5.92	6.65	7.52	8.41	6.61	7.49	6.36
Tb	0.89	0.90	0.97	1.08	1.31	0.92	1.07	0.92
Dy	4.76	4.92	5.12	5.71	7.38	4.97	5.82	5.12
Ho	0.84	0.89	0.90	1.02	1.41	0.89	1.05	0.94
Er	2.10	2.23	2.23	2.58	3.85	2.19	2.56	2.30
Tm	0.27	0.29	0.29	0.33	0.55	0.28	0.32	0.30
Yb	1.67	1.84	1.74	2.03	3.55	1.70	1.94	1.75
Lu	0.23	0.26	0.24	0.29	0.50	0.24	0.27	0.24
Hf	4.39	4.37	5.68	6.98	14.5	5.36	6.34	5.33
Ta	2.46	2.47	2.72	4.23	9.08	3.04	3.52	2.89
Pb	1.92	1.85	1.42	2.30	6.26	1.93	1.89	1.86
Th	3.34	3.33	3.95	5.80	11.9	3.67	4.01	3.42
U	0.85	0.89	1.03	1.63	3.19	1.08	1.23	1.04
⁸⁷ Sr/ ⁸⁶ Sr	0.703640		0.704264	0.703627	0.703594	0.703743	0.703501	0.703537
¹⁴³ Nd/ ¹⁴⁴ Nd	0.51289	0.51292	0.51281	0.51291	0.51290	0.51289		
ε Nd	4.88	5.56	3.39	5.31	5.15	4.86		
²⁰⁶ Pb/ ²⁰⁴ Pb	19.53	19.50	19.69			19.65		
²⁰⁷ Pb/ ²⁰⁴ Pb	15.61	15.59	15.68			15.63		
²⁰⁸ Pb/ ²⁰⁴ Pb	39.35	39.23	39.75			39.51		
²⁰⁸ Pb/ ²⁰⁶ Pb	2.014	2.011	2.019			2.011		
²⁰⁸ Pb*/ ²⁰⁶ Pb*	0.965	0.957	0.989			0.971		
¹⁷⁶ Hf/ ¹⁷⁷ Hf	0.282970		0.282897	0.282978		0.282986		
ε Hf	6.01		3.43	6.29		6.58		

Table 3.1: continued

Sample	SM9712	SM9714	SM9716	SM9718	SM9719	BHVO-1	BHVO-1		
Location	Povoacao, São Miguel	Pico Longo, São Miguel	Agua Retorta, São Miguel	Agua Retorta, São Miguel	Agua Retorta, São Miguel	XRF	n=23	ICP-MS	n=12
Latitude [°N]	37°45.450	37°77.134	37°45.900	37°45.900	37°45.900				
Longitude [°W]	25°14.500	25°21.150	25°09.800	25°09.800	25°09.800				
	Subaeral	Subaeral	Subaeral	Subaeral	Subaeral	Standard	standard deviation	Standard	standard deviation
TAS classification	Trachyte	Trachybasalt	Basalt	Trachybasalt	Basalt	Basalt		Basalt	
Age [Ma]			2.04		4.40				
Melting pressure [GPa]									
WR/GL	GL	WR	WR	WR	WR	WR		WR	
[wt.%]									
SiO ₂	64.66	52.70	48.33	49.68	42.95	49.94	± 0.14		
TiO ₂	0.72	2.27	3.92	3.21	3.45	2.76	± 0.01		
Al ₂ O ₃	18.55	17.61	14.69	17.08	9.73	13.57	± 0.07		
Fe ₂ O ₃		8.07	13.06	11.37	13.57	12.22	± 0.04		
FeO	2.44								
MnO	0.16	0.17	0.16	0.16	0.17	0.17	± 0.00		
MgO	0.39	3.28	5.52	3.32	12.58	7.18	± 0.06		
CaO	1.13	6.00	8.80	7.39	10.12	11.46	± 0.04		
Na ₂ O	5.86	3.97	2.98	3.74	1.50	2.40	± 0.07		
K ₂ O	6.90	3.82	2.08	2.56	1.44	0.53	± 0.01		
P ₂ O ₅	0.07	0.72	0.54	0.75	0.45	0.28	± 0.00		
SO ₃	0.03								
Cl	0.19								
LOI	0.00	0.00	0.00	0.00	0.00				
Total	101.10	98.61	100.08	99.26	95.96	100.52			
[ppm]									
Sc	2.29	8.81	19.2	12.4	24.5			32.9	± 1.54
Cr	7.85	86.3	152	7.00	597	282	± 4.85	291	± 9.84
Co	1.72	11.8	40.0	24.9	52.3			45.5	± 1.95
Ni		25.4	95.0	39.0	315	107	± 7.30	120	± 4.54
Cu	1.99	12.1	28.1	13.8	81.2			135	± 9.81
Zn		95.4	99.5	103	91.6	106	± 4.04	104	± 4.22
Mo	6.77	1.66	2.41	2.55	1.01			1.06	± 0.09
Rb	139	106	55.3	64.8	38.7	9.91	± 1.85	9.36	± 0.30
Sr	41.2	847	624	698	410	398	± 2.52	394	± 12.7
Y	34.9	48.4	38.8	42.4	30.2			26.4	± 1.29
Zr	815	572	389	441	265	188	± 2.38	175	± 6.47
Nb	136	111	62.4	77.6	50.7	17.6	± 1.34	17.5	± 0.46
Cs	1.22	0.49	0.16	0.05	0.32			0.10	± 0.00
Ba	172	968	487	633	385	160		18.4	± 2.54
La	109	107	59.1	62.5	50.1			15.2	± 0.38
Ce	205	185	112	129	91.5	10.2	± 3.66	37.8	± 0.58
Pr	22.5	25.1	13.6	15.1	12.9			5.50	± 0.07
Nd	75.4	94.6	53.0	59.6	51.6			24.9	± 0.31
Sm	12.5	17.0	10.5	12.0	10.1			6.20	± 0.13
Eu	2.96	4.86	3.04	3.53	2.89			2.13	± 0.06
Gd	9.01	14.6	9.75	10.9	9.13			6.20	± 0.20
Tb	1.38	2.05	1.34	1.54	1.29			0.96	± 0.03
Dy	7.73	10.6	7.67	8.42	6.81			5.39	± 0.15
Ho	1.48	1.92	1.43	1.54	1.23			0.98	± 0.04
Er	3.95	4.92	3.69	3.91	3.04			2.47	± 0.08
Tm	0.55	0.65	0.50	0.52	0.39			0.33	± 0.01
Yb	3.53	3.94	3.06	3.21	2.33			2.02	± 0.07
Lu	0.51	0.56	0.44	0.45	0.33			0.28	± 0.01
Hf	20.3	14.7	8.99	9.69	7.79			4.40	± 0.08
Ta	8.96	7.32	4.18	4.95	3.54			1.08	± 0.04
Pb	10.2	6.54	3.46	3.84	3.01			1.94	± 0.23
Th	17.3	14.1	6.98	8.15	5.99			1.21	± 0.09
U	5.05	3.31	1.59	1.71	1.02			0.42	± 0.02
⁸⁷ Sr/ ⁸⁶ Sr	0.705090		0.706210						
¹⁴³ Nd/ ¹⁴⁴ Nd			0.51268						
ε Nd			0.78						
²⁰⁶ Pb/ ²⁰⁴ Pb		20.00	20.16	19.97	19.98				
²⁰⁷ Pb/ ²⁰⁴ Pb		15.75	15.80	15.77	15.77				
²⁰⁸ Pb/ ²⁰⁴ Pb		40.34	40.43	40.20	40.38				
²⁰⁸ Pb/ ²⁰⁶ Pb		2.017	2.005	2.013	2.021				
²⁰⁸ Pb*/ ²⁰⁶ Pb*		1.016	1.009	1.006	1.022				
¹⁷⁶ Hf/ ¹⁷⁷ Hf									
ε Hf									

this glass was separated, hand-picked, washed, and used for the geochemical analyses. Where glass was not present, fresh cores of whole rock samples were cut, coarse crushed, washed thoroughly in deionised water, and crushed in an agate mill.

For whole rocks, 0.6 grams of sample were mixed with lithium tetraborate and ammonium nitrate, fused to a homogeneous glass bead, and analysed using a Philips 1400 XRF spectrometer calibrated against international rock standards (Table 3.1). For most elements, precision was better than 0.8 % (2σ) and accuracy better than 1 % (2σ).

For the glasses, major element analyses were carried out on a JEOL JXA 8900 Superprobe electron microprobe at the Institut für Geowissenschaften, University of Kiel. The major elements SiO_2 , TiO_2 , Al_2O_3 , FeO^T , MnO , MgO , CaO , Na_2O , K_2O , P_2O_5 , Cr_2O_3 and, in some cases, also Cl and NiO were measured using an accelerating voltage of 15 kV, a probe current of 15 nA with a beam diameter of $12\mu\text{m}$. Counting times were set to 20 and 10 seconds ($\text{Na}_2\text{O} = 10/5$ sec; $\text{Cl} = 120/60$ sec; $\text{Ni} = 40/15$ sec) for peaks and single backgrounds, respectively. The precision and accuracy was generally better than 1 % (2σ) of the measured values.

The trace element analyses were carried out using an Agilent 7500c/s Quadrupole Inductively Coupled Plasma Mass Spectrometer (ICP-MS) at the Institut für Geowissenschaften, University of Kiel. The samples were prepared following the pressurised HF-HClO_4 -aqua regia acid digestion procedure described by Garbe-Schönberg (1993). Trace element analyses of the samples and of international rock standards are shown in Table 3.1 indicating a precision and accuracy of $< 5\%$ and $< 8\%$ (2σ) from multiple measurements of BHVO-1 ($n = 12$), respectively.

For isotopic determinations, 100 mg of powdered sample material was dissolved in HF-HNO_3 followed by Pb, Sr and Nd separation using the ion exchange techniques described in detail in Hoernle *et al.* (1991). The Sr and Nd isotopic ratios of 15 samples were determined at the Zentrallaboratorium für Geochronologie in Münster with a VG Sector 54 multicollector mass spectrometer in dynamic collection mode (Table 3.1). $^{86}\text{Sr}/^{88}\text{Sr} = 0.1194$ and $^{146}\text{Nd}/^{144}\text{Nd} = 0.7219$ were used for instrumental mass fractionation correction, respectively. The average values of the NBS 987 Sr and the La Jolla Nd standard are $^{87}\text{Sr}/^{88}\text{Sr} = 0.710299$ ($n = 16$; $2\text{SD} = 0.000026$) and $^{143}\text{Nd}/^{144}\text{Nd} = 0.511862$ ($n = 14$; $2\text{SD} = 0.000024$), respectively. Another 13 samples were analysed in static mode at the IFM-GEOMAR in Kiel on a Finnigan MAT 262 RPQ2+ and on a Finnigan Triton mass spectrometer. On the Triton, the average $^{87}\text{Sr}/^{88}\text{Sr}$ ratio for the Sr standard NBS987 is 0.710273 ($n = 14$; $2\text{SD} = 0.000005$) and the average $^{143}\text{Nd}/^{144}\text{Nd}$ ratios of the Nd Spex standard is 0.511710 ($n = 5$; $2\text{SD} = 0.000005$) corresponding to a La Jolla value of 0.511828 . All Sr isotope analyses are reported relative to $^{87}\text{Sr}/^{88}\text{Sr} = 0.710250$ in the NBS987 Sr and $^{143}\text{Nd}/^{144}\text{Nd} = 0.511828$ in the La Jolla Nd standard, respectively. Procedural blanks in both laboratories were generally better than 0.2 ng and 0.1 ng for Sr and Nd. The Pb isotopes were carried out on a Finnigan MAT 262 mass spectrometer in static mode at the IFM-GEOMAR in Kiel. For Pb, the analyses were fractionation corrected using repeated measurement of NBS-981 ($n = 34$; errors are 2σ values; $^{206}\text{Pb}/^{204}\text{Pb} = 16.904 \pm 0.018$, $^{207}\text{Pb}/^{204}\text{Pb} = 15.447 \pm 0.024$, $^{208}\text{Pb}/^{204}\text{Pb} = 36.559 \pm 0.075$) normalised to the values of Todt *et al.* (1996).

The Hf isotope analyses were carried out at the Max-Planck-Institut für Chemie in Mainz following the chemical separation procedure described by Münker *et al.* (2001). Hf isotope ratios were measured on a Nu Plasma Multi-Collector ICP-MS (MC-ICP-MS) in static mode using a CETAC Aridus inlet system fitted with a ESI Teflon nebulizer with a $50\mu\text{l}$ flow rate. All isotope ratios were corrected with an exponential fractionation law

using $^{179}\text{Hf}/^{177}\text{Hf} = 0.7325$. Repeated measurements of the JMC 475 Hf standard averaged $^{176}\text{Hf}/^{177}\text{Hf} = 0.282170$ ($n = 13$; $2\text{SD} = 0.000008$) during the analysis period and are in good agreement with the long-term average of 0.282161 ($n = 415$; $2\text{SD} = 0.000016$).

3.5 RESULTS

The São Miguel samples are mostly alkali basalts with MgO concentrations up to 14.1 wt. %, but range to more evolved rocks with MgO as low as 0.2 wt. % (Fig. 3.2). The Sete Cidades samples cover the whole range of MgO contents, whereas samples from the Agua de Pau volcanic system have a more restricted range between 13.0 and 4.4 wt. % MgO. Samples from the Nordeste volcano are more evolved with MgO between 5.5 and 2.9 wt. %, with only one high-MgO sample (12.6 wt. %) that shows petrographic and chemical evidence for the accumulation of olivine and clinopyroxene similar to the other high MgO (> 12 wt. % MgO) samples from Sete Cidades and Agua de Pau. The samples from each volcanic system lie on a single liquid line of descent which is comparable to that of the well-determined Sete Cidades volcano (Beier *et al.*, 2006), indicating progressive fractionation from primary magma compositions with about 12 wt. % MgO (inferred from the Ni-MgO systematics of olivines, whole rocks, and glasses, Beier *et al.*, 2006). The similarities in Na_2O , FeO^{T} , and SiO_2 of lavas from the Agua de Pau and Nordeste volcanoes compared to those from Sete Cidades indicate similar degrees and pressures of partial melting (Fig. 3.2). Thus, the fractionation-corrected major elements (corrected to MgO = 12 wt. %) show only small differences between the eastern and western volcanoes with slightly lower CaO and higher FeO^{T} in the eastern volcanoes.

The trace element compositions of the eastern and western São Miguel lavas are, in general, relatively similar (Fig. 3.3). The major differences are the higher incompatible and REE concentrations of the Nordeste (East) compared to the Sete Cidades lavas (West, Fig. 3.3). The elevated HREE concentrations of Nordeste suggest a smaller amount of residual garnet in the Nordeste mantle source. The REE concentrations and ratios of samples from both volcanic systems (e.g. Ce/Yb, Sm/Yb, La/Sm) as well as the fractionation-corrected major elements (Na, Ti) do not give any evidence for large differences in degrees of partial melting between samples from the different volcanic systems on São Miguel (Fig. 3.2). Comparison of the average primitive Nordeste and Sete Cidades samples (MgO contents of 5 to 12 wt. %, Fig. 3.3d) shows that the Nordeste lavas are relatively more enriched in Cs, Rb, Th, U, and Pb but depleted in Sr, Ba, Ti, and to a lesser degree in Eu than the Sete Cidades lavas. The trace element concentrations of the Agua de Pau volcano are intermediate between the Sete Cidades and the Nordeste lavas, indicating a gradual increase in the relative enrichment in some incompatible element concentrations from the west to the east (Fig. 3.3).

Although influence of crystal fractionation processes on the highly incompatible element ratios has been observed at Sete Cidades (Beier *et al.*, 2006), the variations between the São Miguel volcanoes are too large to be explained by fractional crystallisation only. The trace element ratios show that both volcanoes have Ce/Pb and U/Nb ratios situated within the oceanic range (Hofmann, 1988). Nordeste has much higher Rb/Sr, Th/U, Th/Nb and Rb/Nb ratios but lower Nb/La, Nb/Zr, Th/Pb and Ba-ratios (e.g. Ba/Th, Ba/Rb) and only slightly lower U/Pb ratios than the lavas from Sete Cidades (Fig. 3.4). The trace element ratios of Th/U and U/Pb show that Th is enriched compared to U at Nordeste relative to Sete Cidades (Fig. 3.4).

Compared to other Ocean Island Basalts (OIB), the average trace element concentrations of both Nordeste and especially the Sete Cidades lavas are similar to those in so-called HIMU (high μ = high $^{238}\text{U}/^{204}\text{Pb}$) basalts

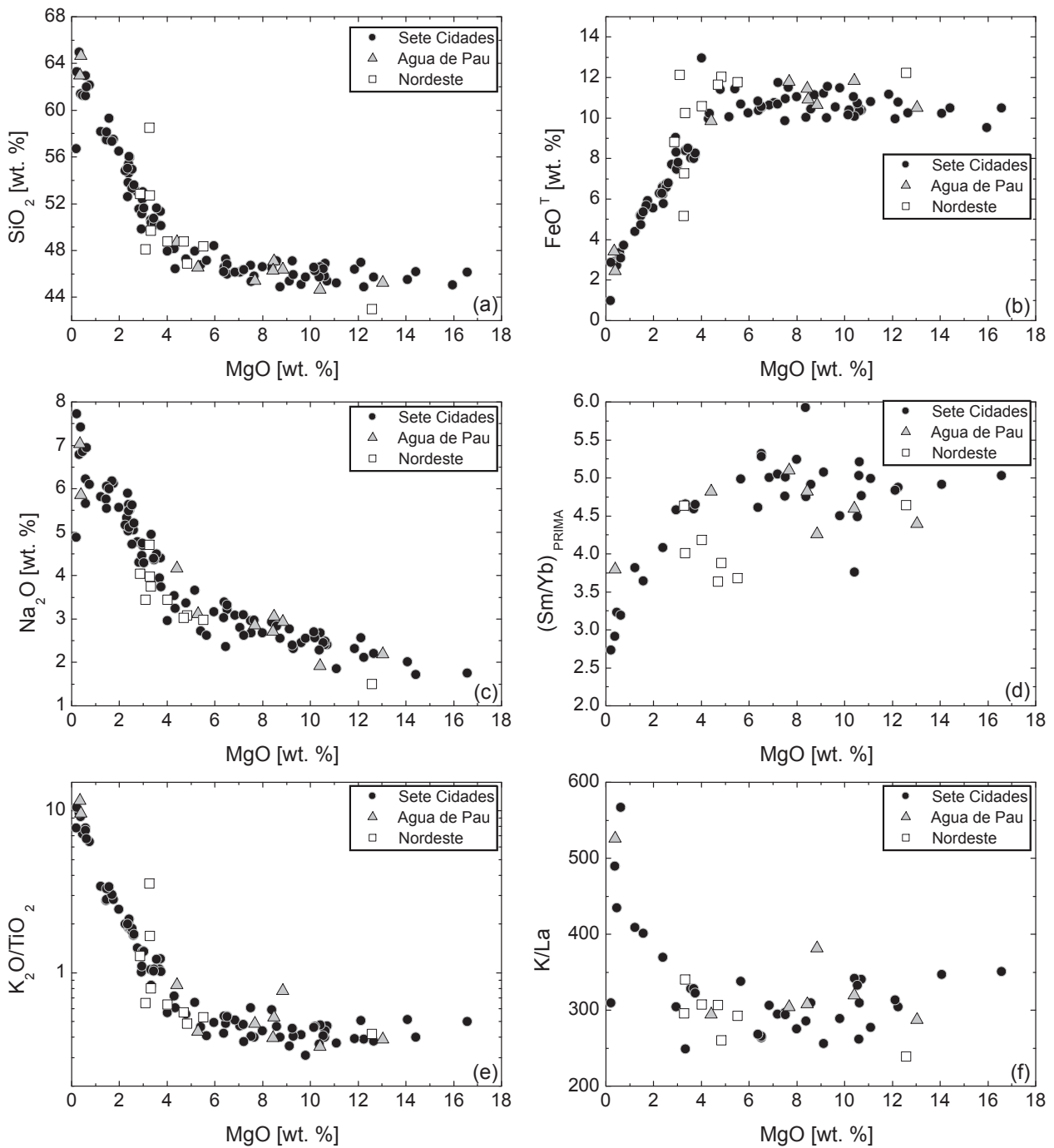


Figure 3.2: Major and trace element data from Sete Cidades, Agua de Pau and Nordeste. The samples from each volcanic system are situated on a single liquid line of decent. The major elements do not give any evidence for differences in degree of partial melting (Na_2O) or melting depth (SiO_2 , FeO^T) but lower HREE ratios (Sm/Yb) give evidence for smaller amounts of residual garnet beneath Nordeste. PRIMA composition from McDonough & Sun (1995).

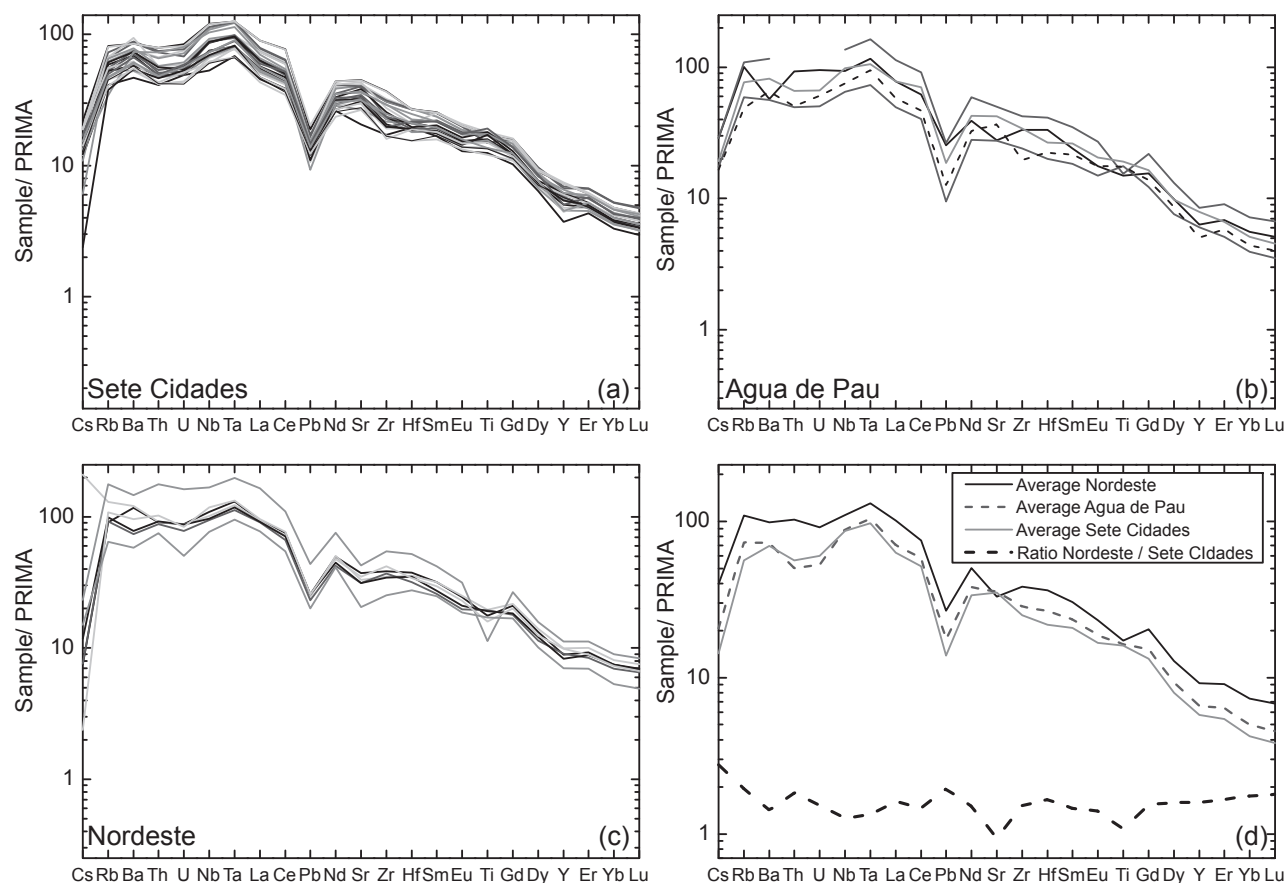


Figure 3.3: Primitive upper mantle (McDonough & Sun, 1995) normalised trace element concentrations from São Miguel; a) primitive Sete Cidades samples, b) primitive Agua de Pau samples, c) primitive Nordeste samples, d) average composition of Nordeste, Agua de Pau and Sete Cidades and the ratio between the Nordeste average and Sete Cidades average compositions (Table 3.2). Note the depletion in Ba, Sr, Ti and Eu in the Nordeste pattern.

(e.g. St. Helena, Tubuaii) but with notably higher Cs, Rb, Ba, and Th concentrations for both volcanoes (Fig. 3.5). The Nordeste volcanic system is also enriched in the LREE, but depleted in Sr and Ti compared to the HIMU basalts. The trace element differences between the São Miguel volcanoes and the HIMU representatives results in differences in several key incompatible trace element ratios (Fig. 3.4), i.e. the Rb/Sr, Rb/Nb, and Ba/Th ratios in rocks from both volcanoes are generally higher than those typical for HIMU basalts, despite the generally enriched incompatible trace element pattern of Nordeste compared to typical HIMU basalts (Fig. 3.5). The São Miguel lavas are generally situated within the HIMU range in the U/Pb and Th/Pb ratios with the Sete Cidades lavas tending towards slightly higher ratios (Fig. 3.4). The Lu/Hf ratios of both volcanoes are slightly lower compared to the HIMU islands and the element ratios of fluid mobile versus fluid immobile elements such as Ba/Th (Sete Cidades and Agua de Pau) and K/La (both volcanoes) are higher.

The Sr, Nd, Pb, and Hf isotope ratios of the São Miguel samples define linear arrays with systematically more enriched isotope ratios towards the east, consistent with previous isotope data on the São Miguel rocks (e.g. Hawkesworth *et al.*, 1979; Allegre *et al.*, 1987; Hart, 1988; Turner *et al.*, 1997; Widom *et al.*, 1997; Elliott *et al.*, resubmitted) and the general enrichment observed in the trace element concentrations across the island (Fig. 3.3). The isotope trends represent binary mixing arrays between the two end-members of the Sete Cidades and Nordeste volcanoes (Fig. 3.6). Considerable isotopic variations exist in a single volcanic system at Sete Cidades

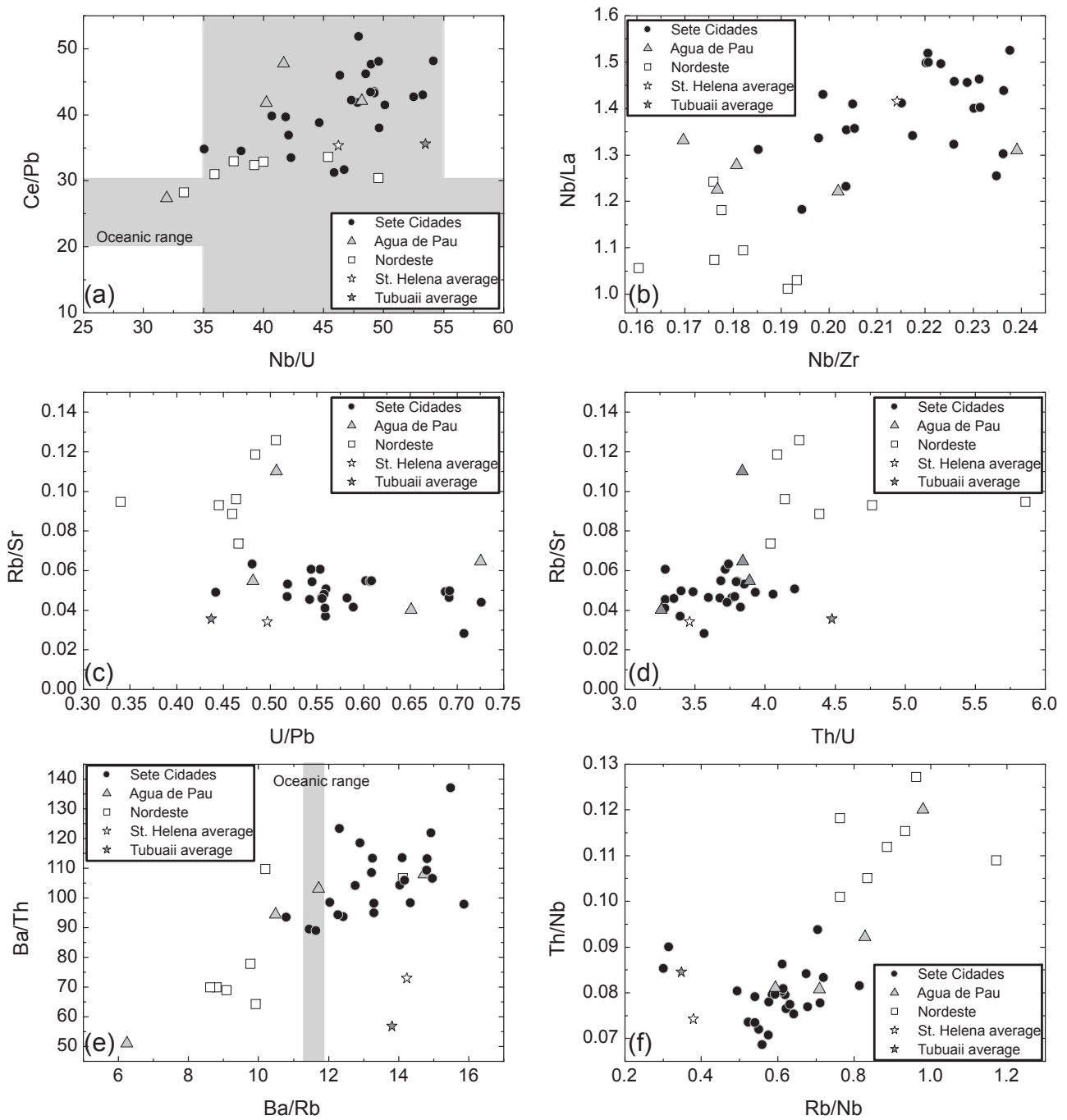


Figure 3.4: Representative trace element ratios of Nordeste, Agua de Pau and Sete Cidades. Grey fields represent the range of oceanic basalts proposed by Hofmann (1988, Fig. 3.4a) and Hofmann & White (1983, Fig. 3.4e). The differences in the incompatible elements reflect the trace element pattern of Figure 3.3. Average St. Helena and Tubuaii values are literature data for comparison (Willbold & Stracke, 2005) also given in Table 3.2.

(ϵNd from 4.35 to 6.82, Haase & Beier, 2003; Beier *et al.*, 2006) but these variations are small, compared to the entire isotopic range observed across the island from Sete Cidades in the west to Nordeste in the east (ϵNd from 0.8 to 6.8). This variation is large compared to the global ocean island range (ϵNd from -5 to 11). Within isotopic multispace, the Sete Cidades lavas are situated within the global arrays with compositions similar to some lavas from other ocean islands in the Atlantic Ocean, such as the Canary islands (e.g. Hoernle *et al.*, 1991), Cape Verdes (e.g. Jorgensen & Holm, 2002; Doucelance *et al.*, 2003), and Ascension (e.g. Weis, 1983; Weis *et al.*, 1987). Lavas from the easternmost Nordeste volcano have the highest $^{87}\text{Sr}/^{86}\text{Sr}$, $^{206}\text{Pb}/^{204}\text{Pb}$, $^{208}\text{Pb}/^{204}\text{Pb}$, and the lowest $^{143}\text{Nd}/^{144}\text{Nd}$ and $^{176}\text{Hf}/^{177}\text{Hf}$ isotope ratios on São Miguel (Fig. 3.6). The Nordeste end-member isotopic compositions are unusual among global OIB in having radiogenic Pb isotope ratios ($^{206}\text{Pb}/^{204}\text{Pb} \sim 20$, $^{208}\text{Pb}/^{204}\text{Pb} \sim 40.2$) coupled to highly radiogenic Sr isotope ratios ($^{87}\text{Sr}/^{86}\text{Sr} \sim 0.706$) and low Nd and Hf isotope ratios ($^{143}\text{Nd}/^{144}\text{Nd}$ and $^{176}\text{Hf}/^{177}\text{Hf} \sim 0.5127$ and ~ 0.28280 , respectively). Only some lavas from the Cook-Austral islands have similar isotopic compositions (e.g. Mauke and Atiu islands; Palacz & Saunders, 1986; Nakamura & Tatsumoto, 1988; Schiano *et al.*, 2001). Despite the similarity of the trace element concentrations to those found in typical HIMU, the isotope ratios of the Nordeste samples are clearly unlike those in typical HIMU islands, which are characterised by low and relatively constant Sr isotope ratios, very high Pb and low Hf for given Nd isotope ratios (Zindler & Hart, 1986; Salters & White, 1998; Stracke *et al.*, 2005). The isotope ratios of the Sete Cidades volcano are similar to those of FOZO as recently re-defined by Stracke *et al.* (2005), while those of the Nordeste lavas are most similar to EM-2, but are distinguished from EM-2 (e.g. Samoa, Society; Zindler & Hart, 1986; Hart, 1988) by their highly radiogenic Pb isotope ratios, which are untypical of EM-2 (Fig. 3.6). Thus, the Nordeste mantle source represents a unique mantle component that is clearly distinguishable from those previously defined by White (1985) and Zindler & Hart (1986).

The observed trace element differences between the Nordeste volcano and HIMU also account for some of the observed isotopic differences (Fig. 3.7). Thus, the higher Rb/Sr ratios are well-correlated to the more radiogenic $^{87}\text{Sr}/^{86}\text{Sr}$ ratios in Nordeste compared to Sete Cidades and HIMU. However, despite their higher $^{206}\text{Pb}/^{204}\text{Pb}$, the Nordeste lavas have lower U/Pb than the Sete Cidades basalts, whereas the elevated Th/U and Th/Pb ratios at comparable U/Pb may account for the higher observed $^{208}\text{Pb}/^{204}\text{Pb}$ for a given $^{206}\text{Pb}/^{204}\text{Pb}$ trend at São Miguel relative to HIMU. The $^{143}\text{Nd}/^{144}\text{Nd}$ and $^{176}\text{Hf}/^{177}\text{Hf}$ ratios of São Miguel extend from the FOZO-like Sete Cidades lavas to lower $^{143}\text{Nd}/^{144}\text{Nd}$ and $^{176}\text{Hf}/^{177}\text{Hf}$ than found in the HIMU lavas (Fig. 3.6), the latter being consistent with lower Lu/Hf ratios found at Nordeste. Generally, most the trace element ratios (e.g. Nb/Zr, Nb/La, Ba/Rb, Fig. 3.7) are well-correlated with the isotope ratios, suggesting that the gradual change in incompatible element enrichment from west to east on São Miguel is a source rather than a crystal fractionation-related feature.

3.6 DISCUSSION

Although it has been shown that there is some temporal variation in the trace element and isotopic composition of the Sete Cidades lavas (Beier *et al.*, 2006), both the trace element and isotopic variations are relatively small compared to the range observed in lavas across the entire island. The progressive enrichment of the trace element and isotope ratios in lavas from the west to the east of São Miguel, the large differences in the isotope ratios, and the good correlation between the incompatible element and the isotope ratios (Fig. 3.7) indicates that the similarities between Sete Cidades and Nordeste are a result of mixing between two distinct mantle sources rather than a result of different degrees of crystal fractionation or partial melting. The similarities in terms of incompatible element compositions (Figs. 3.2 & 3.3) and the close spatial connection of the two endmembers may imply a close genetic relationship between them.

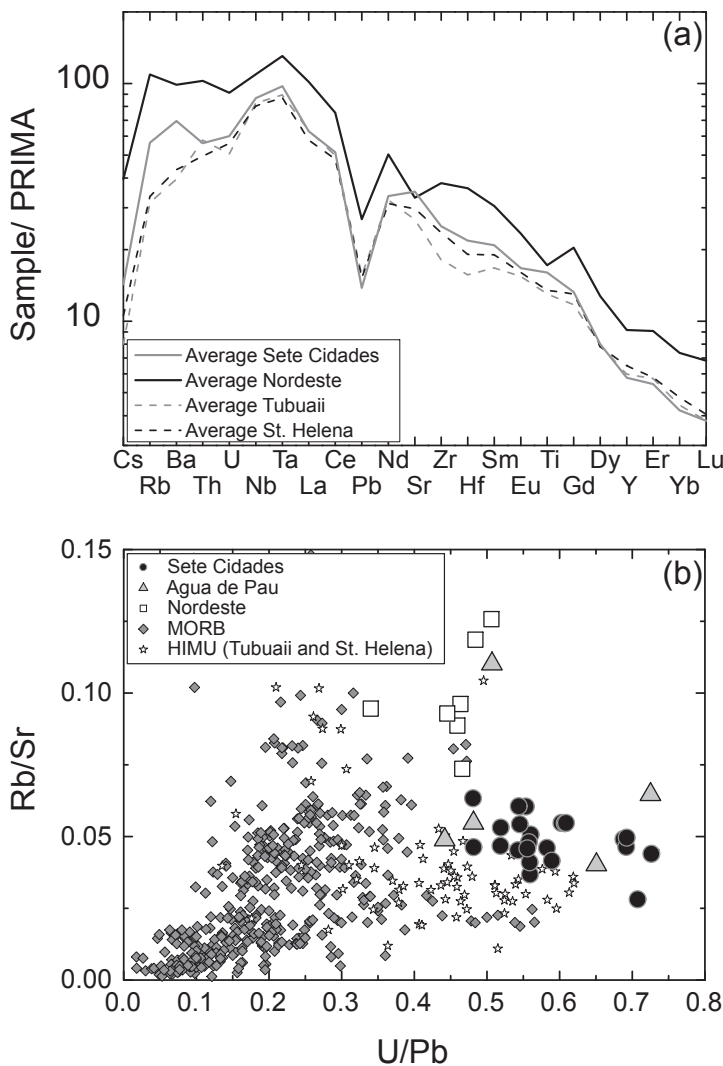


Figure 3.5: (a) Sete Cidades and Nordeste average trace element pattern compared to the average compositions of Tubuaii and St. Helena (Willbold & Stracke, 2005). Both islands are commonly related to the so-called HIMU compositions (high μ = high $^{238}\text{U}/^{204}\text{Pb}$). Remarkable similarities exist between the HIMU islands and São Miguel, however, the incompatible elements also indicate some differences, e.g. elevated Rb and Ba relative to Th and U. (b) Rb/Sr versus U/Pb ratios of São Miguel, MORB and the HIMU islands. MORB and HIMU data were compiled from the GEOROC database <http://georoc.mpch-mainz.gwdg.de/georoc/> and from Willbold & Stracke (2005)

of Sete Cidades and HIMU are situated within the same range with the HIMU samples ranging towards lower U/Pb (Figs. 3.4 & 3.5), however the isotopic differences indicate lower time integrated U/Pb and Th/Pb ratios for Sete Cidades. The composition of FOZO is interpreted to be recycled oceanic crust with variable isotopic compositions that is relatively little affected by alteration compared to the HIMU mantle sources, which have likely experienced significant chemical modification during sub-arc alteration (Stracke *et al.*, 2003). If the Sete Cidades isotopic signature would be derived from recycled oceanic crust without significant alteration, the higher Sr and Pb isotopic ratios require a relatively enriched MORB composition. However, even enriched MORB have Th/Pb and U/Pb ratios (Fig. 3.5) that are too low to be a possible component in the Sete Cidades mantle source and a change of their incompatible element compositions is required, for example, U needs to be increased over Th. The modification during subduction alteration of any subducted oceanic crust leads to

3.6.1 The Sete Cidades mantle source

The relatively similar incompatible element patterns (Figs. 3.3 & 3.5) of the Sete Cidades and the HIMU basalts suggests a relationship of the two sources. Furthermore, the isotopic composition of Sete Cidades with $^{87}\text{Sr}/^{86}\text{Sr} \sim 0.7033$, $^{143}\text{Nd}/^{144}\text{Nd} \sim 0.51295$, $\epsilon_{\text{Hf}} \sim 7$, $^{206}\text{Pb}/^{204}\text{Pb} \sim 19.3$ and $^{208}\text{Pb}/^{204}\text{Pb} \sim 39.0$ is situated at the lower end of the recently re-defined FOZO composition (Fig. 3.6; Stracke *et al.*, 2005). This may indicate that the Sete Cidades lavas are derived from a mantle source similar to that invoked for HIMU and FOZO which has been proposed to represent recycled oceanic lithosphere (Hofmann & White, 1980; Hart *et al.*, 1992). Such an origin is supported by the low oxygen isotope compositions in the São Miguel lavas (Widom & Farquhar, 2003). However, although some similarity exist between the HIMU and Sete Cidades trace element pattern, they also exhibit differences; i.e. the Rb and Ba concentrations are significantly enriched relative to Th and U, and Ba is more enriched than Rb at Sete Cidades compared to the HIMU lavas (Fig. 3.4). The Sete Cidades component most likely has high $^3\text{He}/^4\text{He}$ ratios (inferred from the “Terceira” component, Moreira *et al.*, 1999), whereas HIMU lavas have low He isotope ratios (Graham *et al.*, 1992). Consequently, a primitive component possibly from the deep undegassed mantle resides in the Sete Cidades mantle source. The recent U/Pb, Th/Pb ratios

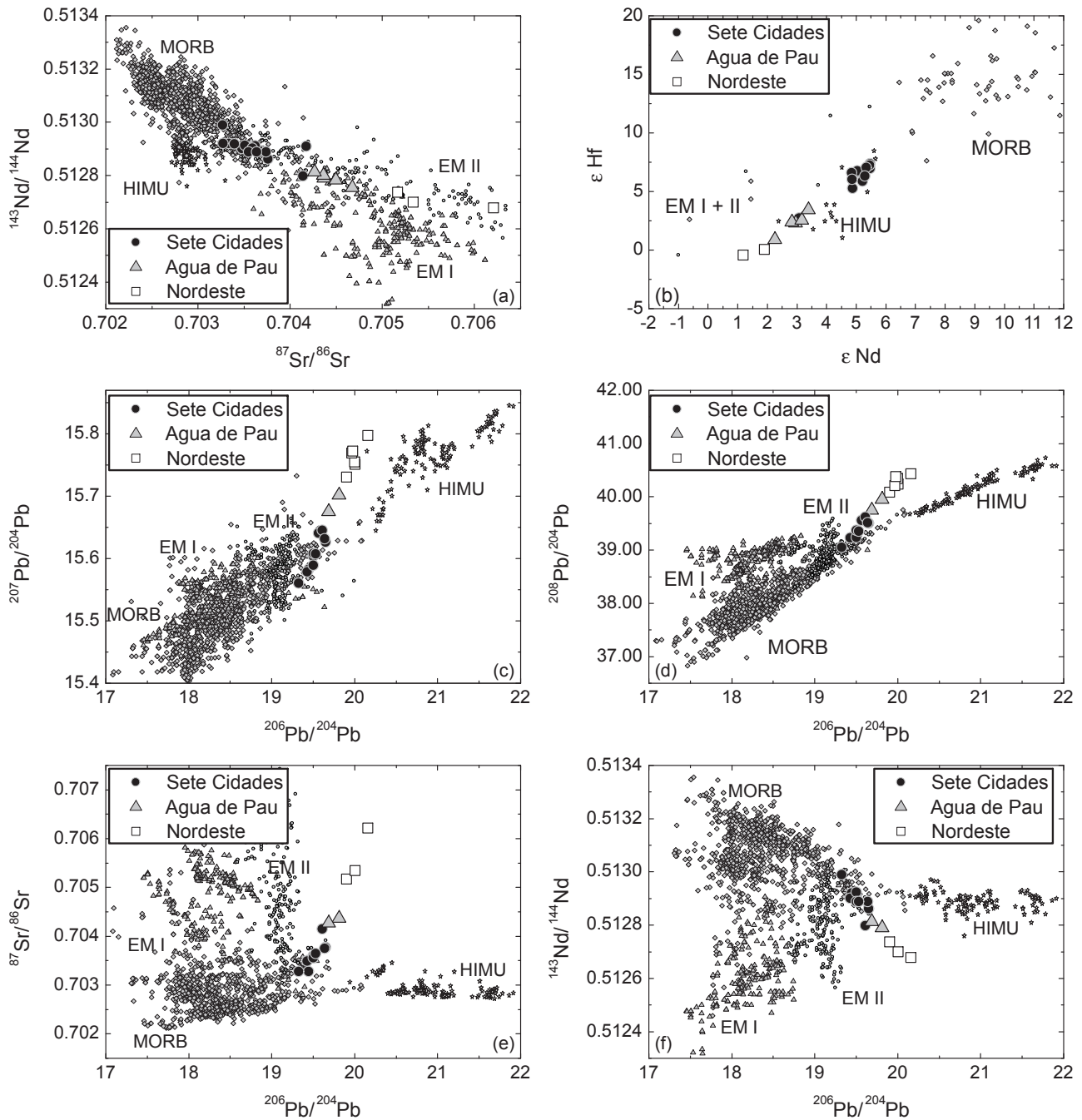


Figure 3.6: Isotope data of the São Miguel volcanoes Sete Cidades in the west, Agua de Pau in the central area and Nordeste in the east. The overlapping isotopic trends of Agua de Pau and Sete Cidades mainly reflect samples from a zone of scoria cones between the two volcanoes, with two overlapping rift zones, each connected to either of the two systems (Haase & Beier, 2003). The HIMU, MORB and Enriched Mantle compositions are referenced in detail in Stracke *et al.* (2003).

Table 3.2: Trace element compositions of Sete Cidades, Nordeste and the discussed models. Sete Cidades and Nordeste average compositions are average concentrations of primitive lavas > 5 wt.% MgO. Sete Cidades model composition refers to subducted, recycled, and slightly altered enriched oceanic crust, whereas the Nordeste model refers to the additional presence of an evolved seamount composition of the Koko seamount from the Hawaiian Emperor Chain (Regelous *et al.*, 2003). Sediment model represents presence (0.2 %) of a GLOSS sediment component mixed into a depleted mantle (Plank & Langmuir, 1998) and melting model represents the interaction of a 0.5 % garnet bearing melt mixed into a depleted mantle as given by Salters & Stracke (2004). Average St. Helena and Tubuaii compositions are calculated from Willbold & Stracke (2005) and references therein.

	Sete Cidades average	Sete Cidades model	Nordeste average	Nordeste model	Sediment model	Melting model	St. Helena Average	Tubuaii Average
[ppm]								
Cs	0.31	0.64	1.28	1.19	133	3.23	0.22	0.17
Rb	34.1	30.9	58.0	72.0	106	106	20.1	18.9
Ba	493	428	546	616	130	1301	286	261
Th	4.46	4.39	6.91	8.20	121	12.9	3.93	4.59
U	1.18	1.32	1.54	1.66	126	3.50	1.13	1.03
Nb	54.2	79.1	61.0	80.6	159	162	53.0	54.4
Ta	3.46	5.41	4.16	5.52	194	10.3	3.21	3.31
La	40.1	56.3	57.5	73.3	123	84.2	37.4	41.1
Ce	84.1	109	111	126	85.7	158	80.7	83.5
Pb	2.12	3.25	3.50	4.71	62.6	7.64	2.28	2.35
Nd	41.5	50.8	56.0	58.4	52.1	65.4	39.0	40.5
Sr	671	596	579	712	37.3	871	591	532
Zr	267	338	346	509	39.7	511	247	190
Hf	6.21	7.73	9.18	10.6	34.1	11.7	5.40	4.43
Sm	8.43	9.08	11.2	11.5	28.0	12.7	7.72	6.80
Eu	2.56	2.35	3.25	2.92	18.9	3.24	2.47	2.37
Ti	12650	15935	22751	19219	16.2	20264	16246	15707
Gd	7.28	5.10	10.2	8.07	11.7	9.18	7.08	6.38
Dy	5.49	4.40	8.02	8.01	8.01	9.08	5.26	5.35
Y	25.4	22.0	36.9	40.5	6.10	47.4	27.9	25.7
Er	2.43	1.90	3.75	3.63	5.23	4.22	2.54	2.52
Yb	1.90	1.56	3.07	3.00	4.24	3.48	2.10	1.96
Lu	0.26	0.20	0.44	0.39	3.56	0.46	0.27	0.26

a significant loss of Pb relative to Ce, Th and U resulting in high Ce/Pb, U/Pb, and Th/Pb ratios (Kogiso *et al.*, 1997), which is generally consistent with the high ratios observed in the Sete Cidades lavas and the more radiogenic Pb isotope compositions compared even to enriched MORB (Fig. 3.6). The general tendency of Sete Cidades towards lower time integrated U/Pb and Th/Pb ratios compared to the HIMU suggests that Sete Cidades has been less affected by subduction modification than the HIMU sources. During subduction, Rb is more mobile than Sr in the circulating fluids (Kogiso *et al.*, 1997), which generally lowers the Rb/Sr ratios, but a possible addition of seawater Sr to the recycled crust could explain increased Sr isotope compositions. The Sete Cidades lavas are enriched in fluid-immobile incompatible elements with Nb/Zr ~ 0.22 (Fig. 3.7b) significantly higher than MORB (~ 0.03) or primitive mantle (~ 0.06). To explain this enrichment the Sete Cidades basalts would have to form from a source with at least primitive mantle composition and a degree of melting of < 1% which appears to low given the major element compositions (e.g. Na, Ti) of the basalts (Fig. 3.2). Consequently, the source of the Sete Cidades basalts needs to be enriched in incompatible elements and most likely contains recycled enriched MORB or alkaline basalts from subducted oceanic intraplate volcanoes. The incompatible element similarities between relatively enriched MORB compositions and relatively depleted alkaline basalts from ocean islands make a differentiation between these two compositions difficult (e.g. Niu & O'Hara, 2003). However, the recycled oceanic crust at Sete Cidades was altered by hydrothermal processes and

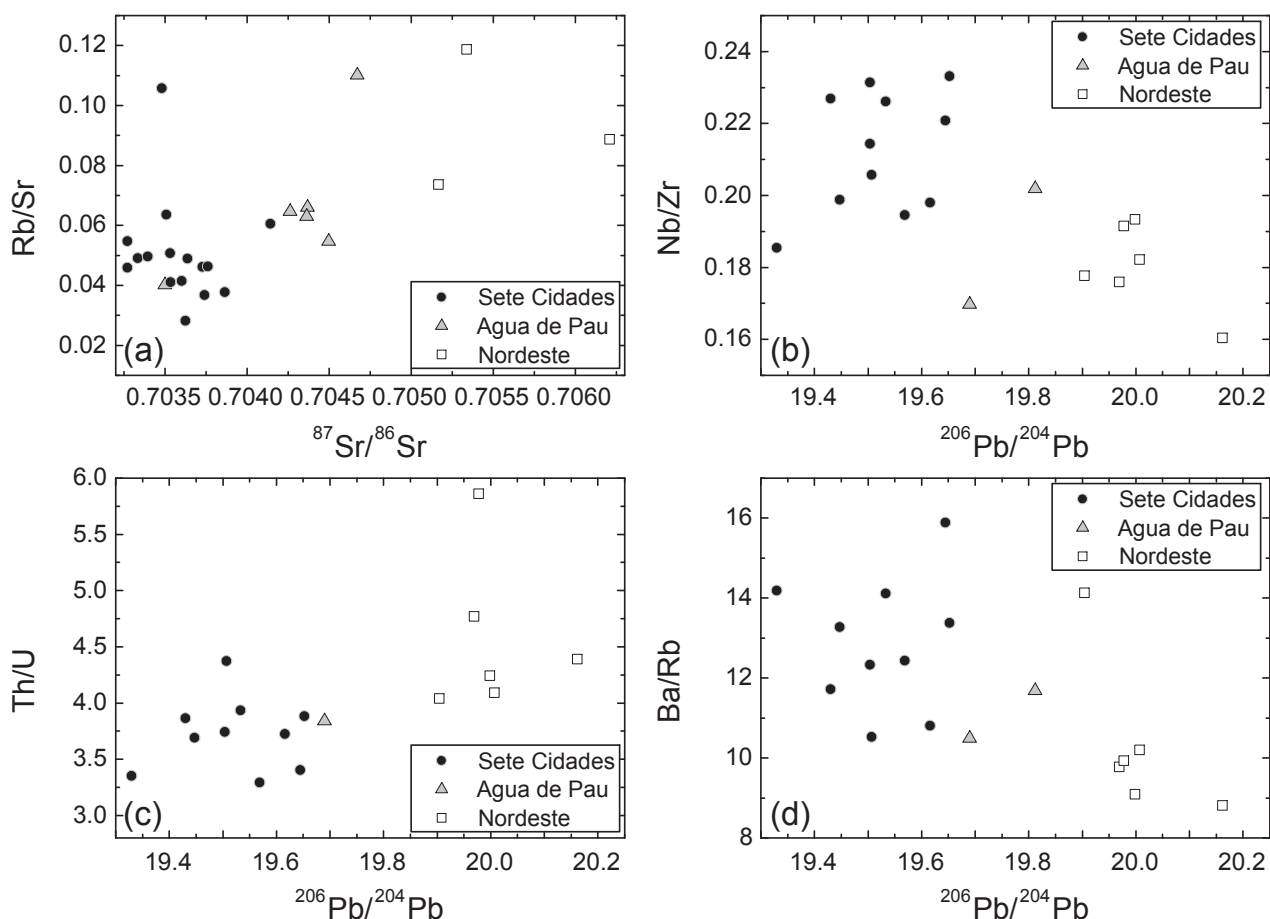


Figure 3.7: Selected trace element and isotope ratios from the São Miguel lavas. The correlations between trace elements and isotope ratios give evidence that both, trace elements and isotopes are influenced by a common process.

the subduction process generating enriched Rb/Sr and U/Pb, but lower Th/Pb as a result of the loss of Pb and only slightly modifying Rb relative to Sr (Fig. 3.8, Table 3.2). Modelling the isotopic composition based on the trace element compositions for the Sete Cidades lavas suggests that the precursor rock formed about 3 Ga ago and was recycled 2 Ga ago leading to the observed Sr-Nd-Pb-Hf isotope compositions.

3.6.2 The Nordeste mantle source

The similarities between the Sete Cidades and Nordeste trace element systematics suggests some similarities of their mantle sources but the Nordeste source has unique Sr, Nd, Pb and Hf isotope compositions (Fig. 3.6). As indicated by the good correlation between the isotopes and the parent-daughter ratios (e.g. Rb/Sr – $^{87}\text{Sr}/^{86}\text{Sr}$, Fig. 3.7), some of the differences in the trace element ratios can also account for the isotopic differences. However, the Pb isotopes of the Nordeste lavas suggest time-integrated U/Pb and Th/Pb ratios even higher than the Sete Cidades source whereas the present Ce/Pb and U/Pb are lower (Figs. 3.4a & 3.5b) than those of Sete Cidades. The U/Pb and especially the Rb/Sr are higher than those known from MORB which might suggest a depletion of Pb during alteration for both São Miguel sources. However, alteration would also lower the Rb/Sr ratios since Rb is more mobile than Sr during alteration. Explaining the difference between the two sources by an increasing amount of alteration of the recycled crust at Nordeste is therefore incompatible with the observation that Nordeste has increased Rb/Sr ratios compared to Sete Cidades. A similar relationship is observed in the Ba/Th versus Ba/Rb ratios where Ba is mobile in fluids relative to Th but less mobile than Rb which should

result in elevated Ba/Th and Ba/Rb ratios rather than low Ba/Rb ratios observed in the Nordeste lavas (Fig. 3.4). Thus, we need a process or source component that does enrich/is enriched in Rb over Sr and U, Th, over Pb and Th relative to U to be responsible for the observed trace element and isotope variations beneath Nordeste (Figs. 3.4, 3.6, 3.7).

3.6.2.1 Sediments

One possibility to explain the enriched Nordeste signatures could be the presence of subducted sediment in the Nordeste mantle source (Turner *et al.*, 1997). In general, the occurrence of recycled sediments would lead to an enrichment of the incompatible elements (Fig. 3.9; Weaver *et al.*, 1986). Also, sediments in general have relatively high Rb/Sr ratios (Plank & Langmuir, 1998) which is in good agreement with the elevated Rb/Sr and $^{87}\text{Sr}/^{86}\text{Sr}$ isotope ratios of Nordeste. Most sedimentary compositions also have lower Sm/Nd and Lu/Hf ratios which also corresponds to the low Nd and Hf isotope compositions at Nordeste (Fig. 3.6). However, sediments in the Nordeste mantle source would also lead to an enrichment in Pb (Weaver *et al.*, 1986), even at very low sediment concentrations in the source ($> 0.2\%$, Table 3.2), which contrasts strikingly with the Nordeste mantle signature having depleted Pb concentrations (Fig. 3.9, Table 3.2). Although the Ce/Pb and Nb/U ratios

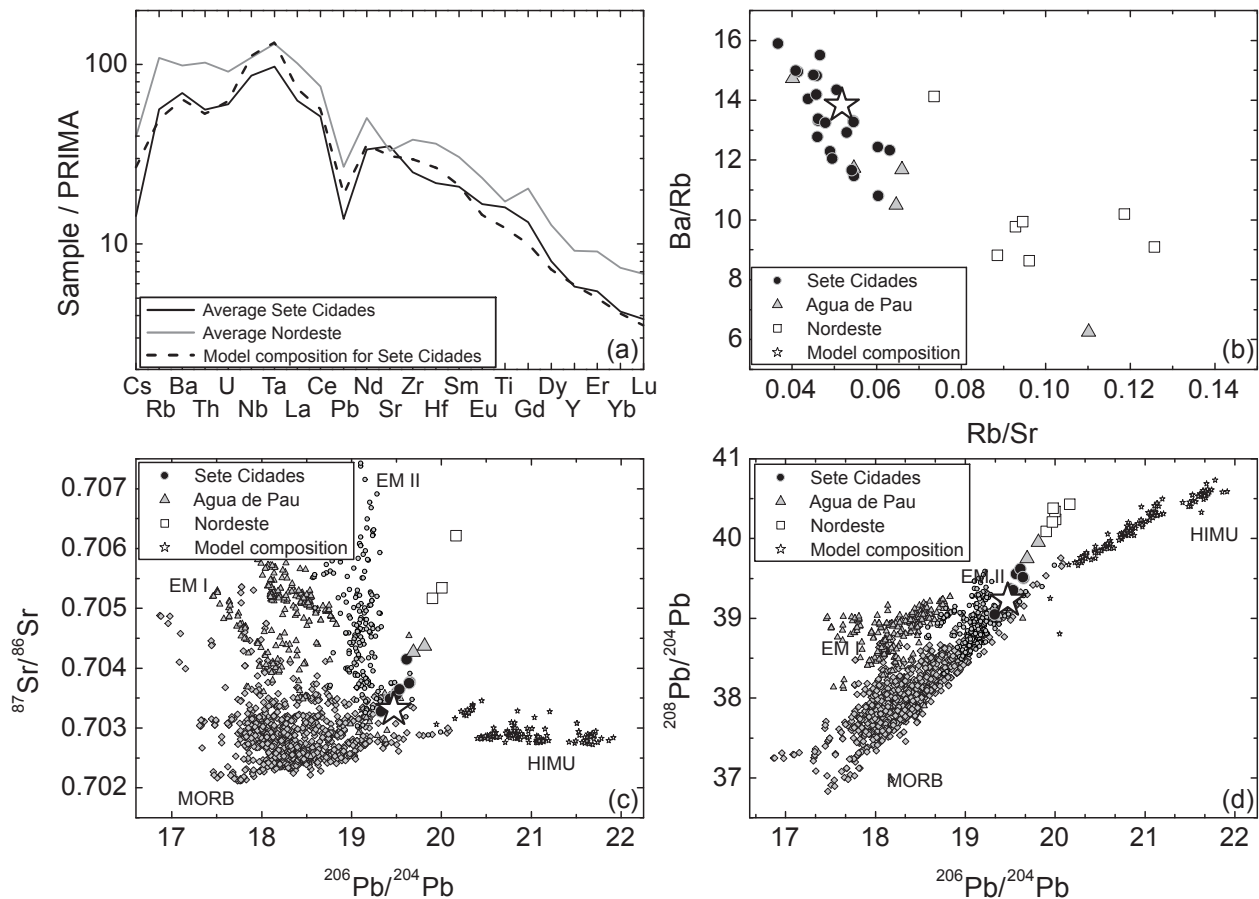


Figure 3.8: Trace element and isotopic model for the Sete Cidades volcanic system; a) shows the trace element pattern of 8 % bulk subducted crust (15 % average E-MORB (Niu & O'Hara, 2003), 18 % altered N-MORB (Kelley *et al.*, 2003), 67 % Gabbro (Hart *et al.*, 1999)) mixed with an ambient mantle source (Salters & Stracke, 2004), b) shows representative trace element ratios, respectively, c) and d) comprise the isotope ratios for 3 Ga derivation age and 2 Ga recycling age for this source composition. (Initial isotopic compositions: $^{206}\text{Pb}/^{204}\text{Pb} = 14.73$, $^{207}\text{Pb}/^{204}\text{Pb} = 15.12$, $^{208}\text{Pb}/^{204}\text{Pb} = 34.10$, $^{87}\text{Sr}/^{86}\text{Sr} = 0.702245$, $^{143}\text{Nd}/^{144}\text{Nd} = 0.510088$, $^{176}\text{Hf}/^{177}\text{Hf} = 0.281521$). The Sete Cidades isotopic composition resembles the so-called FOZO array (White, 1985; Zindler & Hart, 1986). Detailed compositions of the calculated trace element model are given in Table 3.2.

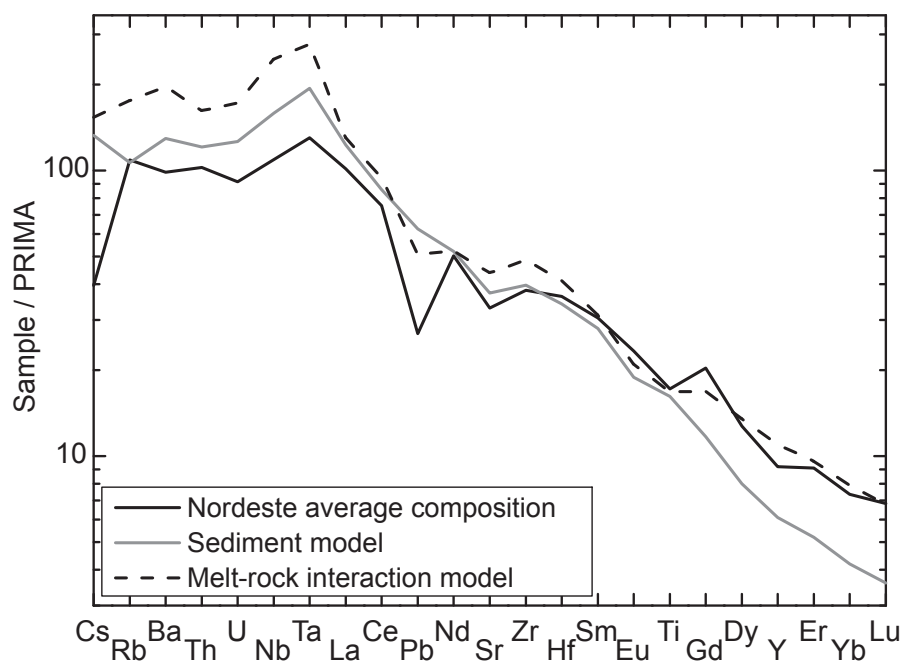


Figure 3.9: Primitive upper mantle (McDonough & Sun, 1995) normalised trace element concentrations of models assuming the involvement of sediments (GLOSS, Plank & Langmuir, 1998) or melt-rock interactions as also proposed by Elliott *et al.* (resubmitted). Both models do not fit to the observed average Nordeste composition. Detailed trace element compositions are given in Table 3.2.

of Nordeste are slightly lower than at Sete Cidades (Fig. 3.4), they cannot be explained by the presence of sediments in the source, because even slight amounts of sediment significantly increase the Pb concentrations leading to much lower Ce/Pb ratios than observed at Nordeste (Table 3.2). An enrichment of Pb would also lead to low U/Pb and Th/Pb and, in turn, to relatively unradiogenic Pb isotope ratios (e.g. Enriched Mantle sources, Fig. 3.6). Especially the combination of radiogenic Sr and unradiogenic Pb isotope ratios in sediments makes their occurrence to appear unlikely at Nordeste. Even the most radiogenic $^{206}\text{Pb}/^{204}\text{Pb}$ ratios found in some marine sediments (Kramers & Tolstikhin, 1997) are not radiogenic enough to account for the Nordeste signature. Other incompatible element ratios such as Ba/Rb and Ba/Th are higher in the majority of the subducted sediments than at Nordeste. Therefore we suggest that sediments are not the origin of the enriched Nordeste signature.

3.6.2.2 Subcontinental lithosphere

An alternative model proposed by Widom *et al.* (1997) suggests the presence of delaminated subcontinental lithosphere beneath Nordeste. Because the Nordeste lavas have lower Ba/Rb ratios than other oceanic basalts (Fig. 3.4; Hofmann & White, 1983), these authors assumed a metasomatised phlogopite, K-richterite bearing mantle source from delaminated continental lithosphere beneath the eastern part of São Miguel. Lithospheric mantle from the opening of the Atlantic may be tapped by rising plume melts (Widom *et al.*, 1997). We do not find any evidence for the influence of neither amphibole nor phlogopite from the major and trace elements. Our samples do not show any significant change in the $\text{K}_2\text{O}/\text{TiO}_2$ and $\text{Na}_2\text{O}/\text{K}_2\text{O}$ ratios between Sete Cidades and Nordeste which would be expected if amphibole or phlogopite would be present in the Nordeste sources (Fig. 3.2). A negative correlation between Ba/Rb and Nb/La could give evidence for the presence of phlogopite, whereas the presence of amphibole would increase the Ba/Rb ratio, only. However, the presence of phlogopite would also fractionate the K/La ratio (Fig. 3.2), because the partition coefficient for K ($K_D = 3.67$) is very much

higher than for La ($K_D = 0.28$) in phlogopite (LaTourrette *et al.*, 1995). Another argument against the presence of a delaminated lithospheric component is that this component cannot account for the high Pb isotope ratios (Hawkesworth *et al.*, 1990). Lastly, the $^{176}\text{Hf}/^{177}\text{Hf}$ isotope ratios and published $^{187}\text{Os}/^{188}\text{Os}$ isotope ratios are also difficult to reconcile with a lithospheric source component. Lithospheric melts are generally characterised by high $^{176}\text{Lu}/^{177}\text{Hf}$ and $^{187}\text{Re}/^{188}\text{Os}$ ratios (Bizimis *et al.*, 2003; Jung *et al.*, 2005; Salters *et al.*, 2006) leading, with time, to very radiogenic Hf and Os isotope ratios (e.g. Ionov *et al.*, 2005) contrary to the ratios observed at Nordeste. Published $^{187}\text{Os}/^{188}\text{Os}$ isotope data (Widom & Shirey, 1996; Schaefer *et al.*, 2002) from several Azorean islands including São Miguel have low $^{187}\text{Os}/^{188}\text{Os}$ isotope ratios (0.13338 - 0.14196) and very low $^{176}\text{Hf}/^{177}\text{Hf}$ isotope ratios (0.28230 - 0.28279). The presence of metasomatised, delaminated subcontinental lithosphere therefore seems unlikely to account for the enriched Nordeste signature.

3.6.2.3 Melt-rock interactions

Another possibility to account for the radiogenic Sr and Pb isotope ratios, unradiogenic Nd and Hf isotope ratios and enriched trace element pattern could be a mantle source enriched by small-degree melts, melt-rock interaction processes or melt metasomatism (Donnelly *et al.*, 2004; Workman *et al.*, 2004). Infiltration of small-degree melts into a depleted mantle source leads to enriched incompatible elements relative to the more compatible and REE elements. It also leads to an enrichment of Rb over Sr, and U and Th over Pb which could indeed explain the radiogenic isotope ratios of Nordeste. Assuming ancient melting processes in the upper mantle (see also Elliott *et al.*, resubmitted), the enriched Sr and Pb isotopic signatures can be modelled using a highly enriched low-degree melt in the garnet stability field of a previously depleted mantle source (Workman & Hart, 2005). If this melt composition remains isolated over at least 2.5 Ga, the Sr and Pb isotopes are even more enriched than originally found in the Nordeste volcanics and the Nd and Hf isotope ratios are lowered to the range of the Nordeste samples. In this case we have to assume that the Nordeste rocks do not only represent the pure end member composition but also represent a binary mixing composition between the most enriched member and the Sete Cidades mantle source. A similar model has recently been suggested by Elliott *et al.* (resubmitted). Their model is mainly based on the Nd and Hf relationships and they suggested that the contrast between isotope ratios and incompatible elements suggests an unusually old component rather than a distinct mantle source composition at Nordeste.

Although such melt-rock interaction scenarios may explain the isotopic variations, severe problems occur concerning the incompatible trace elements. The melt-rock interaction model leads to an increase of the incompatible element concentrations which results in a steeper trace element pattern than observed at São Miguel (Fig. 3.9, Table 3.2). Consequently, the incompatible trace element ratios ((Rb, Ba, Th, U)/La) significantly increase leading to trace element patterns which are comparable to those observed in lavas from EM-related islands (e.g. Society; Willbold & Stracke, 2005). The melt model also increases the Nb/La and Nb/Zr ratios, whereas the Nordeste lavas show lower Nb/Zr than the Sete Cidades basalts (Fig. 3.4). Although an increase of the U/Pb and Th/Pb suggests a fit of the model, the less depleted Pb relative to Nd and Sr does not fit to the observations (Fig. 3.9). Hence, the increasing U/Pb and Th/Pb ratios are a result of the disproportional enrichment of Th and U relative to the enrichment of Pb rather than by an enrichment of Th and U, only. The discrepancies between isotope and trace element systematics of the melt-rock interaction models were also observed by Elliott *et al.* (resubmitted) and, as a result, they proposed a decoupled behaviour of the trace elements and isotopes at São Miguel. Whereas the isotopic signature of their model is a result of an ancient modest-degree melt, the incompatible trace element signatures of this model are thought to be of secondary

origin, suggesting the assimilation of syenite nodules into the rising magma. We do not find any evidence for the presence of syenite in the most enriched eastern lavas from Nordeste and the trace element ratios such as K_2O/TiO_2 do not give any evidence for the assimilation of syenite (Fig. 3.2). Some syenite nodules were found at the NW-flank of Agua de Pau and at the western flank of Sete Cidades (Beier *et al.*, 2006), nonetheless, even though these magmas contain syenites, they do not show any major or trace element evidence that the nodules were significantly assimilated into the magma.

The conspicuous correlation of the Rb/Sr ratios and $^{87}Sr/^{86}Sr$ isotope ratios (Fig. 3.7) makes a decoupled behaviour of the trace element and isotope systematics to appear unlikely. Summarizing we suggest that the occurrence of melt-rock interaction processes may be able to explain the isotopic variations in the enriched São Miguel lavas, but fails to explain the trace element variations. The correlation of the trace elements and isotope ratios gives evidence for a source, rather than a secondary assimilation signature and should therefore be taken into consideration.

3.6.2.4 Subduction of enriched basalts and trachytes

The similarities of the Sete Cidades and Nordeste major and trace element pattern suggest that both source components originated from similar precursors. Since the Sete Cidades mantle source contains some kind of recycled enriched MORB or alkaline basaltic material it seems reasonable, because of the spatial proximity between the two volcanoes, to assume that the enriched mantle source at Nordeste also originates from recycling. From the previous discussion, we can exclude several processes commonly associated with the origin of radiogenic isotope signatures, such as alteration processes that would lead to the isotopic compositions of HIMU or the presence of sediments leading to less radiogenic Pb isotope and much lower Ce/Pb and Nb/U ratios. Compared to Sete Cidades, however, the recycled crust involved at Nordeste must be more enriched in several elements (e.g. Rb relative to Ba, U relative to Th) and thus is likely to represent a more enriched oceanic crust than in the Sete Cidades mantle source. A ubiquitous source of enriched lavas on the ocean floor are seamounts; i.e. the compositions of seamounts generally resemble the trace element compositions of OIB (McKenzie *et al.*, 2004) and range from incompatible element depleted tholeiitic basalts to incompatible element enriched transitional and alkali basalts (Zindler *et al.*, 1984). The Sr, Nd and Pb isotope ratios range from MORB-like depleted tholeiites to relatively radiogenic compositions in the alkali basalts (Graham *et al.*, 1988) covering a large range in isotopic and trace element compositions. In addition, the trace element pattern of Nordeste exhibit depletions in Sr (relative to Nd), Eu, Ti (relative to Gd) and Rb relative to Ba (Fig. 3.3). These depletions could indicate a possible precursor rock with an intermediate to evolved composition because the crystallisation of typical mineral assemblages at oceanic islands such as alkali feldspar and Fe-Ti oxides lead to strongly decreased Sr and Rb and slightly decreased Eu (alkali feldspar) and Ti (Fe-Ti oxides) as a result of the high compatibility of these elements to the referring mineral assemblage. Adding a small amount (~ 0.8 - 2 %) of a trachyte from the Koko volcano at the Hawaiian-Emperor chain (Regelous *et al.*, 2003) to the modelled composition of the Sete Cidades mantle source fits best to the Nordeste trace element pattern (Fig. 3.10). The Koko seamount rocks are depleted in Ba, Sr, and Ti due to the fractionation of alkali feldspar and Fe-Ti oxides. This evolved composition also fits the observed Th/Pb, U/Pb, and Th/U ratios, i.e. it increases the Th/Pb and U/Pb and decreases Nb/La and Nb/Zr ratios relative to the Sete Cidades compositions (Table 3.2).

We conclude that adding a seamount trachyte to the Sete Cidades mantle source is able to explain the isotope systematics and incompatible element compositions at Nordeste. Assuming a recycling age of 1.25 Ga and

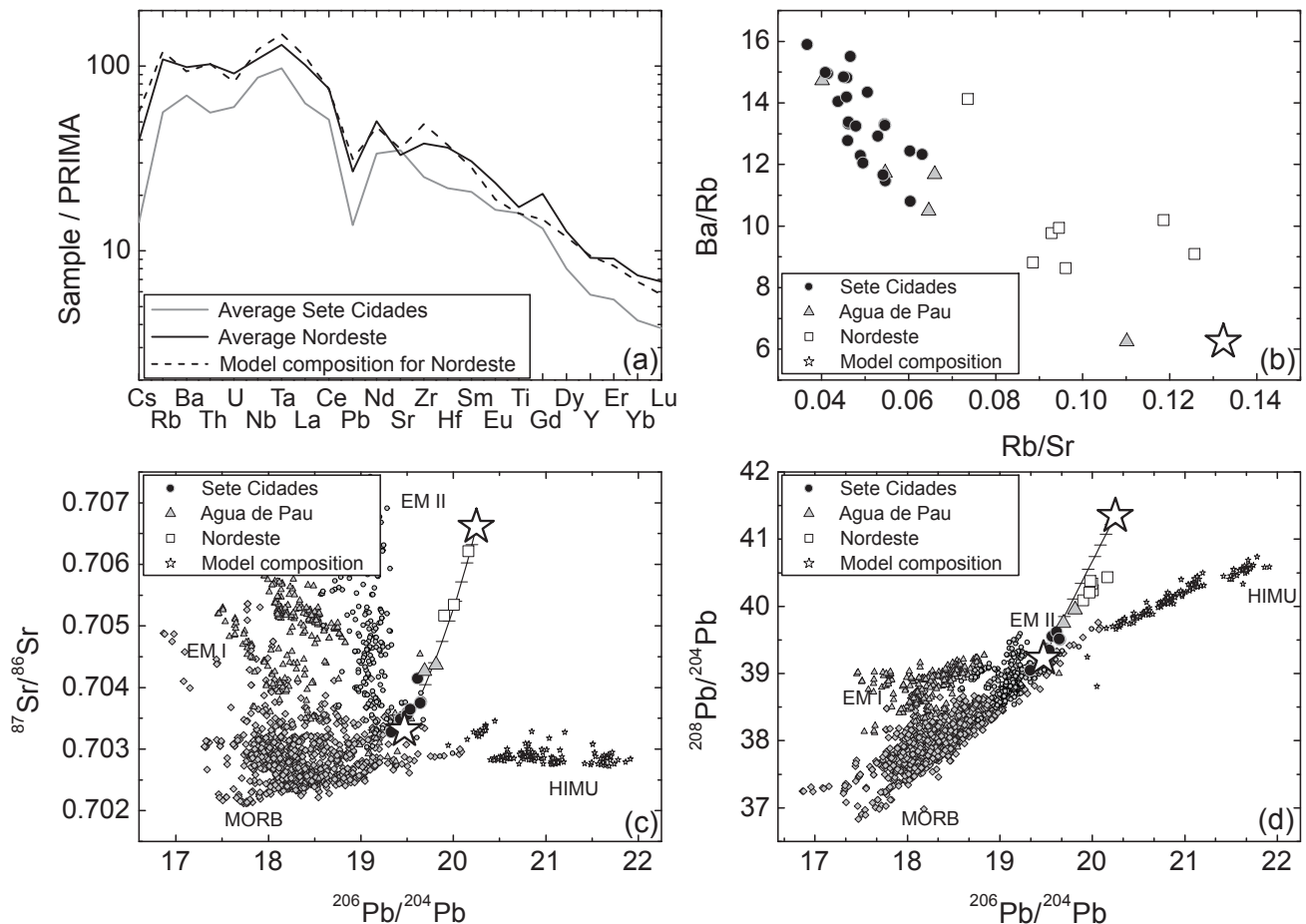


Figure 3.10: Trace element and isotopic model for Nordeste volcanic system; a) shows the trace element pattern of 5 % bulk subducted crust (17 % E-MORB (Niu & O'Hara, 2003), 18 % altered N-MORB (Kelley *et al.*, 2003), 65 % Gabbro (Hart *et al.*, 1999)) mixed with an ambient mantle source (Salters & Stracke, 2004), and an evolved composition (~ 2 %) from the Hawaiian-Emperor Chain (Regelous *et al.*, 2003). b) shows representative trace element ratios, respectively, c) and d) comprise the isotope ratios for 3 Ga derivation age and 1.25 Ga recycling age. (Initial isotopic compositions: $^{206}\text{Pb}/^{204}\text{Pb} = 15.96$, $^{207}\text{Pb}/^{204}\text{Pb} = 15.34$, $^{208}\text{Pb}/^{204}\text{Pb} = 35.35$, $^{87}\text{Sr}/^{86}\text{Sr} = 0.702679$, $^{143}\text{Nd}/^{144}\text{Nd} = 0.511196$, $^{176}\text{Hf}/^{177}\text{Hf} = 0.282152$). Tick marks of the mixing array represent 10 % steps of the mixing array between the calculated Sete Cidades and Nordeste mantle sources.

a derivation age of 3 Ga from bulk silicate earth we are able to reproduce both the trace element pattern of Nordeste and the isotopic ratios (Fig. 3.10). The recycling of both slightly altered trachytic and basaltic material significantly increases the Rb/Sr, U/Pb, Th/Pb and Th/U ratios and, in turn, is able to produce the radiogenic Nordeste signatures. The elevated Rb/Sr and Th/Pb ratios and lower Sm/Nd and Lu/Hf in the trachyte also lead to enriched $^{87}\text{Sr}/^{86}\text{Sr}$, $^{208}\text{Pb}/^{204}\text{Pb}$ and lower $^{143}\text{Nd}/^{144}\text{Nd}$ and $^{176}\text{Hf}/^{177}\text{Hf}$ isotope ratios which is observed at Nordeste. To that extent our model is consistent with Elliott *et al.* (resubmitted) assuming an evolved component to be responsible for the Nordeste trace element systematics. We differ from these authors that the evolved signature is of recent origin due to the fact that the trace elements are well correlated to the isotopes (Fig. 3.7), and, in case of a recent assimilation of syenite, the major elements would also be changed (Fig. 3.2).

Whereas a recycled seamount containing significant amounts of evolved lavas might best explain the combined trace element and isotope systematics at Nordeste, the Sete Cidades mantle source may contain only enriched alkaline basaltic material; i.e. both sources have a similar geodynamic origin from recycling of oceanic crust. This is also consistent with the low oxygen isotopes found in olivines from the São Miguel lavas (Widom & Farquhar, 2003).

The unique occurrence of the Nordeste isotope signature among the world's known isotopic compositions can be explained by the rare occurrence of evolved seamount lavas compared to primitive compositions but also by the scarce subduction of seamounts that are accreted rather than subducted. Although rare, seismic velocity images (Kodaira *et al.*, 2000) and the investigation of magnetic anomalies (Yamazaki & Okamura, 1989) revealed that seamounts are subducted as recently observed along the Japan Trench (Lallemand & Le, 1987).

3.7 CONCLUSIONS

The similarities of the trace elements and isotopes between the São Miguel samples and the so-called HIMU islands such as Tubuaii and St. Helena suggest that these mantle source have a common origin although variations in the incompatible trace elements and isotopes indicate differences in degree of alteration and composition of the recycled components. We suggest that the mantle sources of both Sete Cidades and Nordeste contain recycled, altered oceanic crust which was altered less during subduction than the HIMU sources. The relatively depleted Sr, Ti, Eu, and Ba concentrations of Nordeste indicate that crystal fractionation must have played an important role in the precursor rock; i.e. the crystallisation of alkali feldspar and Fe-Ti oxides in evolved lavas leads to depletions in these elements. Modelling the western Sete Cidades mantle source in terms of trace elements and Sr-Nd-Hf-Pb isotopes leads to the assumption that a subduction of altered, recycled, enriched oceanic crust might best explain this volcanoes pattern. The Nordeste trace element and isotopic systematics can be modelled modifying the Sete Cidades mantle source with an evolved seamount composition. Very small amounts (~ 0.8-2 %) of a subducted, altered trachytic composition account for an enrichment of the Nordeste lavas relative to the Sete Cidades rocks and HIMU (Fig. 3.10). A derivation age of 3 Ga for both sources not only reflects their similar origin, but also reflects the formation of the oceanic lithosphere at the time of increased crustal growth as inferred from Sm-Nd age constraints (Hurley & Rand, 1969; DePaolo & Wasserburg, 1979; Veizer & Jansen, 1979; McLennan & Taylor, 1982). The subduction of a seamount would be the most likely geological scenario possible (Cloos, 1993), because it is not only able to explain the similarity between the two sources as well as similar derivation ages but also reflects a common geodynamic process (recycling) for the origin of mantle source signatures.

3.8 ACKNOWLEDGMENTS

We gratefully acknowledge the help of H. Baier, K. Mezger, and F. Hauff with the isotope analyses and D. Garbe-Schönberg with the ICP-MS analyses. This study has been funded by the Deutsche Forschungsgemeinschaft through grants Ha 2568/6-1, Ha 2568/9-2, and Ha 2100/7-1.

REFERENCES

- Abdel Monem, A.A., Fernandez, L.A. and Boone, G.M. (1975) K-Ar-Ages from the eastern Azores group (Santa Maria, Sao Miguel and the Formigas islands). *Lithos* **8**, 247-254.
- Allegre, C.J., Hamelin, B., Provost, A. and Dupre, B. (1987) Topology in isotopic multispace and origin of mantle chemical heterogeneities. *Earth and Planetary Science Letters* **81**, 319-337.
- Beier, C., Haase, K.M. and Hansteen, T.H. (2006) Magma evolution of the Sete Cidades volcano, São Miguel, Azores. *Journal of Petrology*, DOI: 10.1093/petrology/egl014.
- Bizimis, M., Sen, G. and Salters, V.J.M. (2003) Hf-Nd isotope decoupling in the oceanic lithosphere: constraints from spinel peridotites from Oahu, Hawaii. *Earth and Planetary Science Letters* **217**, 43-58.
- Booth, B., Croasdale, R., Walker, G.P.L. and F.R.S. (1978) A quantitative study of five thousand years of volcanism on Sao Miguel, Azores. *Philosophical Transactions of the Royal Society of London* **288**, 271-319.
- Cloos, M. (1993) Lithospheric buoyancy and collisional orogenesis; subduction of oceanic plateaus, continental margins, island arcs, spreading ridges, and seamounts. *Geological Society of America Bulletin* **105**, 715-737.
- Davies, G.R., Norry, M.J., Gerlach, D.C. and Cliff, R.A. (1989) A combined chemical and Pb-Sr-Nd isotope study of the Azores and Cap Verde hot-spots: the geodynamic implications. In: Saunders, A. D. and Norry, M. J. (eds.) *Magmatism in the Oceanic Basins*. pp. 231-255. Geological Society Special Publications.
- DePaolo, D.J. and Wasserburg, G.J. (1979) Sm-Nd age of the Stillwater Complex and the mantle evolution curve for neodymium. *Geochimica et Cosmochimica Acta* **43**, 999-1008.
- Donnelly, K.E., Goldstein, S.L., Langmuir, C.H. and Spiegelman, M. (2004) Origin of enriched ocean ridge basalts and implications for mantle dynamics. *Earth and Planetary Science Letters* **226**, 347-366.
- Doucelance, R., Escrig, S., Moreira, M., Gariépy, C. and Kurz, M.D. (2003) Pb-Sr-He isotope and trace element geochemistry of the Cape Verde Archipelago. *Geochimica et Cosmochimica Acta* **67**, 3717-3733.
- Elliott, T., Blichert-Toft, J., Heumann, A., Koetsier, G. and Forjaz, V. (resubmitted) The origin of enriched mantle beneath São Miguel, Azores. *Geochimica et Cosmochimica Acta*.
- Garbe-Schönberg, C.-D. (1993) Simultaneous determination of thirty-seven trace elements in twenty-eight international rock standards by ICP-MS. *Geostandards Newsletters* **17**, 81-97.
- Graham, D.W., Humphris, S.E., Jenkins, W.J. and Kurz, M.D. (1992) Helium isotope geochemistry of some volcanic rocks from Saint Helena. *Earth and Planetary Science Letters* **110**, 121-131.
- Graham, D.W., Zindler, A., Kurz, M.D., Jenkins, W.J., Batiza, R. and Staudigel, H. (1988) He, Pb, Sr and Nd isotope constraints on magma genesis and mantle heterogeneity beneath young Pacific seamounts. *Contribu-*

tions to *Mineralogy and Petrology* **99**, 446-463.

Haase, K.M. (1996) The relationship between the age of the lithosphere and the composition of oceanic magmas: Constraints on partial melting, mantle sources and the thermal structure of the plates. *Earth and Planetary Science Letters* **144**, 75-92.

Haase, K.M. and Beier, C. (2003) Tectonic control of ocean island basalt sources on Sao Miguel, Azores? *Geophysical Research Letters* **30**, 1856.

Hart, S.R. (1988) Heterogeneous Mantle Domains - Signatures, Genesis and Mixing Chronologies. *Earth and Planetary Science Letters* **90**, 273-296.

Hart, S.R., Blusztajn, J., Dick, H.J.B., Meyer, P.S. and Muehlenbachs, K. (1999) The fingerprint of seawater circulation in a 500-meter section of ocean crust gabbros. In: *A group of papers in honor of Claude Allegre on his sixtieth birthday*. pp. 4059-4080. Pergamon: Oxford, International.

Hart, S.R., Hauri, E.H., Oschmann, L.A. and Whitehead, J.A. (1992) Mantle plumes and entrainment; isotopic evidence. *Science* **256**, 517-520.

Hart, S.R. and Zindler, A. (1989) Constraints on the nature and development of chemical heterogeneities in the mantle. In: *Mantle convection; plate tectonics and global dynamics*. pp. 261-387. Gordon & Breach Science Publishers: New York, NY, United States.

Hawkesworth, C.J., Erlank, A.J., Kempton, P.D. and Waters, F.G. (1990) Mantle metasomatism; isotope and trace-element trends in xenoliths from Kimberley, South Africa. *Chemical Geology* **85**, 19-34.

Hawkesworth, C.J., Norry, M.J., Roddick, J.C. and Vollmer, R. (1979) $^{143}\text{Nd}/^{144}\text{Nd}$ and $^{87}\text{Sr}/^{86}\text{Sr}$ ratios from the Azores and their significance in LIL-element enriched mantle. *Nature* **280**, 28-31.

Hoernle, K., Tilton, G. and Schmincke, H.-U. (1991) Sr-Nd-Pb isotopic evolution of Gran Canaria: evidence for shallow enriched mantle beneath the Canary Islands. *Earth and Planetary Science Letters* **106**, 44-63.

Hofmann, A.W. (1988) Chemical differentiation of the Earth: the relationship between mantle, continental crust, and oceanic crust. *Earth and Planetary Science Letters* **90**, 297-314.

Hofmann, A.W. and White, W.M. (1980) The role of subducted oceanic crust in mantle evolution. *Year Book - Carnegie Institution of Washington* **79**, 477-483.

Hofmann, A.W. and White, W.M. (1983) Ba, Rb and Cs in the Earth's mantle. *Zeitschrift fur Naturforschung* **38 a**, 256-266.

Hurley, P.M. and Rand, J.R. (1969) Pre-drift continental nuclei. *Science* **164**, 1229-1242.

- Ionov, D.A., Blichert-Toft, J. and Weis, D. (2005) Hf isotope compositions and HREE variations in off-craton garnet and spinel peridotite xenoliths from central Asia. *Geochimica et Cosmochimica Acta* **69**, 2399-2418.
- Jorgensen, J.O. and Holm, P.M. (2002) Temporal variation and carbonatite contamination in primitive ocean island volcanics from Sao Vicente, Cape Verde Islands. *Chemical Geology* **192**, 249-267.
- Jung, S., Pfänder, J., Brüggmann, G. and Stracke, A. (2005) Sources of primitive alkaline volcanic rocks from the Central European Volcanic Province (Rhön, Germany) inferred from Hf, Os and Pb isotopes. *Contributions to Mineralogy and Petrology* **150**, 546-559.
- Kelley, K.A., Plank, T., Ludden, J. and Staudigel, H. (2005) Subduction cycling of U, Th, and Pb. *Earth and Planetary Science Letters* **234**, 369-383.
- Kelley, K.A., Plank, T., Ludden, J.N. and Staudigel, H. (2003) Composition of altered oceanic crust at ODP Sites 801 and 1149. *Geochemistry, Geophysics, Geosystems* **4**, DOI: 10.1029/2002GC000435
- Kodaira, S., Takahashi, N., Nakanishi, A., Miura, S. and Kaneda, Y. (2000) Subducted seamount imaged in the rupture zone of the 1946 Nankaido earthquake. *Science* **289**, 104-106.
- Kogiso, T., Tatsumi, Y. and Nakano, S. (1997) Trace element transport during dehydration processes in the subducted oceanic crust; 1, Experiments and implications for the origin of ocean island basalts. *Earth and Planetary Science Letters* **148**, 193-205.
- Kramers, J.D. and Tolstikhin, I.N. (1997) Two terrestrial lead isotope paradoxes, forward transport modelling, core formation and the history of the continental crust. In: *Highlights of the Goldschmidt meeting, in honor of A. W. Hofmann*. pp. 75-110. Elsevier: Amsterdam, Netherlands.
- Lallemand, S. and Le, P.X. (1987) Coulomb wedge model applied to the subduction of seamounts in the Japan Trench. *Geology (Boulder)* **15**, 1065-1069.
- LaTourrette, T., Hervig, R.L. and Holloway, J.R. (1995) Trace element partitioning between amphibole, phlogopite, and basanite melt. *Earth and Planetary Science Letters* **135**, 13-30.
- McDonough, W.F. and Sun, S.-S. (1995) The composition of the Earth. *Chemical Geology* **120**, 223-253.
- McKenzie, D., Stracke, A., Blichert, T.J., Albarede, F., Gronvold, K. and O, N.R.K. (2004) Source enrichment processes responsible for isotopic anomalies in oceanic island basalts. *Geochimica et Cosmochimica Acta* **68**, 2699-2724.
- McLennan, S.M. and Taylor, S.R. (1982) Geochemical constraints on the growth of the continental crust. *Journal of Geology* **90**, 347-361.
- Moore, R.B. (1990) Volcanic geology and eruption frequency, Sao Miguel, Azores. *Bulletin of Volcanology* **52**, 602-614.

- Moore, R.B. (1991) Geology of three late Quaternary stratovolcanos on Sao Miguel, Azores. pp. 1-46. In: *U.S. Geological Survey Bulletin*. U.S. Geological Service.
- Moreira, M., Doucelance, R., Kurz, M.D., Dupre, B. and Allegre, C.J. (1999) Helium and lead isotope geochemistry of the Azores Archipelago. *Earth and Planetary Science Letters* **169**, 189-205.
- Münker, C., Weyer, S., Scherer, E. and Mezger, K. (2001) Separation of high field strength elements (Nb, Ta, Zr, Hf) and Lu from rock samples for MC-ICPMS measurements. *Geochemistry, Geophysics, Geosystems* **2**, DOI: 10.1029/2001GC000183.
- Nakamura, Y. and Tatsumoto, M. (1988) Pb, Nd, and Sr isotopic evidence for a multicomponent source for rocks of Cook-Austral Islands and heterogeneities of mantle plumes. *Geochimica et Cosmochimica Acta* **52**, 2909-2924.
- Niu, Y. and O'Hara, M.J. (2003) Origin of ocean island basalts; a new perspective from petrology, geochemistry, and mineral physics considerations. *Journal of Geophysical Research, B, Solid Earth and Planets* **108**, DOI: 10.1029/2002JB002048.
- Palacz, Z.A. and Saunders, A.D. (1986) Coupled trace element and isotope enrichment in the Cook-Austral-Samoa islands, Southwest Pacific. *Earth and Planetary Science Letters* **79**, 270-280.
- Plank, T. and Langmuir, C.H. (1998) The chemical composition of subducting sediment and its consequences for the crust and mantle. In: *Geochemical Earth Reference Model (GERM)*. pp. 325-394. Elsevier: Amsterdam, Netherlands.
- Regelous, M., Hofmann, A.W., Abouchami, W. and Galer, S.J.G. (2003) Geochemistry of Lavas from the Emperor Seamounts, and the Geochemical Evolution of Hawaiian Magmatism from 85 to 42 Ma. *Journal of Petrology* **44**, 113-140.
- Salters, V., Blichert-Toft, J., Fekiacova, Z., Sachi-Kocher, A. and Bizimis, M. (2006) Isotope and trace element evidence for depleted lithosphere in the source of enriched Ko'olau basalts. *Contributions to Mineralogy and Petrology* **151**, 297-312.
- Salters, V.J.M. and Stracke, A. (2004) Composition of the depleted mantle. *Geochemistry, Geophysics, Geosystems* **5**, DOI: 10.1029/2003GC000597.
- Salters, V.J.M. and White, W.M. (1998) Hf isotope constraints on mantle evolution. In: *Geochemical Earth Reference Model (GERM)*. pp. 447-460. Elsevier: Amsterdam, Netherlands.
- Schaefer, B.F., Turner, S., Parkinson, I., Rogers, N. and Hawkesworth, C. (2002) Evidence for recycled Archaean oceanic mantle lithosphere in the Azores plume. *Nature* **420**, 304-307.
- Schiano, P., Burton, K.W., Dupre, B., Birck, J.L., Guille, G. and Allegre, C.J. (2001) Correlated Os-Pb-Nd-Sr

- isotopes in the Austral-Cook Chain basalts; the nature of mantle components in plume sources. *Earth and Planetary Science Letters* **186**, 527-537.
- Stracke, A., Bizimis, M. and Salters, V.J.M. (2003) Recycling oceanic crust: Quantitative constraints. *Geochemistry, Geophysics, Geosystems* **4**, DOI: 10.1029/2001GC000223.
- Stracke, A., Hofmann, A.W. and Hart, S.R. (2005) FOZO, HIMU and the rest of the mantle zoo. *Geochemistry, Geophysics, Geosystems* **6**, DOI: 10.1029/2004GC000824.
- Todt, W., Cliff, R.A., Hanser, A. and Hofmann, A.W. (1996) Evaluation of a ^{202}Pb - ^{205}Pb double spike for high-precision lead isotope analyses. In: AGU (ed.) *Earth-Processes: Reading the isotopic code*. pp. 429-437.
- Turner, S., Hawkesworth, C., Rogers, N. and King, P. (1997) U-Th isotope disequilibria and ocean island basalt generation in the Azores. In: Hawkesworth, C. and Arndt, N. T. (eds.) *Highlights of the Goldschmidt meeting, in honor of A. W. Hofmann*. pp. 145-164. Elsevier: Amsterdam, Netherlands.
- Veizer, J. and Jansen, S.L. (1979) Basement and sedimentary recycling and continental evolution. *Journal of Geology* **87**, 341-370.
- Vogt, P.R. and Jung, W.Y. (2004) The Terceira Rift as hyper-slow, hotspot-dominated oblique spreading axis: A comparison with other slow-spreading plate boundaries. *Earth and Planetary Science Letters* **218**, 77-90.
- Weaver, B.L., Wood, D.A., Tarney, J. and Joron, J.L. (1986) Role of subducted sediment in the genesis of ocean-island basalts; geochemical evidence from South Atlantic Ocean Islands. *Geology (Boulder)* **14**, 275-278.
- Weis, D. (1983) Pb isotopes in Ascension Island rocks; oceanic origin for the gabbroic to granitic plutonic xenoliths. *Earth and Planetary Science Letters* **62**, 273-282.
- Weis, D., Demaiffe, D., Cauet, S. and Javoy, M. (1987) Sr, Nd, O and H isotopic ratios in Ascension Island lavas and plutonic inclusions; cogenetic origin. *Earth and Planetary Science Letters* **82**, 255-268.
- White, W.M. (1985) Sources of oceanic basalts: radiogenic isotopic evidence. *Geology* **13**, 115-118.
- Widom, E., Carlson, R.W., Gill, J.B. and Schmincke, H.U. (1997) Th-Sr-Nd-Pb isotope and trace element evidence for the origin of the Sao Miguel, Azores, enriched mantle source. *Chemical Geology* **140**, 49-68.
- Widom, E. and Farquhar, J. (2003) Oxygen isotope signatures in olivines from Sao Miguel (Azores) basalts: implications for crustal and mantle processes. *Chemical Geology* **193**, 237-255.
- Widom, E. and Shirey, S.B. (1996) Os isotope systematics in the Azores: implications for mantle plume sources. *Earth and Planetary Science Letters* **142**, 451-465.

Willbold, M. and Stracke, A. (2005) The trace element composition of mantle end-members: implications for recycling of oceanic and upper/lower continental crust. *Geochemistry, Geophysics, Geosystems* **7**, DOI: 10.1029/2005GC001005.

Workman, R.K. and Hart, S.R. (2005) Major and trace element composition of the depleted MORB mantle (DMM). *Earth and Planetary Science Letters* **231**, 53-72.

Workman, R.K., Hart, S.R., Jackson, M., Regelous, M., K.A., F., Blusztajn, J., Kurz, M.D. and Staudigel, H. (2004) Recycled metasomatized lithosphere as the origin of the Enriched Mantle II (EM2) end-member: Evidence from the Samoan Volcanic Chain. *Geochemistry, Geophysics, Geosystems* **5**, DOI:10.1029/2003GC000623.

Yamazaki, T. and Okamura, Y. (1989) Subducting seamounts and deformation of overriding forearc wedges around Japan. In: *Subduction zones; the Kaiko Project*. pp. 207-229. Elsevier: Amsterdam, Netherlands.

Zindler, A. and Hart, S. (1986) Chemical Geodynamics. *Annual Review of Earth and Planetary Science Letters* **14**, 493-571.

CHAPTER IV

MAGMA EVOLUTION OF THE SETE CIDADES VOLCANO, SÃO MIGUEL, AZORES

Christoph Beier^{1,2}, Karsten M. Haase^{1,3}, and Thor H. Hansteen⁴

¹Institut für Geowissenschaften, Christian-Albrechts-Universität zu Kiel, Ludewig-Meyn-Straße 10, 24118 Kiel, Germany, Email: chb@gpi.uni-kiel.de

²Max-Planck-Institut für Chemie (Otto-Hahn-Institut), Abteilung Geochemie, Joh.-Joachim-Becher-Weg 27, 55128 Mainz, Germany

³Department of Earth Sciences, University of Aarhus, C.F. Møllers Allé 110, 8000 Aarhus C, Denmark

⁴IFM-GEOMAR, Leibniz-Institut für Meereswissenschaften, Wischhofstr. 1-3, 24148 Kiel, Germany

4.1 ABSTRACT

The Sete Cidades volcano (São Miguel, Azores) is situated at the eastern end of the ultraslow spreading Terceira rift axis. The volcano comprises several dominantly basaltic pre-caldera eruptions, a trachytic caldera-forming stage, and a post-caldera stage consisting of alternating trachytic and basaltic eruptions. The post-caldera flank lavas are more primitive (> 5wt. % MgO) than the pre-caldera lavas implying extended fractional crystallization and longer crustal residence times for the pre-caldera shield-building lavas. Thermobarometric estimates show that the ascending alkali basaltic magmas stagnated and crystallized at the crust-mantle boundary (~ 15 km depth), whereas the more evolved magmas mainly fractionated in the upper crust (~ 3 km depth). The caldera-forming eruption was triggered by a basaltic injection into a shallow trachytic magma chamber. Lavas from all stages follow a single, continuous liquid line of descent from alkali basalt to trachyte, although slight differences in incompatible element (e.g. Ba/Nb, La/Nb) and Sr isotope ratios imply some heterogeneity of the mantle source. Major and trace element data suggest similar partial melting processes throughout the evolution of the volcano. Slight geochemical differences between post- and pre-caldera stage lavas from the Sete Cidades volcanic system indicate a variation in the mantle source composition with time. The oxygen fugacity increased from the pre-caldera to the post-caldera stage lavas, probably due to the assimilation of crustal rocks; this is supported by the presence of crustal xenoliths in the lavas of the flank vents. The lavas from the Sete Cidades volcano generally have low Sr isotope ratios; however rocks from one post-caldera vent on the western flank indicate mixing with magmas resembling the lavas from the neighbouring Agua de Pau volcano, having higher Sr isotope ratios. The different magma sources at Sete Cidades and the adjacent Agua de Pau volcano imply that, despite their close proximity, there is only limited interaction between them.

4.2 INTRODUCTION

Oceanic intraplate volcanoes provide insights into both the composition of the Earth's mantle and processes of magma generation and evolution during magma ascent. Ocean island magmatic systems often develop through several stages of volcanism, in which each stage typically shows a distinct chemical and isotopic composition (Woodhead, 1992). The best studied oceanic volcanoes are those of the Hawaiian islands that have evolved through four stages: (1) pre-shield, (2) shield, (3) post-shield or post-caldera, and (4) post-erosional volcanism (Clague, 1987). Although each stage has distinct geochemical variations (e.g. Chen & Frey, 1983; Abouchami *et al.*, 2000), these different stages are thought to reflect variations in source compositions and melting processes due to the movement of the lithosphere across a deep-seated mantle plume (Griffiths & Richards, 1989; Frey & Rhodes, 1993; Frey *et al.*, 1994). The Hawaiian plume is, however, unusually strong with an estimated plume buoyancy flux of 6.5 to 8.7 Mg/s, compared with a plume buoyancy flux of 1.2 Mg/s for the Azores (Sleep, 1990). Coupled with a much lower plate velocity for the Azores and other Atlantic island groups such as the Canary Islands and Madeira, melt generation and subsequent evolutionary processes may be distinct from those at Hawaii. The repeated volcanic cycles over periods of millions of years for several Atlantic islands appear to be a direct result of the relatively slow plate movement (e.g. Hoernle & Schmincke, 1993; Geldmacher *et al.*, 2000).

Chemical interaction between ascending magmas and the oceanic lithosphere can occur beneath ocean islands. Geochemical studies have shown that assimilation of old oceanic lithosphere and rocks forming the pedestal of the volcano have important consequences for the interpretation of magma compositions as indicators of the composition of the mantle source (e.g. Thirlwall *et al.*, 1997; Wolff *et al.*, 2000; Hansteen & Troll, 2003). Thus, the ascent of magmas beneath oceanic intraplate volcanoes requires detailed study in order to distinguish primary and contaminated basalts and the different possible magma sources. Although the exceptionally large range of geochemical heterogeneity in the São Miguel lavas has been the subject of several studies (Hawkesworth *et al.*, 1979; Davies *et al.*, 1989; Widom *et al.*, 1997; Haase & Beier, 2003; Widom & Farquhar, 2003), the geochemical evolution of single volcanoes on São Miguel has not yet been investigated.

The primary aim of this work is to describe the temporal magmatic evolution and the compositional variations of the Sete Cidades volcanic system, based on a series of stratigraphically well constrained samples. The Sete Cidades volcanic system has been postulated to represent one end-member of a heterogeneous São Miguel mantle source (Hawkesworth *et al.*, 1979; Widom, 1991; Widom *et al.*, 1997). Our data show a distinct evolution of mafic magmas through the stratigraphy as a result of fractional crystallization processes. We propose a petrogenetic model for the subaerial part of the Sete Cidades volcano (< 210,000 years), which emphasises the importance of both fractional crystallization and mixing processes.

4.3 GEOLOGICAL BACKGROUND

4.3.1 Geological setting of São Miguel

The eastern Azores platform is dominated by three major tectonic structures; (1) the East Azores Fracture Zone (EAFZ) in the south, (2) the NW-SE striking Terceira rift axis in the northern part of the platform, and (3) the Mid-Atlantic Ridge (MAR) in the west (Fig. 4.1). The Terceira rift axis represents the plate boundary between the Eurasian and the African plates (Krause & Watkins, 1970; Luis *et al.*, 1994) and appears to be an ultraslow

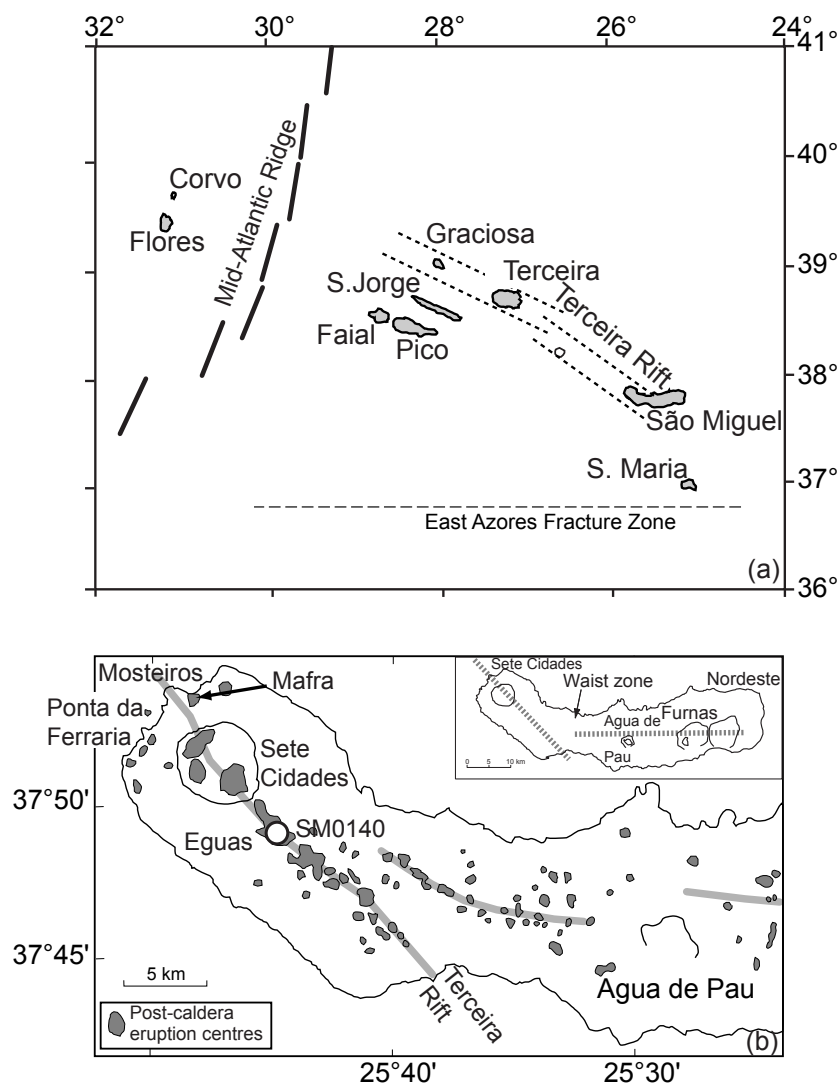


Figure 4.1: a) Map of the Azores archipelago illustrating the Azores islands and associated tectonic features based on Widom & Shirey (1996). b) Map of São Miguel, showing the western end of the island with the volcanic systems of Sete Cidades and Agua de Pau and the post-caldera eruption centres. The sample SM0140 (white circle) was taken from the post-caldera Eguas eruption centre. The inset illustrates São Miguel as a whole and the associated tectonic lineaments (Moore, 1991a). The grey lines indicate the Terceira rift axis and the Agua de Pau scoria cone line.

spreading rift with an extension rate of 2 to 4 mm/year (Searle, 1980; Luis *et al.*, 1998; Vogt & Jung, 2004). Geochemical studies of volcanic rocks from the islands and the adjacent MAR suggest the presence of a mantle plume beneath the Azores, which is also influencing the spreading axis (Schilling, 1975a; Schilling, 1975b; Widom & Shirey, 1996). Seismic tomography data show that there is a negative P-wave velocity anomaly beneath the Azores, probably reflecting a mantle plume, which according to Ritsema & Allen (2003) is restricted to the uppermost 200 km of the mantle, but according to Montelli *et al.* (2004) extends into the lower mantle.

The island of São Miguel lies at the eastern end of the Azores archipelago (Fig. 4.1) and consists of four large stratovolcanoes and a region of overlapping volcanic rift zones (Waist Zone) between the volcanoes of Sete Cidades to the west and Agua de Pau to the east (Moore, 1990; Haase & Beier, 2003). São Miguel is situated at the intersection of two regional tectonic lineaments that influence the volcanism on the island. The Sete Cidades volcano at the western end of São Miguel is situated on the Terceira rift axis, whereas the eastern three volcanoes of Agua de Pau, Furnas, and Nordeste are aligned along an E-W trend parallel to the EAFZ (Fig. 4.1). All four volcanoes have been active in the last 100,000 years although the Nordeste volcano in the far east appears

to be extinct and is significantly eroded (Abdel Monem *et al.*, 1975; Feraud *et al.*, 1980; Johnson *et al.*, 1998). Lavas from São Miguel show one of the largest ranges of isotopic compositions known from any oceanic island, with Sr isotope ratios, for example, varying between 0.7033 and 0.7052 (Hawkesworth *et al.*, 1979). The Sete Cidades lavas have distinct compositions compared to rocks from the other three volcanoes, with the lowest Sr and Pb isotope ratios observed on the island (Hawkesworth *et al.*, 1979; Widom *et al.*, 1997). However, these distinctions were based on only three Sete Cidades samples and, thus, do not accurately represent the chemical evolution and compositional span of the volcano.

4.3.2 The stratigraphy of Sete Cidades volcano

Stratigraphic observations of Moore (1990; 1991b) and our own field work (Figs. 4.2 & 4.3) show that Sete Cidades developed through three major phases of volcanic activity: (1) a dominantly alkali basaltic, pre-caldera, shield-building phase, (2) a trachytic caldera-forming phase, and (3) a mainly trachytic, effusive, post-caldera phase associated with small basaltic flank eruptions (Figs. 4.2 & 4.3). The pre-caldera stage appears to dominate the volcano evolution, covering a time span from > 210,000 years and lasting until the caldera forming eruptions, which comprise a sequence of explosive eruptions that occurred 36,000, 29,000, and 16,000 years ago (Pacheco *et al.*, 2005). The post-caldera stage thus covers the shortest time span in the volcano's evolution. Hence, the thicknesses and volumes of the three stages differ accordingly. The thickness of the subaerial pre-caldera stage deposits is estimated from coastal outcrops at Mosteiros and Ponta da Ferraria to be at least 200 m, covering an age range from 74,000 years (oldest unit at Ponta da Ferraria) to 36,000 years (first caldera-related eruption; Fig. 4.3). However, the maximum thickness of the pre-caldera stage is thought to be significantly larger, because most of the volcano's pre-caldera deposits are either submarine or were covered by younger eruptions. The stratigraphy of Sete Cidades shows several fractionation cycles from basaltic to trachytic compositions over the last 210,000 years (Moore, 1991b) of subaerial activity. For example, the upper stratigraphic section at the sea cliff of Ponta da Ferraria (Fig. 4.3) shows four changes from basaltic lava flows to trachytic pumice, suggesting that the volcano regularly erupted magmas of different compositions during the pre-caldera stage. The intermediate and evolved magmas erupted from Sete Cidades volcano show ~ 11 changes between a basaltic to intermediate and an evolved composition in the last 16,000 years.

The caldera outflow stage comprises a sequence of explosive eruptions producing trachytic airfall deposits and pyroclastic flow deposits that culminated in the caldera collapse. The caldera-outflow deposits have a maximum thickness of 50 to 60 meters at the south-eastern caldera rim. The post-caldera ash deposits are generally thicker (up to 40 m) on the south-eastern flank than on the western and north-western flanks (cm to m range), indicating north-westerly winds at the time of eruption (Booth *et al.*, 1978). The trachytic post-caldera stage eruptive units have a variable maximum thickness between 70 and 110 meters at the eastern caldera flank and thin out to the m-range in the vicinity of the Mosteiros and Ponta da Ferraria outcrops (Fig. 4.3). Booth *et al.* (1978) calculated the volume of these explosive eruptions, subdivided into several eruptive events termed Sete A-L, as being up to 3.78 km³. The explosive post-caldera deposits are intercalated with local basaltic lava flows of variable thicknesses from 2-30 meters. Although the pre-caldera units are intercalated with thin ash layers of evolved composition, the majority of the pre-caldera stage consists of basaltic and intermediate lavas. In contrast the post-caldera stage is dominated by larger volumes of evolved pyroclastic deposits and lavas intercalated with smaller basaltic flank eruptions.

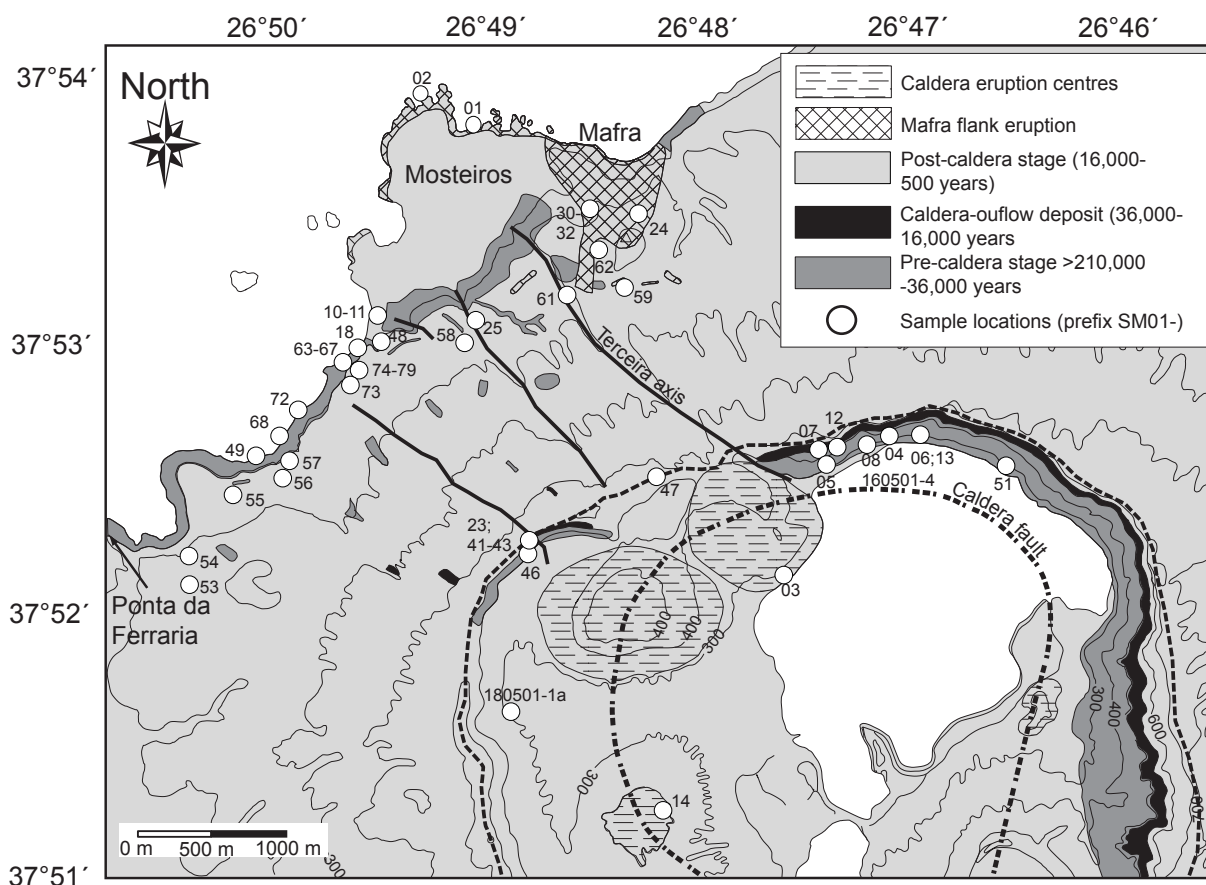


Figure 4.2: Simplified geological map of the NW part of the Sete Cidades volcano. The post-caldera stage mainly consists of younger (< 16,000 years) pyroclastic deposits covering the pre-caldera lava flows. Sample numbers are related to Table 4.1, e.g. 10-11 corresponds to SM0110-SM0111. Topographic contours are in 100 m intervals.

The volcano's morphology is influenced by two major tectonic structures: (1) the Terceira rift axis striking through the volcano in a NW-SE direction, and (2) the post-caldera ring fault (Fig. 4.2). The latter represented a major conduit through which most of the post-caldera trachytes were erupted. On the eastern flank of Sete Cidades, two rows of scoria cones have erupted numerous young lava flows (Fig. 4.1). The southern row of scoria cones marks a lineament showing a structural connection to the SE-striking Terceira rift axis running through the Sete Cidades volcano (Fig. 4.1). The Sr isotope compositions of the lavas from these eruption centres indicate that they belong to the Sete Cidades volcanic system (Haase & Beier, 2003). In contrast, the northern row of cones in the Waist Zone strikes more easterly and the lavas have higher $^{87}\text{Sr}/^{86}\text{Sr}$ suggesting their derivation from the neighbouring Agua de Pau volcano.

4.4 SAMPLING STRATEGY AND ANALYTICAL METHODS

4.4.1 Sampling and sample treatment

Selected areas of the Sete Cidades volcano were partly mapped and sampled stratigraphically in May 2001 (Figs. 4.2 & 4.3). The sampling was carried out based on our stratigraphic investigations and previous studies of the evolution of the subaerial volcanic activity of Sete Cidades (Booth *et al.*, 1978; Moore, 1990; Moore, 1991b). Most samples are optically fresh and lack alteration of olivine crystals and vesicle fillings. However, a few samples show signs of a hydrothermal overprint with iddingsitized olivine rims and clay mineral fillings

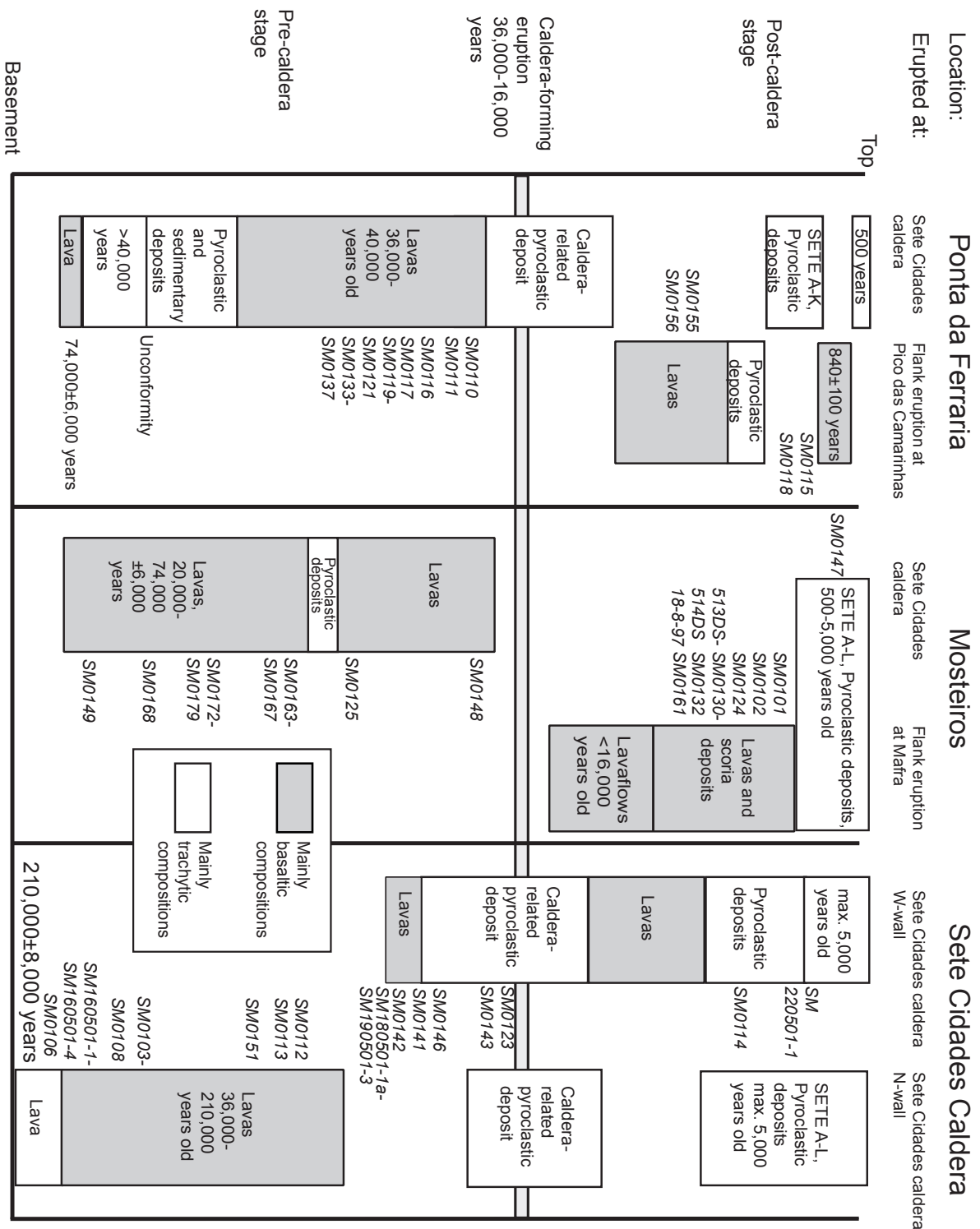


Figure 4.3: Stratigraphy of the Sete Cidades volcano. The localities Ponta da Ferraria and Mosteiros are divided into deposits from the Sete Cidades caldera vent on the left and local flank eruptions on the right. Age constraints are from Moore (1991a, 1991b) and Moore & Rubin (1991) for the pre-caldera rocks and the flank eruptions, and from Booth *et al.* (1978) for the Sete A-L pyroclastic deposits. The caldera-related deposits were estimated to be 36,000-16,000 years old by Pacheco *et al.* (2005). The vertical axis schematically represents the thickness of each deposit; these vary, especially for the pyroclastic deposits, between individual locations due to the influence of the wind during eruption. Sample numbers correspond to the stratigraphic position of the analysed samples.

Table 4.1: Selected major element, trace element and Nd-Sr isotope data of the Sete Cidades lavas and international rock standards. Additional data are available in the Appendix. The whole-rock (WR) major element data were determined by XRF and the trace element data by ICP-MS.

Sample no.	SM0104	SM0106	SM0116	SM0120	SM0133	SM0134	SM0136	SM0176	SM160501-4	SM0114
Location	NNW-cald. wall	N-cald. wall	Ponta da Ferraria	Ponta da Ferraria	Ponta da Ferraria	Ponta da Ferraria	Ponta da Ferraria	Cliffs in Mosteiros	N-cald. wall	Caldeira seca
Long. [°N]	37.525	37.526	37.516	37.515	37.516	37.516	37.516	37.532	37.528	37.518
Lat. [°W]	25.474	25.468	25.516	25.513	25.516	25.516	25.516	25.493	25.468	25.481
Volcanic stage	pre-caldera	pre-caldera	pre-caldera	pre-caldera	pre-caldera	pre-caldera	pre-caldera	pre-caldera	pre-caldera	post-caldera
TAS classification	Basalt	Trachyandesite	Basalt	Trachyandesite	Basalt	Basaltic	Basalt	Basaltic trachyandesite	Basalt	Trachyte
[wt.%]										
SiO ₂	46.71	61.23	46.09	58.16	47.09	54.56	46.85	50.08	46.17	63.28
TiO ₂	2.98	0.72	3.55	1.27	3.40	1.92	3.17	2.61	3.49	0.49
Al ₂ O ₃	14.05	17.64	14.74	17.99	13.33	17.35	11.89	16.87	14.18	15.56
Fe ₂ O ₃	10.94	3.02	11.81	4.87	11.60	7.33	11.47	9.16	12.01	3.16
MnO	0.18	0.17	0.18	0.17	0.17	0.19	0.17	0.18	0.17	0.24
MgO	7.51	0.48	6.85	1.24	8.60	2.41	10.63	3.75	6.38	0.23
CaO	9.96	1.46	9.92	3.23	11.03	4.86	11.96	7.35	10.76	0.50
Na ₂ O	2.95	6.85	3.08	5.81	2.83	5.63	2.48	3.73	3.02	7.72
K ₂ O	1.80	5.17	1.80	4.31	1.58	3.61	1.38	2.65	1.47	5.10
P ₂ O ₅	0.69	0.09	0.59	0.31	0.57	0.62	0.52	0.92	0.52	0.05
LOI	0.51	0.15	0.00	0.47	0.00	0.03	0.11	2.34	0.71	2.30
Total	98.28	96.98	98.61	97.83	100.20	98.51	100.63	99.64	98.88	98.63
[ppm]										
Sc	20.2	1.91	22.4	2.76	28.1	5.63	28.4	9.77	22.2	2.20
V	226	10.4	271	48.0	297	95.0	261	156	299	2.97
Cr	344	1.07	162	2.87	449	1.38	662	12.0	211	1.39
Co	35.8	0.58	40.8	3.43	44.9	8.28	47.4	17.5	41.9	6.06
Ni	117	0.26	57.4	0.72	122	0.39	198	7.27	77.1	0.30
Cu	54.8	1.53	43.8	2.28	67.8	3.42	87.7	10.9	95.3	0.99
Zn	101	92.1	104	97.7	98.7	113	88.4	105	110	154
Mo	2.24	2.06	2.44	3.76	2.02	2.57	1.56	1.55	2.22	11.2
Rb	39.8	133	40.9	102	39.0	86.1	31.6	56.7	20.6	177
Sr	786	313	833	743	715	814	638	893	733	4.14
Y	28.7	39.7	26.3	36.8	28.2	41.8	21.7	33.5	26.6	64.0
Zr	321	808	336	646	305	572	238	414	305	1214
Nb	73.5	166	74.1	148	60.7	130	56.5	98.3	68.1	272
Cs	0.36	0.29	0.29	0.51	0.23	0.62	0.25	0.20	0.28	1.78
Ba	571	1398	502	1301	518	1008	381	752	484	6.84
La	50.5	98.8	48.8	87.6	42.5	81.3	37.0	68.4	45.5	137
Ce	106	190	102	170	88.3	164	78.9	138	91.0	265
Pr	12.9	19.0	12.5	19.3	11.0	19.1	9.74	16.1	11.1	28.6
Nd	51.2	63.4	49.2	69.8	44.1	71.6	39.1	61.2	43.8	95.0
Sm	10.2	10.3	9.65	12.2	8.82	13.4	7.88	11.6	8.74	16.4
Eu	3.04	2.88	2.89	3.60	2.67	3.98	2.36	3.40	2.65	2.47
Gd	8.64	7.92	8.06	9.82	7.54	11.2	6.63	9.56	7.52	13.1
Tb	1.23	1.23	1.13	1.41	1.08	1.62	0.94	1.35	1.08	2.11
Dy	6.44	6.65	5.94	7.66	5.57	8.81	4.83	7.20	5.71	12.2
Ho	1.16	1.26	1.05	1.44	0.98	1.62	0.86	1.29	1.02	2.41
Er	2.91	3.52	2.62	3.83	2.45	4.23	2.10	3.28	2.58	6.73
Tm	0.38	0.51	0.33	0.53	0.31	0.57	0.27	0.43	0.33	0.98
Yb	2.30	3.42	2.07	3.42	1.93	3.54	1.62	2.67	2.03	6.43
Lu	0.32	0.50	0.28	0.50	0.27	0.50	0.23	0.38	0.29	0.93
Hf	7.59	14.4	7.71	13.9	6.33	12.4	6.01	9.03	6.98	26.8
Ta	4.67	8.28	4.72	8.32	3.64	7.62	3.58	5.94	4.23	15.5
Pb	2.46	7.13	2.22	6.61	2.04	4.44	1.64	3.51	2.30	10.6
Th	5.81	15.3	5.33	12.8	4.57	11.0	3.87	8.00	5.80	23.8
U	1.38	3.49	1.53	2.99	1.24	2.84	1.14	2.15	1.63	6.53
⁸⁷ Sr/ ⁸⁶ Sr	0.70353	0.70359	0.70334	0.70365	0.70327	0.70348	0.70340	0.70351	0.70363	0.70418
¹⁴³ Nd/ ¹⁴⁴ Nd	0.51290	0.51291	0.51292	0.51290	0.51292	0.51290	0.51292	0.51291	0.51291	0.51291

Table 4.1: continued

Sample no.	SM220501-1	SM0203	SM9704-a	SM9710	513DS-1	515DS-1	SM0101	SM0102	SM0161
Location	N of Ginetes, flank vent	Pico da Pintona	Relva, Waist Zone	Serra Gorda Waist Zone	W-flank subm.	W-flank subm.	Mafra flank vent	Mafra flank vent	Mafra flank vent
Long. [°N]	37.514	37.798	37.750	37.820	37.866	37.865	37.539	37.540	37.534
Lat. [°W]	25.504	25.701	25.710	25.739	25.938	25.998	25.490	25.492	25.485
Volcanic stage	post-caldera stage	post-caldera stage	post-caldera stage	post-caldera stage	post-caldera stage	post-caldera stage	post-caldera stage	post-caldera stage	post-caldera stage
TAS classification	Trachyte	Basalt	Basalt	Basalt	Basalt	Trachyte	Basalt	Basalt	Basalt
[wt.%]									
SiO ₂	61.98	46.56	45.71	46.39	46.95	59.29	44.87	45.47	45.36
TiO ₂	0.78	2.43	3.44	3.00	2.74	1.28	3.08	2.74	3.59
Al ₂ O ₃	16.88	12.52	12.76	12.64	12.33	18.69	10.96	10.25	13.05
Fe ₂ O ₃	3.42	11.18	12.75	11.91	11.06	5.93	11.96	11.34	12.44
MnO	0.19	0.16	0.17	0.17	0.17	0.19	0.17	0.16	0.18
MgO	0.64	10.42	9.81	10.55	12.13	1.58	12.26	14.09	9.14
CaO	1.16	11.58	11.14	11.27	10.97	3.53	11.62	10.52	10.81
Na ₂ O	6.94	2.67	2.55	2.45	2.56	5.99	2.11	2.01	2.76
K ₂ O	5.21	1.15	1.06	1.22	1.38	4.32	1.19	1.40	1.26
P ₂ O ₅	0.15	0.40	0.52	0.48	0.48	0.38	0.52	0.45	0.69
LOI	1.13	0.23	0.00	0.00	0.00	0.00	0.00	0.00	0.00
Total	98.48	99.30	99.91	100.08	100.77	101.18	98.74	98.43	99.28
[ppm]									
Sc	29.8	31.2	19.9	26.1	24.1	3.16	30.9	29.0	24.4
V	22.7	262				40.6	263	229	289
Cr	6.78	788	670	784	996	2.25	654	705	405
Co	7.34	50.3	48.6	41.1	44.6	4.95	55.8	59.7	47.1
Ni	2.47	212	185	289	319	1.75	225	311	139
Cu	2.53	86.2	25.9	99.4	70.5	3.29	83.5	74.9	36.7
Zn	115	89.7	82.6	95.0	90.0	92.1	85.0	84.3	99.0
Mo	6.37	1.71	1.86	1.63	1.90	0.97	1.68	1.84	1.99
Rb	95.0	33.3	22.6	24.3	28.5	1090	27.1	32.3	33.1
Sr	110	527	615	594	622	543	589	534	797
Y	37.1	25.8	23.2	19.1	19.3	33.7	20.4	19.5	25.4
Zr	698	177	207	168	259	607	200	226	248
Nb	168	40.9	45.7	39.7	48.0	130	43.6	44.8	57.4
Cs	0.95	0.40	0.05	0.30	0.32	0.26	0.25	0.28	0.32
Ba	730	411	359	364	404		347	348	494
La	76.4	28.0	30.5	30.5	36.6	89.5	32.5	33.5	40.9
Ce	152	57.8	64.6	64.1	75.5	173	69.3	71.4	86.5
Pr	17.0	7.26	8.04	8.12	9.51	19.4	8.71	8.85	10.8
Nd	59.9	29.5	33.5	33.4	38.3	68.0	35.5	35.5	44.3
Sm	10.5	6.44	7.13	7.32	7.93	11.8	7.37	7.17	8.97
Eu	2.69	2.04	2.22	2.27	2.43	3.32	2.25	2.13	2.77
Gd	8.41	5.92	6.61	6.36	6.70	9.65	6.40	6.04	7.59
Tb	1.31	0.90	0.92	0.92	0.96	1.44	0.91	0.86	1.07
Dy	7.38	4.92	4.97	5.12	5.16	7.76	4.75	4.51	5.60
Ho	1.41	0.89	0.89	0.94	0.93	1.44	0.84	0.80	1.00
Er	3.85	2.23	2.19	2.30	2.28	3.81	2.09	1.97	2.47
Tm	0.55	0.29	0.28	0.30	0.29	0.54	0.27	0.26	0.31
Yb	3.55	1.84	1.70	1.75	1.76	3.49	1.62	1.57	1.90
Lu	0.50	0.26	0.24	0.24	0.24	0.50	0.21	0.22	0.26
Hf	14.5	4.37	5.36	5.33	5.98	15.1	5.43	5.95	5.94
Ta	9.08	2.47	3.04	2.89	3.34	8.73	2.86	2.94	3.65
Pb	6.26	1.85	1.93	1.86	2.05	6.13	1.59	1.84	1.80
Th	11.9	3.33	3.67	3.42	3.82	13.5	3.33	3.73	4.06
U	3.19	0.89	1.08	1.04	1.14	1.76	0.89	1.00	1.06
⁸⁷ Sr/ ⁸⁶ Sr	0.70359		0.70374	0.70354	0.70327	0.70355	0.70373	0.70414	0.70360
¹⁴³ Nd/ ¹⁴⁴ Nd	0.51290	0.51292	0.51289		0.51299	0.51289	0.51289	0.51280	0.51291

Table 4.1: continued

Sample no.	AGV-1	Deviation	BCR-2	Deviation	BHVO-1	Deviation	JA-2	Deviation	BR	Deviation
[wt.%]										
SiO ₂	59.06	0.26	54.53	0.78	49.81	0.31	56.05	0.16		
TiO ₂	1.05	0.00	2.26	0.02	2.74	0.01	0.66	0.00		
Al ₂ O ₃	17.09	0.08	13.61	0.28	13.65	0.11	15.44	0.10		
Fe ₂ O ₃	6.72	0.03	13.80	0.15	12.16	0.12	6.25	0.03		
MnO	0.10	0.00	0.19	0.00	0.17	0.00	0.11	0.00		
MgO	1.53	0.01	3.67	0.07	7.20	0.08	7.91	0.07		
CaO	4.87	0.04	7.10	0.04	11.39	0.04	6.32	0.03		
Na ₂ O	4.26	0.10	3.29	0.15	2.37	0.12	3.07	0.08		
K ₂ O	2.93	0.00	1.79	0.02	0.53	0.01	1.75	0.01		
P ₂ O ₅	0.50	0.00	0.37	0.01	0.28	0.01	0.15	0.00		
LOI	0.00		0.00							
Total	98.11		100.61		100.33		97.72			
Trace element deviation (ICP-MS) of measured standards from published values of Govindaraju (1995)										
[ppm]										
Sc	11.7	0.31			30.4	1.03	18.2	1.03	19.3	4.02
V	130	6.82			298	13.6	134	6.68	213	15.6
Cr*	9.12				276	9.15	442	16.1	358	15.2
Co	14.6	0.45			42.9	1.49	27.5	1.74	53.6	1.17
Ni*	14.2	1.30			111	7.29	130	8.19	240	13.8
Cu	53.5	4.58			130		26.8		65.2	
Zn*	84.3	2.63			102	2.00	58.3	3.11	155	3.88
Mo	2.06	0.45			107	0.04	0.53	0.01	2.20	0.14
Rb	66.6	0.49			9.32	1.19	67.5	0.34	44.0	2.14
Sr	678	11.2			420	11.7	245	4.79	1129	135
Y	18.0	1.41			25.1	1.77	15.4	1.92	27.2	1.99
Zr	220	4.64			170	6.10	102	11.8	281	14.7
Nb	13.4	1.11			18.0	0.66	8.47	0.94	110	8.14
Cs	120	0.05			0.09	0.03	4.39	0.13	0.63	
Ba	1226				137		304	9.27	1077	19.5
La	37.9	0.04			15.7	0.03	15.0	0.89	80.9	0.79
Ce	69.0	1.43			39.4	0.28	31.6		150	0.45
Pr	8.35	0.53			5.55	0.10	3.54	0.59	16.9	0.06
Nd	31.6	0.96			25.4	0.12	13.7	0.02	64.4	0.42
Sm	5.84	0.04			6.37	0.13	2.95	0.12	11.9	0.23
Eu	1.58	0.04			2.12	0.04	0.85	0.06	3.50	0.14
Gd	4.78	0.15			6.36	0.03	2.91	0.14	9.63	0.10
Tb	0.66	0.02			0.99	0.02	0.47	0.04	1.27	0.01
Dy	3.62	0.02			5.55	0.25	2.86	0.10	6.22	0.12
Ho	0.69	0.02			1.04	0.04	0.58	0.09	1.05	0.03
Er	1.87	0.12			2.62	0.16	1.69	0.23	2.50	0.00
Tm	0.25	0.06			0.34	0.01	0.24	0.04	0.30	0.00
Yb	1.66	0.04			2.11	0.07	1.65	0.01	1.77	0.02
Lu	0.24	0.02			0.28	0.00	0.24	0.02	0.23	0.01
Hf	5.33	0.17			4.92	0.38	2.92	0.02	5.92	0.23
Ta	0.86	0.03			1.22	0.09	0.65	0.03	5.61	0.41
Pb	34.3	1.27			1.92	0.01	17.3	1.38	4.43	0.40
Th	6.44	0.04			1.32	0.18	4.77	0.05	10.5	0.35
U	1.90	0.01			0.43	0.01	2.11	0.20	2.49	0.00

Table 4.2: Major element and trace element compositions of glass samples from Sete Cidades. The major element compositions were determined by electron microprobe and the trace element data by ICP-MS.

Sample no.	SM0103	SM0123	SM0143	SM9701	513DS-3	513DS-6	SM0101	SM0102	SM0131
Location	NW-cald wall	W-cald. wall	W-cald. wall	Miradoro do Carvao	W-flank Sete Cidades	W-flank Sete Cidades	Mafra flank vent	Mafra flank vent	Mafra flank vent
Long. [°N]	37.523	37.524	37.524	37.750	37.866	37.866	37.539	37.540	37.533
Lat. [°W]	25.474	25.486	25.486	25.710	25.938	25.938	25.490	25.492	25.483
Volcanic stage	pre-caldera stage	caldera-related deposit	caldera-related deposit	post-caldera stage	post-caldera stage	post-caldera stage	post-caldera stage	post-caldera stage	post-caldera stage
TAS classification	Trachyte	Trachyte	Trachyte	Basalt	Basalt	Basalt	Basalt	Basalt	Trachy-andesite
[wt.%]									
SiO ₂	64.93	61.20	62.92	47.10	48.39	47.92	46.73	47.26	56.69
TiO ₂	0.59	0.77	0.76	3.86	3.22	4.33	4.22	3.62	0.35
Al ₂ O ₃	17.69	17.72	18.34	14.66	15.41	14.45	15.17	13.75	25.97
FeO ^T	2.88	3.35	3.11	10.66	10.22	12.93	11.41	10.57	0.97
MnO	0.21	0.15	0.14	0.15	0.19	0.20	0.17	0.18	0.05
MgO	0.33	0.60	0.60	5.66	5.97	4.02	5.42	6.46	0.20
CaO	0.62	1.49	1.60	12.12	11.98	8.74	11.85	12.91	8.07
Na ₂ O	6.78	5.65	6.22	2.62	3.16	2.95	2.72	2.35	4.87
K ₂ O	5.71	5.97	5.71	1.57	1.58	2.45	1.95	1.75	2.70
P ₂ O ₅	0.08	0.19	0.17	0.51	0.48		0.84	0.68	0.10
SO ₃	0.01	0.02	0.02	0.05			0.03	0.01	0.01
F				0.32					
Cl	0.23	0.27	0.29	0.09			0.05	0.05	0.02
Total	100.06	97.37	99.88	99.37	100.59	97.98	100.56	99.59	100.00
[ppm]									
Sc				26.4					
V									
Cr				330					
Co				43.4					
Ni				116					
Cu				89.8					
Mo				2.00					
Rb				29.8					
Sr				660					
Y				21.6					
Zr				206					
Nb				48.4					
Cs				0.35					
Ba				442					
La				38.6					
Ce				87.0					
Pr				10.2					
Nd				41.1					
Sm				8.73					
Eu				2.68					
Gd				7.44					
Tb				1.06					
Dy				5.72					
Ho				1.03					
Er				2.50					
Tm				0.32					
Yb				1.88					
Lu				0.27					
Hf				6.15					
Ta				3.28					
Pb				2.19					
Th				3.91					
U				1.19					

Table 4.3: Descriptions of sample localities and the petrology of representative samples.

Sample no.	Location name:	Rock type	Description of petrology:
Pre-caldera stage:			
SM0103	NW-caldera wall Lagoa Azul	Trachyte	Fresh, fine grained trachyte with glass, ~3 % Pl xenocrysts up to 4 mm, ~3 % Fe-Ti oxides xeno- and phenocrysts (< 0.5 mm), 1 % Cpx xenocrysts (< 1 mm), < 0.5 % Bt phenocrysts (< 0.5 mm)
SM0106	N-caldera wall Lagoa Azul	Trachyte	Fine to coarse grained trachyte, ~50 % Pl phenocrysts up to 1 mm, ~3 % Pl xenocrysts up to 3 mm, < 1 % Kaer xenocrysts (< 1 mm), < 0.5 % Bt xenocrysts (< 0.5 mm), sample contains a large accumulation of coarse grained (< 5 mm) Pl (~80 %), Cpx (10 %), and Fe-Ti oxide (~10 %) xenocrysts
SM0108	N-caldera wall Lagoa Azul, E of SM0106	Basalt	Fine-grained basalt, ~10 % Pl phenocrysts up to 0.5 mm, ~5 % Cpx xenocrysts up to 2 mm, ~3 % Ol with corroded rims, very fine-grained Fe-Ti oxides in matrix, ~0.5 % Kaer (< 1 mm) xenocrysts, resorbed Fe-oxide rims
SM0111	Coastline at Mosteiros	Basaltic trachyandesite	Fine-grained intermediate composition with 10 % Pl xenocrysts (< 3 mm), fine-grained Fe-Ti oxides and Pl phenocrysts in matrix (< 0.2 mm)
SM0137	Ponta da Ferraria	Trachybasalt	Fine-grained Trachybasalt, ~40 % Pl phenocrysts (< 0.5 mm), 7 % sieve textured Pl xenocrysts (< 1 mm), 3 % Cpx and Ol xenocrysts (< 1 mm), 1 % Kaer phenocrysts (< 4 mm) with a 100-200 µm opacitized reaction rim with Fe-Ti oxides, Pl and Cpx (~1-5 µm)
SM0149	Relva Velha, S of Mosteiros	Trachyte	Fine-grained trachyte, 10 % Pl phenocrysts (< 2 mm), 5 % of Fe-Ti oxide pheno- and xenocrysts (< 0.5 mm), 5 % Pl xenocrysts (< 1 mm)
SM0166	Coastline S of Mosteiros	Basaltic trachyandesite	Fine-grained evolved rock, ~30 % Pl phenocrysts (< 0.5 mm), 1% Cpx xenocrysts (< 0.5 mm)
SM0176	Coastline S of Mosteiros	Basaltic trachyandesite	Fine-grained intermediate composition, ~5 % Pl phenocrysts (< 2mm), ~2 % Fe-Ti oxide xenocrysts (< 1 mm), matrix consists of fine-grained Fe-Ti oxides and Pl phenocrysts
SM 160501-1	W-caldera wall	Trachy- andesite	Fine-grained porous intermediate composition, 3 % Pl phenocrysts (< 0.5 mm), < 1 % Cpx xenocrysts (< 0.5 mm)
Caldera related deposits:			
SM0123	NW-caldera rim	Trachyte	Fine-grained to glassy porous (~15 %) matrix with elongated glass shards (< 20 mm), ~2 % Ol (< 1 mm), ~2 % Cpx (< 1 mm), 1-2 % Pl (< 1 mm), 0.5 % Kaer (< 2 mm) xenocrysts, < 0.5 % Bt xenocrysts (< 5 mm)
SM0143	NW-caldera rim	Trachyte	Fine-grained matrix with elongated glass shards (< 30 mm), 1 % Ol (< 1 mm), 1 % Cpx (< 1 mm), 1 % Pl (< 1 mm), < 0.5 % Bt xenocrysts (< 0.5 mm)
Post-caldera stage:			
SM0101	Beira Mar de Beixo Coast at Mosteiros	Basalt	Fresh, fine grained basalt with glass, ~15 % Ol and 10 % Cpx phenocrysts (< 4 mm), ~5 % Cpx and Ol xenocrysts, < 1 % Fe-Ti oxides (< 0.5 mm)
SM0102	Beira Mar de Beixo Coast at Mosteiros	Basalt	Fresh, fine grained basalt with glass, ~10 % Ol and 7 % Cpx phenocrysts (< 5 mm), ~3 % Cpx and Ol xenocrysts
SM0131	W-flank of Mafra	Basalt	Fine-grained basalt, 5 % Cpx phenocrysts (< 10 mm), 5 % Ol (< 2 mm), 3 % Pl (< 1 mm) xenocrysts
SM0140	Eguas flank vent E-flank of Sete Cidades	Basalt	Fine-grained basalt, ~5 % Cpx and 5 % Ol phenocrysts (< 2 mm) 2 % Cpx and Ol xenocrysts (< 3 mm)
SM0161	WSW- flank of Mafra vent	Basalt	Fine-grained basalt, 12 % Cpx, 8 % Ol phenocrysts (< 1 mm), contains a cumulate with 75 % Cpx, 15 % Ol, 10 % Pl (~3 mm)
SM 220501-1	N of Ginetes, W-flank of Sete Cidades	Trachyte	Fine-grained to glassy trachyte, 7 % Pl xenocrysts (< 1.5 mm), 3 % Fe-Ti oxide xenocrysts (< 0.5 mm), < 1 % Cpx xenocrysts (< 1 mm)

Table 4.4: continued

Sample	SMD0137	SMD0137	SMD0140	SMD0143	SMD180501	SMD0140	SMD0103	SMD0106	SMD0123	SMD0143	SMD0101	SMD0101	SMD0106	SMD0123
Volcanic stage	pre-caldera	pre-caldera	post-caldera	caldera-related	pre-caldera	post-caldera	pre-caldera	caldera-related	caldera-related	caldera-related	post-caldera	post-caldera	pre-caldera	caldera-related
Mineral	Kaer core	Kaer rim	Mag core	Mag core	Kaer core	Mag-Chr core	Bt core	Bt core	Bt core	Bt core	Chr core	Mag core	Mag core	Mag core
Total no. of analyses per sample	29 ss core-rim analyses			12 ss	10 ss	12 ss	15 ss	7 ss	16 ss	4 ss	25 ss	22 ss	9 ss	
SiO ₂	39.56	43.80	39.78	39.03	40.96	38.87	38.74	36.70	36.48	35.97	0.00	0.00	0.00	0.11
TiO ₂	5.93	5.42	5.53	7.04	6.10	6.79	5.65	6.51	7.14	7.25	3.81	3.81	14.68	17.86
Al ₂ O ₃	13.36	8.05	13.14	11.35	11.82	12.46	12.20	13.30	13.69	13.66	14.07	14.07	1.50	5.59
Cr ₂ O ₃	0.00	0.00	0.00	0.00	0.00	0.04	0.00	0.00	0.03	0.00	36.20	0.02	0.00	0.06
FeO	0.38	6.92	0.24	5.71	0.81	13.01	15.00	9.01	15.98	10.76	18.51	39.25	39.50	37.73
Fe ₂ O ₃	11.24	1.89	11.16	4.05	10.30	0.00	0.00	6.85	0.00	5.64	14.42	40.01	39.48	30.99
MgO	12.77	11.44	12.93	9.55	13.32	11.46	14.68	13.91	12.97	12.95	12.07	1.77	1.98	6.75
MnO	0.08	0.15	0.11	0.23	0.24	0.25	0.53	0.41	0.30	0.35	0.34	2.63	1.96	0.42
CaO	11.95	21.33	11.72	21.56	11.81	11.25	0.01	0.00	0.01	0.00	0.00	0.00	0.00	0.00
Na ₂ O	2.29	0.53	2.31	0.52	2.57	2.68	0.93	0.97	0.98	0.92	0.00	0.00	0.00	0.00
K ₂ O	1.14	0.00	1.12	0.00	0.99	0.94	8.98	8.71	8.50	8.69	0.00	0.00	0.00	0.00
NiO													0.01	0.08
ZnO													0.23	0.03
Total	98.70	99.53	98.04	99.04	98.92	97.75	96.72	96.37	96.08	96.19	99.42	99.32	99.35	99.61
Sample	SMD0137	SMD0137	SMD0140	SMD0143	SMD180501	SMD0140	SMD0137	SMD0123	SMD0106	SMD0123	SMD0137	SMD0103		
Volcanic stage	pre-caldera	pre-caldera	post-caldera	caldera-related	pre-caldera	post-caldera	pre-caldera	caldera-related	pre-caldera	caldera-related	pre-caldera	pre-caldera		
Mineral	Mag core	Mag rim	Mag core	Mag core	Mag core	Mag-Chr core	Ti-Mag core	Ti-Mag core	Ilm core	Ilm core	Ilm core	Ilm core		
Total no. of analyses per sample	38 ss	6 ss	11 ss	17 ss	14 ss	2 ss	1 ss	4 ss	6 ss	5 ss	6 ss	6 ss		
SiO ₂	0.00	0.00	0.00	0.00	0.10	0.00	0.00	0.08	0.00	0.00	0.05	0.00	0.00	66.29
TiO ₂	14.93	17.73	16.77	17.12	18.35	2.90	20.47	29.68	46.94	45.93	49.82	46.42	0.00	0.00
Al ₂ O ₃	5.48	4.93	4.85	1.65	3.01	14.81	4.39	1.53	0.05	0.10	0.17	0.48	19.36	0.00
Cr ₂ O ₃	0.00	0.00	0.00	0.00	0.00	37.75	0.00	0.00	0.01	0.00	0.00	0.00	0.00	0.00
FeO	37.71	40.41	39.52	42.14	42.68	14.57	42.36	55.08	36.60	36.39	36.76	30.01	0.30	0.30
Fe ₂ O ₃	35.85	30.32	32.64	34.48	29.47	12.38	26.61	7.09	10.63	12.48	6.17	15.42	0.00	0.00
MgO	4.90	4.59	4.58	2.07	2.20	13.50	4.99	1.11	1.38	1.04	3.37	6.31	0.00	0.00
MnO	0.40	0.42	0.58	1.63	1.76	0.33	0.52	0.66	2.99	2.95	1.96	0.44	0.00	0.00
CaO	0.00	0.00	0.00	0.00	0.00	0.00	0.00	0.00	0.00	0.00	0.00	0.00	0.00	0.45
Na ₂ O	0.00	0.00	0.00	0.00	0.00	0.00	0.00	0.00	0.00	0.00	0.00	0.00	0.00	7.02
K ₂ O	0.00	0.00	0.00	0.00	0.00	0.00	0.00	0.00	0.00	0.00	0.00	0.00	0.00	6.55
NiO														
ZnO					0.03	0.03	0.13	0.03	0.06	0.06	0.01	0.01		
Total	99.27	98.40	98.94	99.08	97.87	96.35	99.48	95.34	98.75	99.00	98.43	99.15		99.98

versity of Kiel. The concentrations of the major elements as well as Cr_2O_3 and, in some cases, also Cl and NiO were measured. The machine was operated at an accelerating voltage of 15 kV, a beam current of 15 nA, using a focused beam with a diameter of 1 μm for minerals, and with a beam diameter of 12 μm for glasses. Counting times were set to 20 and 10 seconds for glasses ($\text{Na}_2\text{O} = 10/5$ sec; Cl = 120/60 sec; Ni = 40/15 sec) and 15 and 7 seconds for mineral peaks and backgrounds, respectively.

4.4.4 Nd-Sr isotopes

The Sr and Nd isotopic compositions of most samples were determined at the Zentrallaboratorium für Geochronologie in Münster using a VG Sector 54 multicollector mass spectrometer. A few samples were analysed in static mode at the IFM-GEOMAR Research Centre in Kiel on a Finnigan MAT 262 RPQ2+ and on a Finnigan Triton mass spectrometer. For isotopic determinations, 100 mg of powdered sample material and standard ion exchange techniques (Hoernle *et al.*, 1991) were used to separate Sr and Nd from the matrix. The samples were leached for 1 h in hot ultrapure 6N HCl before dissolution. Procedural blanks in both laboratories were generally better than 0.2 ng for Sr and 0.1 ng for Nd. Sr isotope ratios were analysed in dynamic mode and isotope fractionation corrections made using $^{86}\text{Sr}/^{88}\text{Sr} = 0.1194$. In Münster, standard runs for Sr isotopes gave NBS 987 ($n = 16$): 0.710299 (2SD = 0.000026). Repeated measurement ($n = 12$) of the LaJolla Nd isotope standard yielded 0.511870 (2SD = 0.000018). In Kiel, the NBS987 ($n = 8$) gave 0.710273 (2SD = 0.000005) and the La Jolla standard yielded 0.511848 (2SD = 0.0000007). All Sr isotope analyses were normalised to NBS987 = 0.710250 and all Nd data are relative to a La Jolla of 0.511855.

4.5 PETROLOGY AND MINERAL CHEMISTRY

4.5.1 Petrology

The sampled rocks from all three different stratigraphic units range in composition from alkali basalt to trachyte based on the Total Alkalis vs. SiO_2 (TAS) classification (Fig. 4.4) of Le Maitre *et al.* (1989). No major compositional gap or bimodality is observed; instead all the samples lie along a well-defined and relatively tight trend in the TAS diagram.

4.5.1.1 Primitive rocks

The mafic rocks of Sete Cidades can be classified as alkali-basalts (Fig. 4.4) with MgO contents between 14 and 5 wt. %. Generally, the lavas from the post-caldera stage on Sete Cidades are more primitive than the pre-caldera lavas. The mafic rocks contain both olivine and clinopyroxene and smaller plagioclase phenocrysts in a fine grained, often glassy matrix. The olivine and clinopyroxene phenocrysts are chemically and optically zoned. The high MgO samples (> 12 wt. % MgO, e.g. sample SM0101 in Tables 4.1, 4.2 & 4.3) show clear optical (xenomorphic shape) and chemical (disequilibrium) evidence for the accumulation of olivine and clinopyroxene xenocrysts. The olivine xenocrysts have corroded cores and are overgrown by clinopyroxene (Fig. 4.5a, Table 4.3). The mafic lavas from the young eruptive centres (e.g. Mafra, Ponta da Ferraria, Fig. 4.1) frequently contain xenoliths of peridotite, gabbro, and syenite which show evidence of partial fusion.

4.5.1.2 Intermediate rocks

The intermediate rocks from Sete Cidades range from 2 to 5 wt. % MgO and are classified as trachybasalt to trachyandesite (Fig. 4.4). Many of these rocks exposed at the coastline are slightly altered by seawater (e.g.

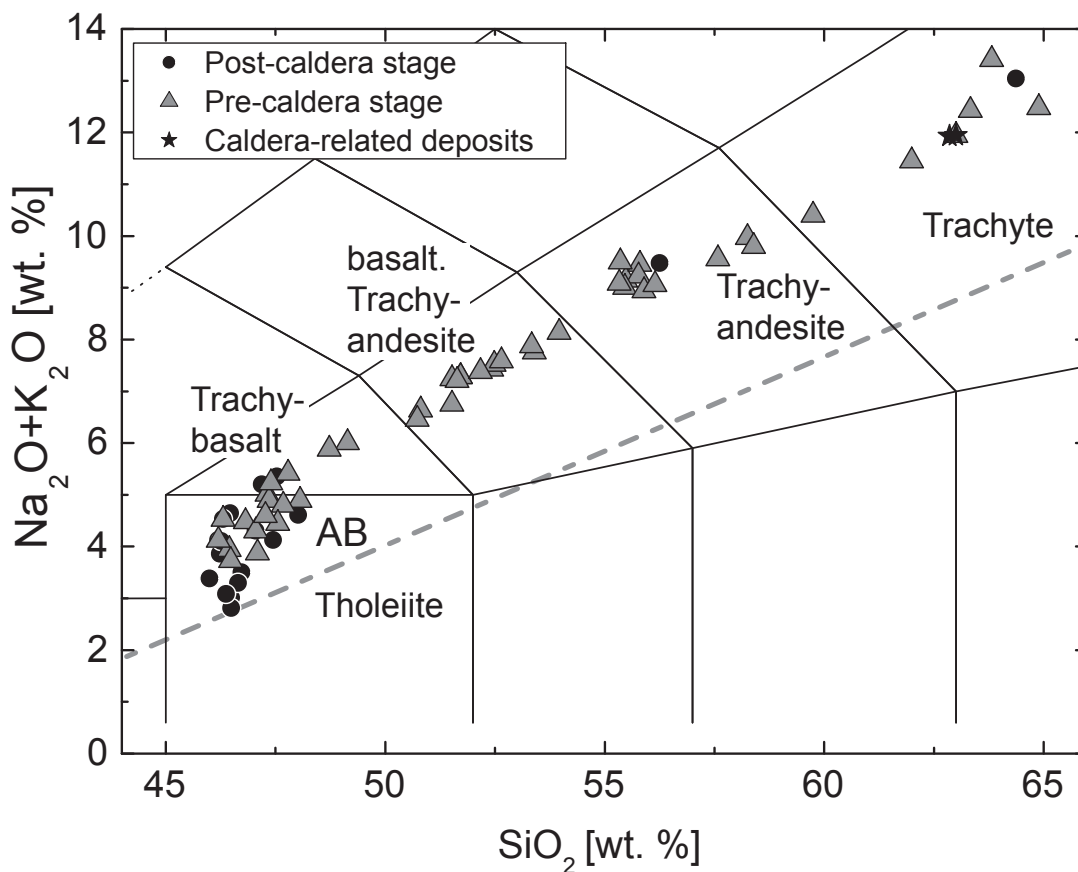


Figure 4.4: Classification of the volcanic rocks of Sete Cidades according to the total-alkali versus SiO_2 diagram of Le Maitre *et al.* (1989). The dividing line between alkaline and tholeiitic compositions was taken from Macdonald (1968). All samples are in the range of the alkali-volcanic series (AB- alkali basalt).

south of Mosteiros). Most intermediate rocks contain phenocrysts of olivine, clinopyroxene, plagioclase, titanomagnetite, ilmenite and apatite (Table 4.3). The olivines often have strongly iddingsitized and corroded rims, and altered cracks filled with red iron oxides and hydroxides. In contrast to the primitive basalts the more evolved rocks contain up to 30 % feldspar laths and up to 3 % magnetite in the matrix (Table 4.3).

4.5.1.3 Evolved rocks (trachytes)

The trachytic lavas of Sete Cidades are mainly exposed on the inner caldera wall, at young eruption centres within the caldera, and at a trachytic dome located on the coast south of Mosteiros (Fig. 4.2). The trachytes have MgO contents of less than 2 wt. % (Fig. 4.4, Table 4.1) and contain plagioclase and alkali feldspar pheno- and xenocrysts, ilmenite, and titanomagnetite and small amounts of kaersutite (Fig. 4.5b, Table 4.3). A few samples contain partly altered biotite crystals and strongly pleochroic aegirine-augite with highly corroded rims. The Sete Cidades volcano erupted a large volume of trachytic, partly glassy, pyroclastic air fall deposits. The matrix of these pyroclastic deposits consists of a glassy, porous shards with plagioclase xenocrysts, and very small amounts of Ti-magnetite and ilmenite. The caldera outflow deposit consists of a fine grained to glassy banded, porous matrix with olivine, pyroxene, plagioclase, and kaersutite xenocrysts (Figs. 4.5c & d, Table 4.3). Other sections of these units consist of a volcanoclastic breccia, glass shards and xenocrysts indicating an explosive eruptive event.

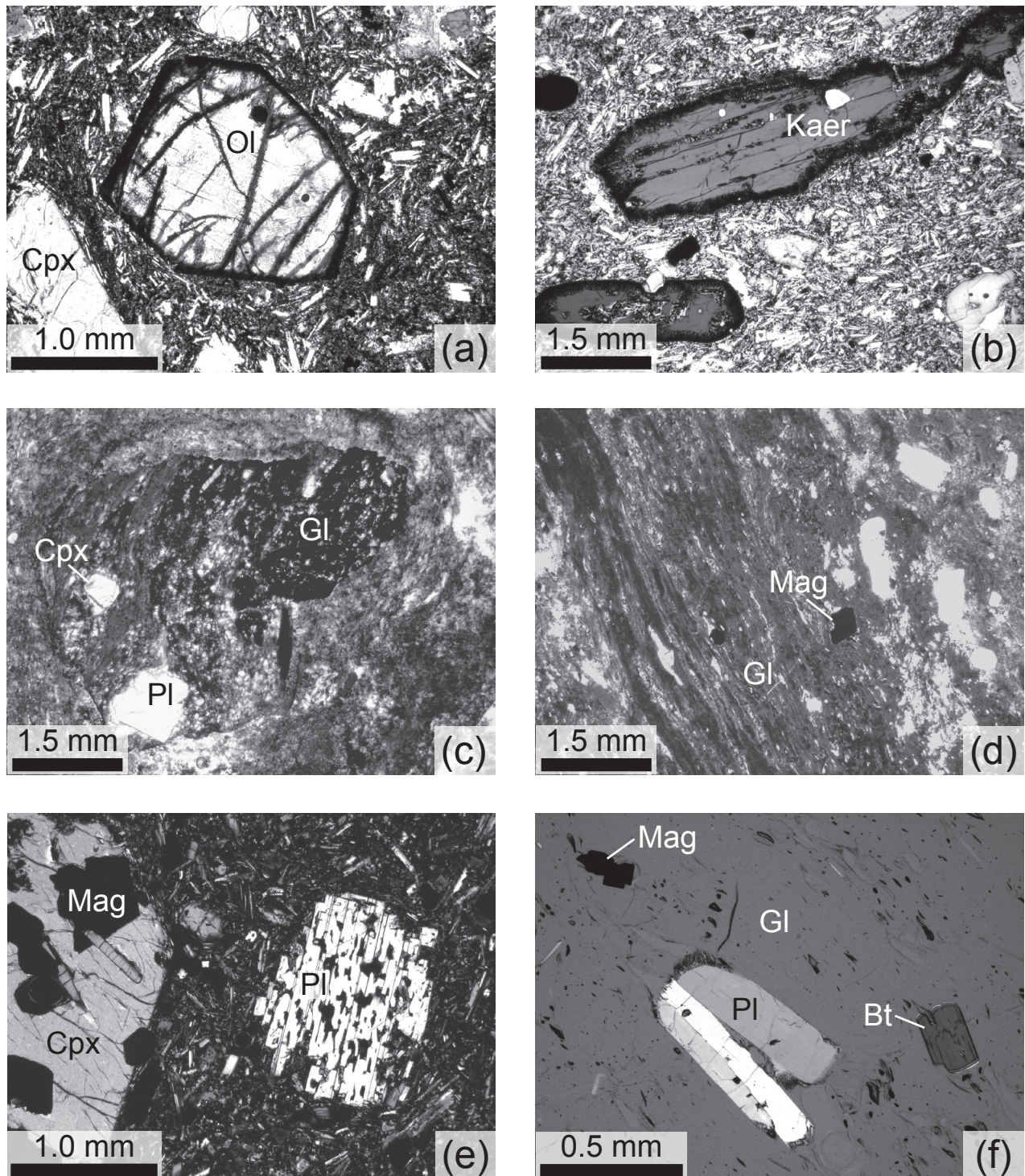


Figure 4.5: Photomicrographs of representative thin sections of the Sete Cidades lavas. (a) Corroded olivine in sample SM0108. (b) Kaersutite (Kaer) phenocrysts with decompression rims in sample SM0137. (c & d) Caldera-related outflow deposits (SM0123, SM0143) showing streaky glass shards (Gl) and plagioclase (Pl) and clinopyroxene (Cpx) xenocrysts as described in Table 4.3. (e) Sieve textured plagioclase crystal in sample SM0137 under crossed polars. (f) Plagioclase, magnetite and biotite crystals in sample SM0103 in a glassy matrix under half-crossed polars.

4.5.2 Mineral chemistry

4.5.2.1 Olivine

The analysed olivines range from Fo_{54-90} in the lavas of Sete Cidades with the higher Fo contents generally characteristic of phenocrysts and xenocrysts in the more mafic rocks. The olivine phenocrysts are normally zoned with a decreasing forsterite content from core to rim. The corroded olivine xenocrysts identified optically by their xenomorphic shape are chemically in disequilibrium with the surrounding glass matrix (Fig. 4.5a). Generally, the pre-caldera olivines have significantly lower Ni-concentrations from 500-1500 ppm (Fo_{70-88}), whereas the post-caldera olivines have higher concentrations from 1000-2500 ppm (Fo_{88-89}). Primitive olivine phenocrysts cores (Fo_{89}) vary widely in their Ni concentrations providing evidence for magma mixing processes. Forsteritic xenocrysts (Fo_{90}) were found in sample SM0140 from the Eguas eruption centre at the eastern flank of Sete Cidades (Fig. 4.1b).

4.5.2.2 Clinopyroxene

The Sete Cidades clinopyroxenes show moderate variations between $\text{Wo}_{39-46}\text{En}_{21-44}\text{Fs}_{17-29}$ and $\text{Wo}_{47-49}\text{En}_{37-48}\text{Fs}_{5-13}$. The majority of the clinopyroxene phenocrysts are normally zoned with decreasing MgO contents from the core towards the rim. However, a few crystals found in the intermediate and evolved rocks are reversely zoned, with higher Mg# in the rims relative to the cores. The Al_2O_3 and TiO_2 contents abruptly increase above En contents of ~ 40 (Fig. 4.6). Augites in the trachytic rocks show the lowest concentrations of Al_2O_3 (> 0.5 wt. %) and TiO_2 (> 0.25 wt. %). In contrast to the other oxides, Al_2O_3 and TiO_2 show a bimodality, with the basaltic rocks having the higher contents. The change in whole-rock compositions from basalt to trachyte is thus accompanied by a sharp decrease in Al_2O_3 and TiO_2 in the pyroxenes, rather than a continuous trend as formerly described by Renzulli & Santi (2000). As observed by Thompson (1974), the proportions of Al_{tot} and $^{\text{VI}}\text{Al}$ are positively correlated with the crystallization pressure of pyroxenes. The clinopyroxenes in the trachytic samples have both lower Al_{tot} and lower $^{\text{VI}}\text{Al}$ than the clinopyroxenes in the basaltic samples. Therefore two different

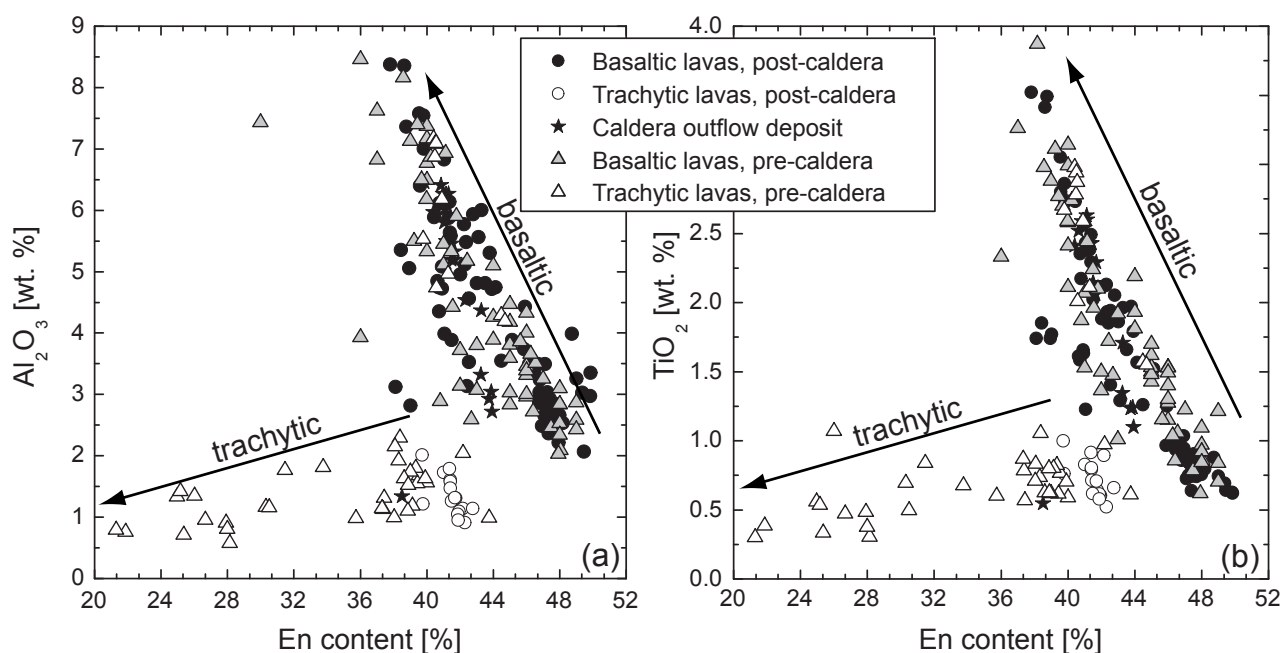


Figure 4.6: Clinopyroxene compositions in lavas from Sete Cidades. (a) and (b) show the Al_2O_3 and TiO_2 (wt.%) vs. mole % En, respectively. Two trends can be distinguished: one having increasing Al_2O_3 and TiO_2 with decreasing En for the basaltic lavas and one with decreasing Al_2O_3 and TiO_2 for the trachytic lavas.

pressure conditions can be inferred: (a) higher pressure conditions for the mafic rocks and (b) shallower level conditions for the more evolved rocks (Pichavant *et al.*, 2002). As the proportion of Na_2O and Fe^{3+} increase with decreasing En content from basalts to trachytes in the Sete Cidades samples, this substitution suggests a relatively high oxygen fugacity during fractional crystallization (Pemberton & Offler, 1985). An enrichment of Na_2O in pyroxenes has been attributed to changes of the $\text{Al}_2\text{O}_3^{\text{liquid}}$ activity and oxygen fugacity by Ewart (1981). However, his work focuses on Na-rich pyroxenes, whereas the Sete Cidades pyroxenes have much lower Na_2O concentrations (up to 1.21 wt. % Na_2O), suggesting that the compositional change in the Sete Cidades clinopyroxenes most likely reflects a pressure decrease in the more evolved lavas.

4.5.2.3 Feldspar

The feldspars in the basaltic rocks are microphenocrysts and phenocrysts with a compositional range from bytownite to labradorite ($\text{Ab}_{15-37}\text{An}_{59-85}\text{Or}_{0-12}$; Fig. 4.7). The plagioclase phenocrysts in the hawaiites generally show a relatively narrow range in the bytownite field ($\text{Ab}_{18-27}\text{An}_{67-82}\text{Or}_{0-6}$), with the higher albite contents reflecting fractional crystallization processes and decreasing CaO content in the melt. The phenocrysts are typically weakly normally zoned. The mugearites show two compositional ranges in the anorthite (An_{86-93}) and bytownite (An_{64-82}) fields implying that the more anorthite-rich crystals likely derived from a more

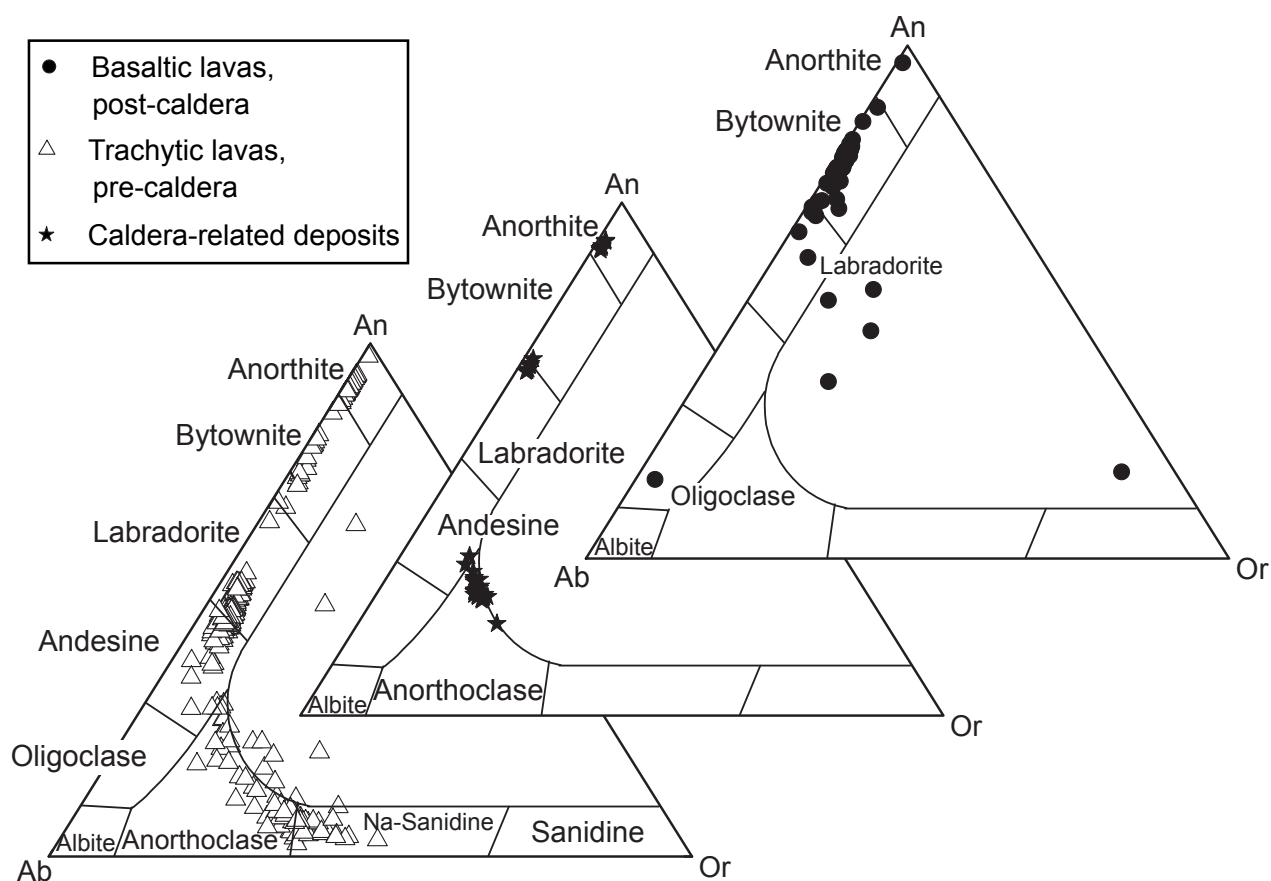


Figure 4.7: Ternary feldspar compositions based on single spot electron microprobe analyses in the Sete Cidades lavas. The feldspars in the basaltic lavas (> 5 wt. % MgO) are relatively anorthite rich in contrast to the intermediate and trachytic samples (< 5 wt. % MgO) which cover a large range in the albite-anorthite fields. The feldspar xenocrysts in the caldera-related deposits show a bimodal distribution in the albite and anorthite fields.

primitive magma. The feldspars in the trachytic rocks range from labradorite-andesine ($\text{Ab}_{42-60}\text{An}_{35-55}\text{Or}_{3-5}$) to anorthoclase-Na-sanidine ($\text{Ab}_{47-63}\text{An}_{3-22}\text{Or}_{14-50}$). The feldspar xenocrysts in sample SM0137 have disequilibrium textures that are commonly referred to as sieve-like textures (Fig. 4.5e) produced either by magma mixing or magmatic decompression (Nelson & Montana, 1992).

4.5.2.4 Spinel and iron-titanium oxides

Some basaltic and intermediate samples contain dark-brown Cr-spinel microphenocrysts. Microprobe analyses reveal that their chemical composition ranges from magnesiochromite to chromite (Table 4.4). The Cr-spinel occurs both as inclusions in olivine and clinopyroxene and in the matrix. The iron-titanium oxides in the Sete Cidades rocks are titanomagnetite in the basaltic and intermediate rocks, whereas ilmenite dominates over titanomagnetite in the more evolved rocks (trachytes and trachyandesites). The oxides can be found both as inclusions in phenocrysts and in the matrix. Some samples show a very dark tachylitic matrix due to presence of very fine grained titanomagnetite crystals.

4.5.2.5 Amphibole

The intermediate (hawaiitic) and trachytic rocks contain abundant amphibole phenocrysts; amphibole xenocrysts occur rarely in the basaltic lavas (Fig. 4.5b). As the content of TiO_2 is approximately 7 wt. % (e.g. SM0108, Table 4.4) the amphiboles are classified as kaersutites. The crystals are not zoned and have wide opacitized rims (SM0137) that are either associated with dehydration or pressure decrease due to magma ascent or with re-heating of the magma above the stability field of hornblende due to magma replenishment (Rutherford & Devine, 1988; Rutherford & Hill, 1993; Nicholis & Rutherford, 2004). Electron backscatter images from the EMP indicate the formation of new phases (1-5 μm) such as Fe-Ti-oxides, plagioclase and Ca-rich clinopyroxene (diopside - hedenbergite); the two latter minerals confirmed by increasing CaO contents towards the rim of the kaersutites. The occurrence of Ca-rich clinopyroxene combined with a relatively thick rim (> 100 μm) could provide evidence that some of these rims may have been generated by an 'overheating' of the magma in the stability field of Ca-rich clinopyroxene (855°C, 0.13 GPa, Rutherford & Devine, 2003). However, the occurrence of sieve-textured, normally-zoned, plagioclase xenocrysts and mostly normally-zoned clinopyroxene xenocrysts in this sample rather suggest decompression processes. Some amphibole phenocrysts show strongly resorbed rims with abundant iron oxides, especially in sample SM0108.

4.5.2.6 Biotite

Biotite crystals were only observed in the trachytic rocks (Fig. 4.5f, Table 4.3). They occur as greenish-brown strongly pleochroic phenocrysts of phlogopite to biotite with a substitution of K_2O by small amounts of Na_2O . According to Burnham (1979) and Wones & Gilbert (1982), crystallization processes in alkaline magmas are sensitive to water pressure and oxygen fugacity. Amphibole crystallizes earlier than biotite at higher pressures; for example, at 750°C amphibole crystallizes between 1-2 kbar whereas biotite crystallizes at pressures \ll 1 kbar (Wones & Gilbert, 1982). The stability of micas is greatly enhanced by lowered SiO_2 activities. The restricted occurrence of biotite in the Sete Cidades trachytic samples suggests that the SiO_2 activity was relatively low; this is confirmed by the absence of quartz in the Sete Cidades lavas. Thus, the trachyte magmas of Sete Cidades are inferred to have had a relatively high water pressure and oxygen fugacity at low SiO_2 activities in order to crystallize amphibole before biotite.

4.5.2.7 Apatite

Small (< 1 mm) idiomorphic to hypidiomorphic apatite crystals occur in the matrix and as inclusions in clinopyroxene phenocrysts in the intermediate rocks (1-3 % MgO), and in mafic and ultramafic xenoliths. The

apatite inclusions in the xenoliths are Cl-F-apatites (Hansteen, unpubl. data), indicating relatively high halogen activities in the crustal magma reservoirs.

4.6 GEOCHEMISTRY

4.6.1 Whole-rock compositions

With decreasing MgO, SiO₂, Na₂O and K₂O show slight increases between 4 and 6 wt. % MgO, but then very abruptly increase in abundance at lower MgO contents (Fig. 4.8). The concentrations of Al₂O₃ and P₂O₅ reach a maximum at 1.5 and 3 wt. % MgO, respectively, and then decrease, while TiO₂ and FeO^T increase to ~ 5 wt. % MgO and then decrease steeply (Fig. 4.8). Lavas with more than 4 wt. % MgO show a positive correlation between MgO and Ni concentrations (Fig. 4.9a); lavas from the Mafra flank eruption show a coherent linear trend extending to high Ni and MgO contents (Fig. 4.9b).

The Sete Cidades pre-and post-caldera lavas are characterised by very similar incompatible element ratios with the exception of (La/Sm)_N, Ba/Nb, and La/Nb which are lower ((La/Sm)_N) and higher (Ba/Nb, La/Nb) in the post-caldera lavas than in the older series at a given MgO content (Fig. 4.10). Whereas (La/Sm)_N, Nb/Ta and Zr/Hf show increasing concentrations with decreasing MgO contents, the Nb/Zr and Ba/Nb of the products of each volcanic stage remain constant over the range of MgO concentrations. La/Nb is constant between 14 and 3 wt. % MgO but decrease significantly at MgO contents lower than 3 wt. %.

The lavas and glasses from Sete Cidades form a broad negative trend in ⁸⁷Sr/⁸⁶Sr versus ¹⁴³Nd/¹⁴⁴Nd extending to much higher ⁸⁷Sr/⁸⁶Sr and lower ¹⁴³Nd/¹⁴⁴Nd isotope ratios than the range of previously published data (Fig. 4.11a). Lavas from the pre-caldera stage generally have lower Sr isotope ratios (< 0.7036) than the post-caldera lavas (0.70355-0.70414), but there is a significant overlap. One sample of the post-caldera stage (SM0114) has a relatively high Sr isotope ratio of 0.70418 at a Nd isotope ratio of 0.51291 which is similar to the bulk of the Sete Cidades lavas. This radiogenic Sr isotope composition most likely reflects seawater-alteration (O'Nions *et al.*, 1977; Whipkey *et al.*, 2000). However, all other samples from Sete Cidades show a coherent correlation between Sr and Nd isotopic ratios, implying a source signature rather than seawater alteration processes. Interestingly, the lavas from the Mafra eruption have extremely heterogeneous Sr-Nd isotope compositions (⁸⁷Sr/⁸⁶Sr: 0.7035-0.7042; Fig. 4.11a). Some literature data from the neighbouring Agua de Pau volcanic system are also plotted in Figure 4.11. The Agua de Pau Sr and Nd isotope ratios extend towards 0.7055 and 0.5127, respectively (White *et al.*, 1979; Feraud *et al.*, 1980; White & Hofmann, 1982; Storey *et al.*, 1989; Turner *et al.*, 1997; Widom *et al.*, 1997). The Rb/Sr and Sr isotope ratios of the Sete Cidades and Agua de Pau samples show a broad positive correlation (Fig. 4.11b) with higher Rb/Sr and Sr isotope ratios at Agua de Pau. Three samples from the Mafra vent define a positive trend towards the fields of Agua de Pau samples.

4.6.2 Glasses

Glasses were found either as crusts on post-caldera flank deposits or in the post-caldera and caldera outflow pyroclastic deposits. The major and trace element compositions of these glasses follow the trends observed in the whole-rock lava samples. Some of the most primitive lavas (SM0101 and SM0102) from the Mafra eruption have MgO whole-rock contents of 12.3 and 14.1 wt. %. These lavas have associated glass crusts with MgO contents of 5.4 and 6.5 wt. %, respectively, implying that the accumulation of olivine and clinopyroxene

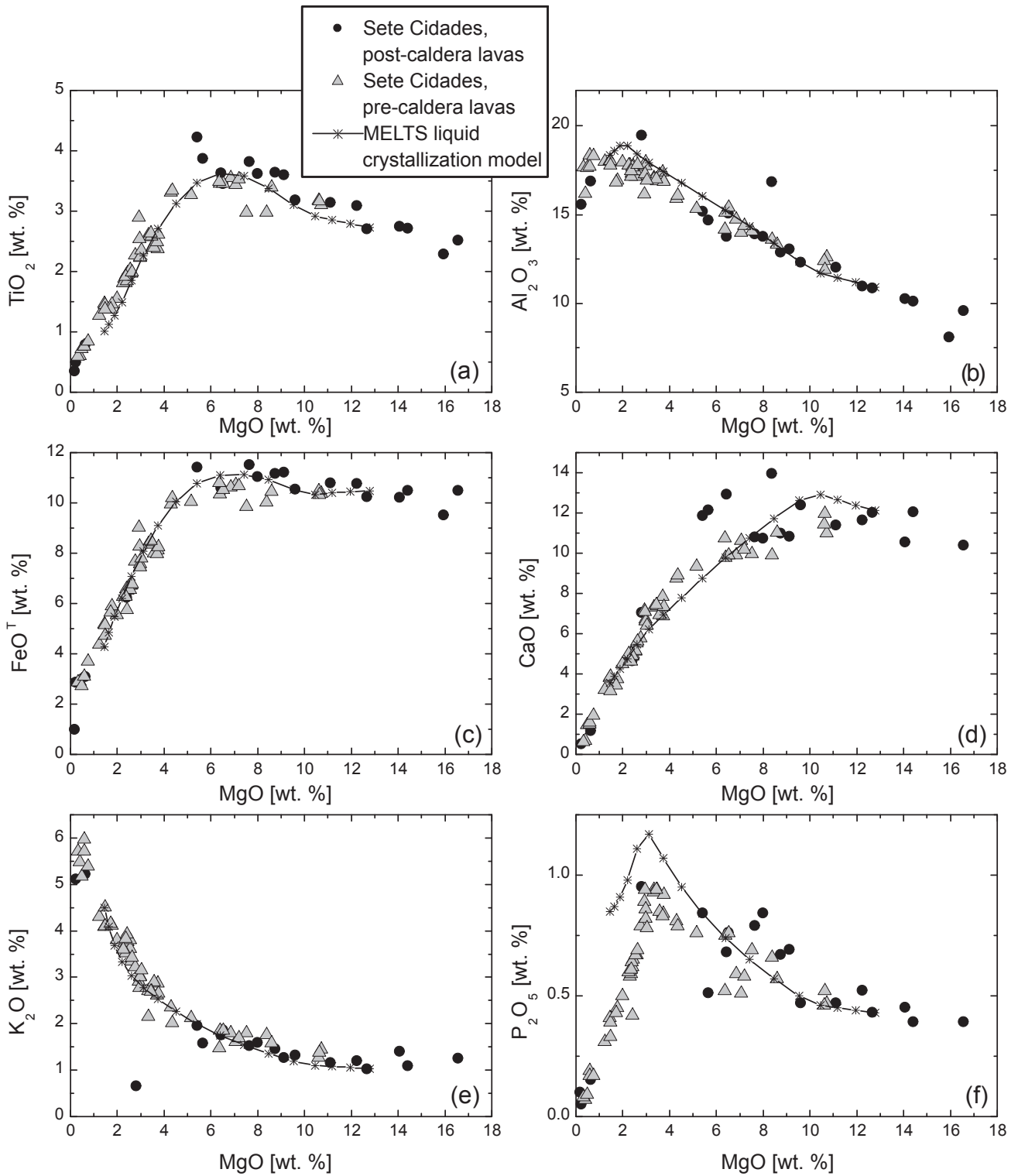


Figure 4.8: Major element contents (a) TiO_2 , (b) Al_2O_3 , (c) FeO^T , (d) CaO, (e) K_2O , (f) P_2O_5 plotted versus MgO contents for the Sete Cidades lavas. Lines indicate fractional crystallization trends modelled by MELTS (Ghiorso & Sack, 1993) using SM0140 as the parental magma as discussed in the text. The tick marks on the model curves indicate temperature steps of 20°C , starting at a temperature of 1311°C and a pressure of 5 kbar.

xenocrysts has modified the bulk-rock composition as already suggested from petrological observations.

4.6.3 The caldera outflow deposit

Thick pyroclastic deposits, suggested to have erupted during caldera formation (Moore, 1990), contain abundant streaky glass shards of heterogeneous chemical compositions between 1.0 and 0.3 wt. % MgO (Fig. 4.12). On major element diagrams, the compositions of larger glass shards lie along linear trends suggesting mixing of two different liquids (Fig. 4.12). The trachytic glass SM0123 from the caldera outflow deposit has a Mg# of 19-33 but contains rare olivines with Fo₈₁, which would be in equilibrium with a liquid of Mg# of ~ 50, supporting mixing of a more primitive magma with an evolved magma composition. Two inversely zoned clinopyroxene xenocrysts have been found in sample SM0123, also providing evidence for magma mixing processes.

4.7 DISCUSSION

4.7.1 Primitive magmas of Sete Cidades and their formation

Primitive magmas from the mantle must be in equilibrium with olivine (Sato, 1977; Hart & Davis, 1978; Hess, 1992), and, thus, the MgO and Ni contents of the most primitive lavas and olivine phenocrysts among the Sete Cidades volcanic rocks can be used to estimate the primary magma composition (Fig. 4.9). The most primitive glasses analysed from the Sete Cidades volcano have MgO contents of about 6.5 wt. % and do not represent primary magma compositions. According to Hess (1992), a primary melt must have at least 10 wt. % MgO and a Ni content of 400 ppm. The Sete Cidades sample SM0140 has a whole-rock MgO content of 12.7 wt. % and a Ni content of 365 ppm, resembling a primary magma formed by 5 % partial melting of a peridotite mantle source (Fig. 4.9) according to the model of Hart & Davis (1978). The olivines in SM0140 (Fo₈₈₋₈₉) are in equilibrium with the bulk-rock composition (Mg# 70) using the olivine-liquid equilibrium of Roeder & Emslie (1970). Although this sample contains small amounts of xenomorphic olivine, the majority of the olivines are idiomorphic to hypidiomorphic, suggesting equilibrium crystallization from the magma. The analysed olivine phenocrysts are the most primitive from Sete Cidades with a Ni concentration range of 1300-2500 ppm at Fo₈₈₋₉₀, suggesting that these olivines crystallized in equilibrium with a melt of similar composition to SM0140. Therefore, we conclude that sample SM0140 represents a near-primary melt composition of the Sete Cidades magma system. Concentrations of MgO higher than ~ 12 wt. % are, thus, considered due to the accumulation of olivine and clinopyroxene as these lavas contain abundant olivine and clinopyroxene xenocrysts (Table 4.1, 4.3 & 4.4). The range of chemical variation in the Sete Cidades volcanic rocks with MgO contents below 12 wt. % is most likely due to fractional crystallization processes.

The primitive magmas of both the pre- and post-caldera stages are similar in terms of their major element compositions, ratios of the heavy rare earth elements, and also in most incompatible element ratios sensitive to the degree of partial melting (Figs. 4.8 & 4.10). Consequently, the degree and the depth of partial melting appear to have remained constant throughout the ~210,000 year-long subaerial evolution of the Sete Cidades volcano. This is in contrast to most other oceanic volcanoes which are fed by magmas formed by variable degrees of partial melting or different depths (e.g. Woodhead, 1992). The relatively constant partial melting processes, and relatively constant melting depth, may be due to adiabatic decompression induced melt generation at the ultraslow spreading axis of the Terceira rift, where the shape of the melting region remains the same as long as extensional movement continues. In contrast, the movement of a lithospheric plate across a mantle plume should

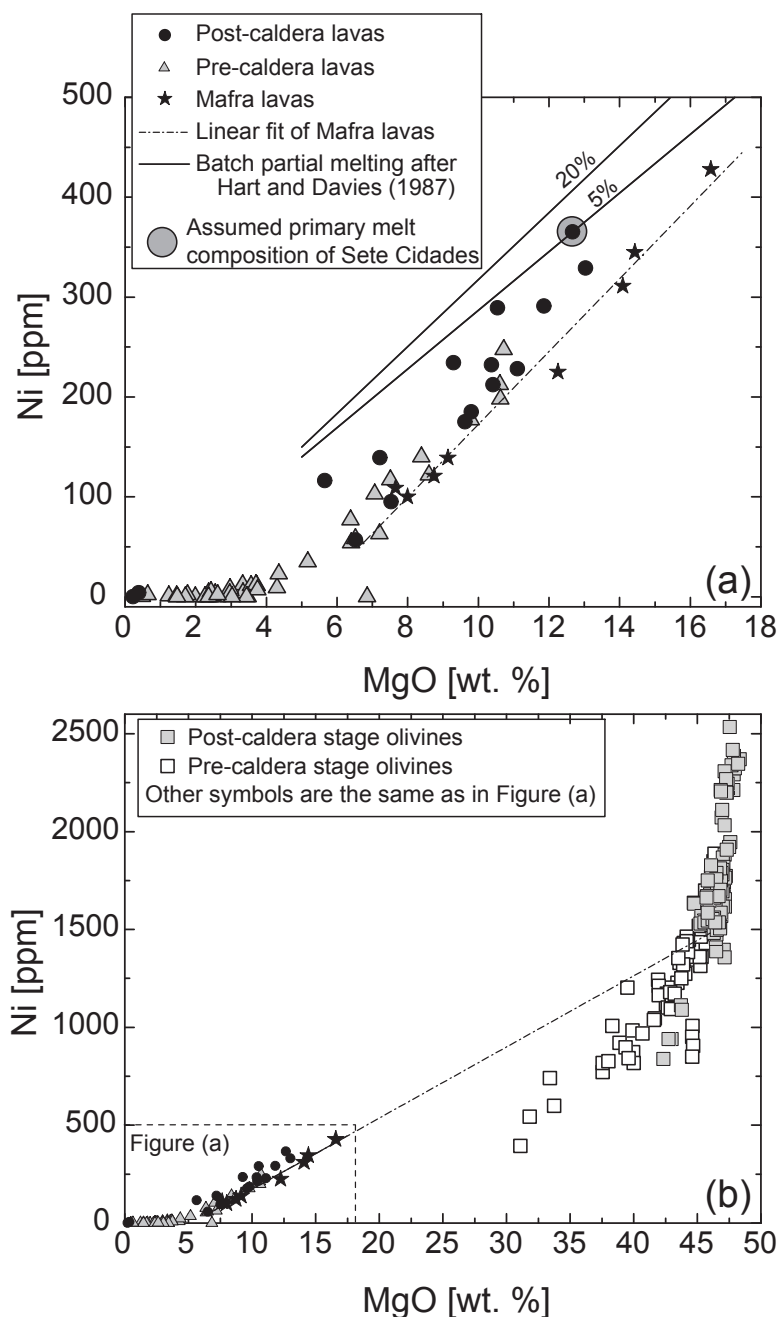


Figure 4.9: (a) Variation of Ni [ppm] versus wt. % MgO in the Sete Cidades lavas. Also shown is the range of primary magma compositions of Hart & Davies (1978) for 5 and 20 % partial melting of a mantle peridotite. (b) lava compositions from (a) and single spot analyses of the Sete Cidades olivine phenocrysts. Dotted line indicates a mixing line between the Sete Cidades primitive basalts with olivine phenocrysts in the Mafra lavas.

lead to variable depths and degrees of partial melting depending on the position of the volcano relative to the plume centre (Watson & McKenzie, 1991). The mantle source feeding the melting region beneath Sete Cidades differs significantly from that of the Agua de Pau volcano 20 km to the east (Fig. 4.11), implying that there is a boundary dividing the ascending magmas and their sources (Haase & Beier, 2003). It is believed that melts in the mantle move by porous flow and an isotopic gradient would be expected between the two volcanoes if there was one large melting region in which magmas from different mantle source regions mixed during ascent. Consequently, the evidence for very limited mixing between the parental magmas of the two volcanoes suggests that two separate melting regions, with efficient focusing of magma into each volcano's plumbing system, exist beneath the Sete Cidades and Agua de Pau volcanoes.

4.7.2 Magma ascent and fractional crystallization processes of the Sete Cidades magmas

4.7.2.1 Geothermobarometry

The magmas of oceanic intraplate volcanoes frequently stagnate and differentiate at different crustal and even mantle levels during their ascent (Hansteen *et al.* 1998). Using the geothermobarometers of Putirka *et al.* (1996), Putirka (1999) and Putirka *et al.* (2003), the crystallization pressures and temperatures can be estimated from co-existing clinopyroxene phenocrysts and liquid compositions. Glass-clinopyroxene equilibrium calculations for primitive samples from Sete Cidades (SM0101 and SM0102: 5.5 and 6.5 wt. % MgO, respectively) gave $1175^{\circ}\text{C} \pm 28^{\circ}\text{C}$ and 5.5 ± 1.7 kbar, representing a crystallization depth of 16.5 ± 5 km. Intermediate samples (SM160501-1) with 2.43 wt. % MgO gave a slightly lower temperature of 1035°C and pressures of 4.2 ± 1.7 kbar, which are within error of the more primitive lavas, although the data are somewhat displaced towards lower pressures. Renzulli & Santi (2000) estimated the temperatures and pressures of crystallization in the Sete Cidades basaltic magmas at $1222 \pm 62^{\circ}\text{C}$ and 4 kbar, respectively, whereas for the evolved rocks they found $698 \pm 3^{\circ}\text{C}$ and 0.2-1.5 kbar using the ternary feldspar geothermometer of Fuhrman & Lindsley (1988) and the geobarometer of Green & Usdansky (1986). In our evolved samples from Sete Cidades we did not find clinopyroxene-liquid equilibrium pairs using the standard error of estimate (SEE) method described by Putirka (1999). None of the Sete Cidades evolved lavas was, therefore, suitable for pressure estimates. However, Thurow & Hansteen (in prep.) determined a pressure of 1.1 ± 0.3 kbar (3.5 ± 1 km) and a temperature of 817°C from fluid inclusions in a co-magmatic hornblende gabbro xenolith interpreted as a solidified magma chamber wall fragment exhumed by the alkali basaltic Pico das Camarinhas eruption (Ponta da Ferraria; sample SM170501-32), resulting from short-term magma stagnation. They further found a lower crustal stagnation level at about 3.0 ± 0.7 kbar for the young alkali basaltic lavas from Mosteiros.

The geobarometric estimates for several basaltic lavas and pyroclastics suggest that the Sete Cidades primitive post-caldera magmas fractionated within the uppermost mantle close to the Moho, which is estimated to lie at about 14 km beneath the Azores platform (Luis *et al.*, 1998; Escartín *et al.*, 2001). Crystallization close to the crust-mantle boundary has also been observed in the Canary Islands and Hawaii (Putirka, 1997; Hansteen *et al.*, 1998b). The deep onset of crystallization requires a relatively cold and probably thick lithosphere above the melting region because the magmas are cooled to about $1150\text{-}1200^{\circ}\text{C}$ within the uppermost mantle. Such a relatively cold lithosphere within the Terceira spreading axis is consistent with geophysical models showing that cooling is more efficient than heat transfer from the ascending mantle in ultraslow spreading regions (Reid & Jackson, 1981). Alternatively, the estimated fractionation depths within the uppermost mantle may correspond to the onset of degassing-induced crystallization, thus representing the depth of CO_2 oversaturation of the magmas. Such upper mantle crystallization has been proposed for Quaternary basanites on the Canary Islands, where CO_2 oversaturation and vigorous crystallization typically starts at 40 to 25 km depth (Hansteen *et al.*, 1998a). After stagnation and crystallization at the crust-mantle boundary, the Sete Cidades magmas typically ascended rapidly to a shallow level of about 3.5 km depth. Such magmas evolved to trachytic compositions and fed the caldera-forming eruption. The occurrence of lower crustal xenoliths in young mafic flank eruptions at Sete Cidades strongly indicates that the magmas also resided intermittently within the lower crust. This is supported by fluid inclusion barometry of mafic and ultramafic xenoliths (Thurow & Hansteen, in prep.), and would imply that the young, mafic magmas could have chemically interacted with the island crust.

Upper mantle magma stagnation and fractional crystallization was also observed at La Palma (Klügel *et al.*, 2000; Klügel *et al.*, 2005), where the pressures were estimated at 4.1 to 7.7 kbar (average 6.0 kbar) using

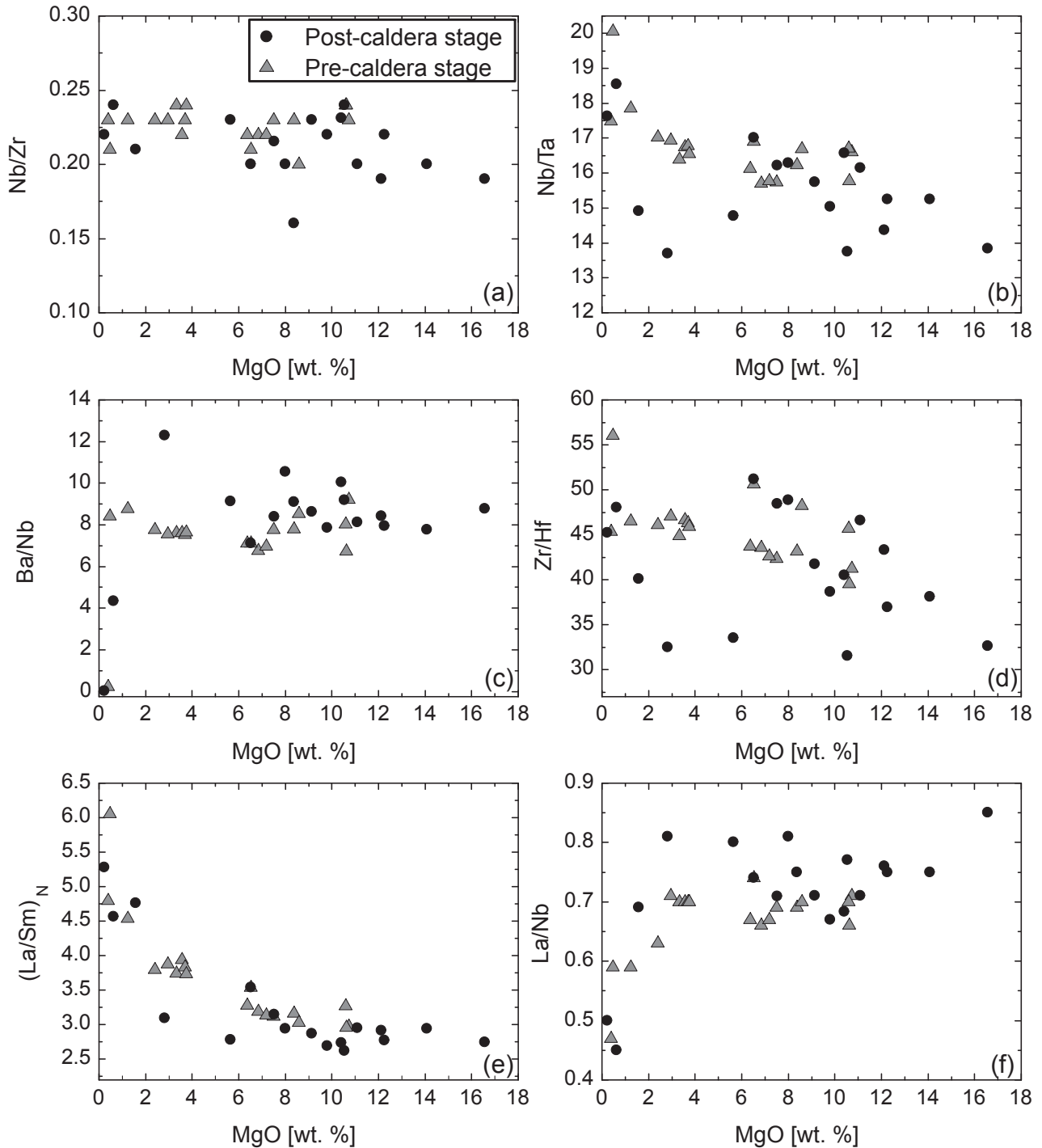


Figure 4.10: Highly incompatible trace element versus wt. % MgO ratios in the lavas from Sete Cidades.

clinopyroxene-melt thermobarometry. Thus the magmas were stored deeper in the lithosphere than beneath Sete Cidades, possibly due to the thicker, older and colder lithosphere beneath the Canary Islands, or to the higher initial CO_2 contents of the magmas. Additional crustal magma accumulation occurred within the lower crust at pressures of 2.4 to 4.7 kbar (average 3.3 kbar) beneath La Palma. Such multi-stage magma ascent and fractionation also occurs beneath other North Atlantic ocean islands (e.g. Madeira; Schwarz *et al.*, 2004).

4.7.2.2 Oxygen fugacity

Coexisting spinel and Fe-Ti oxides (preferentially cores) were used to determine the oxygen-fugacities of the magmas using the fugacity modelling program QUILF of Andersen *et al.* (1993). The equilibrium of the oxides was tested using the $\log(\text{Mg/Mn})_{\text{mag}}$ and $\log(\text{Mg/Mn})_{\text{ilm}}$ ratios of Bacon & Hirschmann (1988). The $f\text{O}_2$ of several lavas was determined and we find that a few basalts lie close to the Ni-NiO buffer curve similar to some evolved lavas from Tenerife (Fig. 4.13), although the Tenerife lavas formed in an open-system, hence they cross the oxygen buffer curves (Bryan *et al.*, 2002). On the other hand, one basalt and two trachyte samples show significantly higher $f\text{O}_2$. The pre-caldera samples have significantly lower $f\text{O}_2$ than the caldera-related deposits and post-caldera samples.

We propose that the higher $f\text{O}_2$ values most likely reflect higher total volatile contents in the post-caldera magmas of Sete Cidades, in both the basaltic and trachytic compositions. This would also be an explanation for the more explosive-style of the volcanism after the caldera-forming eruption. Therefore, the post-caldera mantle source must be characterised by a higher volatile component, increasing the $\log f\text{O}_2$ in the younger lavas. One possibility to increase the volatile content of a magma would be the assimilation of crustal rocks, consistent with the occurrence of crustal xenoliths in the lavas of Ponta da Ferraria and Mafra.

4.7.2.3 Fractional crystallization and modelling using MELTS

Based on the petrological observations and the geochemical data, the following phases crystallized from the Sete Cidades magmas: olivine, clinopyroxene, magnetite, ilmenite, plagioclase, apatite, alkali feldspar, amphibole, and biotite. The major element composition of the Sete Cidades lavas indicates that the samples lie along a single liquid line of descent (Fig. 4.8), although the slight differences in incompatible trace element (e.g. Ba/Nb, La/Nb) and radiogenic isotope ratios (Figs. 4.10 & 4.11) imply that the magmas are not all comagmatic. The fractionation of olivine leads to decreasing MgO and Ni contents (Fig. 4.9), while the decrease of CaO (Fig. 4.8) can be explained by the crystallization of clinopyroxene from magmas with MgO contents between 12 and 3 wt. %, and plagioclase at MgO contents < 3 wt. %. Plagioclase also occurs in the more primitive rocks, but is modally of minor importance; the enrichment in Al_2O_3 in lavas with between 16 and 2 wt.% MgO also suggests minor fractionation of plagioclase. The sharp decrease in Al_2O_3 content at ~ 2 wt. % MgO shows that crystallization of feldspars dominates the fractionation assemblage in the evolved rocks (Fig. 4.8). The crystallization of ilmenite and magnetite decreases the concentrations of TiO_2 and FeO^{T} in the lavas with less than 6 wt. % MgO. The decreasing P_2O_5 content at MgO contents below 3 wt. % is due to the fractionation of apatite.

The major element compositions of the Sete Cidades rocks can be fitted by a fractional crystallization trend calculated using MELTS (Ghiorso, 1997) with sample SM0140 as the parent magma (Fig. 4.8). The oxygen fugacity has been estimated at $\log f\text{O}_2 = -10$ using co-existing Fe-Ti oxides (Fig. 4.13). At a pressure of 5 kbar and estimated H_2O and CO_2 contents of 0.5 wt. %, MELTS calculates a liquidus temperature of 1311°C for sample SM0140. The actual trends from Sete Cidades and the modelled MELTS fractionation trends fit relatively well, confirming that the major element compositional variation of the Sete Cidades lavas is mainly due to fractional crystallization processes. Contrary to other oceanic intraplate volcanoes (e.g. Tenerife, Ablay *et al.*, 1998; Bryan *et al.*, 2002) Sete Cidades does not show a bimodal distribution of the lava compositions. The occurrence of bimodal lava compositions in many magmatic systems has been explained in terms of a density barrier for intermediate magmas, i.e. due to the increased Fe contents of intermediate magmas which are too dense to rise to the surface in most regions (Stolper *et al.*, 1981). The Fe content does not increase significantly during crystal fractionation in the Sete Cidades magmas (Fig. 4.8) and this could explain the eruption of the

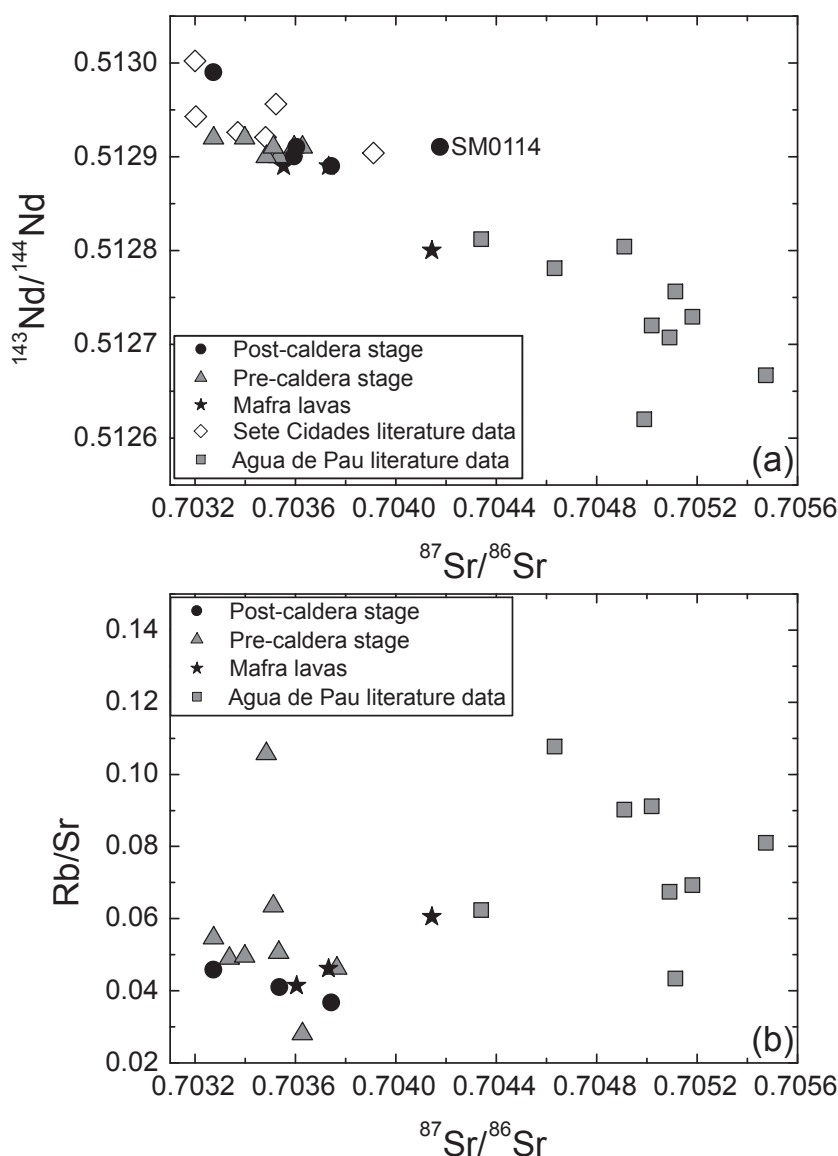


Figure 4.11: (a) Variation of $^{87}\text{Sr}/^{86}\text{Sr}$ versus $^{143}\text{Nd}/^{144}\text{Nd}$ for the Sete Cidades lavas and Agua de Pau data from the literature (White *et al.*, 1979; Feraud *et al.*, 1980; White & Hofmann, 1982; Storey *et al.*, 1989; Turner *et al.*, 1997; Widom *et al.*, 1997). Literature data from Sete Cidades are also plotted for comparison (White *et al.*, 1975; Hawkesworth *et al.*, 1979; Davies *et al.*, 1989; Turner *et al.*, 1997; Widom *et al.*, 1997). (b) Rb/Sr versus $^{87}\text{Sr}/^{86}\text{Sr}$ for the Sete Cidades and Agua de Pau volcanic systems. Sources of data as in (a).

entire compositional range of magmas. The fractional crystallization model using the MELTS program supports this conclusion because the melt density is predicted to decrease continuously from the primitive magma starting composition of SM0140 (2.77 g/cm^3) to 2.52 g/cm^3 in the trachytic melts.

4.7.2.4 Effects of fractional crystallization processes on incompatible element ratios

The coherent fractional crystallization trend allows us to determine the effects of fractionation of different mineral phases on the abundances of incompatible elements and their ratios. Understanding the effects of crystal fractionation processes on incompatible element concentrations and ratios is important because highly incompatible element ratios in lavas are often used as a proxy for the compositions of the mantle source of the lavas (e.g. Kamber & Collerson, 2000a). The Nb/Zr ratio is not affected by crystal fractionation processes (Fig. 4.10a) implying that these two elements have similar distribution coefficients and can be used to distinguish

different mantle sources (Kamber & Collerson, 2000b). In contrast, the highly incompatible element ratios Nb/Ta and Zr/Hf both increase significantly with decreasing MgO in the Sete Cidades sample suite (Figs. 4.10b and d), showing that Nb and Zr are more incompatible than Ta and Hf, respectively, during fractional crystallization. Consequently, the use of these element ratios to compare the mantle sources of different suites of rocks is limited by the effects of fractional crystallization processes. The increasing Zr/Hf in OIB has been explained by the fractionation of clinopyroxene (David *et al.*, 2000). However, whereas the increasing $(La/Sm)_N$ ratios in the more evolved lavas can be explained by extensive fractionation of clinopyroxene (Fig. 4.14a), a model using recently published clinopyroxene distribution coefficients (Hart & Dunn, 1993) and 55 % clinopyroxene in the fractionating mineral assemblage fails to reproduce the observed Zr/Hf trend (Fig. 4.14b). Increasing Nb/Ta in alkaline lava series has been attributed to the presence of titanite in the fractionating assemblage (Wolff, 1984; Green, 1995); however, the Sete Cidades alkali basalts do not contain titanite. Other phases such as olivine and plagioclase that crystallize from the Sete Cidades alkali basalts have only low contents of Zr, Hf, Nb and Ta and do not show large differences between the distribution coefficients of the respective elements (Green, 1995). Thus, the partition coefficients of Nb relative to Ta, and Zr relative to Hf for the Sete Cidades clinopyroxenes may be too low, especially because they are Ti-augites. Alternatively, extensive magnetite fractionation could explain the trends; Green & Pearson (1987) have shown that Nb ($K_D = 0.40$) and Zr ($K_D = 0.10$) are more incompatible than Ta ($K_D = 1.0-10$) and Hf ($K_D = 2.0-4.0$), respectively in magnetite.

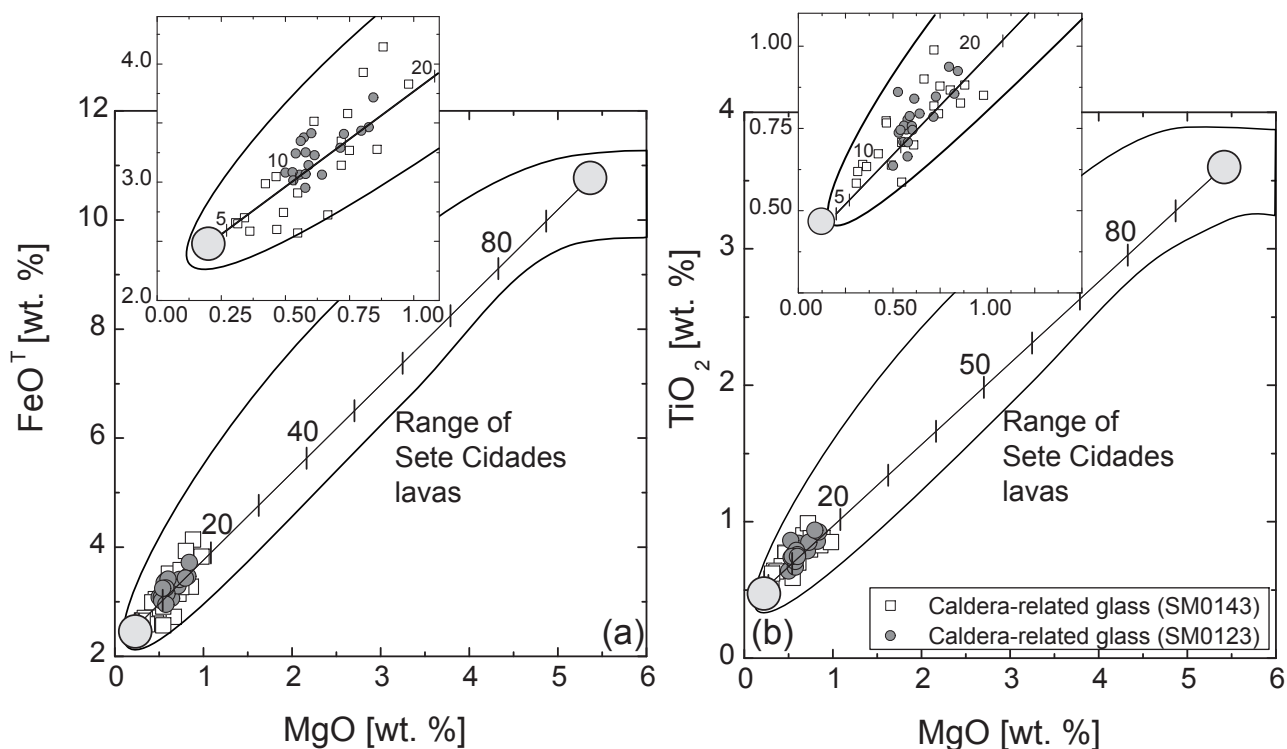


Figure 4.12: Variation of FeO^T (a) and TiO_2 (b) versus MgO (wt. %) in glass shards from two samples of the caldera-related pyroclastic deposit indicating strong heterogeneity within the glasses and possible mixing trends between intermediate and basaltic melt. Field shows the range of the Sete Cidades pre- and post-caldera lavas. The grey circles indicate the end-members of the mixing array. The basaltic magma MgO content has been estimated at about 5 wt. % MgO based on olivine xenocrysts in the glasses of the caldera outflow deposit. The insets illustrate the variation of the caldera-related deposits in more detail.

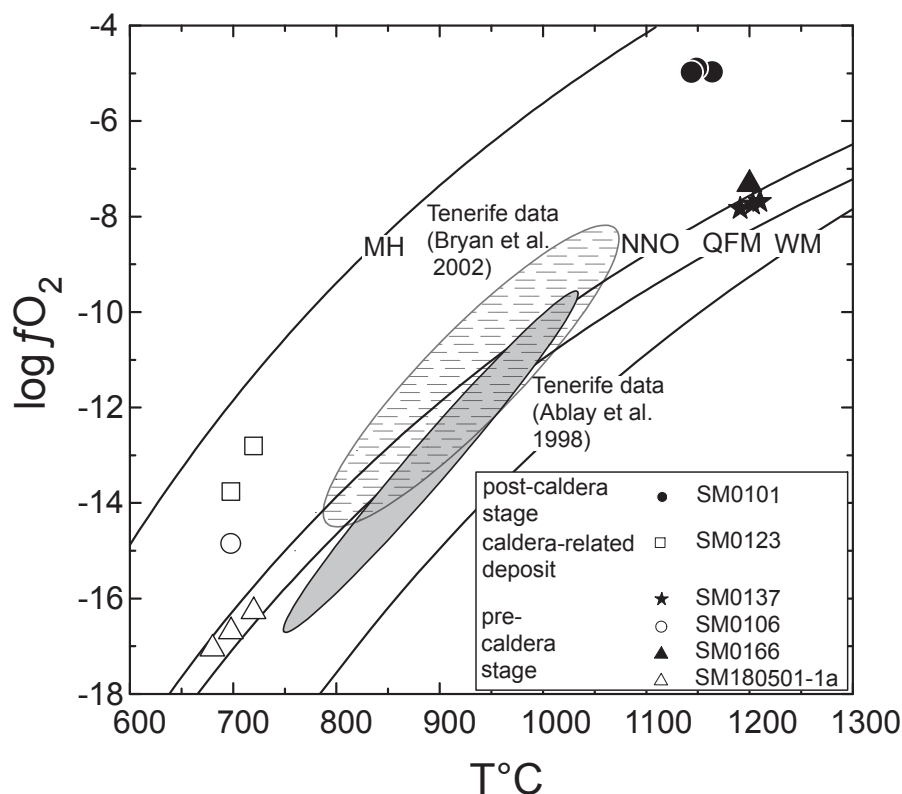


Figure 4.13: Log f_{O_2} versus temperature ($^{\circ}C$) for the Sete Cidades lavas compared to lavas from Tenerife (Ablay *et al.*, 1998; Bryan *et al.*, 2002). Filled symbols are basaltic samples; open symbols represent trachytic compositions.

The trace elements Ba, Eu, and Sr are depleted in the evolved rocks, supporting the late-stage fractionation of feldspar. The decreasing La/Nb at about 3 wt. % MgO coincides with the onset of apatite fractionation (Fig. 4.8f) and most likely, apatite depletes the magma in La relative to Nb (Fujimaki, 1986). Only the most evolved lavas show low Ba/Nb, possibly due to the late-stage fractionation of biotite, withdrawing preferentially Ba ($K_D^{Biotite/Melt} \sim 23.5$) relative to Nb ($K_D^{Biotite/Melt} \sim 6.4$) (Nash & Crecraft, 1985). We conclude that in alkaline rock series even the ratios of highly incompatible elements can be fractionated; this has to be considered when these ratios are used to constrain the compositions of the mantle sources of lavas from different volcanoes.

4.7.3 Time-scales of magma evolution and ascent beneath Sete Cidades

The stratigraphy at Sete Cidades show several fractionation cycles from basaltic to trachytic compositions over the last 210,000 years (Moore, 1991b). The Sete Cidades post-caldera stage consists of 11 changes between basaltic and trachytic compositions in the last 16,000 years. The trachytic post-caldera eruptions were mostly erupted from the caldera vent, suggesting the existence of a shallow magma chamber beneath the centre of the volcano, whereas all the post-caldera basalts were erupted from flank vents along rift zones, thereby generating the alternating post-caldera stage stratigraphy. Consequently, there appears to be no connection between the trachytic magma chamber and the basaltic magma systems on the volcano flanks. In contrast, the subaerial pre-caldera stage observed in the Sete Cidades caldera wall contains at least 7 compositional changes from 210,000 to 36,000 years (Fig. 4.3), and these lavas erupted from the central summit only. On average, the composition changed every 25,000 years in the pre-caldera stage, consistent with observations on the neighbouring Agua de Pau volcano (Widom *et al.*, 1992; Widom *et al.*, 1993). Similar temporal compositional variations have been

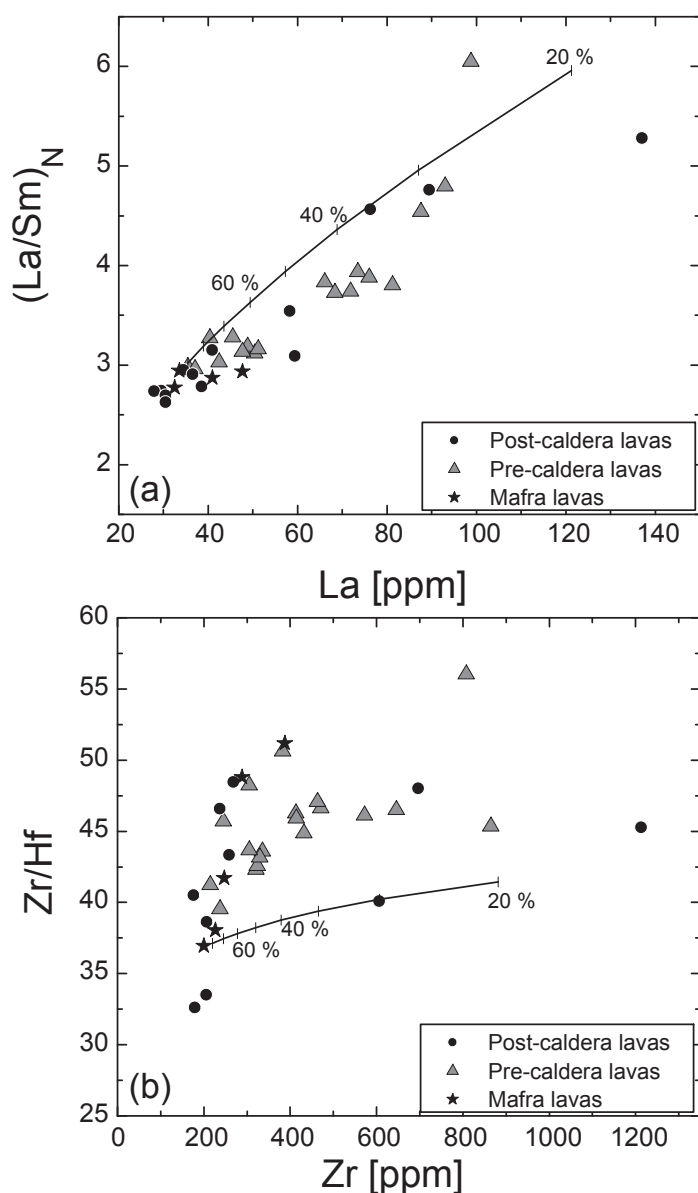


Figure 4.14: Fractionation trends for (a) $(La/Sm)_N$ versus La and (b) Zr/Hf versus Zr for 10 % increments of a crystallization assemblage with 55 % clinopyroxene, 35 % olivine, 5 % plagioclase, 4 % ilmenite and 1 % apatite. Tick marks represent degrees of Rayleigh fractionation in increments of 10 %. Partition coefficients for La, Zr, and Hf in olivine are from Zanetti *et al.* (2004); Sm in olivine and plagioclase from Dunn & Sen (1994); clinopyroxene from Hart & Dunn (1993); magnetite from Nielsen *et al.* (1992); apatite from Fujimaki (1986).

found on Tenerife where two different time-scales have to be taken into consideration. Firstly, the overall differentiation time from a basaltic to a phonolitic composition including the formation of a shallow magma chamber, is $\sim 200,000$ years (Hawkesworth *et al.*, 2000). Secondly, fractionation within trachytic magmas occurs within shorter time-scales of 100's to 1000's of years. These short-term fractionation scales have not been observed at Sete Cidades, but the overall differentiation from a dominantly basaltic to a dominantly trachytic eruptive stage seems to be of the same temporal order at both volcanoes.

The trachytic caldera-forming eruption was probably triggered by basaltic replenishment of the shallow magma chamber, indicated by the occurrence of olivine xenocrysts (Fo_{81}) and inversely zoned clinopyroxene xenocrysts. The large compositional variation of the streaky glass shards in the caldera-forming deposits suggests mixing between an evolved magma and a basaltic magma in equilibrium with olivine with Fo_{81} (Fig. 4.12). Such a basaltic replenishment into an evolved magma chamber could also explain the occurrence of opacitized rims around kaersutite crystals (SM0137), as the heating of an evolved to intermediate magma by the intrusion of hot basaltic magma may raise the magma temperature into the Ca-pyroxene stability field (855°C , 0.13GPa ; Rutherford & Devine, 2003). The intrusion of a hot basaltic magma into an evolved magma could also result in

reversely zoned clinopyroxene and plagioclase crystals. However, although a few clinopyroxene xenocrysts are reversely zoned, with increasing Mg# towards the rim, the majority of the clinopyroxene crystals shows normal zoning, making decompression more likely, where the formation of new mineral phases can be used as an indicator of magma ascent rate (Rutherford & Devine, 1988; Rutherford & Hill, 1993). These authors concluded that Fe-oxide dehydration rims on amphibole form either by decreasing H_2O in the melt during magma ascent or during magma chamber storage. Decreasing H_2O in the Sete Cidades magmas seems unlikely as this would not result in the decompression textures observed in the plagioclase xenocrysts. The experiments show that amphiboles without reaction rims ascended from 8 km depth to the surface in less than 5 days, and that the thickness of the rims correlates with the storage time at less than 6.5 km depth (Rutherford & Devine,

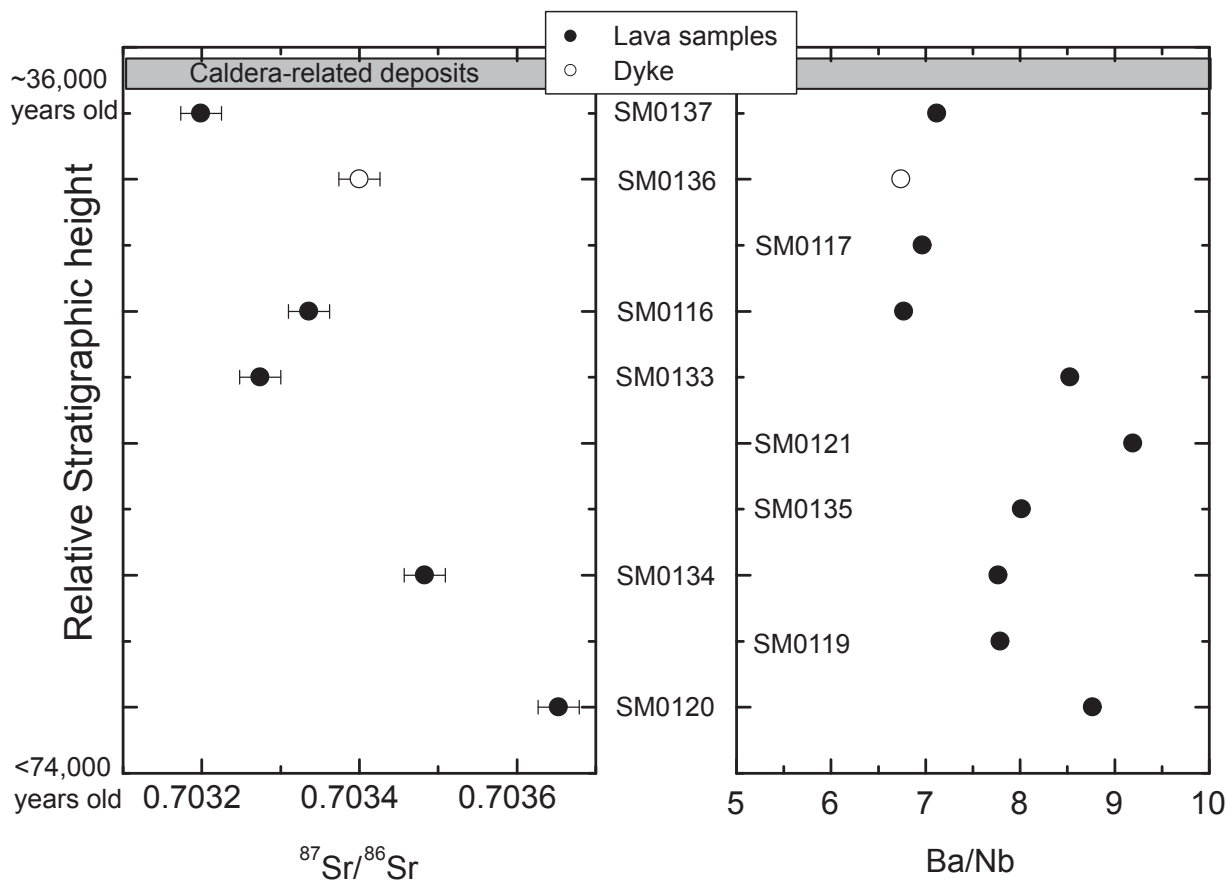


Figure 4.15: Variation of the pre-caldera $^{87}\text{Sr}/^{86}\text{Sr}$ and Ba/Nb ratios with stratigraphic height in the seacliff section at Ponta da Ferraria. The stratigraphic heights represent an age range from < 74,000 to ~ 36,000 years (Moore & Rubin, 1991; Pacheco *et al.*, 2005). The lower lava flows have a distinct composition from the upper units. The error bar represents a maximum 2σ -error of 0.00026.

1988; Nicholis & Rutherford, 2004). The kaersutite reaction rims in sample SM0137 show minimum widths of $100\mu\text{m}$ and a maximum width of $200\mu\text{m}$, measured from backscattered electron images. The experiments of Rutherford and Hill (1993) gave rim width of $30\text{--}50\mu\text{m}$ for an experimental stagnation time of 9–17 days. We conclude that some of the Sete Cidades magmas (e.g. sample SM0137) resided at maximum for a few weeks in a shallow magma chamber at $\sim 3.5\text{ km}$ depth until they ascended to the surface.

4.7.4 Temporal variations in the petrogenesis of the Sete Cidades lavas

The fact that there is no systematic change in the major and in most trace element compositions of the primitive magmas of the pre- and post-caldera lavas at Sete Cidades indicates that mantle partial melting processes did not change significantly during the last 210,000 years. In this respect, the magmatic evolution of the Sete Cidades volcano differs from the systematic temporal variation in the degree of partial melting observed at most oceanic intraplate volcanoes (e.g. Woodhead, 1992). However, the variation of $(\text{La}/\text{Sm})_{\text{N}}$, Ba/Nb, and La/Nb ratios, as well as of Sr and Nd isotope compositions suggests small-scale heterogeneity within the Sete Cidades mantle source and binary mixing, with the two endmember components having varying influences with time (Figs. 4.10 & 4.11). Thus, the post-caldera lavas have higher Ba/Nb, but lower $(\text{La}/\text{Sm})_{\text{N}}$ and Nb/La, than the pre-caldera lavas, indicating a slight systematic change in the mantle source at the time of caldera formation. Because the post-caldera magmas have higher Ba/Nb (Fig. 4.10c), and Ba is more incompatible than Nb, this variation cannot be due to increasing depletion of the source because of the previous melting events forming the

pre-caldera magmas, as observed at other volcanoes (e.g. Reiners, 1998). On a smaller scale, the stratigraphic section at Ponta da Ferraria (Fig. 4.3) shows slight variations in the pre-caldera magma sources with time (Fig. 4.15). For example, the lower lavas in the Ponta da Ferraria section have higher $^{87}\text{Sr}/^{86}\text{Sr}$ and Ba/Nb than the upper lavas (Fig. 4.15). These variations reflect changes in the mantle source of the pre-caldera magmas rather than increasing depletion of the source because other incompatible element ratios such as Nb/Zr or $(\text{La}/\text{Sm})_N$ do not decrease towards the upper part of the section.

One notable systematic difference between the pre- and post-caldera lavas is the MgO content of the two lava series; the pre-caldera lavas exhibit a continuous compositional range between 11 and 0 wt.% MgO (Fig. 4.8). In contrast, the post-caldera stage is divided into trachytic eruptions in the caldera, and basaltic eruptions with more than 6 wt.% MgO on the flank, i.e. the post-caldera stage shows an apparently bimodal distribution. This change in the magma evolution may be due to the presence of a shallow magma chamber that developed at the end of the pre-caldera stage of the Sete Cidades volcano and may have acted as a density barrier, preventing the eruption of primitive lavas from the caldera vent during the post-caldera stage. As long as the felsic magma chamber existed, the basaltic and intermediate lavas were erupted along the volcano's flanks, for example, at Mafra and Ponta da Ferraria (Figs. 4.1, 4.2 & 4.3). The post-caldera stage is dominated by very primitive basaltic flank eruptions (Ponta da Ferraria, Mafra) and a few coeval trachytic eruptions within the caldera. For example, the trachytic eruption of Caldera Seca (Inner Caldera) occurred ~ 500 years ago, while the alkali basalts of Ponta da Ferraria (western flank) erupted 840 years ago (Moore, 1990). The youngest flank eruptions, including Mafra and Ponta da Ferraria, contain abundant mafic and ultramafic xenoliths, implying relatively short crustal residence times. High magma supply rates into the lithosphere during the pre-caldera stage may have induced the formation of a stable magma reservoir in which relatively evolved magmas formed by crystal-liquid fractionation. A decreased magma production rate since caldera formation has resulted in only small volume eruptions of relatively primitive magmas on the flanks of Sete Cidades.

In summary, three important differences exist between the pre- and post-caldera rocks; a) a higher oxygen fugacity in the post-caldera basalts, b) differences in some incompatible trace element ratios in the primitive post-caldera samples (e.g. higher Ba/Nb, La/Nb, lower $(\text{La}/\text{Sm})_N$), and c) a bimodal distribution in the post-caldera lavas, contrasting with a continuous lava trend in the pre-caldera stage.

4.7.5 Evidence for magma mixing?

The Sete Cidades alkali basalts frequently contain olivine xenocrysts with large compositional variations and Fo contents between 52 and 90. The intermediate and evolved lavas contain reversely zoned clinopyroxene xenocrysts (e.g. SM0137, SM0149), suggesting crystallization from different magmas and thus, probably, magma mixing processes. The plagioclase crystals in the intermediate lavas also show a large compositional range; the presence of anorthite-rich crystals which accumulated from a more primitive magma is consistent with the occurrence of reversely zoned clinopyroxenes. In one of these samples (SM0108), a sanidine phenocrysts was also observed, suggesting that the primitive and intermediate magmas assimilated crystals of more evolved magmas before the eruption. Consequently, the replenishment of the evolved magma chamber by basaltic liquids appears to have occurred frequently during the evolution of the volcano and may have been the trigger for eruptions.

The initiation of the caldera-forming eruption of the Sete Cidades volcano about 16,000-36,000 years ago also appears to be related to magma mixing. Calderas are formed by extensive, explosive eruptions emptying the magma chamber, during which the roof sags into the magma chamber and may leave pockets of remaining

melt that can erupt through the caldera-ring faults and form eruption centres on the inner caldera ring (Folch *et al.*, 2001). Two mechanisms may be responsible for the initiation of the caldera-forming eruptions; (1) step-wise degassing of intermediate and trachytic magma may lead to the sagging of the magma chamber roof (Gudmundsson, 1998), or (2) hot basaltic magma injections into a magma chamber containing a cooler, evolved magma, leading to vigorous convection and a pressure increase in the magma chamber triggering an explosive eruption (Sparks *et al.*, 1977). The glasses of the caldera outflow deposit contain elongated glassy shards with very heterogeneous compositions (Fig. 4.12). The glass chemical data of the outflow pyroclastic deposit mostly lie on linear trends that probably reflect mixing between a trachytic and a more primitive melt. The trachytic glass SM0123 from the caldera outflow deposit has an Mg# of 19-33, but contains rare olivines with Fo_{81} which would be in equilibrium with a liquid of Mg# of ~50, supporting mixing of a trachytic melt with a basalt with MgO of about 5 wt. %. Further evidence is given by the occurrence of inversely zoned clinopyroxene xenocrysts with a higher Mg# in the crystal's rim than in its core. Consequently, a possible explanation is the intrusion of a hot, more primitive basaltic melt into a cooler evolved melt stored in a crustal reservoir, leading to overheating of the trachytic magma (Sparks *et al.*, 1977). We conclude that the caldera-related eruptions have been triggered by the inflow of hot basaltic melt into a shallow magma chamber containing trachytic magma.

Nine alkali basaltic samples from the Mafra flank eruption (Fig. 4.1 & 4.2) were analysed and show variations of 1.08-1.40 wt. % K_2O , Nb/Zr of 0.19-0.23, $^{143}Nd/^{144}Nd$ of 0.51291-0.51280, and $^{87}Sr/^{86}Sr$ of 0.70361-0.70414, suggesting compositionally distinct magma sources feeding this single eruption. The lava (SM0102, Table 4.1) with the highest $^{87}Sr/^{86}Sr$ comes from the lava delta most distant from the eruptive fissure, while sample SM0101 of intermediate composition is slightly closer, and the relatively unradiogenic sample SM0161 was taken from the youngest cinder cone on this fissure, possibly indicating a temporal decrease in the Sr isotope ratios. Thus, the Mafra eruption apparently shows chemical evolution of its products similar to the variations observed, for example, during the Puu Oo eruption of Kilauea volcano, Hawaii (Garcia *et al.*, 1996). The temporal compositional variation in oceanic basalts has been explained by crustal contamination, different degrees of partial melting, or mixing of melts from chemically distinct sources (e.g. Reiners, 2002). Crustal contamination within the oceanic crust leading to lower $^{143}Nd/^{144}Nd$ appears unlikely beneath Sete Cidades volcano because both the MORB-like oceanic crust and the lavas of the volcano have higher Nd isotope ratios than the Mafra lavas. The constant major element compositions (e.g. Na_2O , FeO^T) and trace element ratios (e.g. Ce/Yb, Sm/Yb) of the Mafra lavas imply similar degrees of partial melting of the magmas feeding the eruption. Thus the Mafra basalts appear to show the increased influence of another mantle source which resembles that of the neighbouring volcano, Agua de Pau, which has much higher Sr isotope but lower Nd isotope ratios (Fig. 4.11a). Most likely, the trend of the Mafra lavas indicates mixing between a magma of typical Sete Cidades composition and a magma derived from the Agua de Pau mantle source. Such a mixing process is supported by the broad linear positive correlation between $^{87}Sr/^{86}Sr$ and Rb/Sr (Fig. 4.11b), ranging between the compositions of Sete Cidades and Agua de Pau lavas. Thus, we speculate that a small volume of magma from the Agua de Pau source must have been present beneath the western flank of the Sete Cidades volcano giving rise to the unusually radiogenic lavas. This is surprising given the relative homogeneity of the rest of the studied lavas from Sete Cidades. Interestingly, the different Mafra lavas also plot on mixing lines between whole-rock/glass compositions and olivine (Fig. 4.9) suggesting that the magmas also entrained large volumes of xenocrystic olivine during their ascent.

4.8 CONCLUSIONS

The geochemical and petrological results of this study, combined with stratigraphic observations, show that over the last 210,000 years the lavas of the Sete Cidades volcano have undergone frequent changes between primitive and evolved compositions. These alternations occurred during the main shield-building stage that contains intercalated trachytic deposits (> 210,000-36,000 years) which form the greater part of the subaerial volume. A series of caldera-forming eruptions occurred from 36,000 to 16,000 years ago, producing mainly trachytic pyroclastic deposits. The post-caldera stage and recent volcanism has been dominated by both trachytic eruptions within the caldera and along the caldera ring fault and coeval basaltic eruptions from parasitic craters around the flanks of the volcano (Fig. 4.16). Major element and most trace element compositions of all lavas of Sete Cidades volcano show that the magmas evolved mainly by crystal fractionation processes, whilst partial melting processes and mantle sources remained relatively constant throughout the evolution of the subaerial part of the volcano, i.e. over a period of time of 210,000 years. However, a slight systematic difference in the Ba/Nb, La/Nb and the Sr isotope ratios between the pre- and post-caldera lavas implies that the caldera eruption event coincided with a change in magma source compositions. Thermobarometric calculations indicate that the basaltic magmas started to fractionate close to the crust-mantle boundary, at about 16 ± 5 km depth, implying that the ultraslow Terceira rift spreading axis is overlain by a relatively cold lithosphere. The more evolved magmas fractionated extensively in a shallow magma chamber at about 3.5 km depth beneath the volcano, whereas basaltic magmas resided for only short periods of time in crustal reservoirs (Fig. 4.16). After

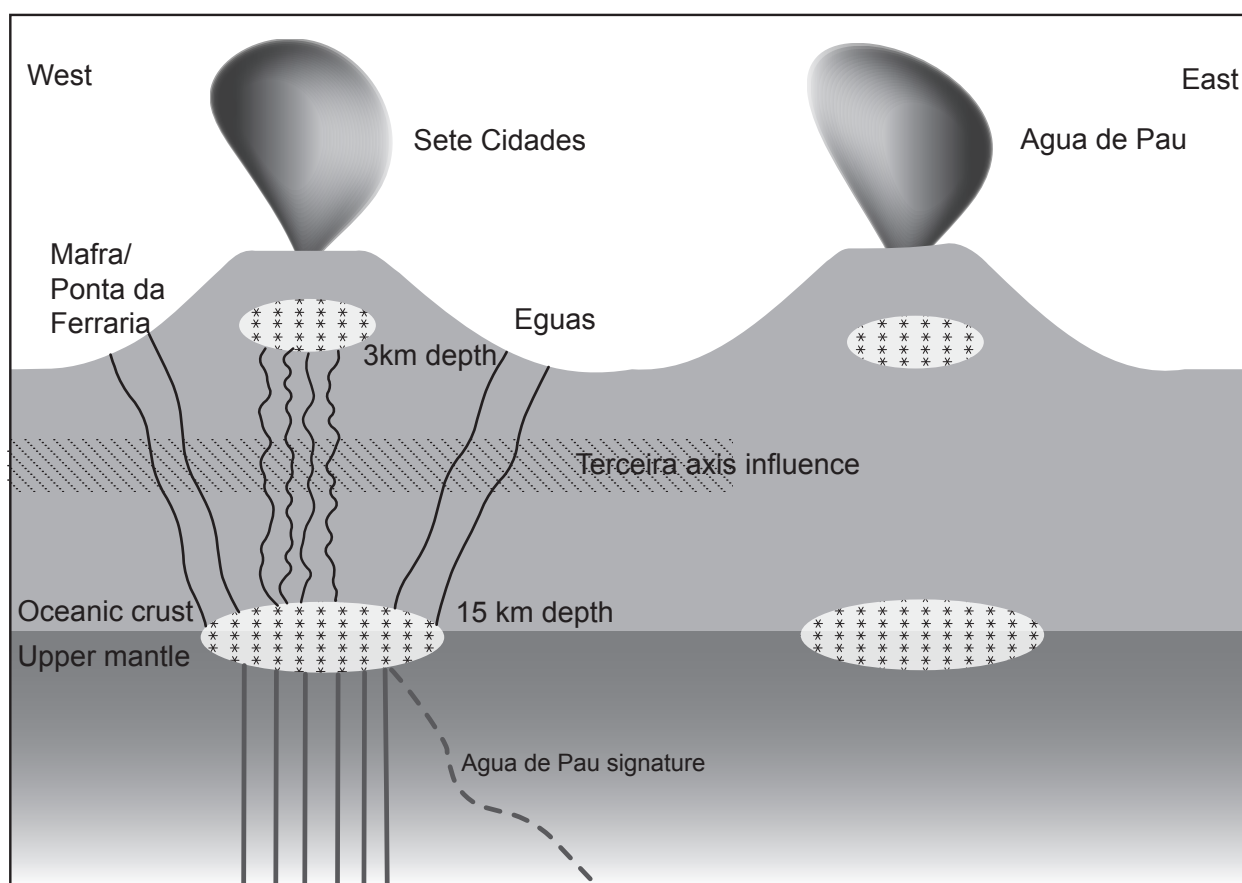


Figure 4.16: Schematic sketch of the Sete Cidades volcano comprising two storage levels (3 km and 15 km). The magmas forming the post-caldera flank eruptions bypassed the shallow magma chamber. Mixing between the Sete Cidades volcanic systems and the Agua de Pau magmas most likely occurs in the upper mantle rather than in the oceanic crust.

caldera formation, residual trachytic magma erupted as lava within the caldera. The more primitive post-caldera magmas reflect rejuvenation of the magmatic system of Sete Cidades volcano and continuing activity along the volcano's rift zone in the Terceira rift. These lavas have the most primitive compositions and contain abundant olivine and clinopyroxene phenocrysts as well as mantle xenoliths, suggesting a relatively fast magma ascent. The alkali volcanic series of Sete Cidades shows clear evidence for fractional crystallization processes in both the major element whole-rock chemistry and in the trace element compositions. The variations observed in the radiogenic isotopes and in the trace element ratios suggest that the lavas from Sete Cidades formed from a mantle source which was heterogeneous on a small scale. The mantle source of the Sete Cidades basalts has a distinct composition compared to that of the adjacent Agua de Pau volcano, situated some 20 km further to the east. Only very limited interaction appears to take place between the two neighbouring magmatic systems; however one of the most recent eruptions on the western flanks of Sete Cidades was fed partly by magmas from the Agua de Pau source.

4.9 ACKNOWLEDGMENTS

We gratefully acknowledge the help of H. Baier, K. Mezger, and F. Hauff with the isotope analyses and D. Garbe-Schönberg with the ICP-MS analyses. This paper benefited significantly from the reviews and helpful comments of S. Bryan, E. Widom, and M. Wilson. This study has been funded by the Deutsche Forschungsgemeinschaft through grants Ha 2568/6-1, Ha 2568/9-2, and Ha 2100/7-1.

REFERENCES

- Abdel Monem, A.A., Fernandez, L.A. and Boone, G.M. (1975) K-Ar-Ages from the eastern Azores group (Santa Maria, Sao Miguel and the Formigas islands). *Lithos* **8**, 247-254.
- Ablay, G.J., Carroll, M.R., Palmer, M.R., Martí, J. and Sparks, R.S.J. (1998) Basanite-Phonolite Lineages of the Teide-Pico Viejo Volcanic Complex Tenerife, Canary Islands. *Journal of Petrology* **39**, 905-936.
- Abouchami, W., Galer, S.J.G. and Hofmann, A.W. (2000) High precision lead isotope systematics of lavas from the Hawaiian Scientific Drilling Project. *Chemical Geology* **169**, 187-209.
- Andersen, D.J., Lindsley, D.H. and Davidson, P.M. (1993) QUILF; a Pascal program to assess equilibria among Fe-Mg-Mn-Ti oxides, pyroxenes, olivine, and quartz. *Computers and Geosciences* **19**, 1333-1350.
- Bacon, C.R. and Hirschmann, M.M. (1988) Mg/ Mn partitioning as a test for equilibrium between coexisting Fe-Ti oxides. *American Mineralogist* **73**, 57-61.
- Booth, B., Croasdale, R., Walker, G.P.L. and F.R.S. (1978) A quantitative study of five thousand years of volcanism on Sao Miguel, Azores. *Philosophical Transactions of the Royal Society of London* **288**, 271-319.
- Bryan, S.E., Marti, J. and Leosson, M. (2002) Petrology and geochemistry of the Bandas del Sur Formation, Las Canadas Edifice, Tenerife (Canary Islands). *Journal of Petrology* **43**, 1815-1856.

- Burnham, C.W. (1979) The importance of volatile constituents. In: Yoder, H. S., Jr. (ed.) *The evolution of the igneous rocks; fiftieth anniversary perspectives*. pp. 439-482. Princeton Univ. Press: Princeton, N.J., United States.
- Chen, C.-Y. and Frey, F.A. (1983) Origin of Hawaiian tholeiite and alkalic basalt. *Nature* **302**, 785-789.
- Clague, D.A. (1987) Hawaiian alkaline volcanism. In: Fitton, J. G. and Upton, B. G. J. (eds.) *Alkaline Igneous Rocks*. pp. 227-252. Geol. Soc. Spec. Publ.
- David, K., Schiano, P. and Allegre, C.J. (2000) Assessment of the Zr/ Hf fractionation in oceanic basalts and continental materials during petrogenetic processes. *Earth and Planetary Science Letters* **178**, 285-301.
- Davies, G.R., Norry, M.J., Gerlach, D.C. and Cliff, R.A. (1989) A combined chemical and Pb-Sr-Nd isotope study of the Azores and Cap Verde hot-spots: the geodynamic implications. In: Saunders, A. D. and Norry, M. J. (eds.) *Magmatism in the Oceanic Basins*. pp. 231-255. Geological Society Special Publications.
- Droop, G.T.R. (1987) A general equation for estimating Fe (super 3+) concentrations in ferromagnesian silicates and oxides from microprobe analyses, using stoichiometric criteria. *Mineralogical Magazine* **51**, 431-435.
- Dunn, T. and Sen, C. (1994) Mineral/ matrix partition coefficients for orthopyroxene, plagioclase, and olivine in basaltic to andesitic systems; a combined analytical and experimental study. *Geochimica et Cosmochimica Acta* **58**, 717-733.
- Escartín, J., Cannat, M., Pouliquen, G. and Rabain, A. (2001) Crustal thickness of V-shaped ridges south of the Azores: Interaction of the Mid-Atlantic Ridge (36°-39°N) and the Azores hot spot. *Journal of Geophysical Research* **106**, 21,719-21,735.
- Ewart, A. (1981) The mineralogy and chemistry of the anorogenic Tertiary silicic volcanics of S.E. Queensland and N.E. New South Wales, Australia. In: *Granites and rhyolites*. pp. 10242-10256. American Geophysical Union: Washington, DC, United States.
- Feraud, G., Kaneoka, I. and Allègre, C.J. (1980) K/Ar Ages and Stress Pattern in the Azores: Geodynamic Implications. *Earth and Planetary Science Letters* **46**, 275-286.
- Folch, A., Codina, R. and Marti, J. (2001) Numerical modeling of magma withdrawal during explosive caldera-forming eruptions. *Journal of Geophysical Research* **106**, 16163-16175.
- Frey, F.A., Garcia, M.O. and Roden, M.F. (1994) Geochemical characteristics of Koolau Volcano: Implications of intershield geochemical differences among Hawaiian volcanoes. *Geochimica et Cosmochimica Acta* **58**, 1441-1462.
- Frey, F.A. and Rhodes, J.M. (1993) Intershield geochemical differences among Hawaiian volcanoes: implications for source compositions, melting processes and magma ascent paths. *Philosophical Transactions of the Royal Society of London* **A342**, 121-136.

- Fuhrman, M.L. and Lindsley, D.H. (1988) Ternary-feldspar modeling and thermometry. *American Mineralogist* **73**, 201-215.
- Fujimaki, H. (1986) Partition coefficients of Hf, Zr, and REE between zircon, apatite, and liquid. *Contributions to Mineralogy and Petrology* **94**, 42-45.
- Garbe-Schönberg, C.-D. (1993) Simultaneous determination of thirty-seven trace elements in twenty-eight international rock standards by ICP-MS. *Geostandards Newsletters* **17**, 81-97.
- Garcia, M.O., Rhodes, J.M., Trusdell, F.A. and Pietruszka, A.J. (1996) Petrology of lavas from the Puu Oo eruption of Kilauea Volcano: III. The Kupaianaha episode (1986-1992). *Bulletin of Volcanology* **58**, 359-379.
- Geldmacher, J., van den Bogaard, P., Hoernle, K. and Schmincke, H.U. (2000) The $^{40}\text{Ar}/^{39}\text{Ar}$ age dating of the Madeira Archipelago and hotspot track (eastern North Atlantic). *Geochemistry, Geophysics, Geosystems* **1**, DOI: 10.1029/1999GC000018
- Ghiorso, M.S. (1997) Thermodynamic models of igneous processes. *Annual Reviews of Earth and Planetary Sciences* **25**, 221-241.
- Ghiorso, M.S. and Sack, R.O. (1993) MELTS; software for the thermodynamic analysis of phase equilibria in magmatic systems. In: *Geological Society of America, 1993 annual meeting*. pp. 96. Geological Society of America (GSA): Boulder, CO, United States.
- Govindaraju, K. (1995) Working values with confidence limits of twenty-six CRPG, ANRT and IWG-GIT Geostandards. *Geostandards Newsletter* **19**, 1-32.
- Green, N.L. and Usdansky, S.I. (1986) Ternary-feldspar mixing relations and thermobarometry. *American Mineralogist* **71**, 1100-1108.
- Green, T.H. (1995) Significance of Nb/Ta as an indicator of geochemical processes in the crust-mantle system. *Chemical Geology* **120**, 347-359.
- Green, T.H. and Pearson, N.J. (1987) An experimental study of Nb and Ta partitioning between Ti-rich minerals and silicate liquids at high pressure and temperature. *Geochimica et Cosmochimica Acta* **51**, 53-62.
- Griffiths, R.W. and Richards, M.A. (1989) The adjustment of mantle plumes to changes in plate motion. *Geophysical Research Letters* **16**, 437-440.
- Gudmundsson, A. (1998) Formation and development of normal-fault calderas and the initiation of large explosive eruptions. *Bulletin of Volcanology* **60**, 160-170.
- Haase, K.M. and Beier, C. (2003) Tectonic control of ocean island basalt sources on Sao Miguel, Azores? *Geophysical Research Letters* **30**, 1856.

- Hansteen, T.H., *et al.* (1998a) Sulfur, chlorine, and fluorine in glass inclusions in olivine and clinopyroxene from basaltic hyaloclastites representing the Gran Canaria shield stage at Sites 953 and 956. *Proceedings of the Ocean Drilling Program, Scientific Results* **157**, 403-410.
- Hansteen, T.H., Kluegel, A. and Schmincke, H.-U. (1998b) Multi-stage magma ascent beneath the Canary Islands; evidence from fluid inclusions. *Contributions to Mineralogy and Petrology* **132**, 48-64.
- Hansteen, T.H. and Troll, V.R. (2003) Oxygen isotope composition of xenoliths from the oceanic crust and volcanic edifice beneath Gran Canaria (Canary Islands); consequences for crustal contamination of ascending magmas. *Chemical Geology* **193**, 181-193.
- Hart, S.R. and Davis, K.E. (1978) Nickel partitioning between olivine and silicate melt. *Earth and Planetary Science Letters* **40**, 203-219.
- Hart, S.R. and Dunn, T. (1993) Experimental cpx/melt partitioning of 24 trace elements. *Contributions to Mineralogy and Petrology* **113**, 1-8.
- Hawkesworth, C.J., Blake, S., Evans, P., Hughes, R., MacDonald, R., Thomas, L.E., Turner, S.P. and Zellmer, G. (2000) Time Scales of Crystal Fractionation in Magma Chambers - Integrating Physical, Isotopic and Geochemical Perspectives. *Journal of Petrology* **41**, 991-1006.
- Hawkesworth, C.J., Norry, M.J., Roddick, J.C. and Vollmer, R. (1979) $^{143}\text{Nd}/^{144}\text{Nd}$ and $^{87}\text{Sr}/^{86}\text{Sr}$ ratios from the Azores and their significance in LIL-element enriched mantle. *Nature* **280**, 28-31.
- Hess, P.C. (1992) Phase equilibria constraints on the origin of ocean floor basalts. In: Phipps Morgan, J., Blackman, D. K. and Sinton, J. M. (eds.) *Mantle flow and melt generation at mid-ocean ridges*. pp. 67-102. Am. Geophys. Union.
- Hoernle, K. and Schmincke, H.U. (1993) The role of partial melting in the 15-Ma geochemical evolution of Gran Canaria; a blob model for the Canary hotspot. *Journal of Petrology* **34**, 599-626.
- Hoernle, K., Tilton, G. and Schmincke, H.-U. (1991) Sr-Nd-Pb isotopic evolution of Gran Canaria: evidence for shallow enriched mantle beneath the Canary Islands. *Earth and Planetary Science Letters* **106**, 44-63.
- Johnson, C.L., Wijbrans, J.R., Constable, C.G., Gee, J., Staudigel, H., Tauxe, L., Forjaz, V.-H. and Salgueiro, M. (1998) $^{40}\text{Ar}/^{39}\text{Ar}$ ages and paleomagnetism of Sao Miguel lavas, Azores. *Earth and Planetary Science Letters* **160**, 637-649.
- Kamber, B.S. and Collerson, K.D. (2000a) Role of "hidden" deeply subducted slabs in mantle depletion. *Chemical Geology* **166**, 241-254.
- Kamber, B.S. and Collerson, K.D. (2000b) Zr/ Nb systematics of ocean island basalts reassessed; the case for binary mixing. In: *In commemoration of Keith Gordon Cox, 1933-1998*. pp. 1007-1021. Oxford University Press: Oxford, United Kingdom.

- Klügel, A., Hansteen, T.H. and Galipp, K. (2005) Magma storage and underplating beneath Cumbre Vieja volcano, La Palma (Canary Islands). *Earth and Planetary Science Letters* **236**, 211-226.
- Klügel, A., Hoernle, K.A., Schmincke, H.-U. and White, J.D.L. (2000) The chemically zoned 1949 eruption on La Palma (Canary Islands): Petrologic evolution and magma supply dynamics of a rift zone eruption. *Journal of Geophysical Research* **105**, 5997-6016.
- Krause, D.C. and Watkins, N.D. (1970) North Atlantic crustal genesis in the vicinity of the Azores. *Geophys. Journ. Roy. Astron. Soc.* **19**, 261-283.
- Le Maitre, R.W., et al. (1989) *A classification of igneous rocks and glossary of terms*. Blackwell: Oxford.
- Luis, J.F., Miranda, J.M., Galdeano, A. and Patriat, P. (1998) Constraints on the structure of the Azores spreading center from gravity data. *Marine Geophysical Researches* **20**, 157-170
- Luis, J.F., Miranda, J.M., Galdeano, A., Patriat, P., Rossignol, J.C. and Mendes Victor, L.A. (1994) The Azores triple junction evolution since 10 Ma from aeromagnetic survey of the Mid-Atlantic Ridge. *Earth and Planetary Science Letters* **125**, 439-459.
- Macdonald, G.A. (1968) Composition and origin of Hawaiian lavas. In: *Studies in volcanology--A memoir in honor of Howel Williams*. pp. 477-522. Geological Society of America (GSA): Boulder, CO, United States.
- Montelli, R., Nolet, G., Dahlen, F.A., Masters, G., Engdahl, E.R. and Hung, S.H. (2004) Finite-frequency tomography reveals a variety of plumes in the mantle. *Science* **303**, 338-343.
- Moore, R.B. (1990) Volcanic geology and eruption frequency, Sao Miguel, Azores. *Bulletin of Volcanology* **52**, 602-614.
- Moore, R.B. (1991a) Geologic Map of Sao Miguel, Azores. U.S. Department of the Interior, U.S. Geological Survey: Denver.
- Moore, R.B. (1991b) Geology of three late Quaternary stratovolcanos on Sao Miguel, Azores. In: *U.S. Geological Survey Bulletin*. U.S. Geological Service, 1-46.
- Moore, R.B. and Rubin, M. (1991) Radiocarbon dates for Lava flows and pyroclastic deposits on Sao Miguel, Azores. *Radiocarbon* **33**, 151-164.
- Nash, W.P. and Crecraft, H.R. (1985) Partition coefficients for trace elements in silicic magmas. *Geochimica et Cosmochimica Acta* **49**, 2309-2322.
- Nelson, S.T. and Montana, A. (1992) Sieve-textured plagioclase in volcanic rocks produced by rapid decompression. *American Mineralogist* **77**, 1242-1249.

- Nicholis, M.G. and Rutherford, M.J. (2004) Experimental constraints on magma ascent rate for the Crater Flat volcanic zone hawaiite. *Geology* **32**, 489-492.
- Nielsen, R.L., Gallahan, W.E. and Newberger, F. (1992) Experimentally determined mineral-melt partition coefficients for Sc, Y and REE for olivine, orthopyroxene, pigeonite, magnetite and ilmenite. *Contributions to Mineralogy and Petrology* **110**, 488-499.
- O'Nions, R.K., Hamilton, P.J. and Evensen, N.M. (1977) Variations in $^{143}\text{Nd}/^{144}\text{Nd}$ and $^{87}\text{Sr}/^{86}\text{Sr}$ ratios in oceanic basalts. *Earth and Planetary Science Letters* **34**, 13-22.
- Pacheco, J.M., Quintero, P.J., Gonçalves, P., Gasparon, M. and Ferreira, T. (2005) Sete Cidades Volcano (S. Miguel, Azores): Constraints to eruptive scenarios. In: Union, E. G. (ed.) *EGU 2005*. Vienna. p. 09772. (Geophysical Research Abstracts)
- Pemberton, J.W. and Offler, R. (1985) Significance of clinopyroxene compositions from the Cudgegong Volcanics and Toolamanang Volcanics; Cudgegong-Mudgee District, NSW, Australia. *Mineralogical Magazine* **49**, 591-599.
- Pichavant, M., Mysen, B.O. and Macdonald, R. (2002) Source and H (sub 2) O content of high-MgO magmas in island arc settings; an experimental study of a primitive calc-alkaline basalt from St. Vincent, Lesser Antilles arc. *Geochimica et Cosmochimica Acta* **66**, 2193-2209.
- Putirka, K. (1997) Magma transport at Hawaii; inferences based on igneous thermobarometry. *Geology (Boulder)* **25**, 69-72.
- Putirka, K. (1999) Clinopyroxene + liquid equilibria to 100kbar and 2450K. *Contributions to Mineralogy and Petrology* **135**, 151-163.
- Putirka, K., Johnson, M., Kinzler, R., Longhi, J. and Walker, D. (1996) Thermobarometry of mafic igneous rocks based on clinopyroxene-liquid equilibria, 0-30 kbar. *Contributions to Mineralogy and Petrology* **123**, 92-108.
- Putirka, K.D., Mikaelian, H., Ryerson, F. and Shaw, H. (2003) New clinopyroxene-liquid thermobarometers for mafic, evolved and volatile-bearing lava compositions, with applications to lavas from Tibet and the Snake River Plain, Idaho. *American Mineralogist* **88**, 1542-1554.
- Reid, I. and Jackson, H.R. (1981) Oceanic spreading rate and crustal thickness. *Marine Geophysical Researches* **5**, 165-172.
- Reiners, P.W. (1998) Reactive Melt Transport in the Mantle and Geochemical Signatures of Mantle-derived Magmas. *Journal of Petrology* **39**, 1039-1061.
- Reiners, P.W. (2002) Temporal -compositional trends in intraplate basalt eruptions: Implications for mantle heterogeneity and melting processes. *Geochemistry, Geophysics, Geosystems* **3**, DOI:10.1029/2001GC000250.

- Renzulli, A. and Santi, P. (2000) Two-stage fractionation history of the alkali basalt-trachyte series of Sete Cidades volcano (Sao Miguel Island, Azores). *European Journal of Mineralogy* **12**, 469-494.
- Ritsema, J. and Allen, R.M. (2003) The elusive mantle plume. *Earth and Planetary Science Letters* **207**, 1-12.
- Roeder, P.L. and Emslie, R.F. (1970) Olivine-liquid equilibrium. *Contributions to Mineralogy and Petrology* **29**, 275-289.
- Rutherford, M.J. and Devine, J.D. (1988) The May 18, 1980, eruption of Mount St. Helens; 3, Stability and chemistry of amphibole in the magma chamber. *Journal of Geophysical Research, B, Solid Earth and Planets* **93**, 11,949-11,959.
- Rutherford, M.J. and Devine, J.D. (2003) Magmatic conditions and magma ascent as indicated by hornblende phase equilibria and reactions in the 1995-2002 Soufriere Hills magma. *Journal of Petrology* **44**, 1433-1454.
- Rutherford, M.J. and Hill, P.M. (1993) Magma ascent rates from amphibole breakdown; an experimental study applied to the 1980-1986 Mount St. Helens eruptions. *Journal of Geophysical Research, B, Solid Earth and Planets* **98**, 19,667-19,685.
- Sato, H. (1977) Nickel content of basaltic magmas: identification of primary magmas and a measure of the degree of olivine fractionation. *Lithos* **10**, 113-120.
- Schilling, J.-G. (1975a) Azores mantle blob: rare-earth evidence. *Earth and Planetary Science Letters* **25**, 103-115.
- Schilling, J.-G. (1975b) Rare-Earth Variations Across 'Normal Segments' of the Reykjanes Ridge, 60°-53°N, Mid-Atlantic Ridge, 29°S, and East Pacific Rise, 2°-19°S, and Evidence on the Composition of the Underlying Low-Velocity layer. *Journal of Geophysical Research* **80**, 1459-1473.
- Schwarz, S., Kluegel, A. and Wohlgemuth, U.C. (2004) Melt extraction pathways and stagnation depths beneath the Madeira and Desertas rift zones (NE Atlantic) inferred from barometric studies. *Contributions to Mineralogy and Petrology* **147**, 228-240.
- Searle, R.C. (1980) Tectonic pattern of the Azores spreading center and triple junction. *Earth and Planetary Science Letters* **51**, 415-434.
- Sleep, N.H. (1990) Hotspots and mantle plumes; some phenomenology. *Journal of Geophysical Research, B, Solid Earth and Planets* **95**, 6715-6736.
- Sparks, S.R.J., Sigurdsson, H. and Wilson, L. (1977) Magma mixing: a mechanism for triggering acid explosive eruptions. *Nature* **267**, 315-318.
- Stolper, E., Walker, D., Hager, B.H. and Hays, J.F. (1981) Melt segregation from partially molten source regions; the importance of melt density and source region size. *Journal of Geophysical Research* **B 86**, 6261-6271.

- Storey, M., Wolff, J.A., Norry, M.J. and Marriner, G.F. (1989) Origin of hybrid lavas from Agua de Pau volcano, Sao Miguel, Azores. In: Saunders, A. D. and Norry, M. J. (eds.) *Magmatism in the Ocean Basins*. pp. 161-180. Geological Society Special Publication.
- Thirlwall, M.F., Jenkins, C., Vroon, P.Z. and Matthey, D.P. (1997) Crustal interaction during construction of ocean islands; Pb-Sr-Nd-O isotope geochemistry of the shield basalts of Gran Canaria, Canary Islands. *Chemical Geology* **135**, 233-262.
- Thompson, R.N. (1974) Some high-pressure pyroxenes. *Mineralogical Magazine* **39**, 768-787.
- Turner, S., Hawkesworth, C., Rogers, N. and King, P. (1997) U-Th isotope disequilibria and ocean island basalt generation in the Azores. In: Hawkesworth, C. and Arndt, N. T. (eds.) *Highlights of the Goldschmidt meeting, in honor of A. W. Hofmann*. pp. 145-164. Elsevier: Amsterdam, Netherlands.
- Vogt, P.R. and Jung, W.Y. (2004) The Terceira Rift as hyper-slow, hotspot-dominated oblique spreading axis: A comparison with other slow-spreading plate boundaries. *Earth and Planetary Science Letters* **218**, 77-90.
- Watson, S. and McKenzie, D. (1991) Melt generation by plumes: a study of Hawaiian volcanism. *Journal of Petrology* **32**, 501-537.
- Whipkey, C.E., Capo, R.C., Chadwick, O.A. and Stewart, B.W. (2000) The importance of sea spray to the cation budget of a coastal Hawaiian soil; a strontium isotope approach. *Chemical Geology* **168**, 37-48.
- White, W.M. and Hofmann, A.W. (1982) Sr and Nd isotope geochemistry of oceanic basalts and mantle evolution. *Nature* **296**, 821-825.
- White, W.M., Schilling, J.G. and Hart, S.R. (1975) Sr-isotope geochemistry of the Azores and the Mid-Atlantic Ridge; 29 degrees N to 60 degrees N. *Eos, Transactions, American Geophysical Union* **56**, 471.
- White, W.M., Tapia, M.D.M. and Schilling, J.-G. (1979) The Petrology and Geochemistry of the Azores Islands. *Contributions to Mineralogy and Petrology*. **69**, 201-213.
- Widom, E. (1991) Petrogenetic processes and timescales of young alkaline volcanic rocks, Sao Miguel, Azores. Doctoral thesis, University of California Santa Cruz, United States.
- Widom, E., Carlson, R.W., Gill, J.B. and Schmincke, H.U. (1997) Th-Sr-Nd-Pb isotope and trace element evidence for the origin of the Sao Miguel, Azores, enriched mantle source. *Chemical Geology* **140**, 49-68.
- Widom, E. and Farquhar, J. (2003) Oxygen isotope signatures in olivines from Sao Miguel (Azores) basalts: implications for crustal and mantle processes. *Chemical Geology* **193**, 237-255.
- Widom, E., Gill, J.B. and Schmincke, H.U. (1993) Syenite nodules as a long-term record of magmatic activity in Agua de Pau Volcano, Sao Miguel, Azores. *Journal of Petrology* **34**, 929-953.

- Widom, E., Schmincke, H.U. and Gill, J.B. (1992) Processes and timescales in the evolution of chemically zoned trachyte; Fogo A, Sao Miguel, Azores. *Contributions to Mineralogy and Petrology* **111**, 311-328.
- Widom, E. and Shirey, S.B. (1996) Os isotope systematics in the Azores: implications for mantle plume sources. *Earth and Planetary Science Letters* **142**, 451-465.
- Wolff, J.A. (1984) Variation in Nb/ Ta during differentiation of phonolitic magma, Tenerife, Canary Islands. *Geochimica et Cosmochimica Acta* **48**, 1345-1348.
- Wolff, J.A., Grandy, J.S. and Larson, P.B. (2000) Interaction of mantle-derived magma with island crust? Trace element and oxygen isotope data from the Diego Hernandez Formation , Las Canadas, Tenerife. *Journal of Volcanology and Geothermal Research* **103**, 343-366.
- Wones, D.R. and Gilbert, M.C. (1982) Chapter 3, Amphiboles in the igneous environment; Introduction. In: Veblen David, R. and Ribbe Paul, H. (eds.) *Amphiboles; petrology and experimental phase relations*. pp. 355-357. Mineralogical Society of America: Washington, DC, United States.
- Woodhead, J.D. (1992) Temporal geochemical evolution in oceanic intra-plate volcanics: a case study from the Marquesas (French Polynesia) and comparison with other hotspots. *Contributions to Mineralogy and Petrology* **111**, 458-467.
- Zanetti, A., Tiepolo, M., Oberti, R. and Vannucci, R. (2004) Trace-element partitioning in olivine: modelling of a complete data set from a synthetic hydrous basanite melt. *Lithos* **75**, 39-54.

APPENDIX/ TABLES

Table 1: Additional major and trace element data used throughout the manuscript. The whole-rock (WR) major elements were determined by XRF and the trace elements by ICP-MS. Where only few trace elements are available, these data were determined by XRF. The major elements of the glasses were determined by electron microprobe and the trace element data by ICP-MS. Chapter I refers to „Geochemical and geochronological constraints on the volcanic evolution of the Azores plateau“, Chapter II refers to „Melting and mantle source variations along an ultraslow spreading rift: the Terceira axis, Azores“, Chapter III refers to „Relics of a subducted seamount: the São Miguel mantle source“, and Chapter IV refers to “Magma evolution of the Sete Cidades volcano, São Miguel, Azores.

Sample	186DS-1	186DS-1	187DS-1	494DS-2	554DS-3	196 DS-2	198 DS-2	198DS-3	198DS-5	198 DS-7	220 DS-3	236 DS-5
Location	Ponta Sul, S of São Miguel	Ponta Sul, S of São Miguel	Ponta Sul, S of São Miguel	Monaco Bank, S of São Miguel	N of Pico Ridge	Pico Ridge	Pico Ridge	Pico Ridge	Pico Ridge	Pico Ridge	Princessa Alice Bank	Condor de Terra
Chapter samples are used in	I & II	I & II	I & II	I & II	I	I	I	I	I	I	I	I
Latitude [°N]	37°06.155	37°10.861	37°10.359	37°38.084	38°08.050	37°55.428	37°58.736	37°58.736	37°58.736	37°58.736	37°44.293	38°32.232
Longitude [°W]	25°45.114	25°42.318	25°42.370	25°54.076	27°23.909	27°21.908	27°21.057	27°21.057	27°21.057	27°21.057	29°12.136	29°03.828
	Submarine	Submarine	Submarine	Submarine	Submarine	Submarine	Submarine	Submarine	Submarine	Submarine	Submarine	Submarine
TAS classification	Basalt	Basalt	Basalt	Basalt	Basalt	Trachyandesite	Basalt	Basalt	Basalt	Trachyandesite	Basalt	Basalt
WR/GL	WR	WR	WR	WR	WR	WR	WR	WR	WR	WR	WR	GL
[wt.%]												
SiO ₂	46.80	46.68	23.24	44.14	45.54	58.13	46.69	48.82	47.95	54.55	48.91	48.04
TiO ₂	2.43	2.42	3.48	3.69	2.54	0.81	3.24	3.15	3.11	1.67	3.60	2.71
Al ₂ O ₃	13.77	13.70	12.12	13.62	14.81	17.38	15.35	15.87	15.51	17.65	12.45	12.65
Fe ₂ O ₃	13.98	13.93	15.16	13.08	10.41	6.04	12.19	9.41	11.04	7.07	15.79	
FeO												11.41
MnO	0.19	0.19	0.20	0.16	0.16	0.14	0.19	0.15	0.19	0.17	0.20	0.21
MgO	6.99	6.93	12.71	8.57	9.28	2.05	4.20	4.03	3.85	1.63	4.64	7.59
CaO	11.08	11.02	12.83	12.38	9.95	4.05	8.82	8.63	8.32	4.34	6.84	13.32
Na ₂ O	2.34	2.38	1.80	1.91	3.24	4.16	3.36	3.87	3.83	5.64	3.81	2.44
K ₂ O	0.31	0.31	0.44	0.86	1.27	4.61	1.82	1.97	2.03	3.26	0.68	0.22
P ₂ O ₅	0.29	0.29	1.09	0.48	0.48	0.33	0.65	0.76	0.77	0.54	0.74	0.37
SO ₃												0.04
Cl												0.03
LOI	1.55	1.55	17.37	0.00	0.00	1.10	2.51	2.50	2.22	2.72	0.89	0.00
Total	99.73	99.40	100.44	98.89	97.68	98.80	99.02	99.16	98.82	99.24	98.55	99.03
[ppm]												
Sc						14.7	17.7				21.8	
Cr	254	251	228	357	346	7.64	0.79				0.38	
Co						17.6	31.2				40.0	
Ni	120	110	241	165	158	10.9	9.24				31.9	
Cu						18.1	4.48				184	
Zn	113	117	154	109	87.0	69.9	129				79.1	
Mo												
Rb	3.00	6.00	6.00	17.0	28.0	80.9	40.6				33.1	
Sr	233	238	662	685	580	629	649				633	
Y						22.2	37.5				56.4	
Zr	149	148	361	252	238	9.28	260				384	
Nb	16.0	16.0	64.0			7.20	74.7				46.9	
Cs						0.36	0.70				1.18	
Ba	65.0	97.0	435			2012	523				206	
La						35.0	51.0				47.2	
Ce			81.0			67.5	99.7				122	
Pr						8.44	12.2				18.2	
Nd						32.3	46.3				80.8	
Sm						5.86	9.02				18.6	
Eu						0.66	2.66				5.74	
Gd						4.78	8.20				16.4	
Tb						0.70	1.25				2.36	
Dy						3.87	7.01				12.3	
Ho						0.74	1.31				2.07	
Er						2.05	3.46				4.93	
Tm						0.29	0.48				0.62	
Yb						1.91	3.06				3.69	
Lu						0.28	0.44				0.49	
Hf						0.34	5.82				10.7	
Ta						0.31	3.90				2.58	
Pb						15.6	3.45				1.36	
Th						0.59	5.68				4.67	
U						0.24	1.66				0.74	

Table 1 continued

Sample	513DS-2	513DS-3	513DS-4	513DS-6	514DS-1	529DS-1	535DS-1	535 DS-2	535DS-3	535DS-3	535DS-4	535DS-5	535DS-6
Location	W slope of São Miguel	W slope of São Miguel	W slope of São Miguel	W slope of São Miguel	W slope of São Miguel	E of Terceira	W flank of Terceira	W flank of Terceira	W flank of Terceira	W flank of Terceira	W flank of Terceira	W flank of Terceira	W flank of Terceira
Chapter samples are used in	I-IV	I-IV	I-IV	I-IV	I-IV	I & II	I & II	I & II	I & II	I & II	I & II	I & II	I & II
Latitude [°N]	37°51.933	37°51.933	37°51.933	37°51.933	37°51.906	38°32.614	38°42.446	38°42.446	38°42.446	38°42.446	38°42.446	38°42.446	38°42.446
Longitude [°W]	25°56.277	25°56.277	25°56.277	25°56.277	25°58.471	26°52.509	27°28.720	27°28.720	27°28.720	27°28.720	27°28.720	27°28.720	27°28.720
	Submarine	Submarine	Submarine	Submarine	Submarine	Submarine	Submarine	Submarine	Submarine	Submarine	Submarine	Submarine	Submarine
TAS classification	Basalt	Basalt	Basalt	Basalt	Basalt	Basalt	Basalt	Basalt	Basalt	Basalt	Basalt	Basalt	Basalt
WR/GL	WR	GL	WR	GL	WR	WR	WR	WR	WR	GL	WR	WR	WR
[wt.%]													
SiO ₂	46.24	48.39	46.55	47.23	47.08	44.16	47.91	46.53	46.70	45.37	48.58	46.05	48.27
TiO ₂	3.05	3.22	3.05	3.89	2.99	1.96	2.88	3.83	3.86	4.26	2.88	3.82	2.88
Al ₂ O ₃	13.34	15.41	12.76	15.30	13.46	15.26	13.27	14.99	15.27	14.27	13.43	14.82	13.76
Fe ₂ O ₃	11.54		11.26		11.10	9.91	11.04	12.95	13.05		11.08	13.11	10.75
FeO		10.22		11.39						12.69			
MnO	0.17	0.19	0.17	0.18	0.16	0.16	0.16	0.17	0.18	0.21	0.16	0.17	0.16
MgO	10.21	5.97	10.16	4.81	9.25	11.25	9.45	6.13	6.31	5.63	9.62	6.03	8.72
CaO	11.76	11.98	10.56	10.07	12.25	10.08	10.05	10.67	10.59	10.67	10.00	10.78	10.02
Na ₂ O	2.56	3.16	2.69	3.36	2.39	2.76	2.93	3.17	3.12	3.30	2.86	3.33	2.96
K ₂ O	1.42	1.58	1.40	2.15	1.35	0.88	0.92	0.84	0.85	0.95	0.96	0.84	0.95
P ₂ O ₅	0.50	0.48	0.55		0.44	0.38	0.38	0.47	0.45	0.46	0.38	0.46	0.38
SO ₃													
Cl													
LOI	0.00	0.00	0.00	0.00	0.00	4.12	0.00	0.00	0.00	0.00	0.00	0.00	0.00
Total	100.79	100.59	99.15	98.37	100.47	100.92	98.99	99.75	100.38	97.81	99.95	99.41	98.85
[ppm]													
Sc	31.3							30.2		24.8	27.3		
Cr	567		621		523	554	454	72.0	72.0	53.1	466	82.0	386
Co	49.4							45.1		36.3	37.6		
Ni	155		250		126	344	180	56.3	56.0	33.9	174	51.0	162
Cu	47.2							40.4		30.6	32.3		
Zn	95.9		97.0		83.0	81.0	91.0	117	109		100	111	94.0
Mo										1.61	1.95		
Rb	32.6		34.0		33.0	22.0	22.0	18.3	22.0	15.6	19.6	20.0	19.0
Sr	669		669		605	422	478	617	591	505	479	590	505
Y	23.1							29.8		24.0	23.9		
Zr	227		331		235	208	272	205	229	166	201	273	280
Nb	49.3							39.1		32.2	38.3		
Cs	0.32							0.14		0.19	0.24		
Ba	400							233		224	256		
La	35.2							26.8		25.1	30.4		
Ce	72.5							56.8		54.1	64.1		
Pr	9.17							7.64		7.16	8.18		
Nd	36.2							31.9		30.6	33.6		
Sm	7.20							7.18		7.43	7.62		
Eu	2.14							2.45		2.44	2.42		
Gd	6.23							6.94		6.99	7.03		
Tb	0.89							1.06		1.07	1.07		
Dy	4.68							5.83		6.10	6.09		
Ho	0.82							1.05		1.13	1.14		
Er	2.04							2.65		2.81	2.90		
Tm	0.27							0.35		0.37	0.38		
Yb	1.66							2.16		2.21	2.29		
Lu	0.23							0.30		0.31	0.33		
Hf	5.24							4.77		5.18	6.16		
Ta	2.76							2.20		2.32	2.72		
Pb	2.23							1.41		1.39	1.77		
Th	3.69							2.32		2.45	3.30		
U	1.07							0.87		0.96	1.25		

Table 1 continued

Sample	523DS-2	523DS-3	523DS-4	524DS-1	525DS-1	525DS-3	525DS-4	525DS-5	526DS-1	556DS-1	556DS-2
Location	Banco João de Castro	Banco João de Castro	Banco João de Castro	Banco João de Castro	Banco João de Castro	Banco João de Castro	Banco João de Castro	Banco João de Castro	Banco João de Castro	Banco João de Castro	Banco João de Castro
Chapter samples are used in	II	II	II	II	II	II	II	II	II	II	II
Latitude [°N]	38°10.455	38°10.455	38°10.455	38°11.287	38°11.746	38°11.746	38°11.746	38°11.746	38°10.673	38°14.777	38°14.777
Longitude [°W]	26°37.895	26°37.895	26°37.895	26°36.761	26°35.852	26°35.852	26°35.852	26°35.852	26°37.951	26°36.657	26°36.657
	Submarine	Submarine	Submarine	Submarine	Submarine	Submarine	Submarine	Submarine	Submarine	Submarine	Submarine
TAS classification	Tephriphonolite	Trachyandesite	Trachyandesite	Trachyte	Basalt	Basalt	Basalt	Basalt	basalt, Trachyandesite	Trachyandesite	Trachyandesite
WR/GL	WR	WR	WR	WR	WR	WR	WR	WR	WR	WR	WR
[wt.%]											
SiO₂	51.19	55.67	55.85	59.19	45.50	46.41	46.20	47.04	51.82	55.50	56.15
TiO₂	2.48	1.64	1.48	0.76	2.10	1.92	2.01	1.98	2.59	1.58	1.61
Al₂O₃	15.14	16.96	17.44	17.36	11.02	9.94	10.30	10.35	16.54	17.31	17.54
Fe₂O₃	9.18	6.34	6.17	4.96	10.54	10.64	10.25	10.47	9.33	7.35	7.51
FeO											
MnO	0.16	0.18	0.15	0.16	0.15	0.16	0.15	0.15	0.19	0.20	0.20
MgO	6.25	1.92	1.53	0.89	14.17	17.29	14.71	15.70	3.49	2.11	2.21
CaO	9.08	4.21	4.26	2.53	11.74	12.00	12.17	12.27	7.04	4.77	4.82
Na₂O	3.87	5.81	5.93	6.27	2.05	1.78	2.08	1.99	4.95	5.53	5.26
K₂O	2.65	4.14	3.69	5.10	1.13	0.88	1.06	1.06	2.98	4.00	3.99
P₂O₅	0.48	0.47	0.43	0.15	0.35	0.31	0.33	0.33	0.93	0.55	0.57
SO₃											
Cl											
LOI	0.00	0.00	0.00	0.00	0.00	0.00	0.00	0.00	0.00	0.00	0.00
Total	100.48	97.34	96.93	97.37	98.75	101.33	99.26	101.34	99.86	98.90	99.86
[ppm]											
Sc	26.5	6.17		1.87	39.6				13.5	5.07	
Cr	206	2.58		2.28	746		1203		13.8	1.48	
Co	29.4	5.50		2.91	55.4				16.4	7.69	
Ni	51.5				326		366		6.97		
Cu	28.1	4.43		2.59	176		125		15.3	4.35	
Zn	94.8	103	99.0	101	79.3		75.0		117	117	
Mo	3.01	5.39		1.62	1.37				3.82	2.32	
Rb	67.5	108		116	27.8				76.0	100	
Sr	562	662		491	434				871	889	
Y	31.4	45.2		32.4	19.8				45.0	39.7	
Zr	243	502		525	158				119	460	
Nb	59.9	104		74.6	35.7				43.6	92.6	
Cs	0.49	0.86		0.23	0.21				0.60	0.44	
Ba	651	1013	988	1171	320		338		900	1101	
La	51.6	83.6		84.2	26.5				74.9	80.3	
Ce	100	159		145	54.4				146	151	
Pr	11.9	18.6		15.6	6.63				17.8	17.6	
Nd	45.5	69.0		51.6	26.6				69.7	64.4	
Sm	8.95	12.8		8.46	5.62				13.7	11.5	
Eu	2.55	3.54		2.40	1.67				4.03	3.42	
Gd	7.57	10.5		6.51	4.96				11.5	9.30	
Tb	1.10	1.52		0.98	0.70				1.61	1.34	
Dy	6.01	8.41		5.62	3.89				8.77	7.27	
Ho	1.11	1.55		1.09	0.71				1.59	1.36	
Er	2.91	4.16		3.09	1.81				4.11	3.64	
Tm	0.40	0.58		0.47	0.24				0.55	0.51	
Yb	2.54	3.74		3.22	1.52				3.43	3.26	
Lu	0.37	0.54		0.49	0.22				0.48	0.48	
Hf	6.58	12.0		11.7	4.25				3.05	11.0	
Ta	3.22	4.73		3.79	1.62				1.78	4.71	
Pb	3.51	4.82		5.92	1.80				4.04	5.17	
Th	5.97	9.84		12.0	2.82				7.05	8.80	
U	1.70	2.93		1.86	0.79				2.10	2.00	

Table 1 continued

Sample	557DS-1	557DS-2	557DS-3	558DS-2	558DS-3	558DS-4	558DS-6	558DS-7	542DS-3	248 DS-3	249 DS-3
Location	Banco João de Castro	Banco João de Castro	Banco João de Castro	W of Banco João de Castro	W of Banco João de Castro	W of Banco João de Castro	W of Banco João de Castro	W of Banco João de Castro	SW of Graciosa	W of Graciosa	W of Graciosa
Chapter samples are used in	II	II	II	II	II	II	II	II	II	II	II
Latitude [°N]	38°15.013	38°15.013	38°15.013	38°13.725	38°13.725	38°13.725	38°13.725	38°13.725	39°05.966	39°05.749	39°06.356
Longitude [°W]	26°35.707 Submarine	26°35.707 Submarine	26°35.707 Submarine	26°39.068 Submarine	26°39.068 Submarine	26°39.068 Submarine	26°39.068 Submarine	26°39.068 Submarine	28°16.412 Submarine	28°10.084 Submarine	28°10.581 Submarine
TAS classification	Basalt	Basalt	Basalt	basalt. Trachyandesite	Trachyandesite	Trachyandesite	Trachyandesite	Trachybasalt	Basanite	Basalt	Basanite
WR/GL	GL	GL	GL	GL	WR	GL	WR	GL	WR	WR	WR
[wt.%]											
SiO₂	49.51	49.66	49.43	52.10	58.02	56.51	57.37	49.53	41.64	46.21	41.14
TiO₂	2.93	2.84	3.14	3.00	1.23	1.60	3.07	3.21	2.67	2.78	2.65
Al₂O₃	15.83	15.59	15.77	15.97	17.81	18.42	17.65	16.36	14.72	14.50	14.24
Fe₂O₃					5.02		5.67		10.69	10.90	10.50
FeO	9.30	10.58	8.51	7.46		5.70		8.36			
MnO	0.19	0.22	0.17	0.24	0.19	0.23	0.21	0.22	0.18	0.16	0.16
MgO	4.52	4.26	5.57	1.77	1.44	2.02	1.85	3.50	11.91	9.20	12.31
CaO	9.60	8.87	10.56	6.60	3.52	4.56	4.28	7.55	10.92	9.72	10.63
Na₂O	3.64	4.30	3.88	4.96	4.84	5.08	4.72	4.17	2.26	3.01	2.44
K₂O	2.59	2.33	1.78	4.84	4.74	4.06	4.44	3.27	0.45	1.14	0.57
P₂O₅				1.04		0.58		0.88	0.50	0.57	0.47
SO₃											
Cl											
LOI	0.00	0.00	0.00	0.00	0.00	0.00	0.00	0.00	0.00	0.38	5.20
Total	98.11	98.65	98.81	97.98	96.81	98.78	99.26	97.05	95.94	98.57	100.31
[ppm]											
Sc				1.56						25.2	
Cr				5.62					474	407	
Co				2.52						44.2	
Ni									223	183	
Cu				3.83						37.6	
Zn				102					95.0	98.9	
Mo				6.11							
Rb				131					5.00	26.1	
Sr				274					483	637	
Y				31.7						27.5	
Zr				426					199	238	
Nb				97.5						49.9	
Cs				1.01						0.25	
Ba				1226						327	
La				79.6						35.5	
Ce				141						74.0	
Pr				15.1						9.47	
Nd				50.5						37.6	
Sm				8.21						7.54	
Eu				2.34						2.42	
Gd				6.57						6.68	
Tb				0.96						0.98	
Dy				5.51						5.34	
Ho				1.07						0.96	
Er				3.03						2.48	
Tm				0.45						0.33	
Yb				3.06						2.10	
Lu				0.46						0.29	
Hf				10.5						5.12	
Ta				3.57						2.72	
Pb				18.3						1.87	
Th				11.5						3.27	
U				3.36						1.05	

Table 1 continued

Sample	249 DS-4	550DS-1	550DS-2	550DS-3	550DS-3	550DS-4	550DS-6	550DS-7	238DS-7	547DS-2	547DS-4	547DS-4	
Location	W of Graciosa	SE of São Jorge	SE of São Jorge	SE of São Jorge	SE of São Jorge	SE of São Jorge	SE of São Jorge	SE of São Jorge	SE of São Jorge	W riftzone of Faial	W of Faial	W of Faial	W of Faial
Chapter samples are used in	II												
Latitude [°N]	39°06.356	38°28.174	38°28.174	38°28.174	38°28.174	38°28.174	38°28.174	38°28.174	38°28.174	38°37.047	38°36.851	38°36.851	38°36.851
Longitude [°W]	28°10.581	27°50.280	27°50.280	27°50.280	27°50.280	27°50.280	27°50.280	27°50.280	27°50.280	28°56.107	28°54.047	28°54.047	28°54.047
	Submarine	Submarine	Submarine	Submarine	Submarine	Submarine	Submarine	Submarine	Submarine	Submarine	Submarine	Submarine	Submarine
TAS classification	Basalt	Basalt	Basalt	Basalt	Basalt	Basalt	Basalt	Basalt	Basalt		Basalt	Basalt	Basalt
WR/GL	WR	WR	WR	WR	GL	GL	GL	GL	GL	GL	WR	GL	WR
[wt.%]													
SiO₂	44.47	44.35	44.88	46.26	47.31	45.78	46.88	47.59			46.76	48.94	47.14
TiO₂	3.41	4.33	4.38	3.53	4.96	4.63	4.70	4.76			2.57	3.20	2.51
Al₂O₃	15.85	15.10	15.28	17.28	13.65	13.87	14.03	14.00			15.15	15.38	14.89
Fe₂O₃	11.02	14.37	14.61	12.25							10.56		10.52
FeO					14.15	12.07	11.72	12.27				9.86	
MnO	0.17	0.18	0.18	0.16	0.22	0.25	0.24	0.25			0.16	0.17	0.16
MgO	6.90	5.08	5.14	4.48	3.93	4.23	4.22	4.54			8.53	5.38	8.62
CaO	11.38	9.57	9.47	9.59	8.83	9.55	9.57	9.50			10.33	10.44	10.31
Na₂O	2.95	3.56	3.56	3.48	3.86	3.34	3.31	3.15			3.38	3.89	3.26
K₂O	0.97	1.11	1.18	1.20	2.01	1.47	1.46	1.51			1.35	1.94	1.39
P₂O₅	0.59	0.59	0.56	0.53	1.01	0.60	0.60	0.65			0.48		0.47
SO₃					0.06								
Cl					0.09								
LOI	2.98	0.00	0.00	0.00	0.00	0.00	0.00	0.00			0.00	0.00	0.00
Total	100.69	98.24	99.24	98.76	100.09	95.79	96.73	98.21			99.27	99.19	99.27
[ppm]													
Sc	31.0									24.0			
Cr	145	23.0	24.0	41.0		296				175	329		348
Co	35.9									29.7			
Ni	52.8	24.0	22.0	33.0		153				77.1	154		142
Cu	46.4									35.5			
Zn	92.0	125	126	113		106				78.3	87.0		88.0
Mo													
Rb	10.3	25.0	28.0	28.0		20.0				23.3	29.0		31.0
Sr	569	602	597	668		835				544	612		603
Y	28.5									23.4			
Zr	240	331	340	315		257				198	284		240
Nb	49.9									34.8			
Cs	0.06									0.22			
Ba	330									297			
La	32.2									26.8			
Ce	68.7									56.3			
Pr	9.06									7.30			
Nd	36.4									29.4			
Sm	7.44									6.11			
Eu	2.31									1.94			
Gd	6.69									5.57			
Tb	0.99									0.83			
Dy	5.48									4.57			
Ho	1.00									0.83			
Er	2.56									2.10			
Tm	0.35									0.28			
Yb	2.21									1.78			
Lu	0.31									0.25			
Hf	5.37									4.44			
Ta	2.76									1.94			
Pb	1.99									2.14			
Th	3.24									2.69			
U	0.47									0.87			

Table 1 continued

Sample	516DS-1	516DS-3	522DS-1	522DS-2	522DS-3	522DS-4	522DS-4	522DS-5	522DS-6	522DS-7	522DS-8	522DS-8	522DS-9
Location	Alcatraz, Terceira axis	Alcatraz, Terceira axis	N Hironnelle Basin	N Hironnelle Basin	N Hironnelle Basin	N Hironnelle Basin	N Hironnelle Basin	N Hironnelle Basin	N Hironnelle Basin	N Hironnelle Basin	N Hironnelle Basin	N Hironnelle Basin	N Hironnelle Basin
Chapter samples are used in	I & II	I & II	II	II	II	II	II	II	II	II	II	II	II
Latitude [°N]	38°08.008	38°08.008	38°28.062	38°28.062	38°28.062	38°28.062	38°28.062	38°28.062	38°28.062	38°28.062	38°28.062	38°28.062	38°28.062
Longitude [°W]	26°00.687	26°00.687	26°34.315	26°34.315	26°34.315	26°34.315	26°34.315	26°34.315	26°34.315	26°34.315	26°34.315	26°34.315	26°34.315
	Submarine	Submarine	Submarine	Submarine	Submarine	Submarine	Submarine	Submarine	Submarine	Submarine	Submarine	Submarine	Submarine
TAS classification	Basanite	Basalt	Trachyte	Basalt	Basalt	Basalt	Basalt	Basalt	Basalt	Trachybasalt	Basalt	Basalt	Basalt
WR/GL	WR	WR	WR	GL	GL	WR	WR	GL	GL	GL	GL	GL	GL
[wt.%]													
SiO ₂	40.81	45.44	61.35	47.21	47.28	43.90	42.89	47.44	47.68	51.26	46.71	46.66	46.79
TiO ₂	4.42	3.80	0.81	4.91	5.08	3.97	3.96	4.89	4.91	3.42	4.86	4.86	4.82
Al ₂ O ₃	15.58	13.97	18.08	14.33	14.04	13.92	13.66	13.88	13.81	16.06	14.28	14.04	14.20
Fe ₂ O ₃	16.35	12.87	5.12			12.47	12.31						
FeO				12.05	12.57			11.91	11.75	9.17	11.93	13.29	11.93
MnO	0.22	0.16	0.17	0.24	0.26	0.15	0.15	0.20	0.21	0.24	0.24	0.21	0.24
MgO	5.49	6.84	0.95	4.74	4.48	5.26	5.12	4.86	4.77	3.62	4.86	4.60	4.85
CaO	8.32	9.78	2.63	9.97	9.47	13.32	13.13	9.93	10.16	7.76	9.94	10.01	9.84
Na ₂ O	3.30	2.93	5.96	3.07	3.30	3.10	3.05	3.09	2.90	4.15	3.30	3.31	3.33
K ₂ O	1.47	1.72	5.13	1.53	1.63	1.14	1.13	1.58	1.63	2.35	1.49	1.54	1.49
P ₂ O ₅	0.77	0.73	0.16	0.69	0.73	0.55	0.55			0.74	0.68	0.85	0.70
SO ₃												0.26	
Cl												0.09	
LOI	0.00	0.00	0.00	0.00	0.00	0.00	0.00	0.00	0.00	0.00	0.00	0.00	0.00
Total	96.73	98.24	100.36	98.75	98.85	97.78	95.95	97.78	97.82	98.77	98.29	99.71	98.19
[ppm]													
Sc			1.98							19.7	29.7		
Cr	244	280	1.40							28.8	60.4		
Co			2.90							24.7	37.1		
Ni	154	157								7.55	29.5		
Cu			2.68							12.1	31.9		
Zn	140	118	109							126	139		
Mo			1.50							2.49	2.52		
Rb	20.0	27.0	121							42.2	31.7		
Sr	957	641	559							634	585		
Y			34.6							39.0	44.7		
Zr	362	312	557							244	363		
Nb			101							46.1	56.9		
Cs			0.21							0.44	0.47		
Ba			1272							442	319		
La			88.7							41.6	41.8		
Ce			151							85.6	93.0		
Pr			16.2							10.8	12.2		
Nd			54.4							44.5	52.1		
Sm			8.99							10.1	12.3		
Eu			2.61							3.10	3.63		
Gd			7.01							9.30	11.2		
Tb			1.02							1.38	1.65		
Dy			5.96							7.72	9.20		
Ho			1.15							1.41	1.66		
Er			3.27							3.60	4.19		
Tm			0.50							0.48	0.56		
Yb			3.34							2.99	3.37		
Lu			0.51							0.42	0.48		
Hf			12.7							6.23	9.24		
Ta			5.66							2.33	2.66		
Pb			6.32							2.58	2.38		
Th			13.1							4.43	4.41		
U			1.78							1.48	1.59		

Table 1 continued

Sample	522DS-10	522DS-11	AZG-03-01	AZG-03-02	AZG-03-03	AZG-03-05	AZG-03-06	AZG-03-09	AZG-03-10	AZG-03-11	AZG-03-12	AZG-03-13
Location	N Hirondele Basin	N Hirondele Basin	Barro Vermelho, Graciosa	Barro Vermelho, Graciosa	W of Barro Vermelho, Graciosa	Baía da Vitória, Graciosa	Baía da Vitória, Graciosa	N of Pico Machado, Graciosa	E of Ponta da Pesqueira, Graciosa	N of Parque Eólico da Graciosa, at NW crater rim of Calderiniha, Graciosa	N of Parque Eólico da Graciosa, at NW crater rim of Calderiniha, Graciosa	S of Serre Branca, Graciosa
Chapter samples are used in	II	II	II	II	II	II	II	II	II	II	II	II
Latitude [°N]	38°28.062	38°28.062	39°05.650	39°05.650	39°05.750	39°04.710	39°04.710	39°04.520	39°05.310	39°02.205	39°02.400	39°01.820
Longitude [°W]	26°34.315	26°34.315	28°01.425	28°01.425	28°01.750	28°03.410	28°03.410	27°59.400	27°59.750	28°01.85	28°01.830	28°02.105
	Submarine	Submarine	Subaeral	Subaeral	Subaeral	Subaeral	Subaeral	Subaeral	Subaeral	Subaeral	Subaeral	Subaeral
TAS classification	Basalt	Trachybasalt	Basalt	Basalt	Basalt	Basalt	Basalt	Basalt	Basalt	Basalt	Basalt	Basalt
WR/GL	GL	WR	WR	WR	WR	WR	WR	WR	WR	WR	WR	WR
[wt.%]												
SiO ₂	47.49	49.55	45.62	45.90	45.53	45.63	44.54	45.70	45.26	47.67	47.55	44.40
TiO ₂	4.94	3.17	3.01	3.32	3.06	3.22	3.16	2.63	2.63	2.64	2.64	4.24
Al ₂ O ₃	14.00	15.47	14.73	15.07	15.71	14.95	14.85	16.42	15.44	16.57	16.67	16.89
Fe ₂ O ₃		11.55	10.81	11.64	11.01	11.04	11.25	10.65	10.88	10.57	10.56	13.08
FeO	11.61											
MnO	0.19	0.18	0.16	0.16	0.15	0.16	0.16	0.16	0.16	0.16	0.16	0.19
MgO	4.81	3.13	9.83	7.26	8.87	9.85	10.40	8.91	9.73	7.30	6.97	4.93
CaO	10.14	8.39	11.22	11.27	10.64	10.82	11.14	10.87	10.40	9.54	9.54	8.24
Na ₂ O	3.01	4.42	2.37	2.70	2.63	2.53	2.08	2.39	2.53	3.46	3.29	2.78
K ₂ O	1.49	2.54	0.86	1.02	0.73	0.90	0.59	0.68	0.72	1.28	1.30	1.73
P ₂ O ₅		1.06	0.42	0.52	0.45	0.46	0.41	0.40	0.48	0.54	0.54	0.66
SO ₃												
Cl												
LOI	0.00	0.00	0.00	0.38	0.86	0.28	0.60	0.93	0.87	0.00	0.00	2.21
Total	97.68	99.46	99.03	99.24	99.64	99.84	99.18	99.74	99.10	99.73	99.22	99.35
[ppm]												
Sc							56.0				25.2	40.2
Cr			453	415	297	410	689	457	424	189	230	6.05
Co							75.3				40.6	51.8
Ni			213	171	161	216	301	201	230	109	115	17.7
Cu							56.8				33.8	27.4
Zn			87.0	92.0	88.0	86.0	110	73.0	97.0	100	96.2	139
Mo							1.06				2.21	1.20
Rb			15.0	21.0	12.0	16.0	8.17		12.0	34.0	36.2	31.4
Sr			522	574	573	556	616	547	516	551	586	667
Y							27.0				28.0	40.2
Zr			225	249	263	257	242	188	233	263	226	335
Nb			43.0	42.0	43.0	45.0	48.1	35.0	42.0	56.0	50.2	69.6
Cs							0.06				0.33	0.12
Ba			264	320	320	310	256	286	309	410	386	517
La							24.3				32.7	47.1
Ce			29.0	46.0	31.0	36.0	55.8	35.0	38.0	56.0	64.3	89.1
Pr							7.31				8.43	11.2
Nd							31.3				33.0	45.7
Sm							6.83				6.79	9.28
Eu							2.24				2.15	2.92
Gd							6.41				6.33	8.36
Tb							0.95				0.91	1.21
Dy							5.16				5.01	6.51
Ho							0.97				0.92	1.22
Er							2.41				2.38	3.05
Tm							0.33				0.32	0.42
Yb							2.01				2.04	2.56
Lu							0.29				0.29	0.37
Hf							4.80				5.22	6.12
Ta							2.36				2.80	3.19
Pb							1.39				1.78	2.90
Th							2.74				3.48	4.46
U							0.69				0.97	1.15

Table 1 continued

Sample	AZG-03-14	AZG-03-15	AZG-03-16	AZG-03-17	AZG-03-18	AZG-03-19	AZG-03-20	AZG-03-21	AZG-03-22	AZG-03-23	AZG-03-25	AZG-03-26
Location	Pico Timao, Graciosa	N of Faja, Graciosa	Entrance of Limeira, Graciosa	Limeira, Graciosa	Limeira, Graciosa	Farol da Folga, Graciosa	Farol da Folga, Graciosa	Between Alto do Sul and Ponta do Sul, Graciosa	N of Carapacho, Graciosa	N of Carapacho, Graciosa	Cruz da Portela Graciosa	Cruz da Portela Graciosa
Chapter samples are used in	II	II	II	II	II	II	II	II	II	II	II	II
Latitude [°N]	39°01.800	39°01.750	39°01.65	39°01.650	39°01.650	39°01.050	39°01.050	39°00.500	39°00.700	39°00.800	39°01.000	39°01.000
Longitude [°W]	28°01.700	28°01.400	28°00.400	28°00.200	28°00.200	28°00.050	28°00.050	27°58.400	27°58.280	27°57.800	27°57.500	27°57.500
	Subaeral	Subaeral	Subaeral	Subaeral	Subaeral	Subaeral	Subaeral	Subaeral	Subaeral	Subaeral	Subaeral	Subaeral
TAS classification	Trachybasalt	Basalt	Basalt	Basalt	Basalt	Trachyandesite	Trachybasalt	Trachybasalt	Basalt	Basalt	basalt, Trachyandesite	Basalt
WR/GL	WR	WR	WR	WR	WR	WR	WR	WR	WR	WR	GL	GL
[wt.%]												
SiO ₂	45.81	45.98	46.56	46.81	46.52	60.99	49.00	49.08	48.94	49.27	54.19	47.78
TiO ₂	4.20	3.14	2.96	2.91	2.91	0.60	2.68	2.56	2.37	2.33	1.56	2.54
Al ₂ O ₃	16.06	15.43	15.16	14.76	14.47	18.20	16.94	17.82	16.50	16.43	16.93	16.19
Fe ₂ O ₃	12.59	11.10	10.25	10.15	10.02	5.13	10.60	9.76	10.10	10.22	9.22	10.33
FeO												
MnO	0.18	0.16	0.15	0.15	0.15	0.14	0.17	0.16	0.16	0.16	0.24	0.15
MgO	5.10	9.34	8.98	8.97	8.86	0.78	5.07	3.69	6.41	6.95	1.92	7.36
CaO	9.23	9.70	10.36	10.51	10.51	2.60	8.56	8.74	9.07	9.05	4.89	10.11
Na ₂ O	3.58	2.61	2.51	2.44	2.59	6.36	3.99	4.09	3.71	3.65	5.67	3.07
K ₂ O	1.63	0.97	1.33	1.45	1.46	3.41	1.47	1.52	1.26	1.28	2.32	1.06
P ₂ O ₅	0.60	0.51	0.49	0.53	0.50	0.21	0.74	0.79	0.50	0.54	0.56	0.42
SO ₃												
Cl												
LOI	0.00	0.67	0.62	0.89	0.42	0.64	0.00	0.04	0.00	0.00	1.31	0.07
Total	98.98	99.61	99.37	99.57	98.41	99.06	99.22	98.25	99.02	99.88	98.81	99.08
[ppm]												
Sc				52.8			21.5		22.2	21.7	14.2	
Cr	25.0	388	406	713	455		65.6	23.0	188	148	4.02	234
Co				64.2			31.3		43.2	33.5	15.2	
Ni	28.0	212	190	219	268		47.3	24.0	88.7	83.7	2.65	129
Cu				59.2			20.4		25.4	15.0	8.31	
Zn	114	95.0	84.0	105	87.0	98.0	103	93.0	87.1	83.7	123	86.0
Mo				1.27			2.03		1.53	1.00	4.07	
Rb	30.0	19.0	17.0	30.4	27.0	74.0	32.4	33.0	23.6	26.9	51.8	23.0
Sr	648	562	608	732	608	387	604	619	548	549	524	516
Y				27.7			32.8		25.3	25.3	49.4	
Zr	306	277	290	314	296	556	239	284	194	198	369	206
Nb	59.0	47.0	48.0	61.3	54.0	87.0	47.9	54.0	36.5	36.9	85.7	36.0
Cs				0.13			0.20		0.11	0.16	0.53	
Ba	462	306	393	436	441	894	414	442	347	363	726	332
La				36.2			33.9		27.1	30.3	57.5	
Ce	59.0	41.0	57.0	78.4	75.0	175	75.0	71.0	56.3	62.1	123	41.0
Pr				9.85			9.50		7.27	7.95	15.3	
Nd				40.0			38.5		29.4	32.7	58.9	
Sm				7.91			8.08		6.20	7.26	12.0	
Eu				2.44			2.65		2.12	2.52	4.12	
Gd				7.03			7.51		5.86	6.98	10.8	
Tb				1.03			1.08		0.84	1.02	1.60	
Dy				5.47			5.91		4.61	5.72	8.86	
Ho				1.02			1.08		0.84	1.05	1.62	
Er				2.57			2.79		2.17	2.70	4.24	
Tm				0.35			0.37		0.29	0.37	0.58	
Yb				2.21			2.33		1.82	2.33	3.72	
Lu				0.32			0.33		0.26	0.33	0.53	
Hf				6.28			5.34		4.78	4.98	8.48	
Ta				3.10			2.73		2.12	2.51	4.03	
Pb				2.62			2.27		1.93	2.15	3.92	
Th				4.33			3.18		2.60	3.00	5.31	
U				1.19			1.00		0.80	0.81	1.63	

Table 1 continued

Sample	AZG-03-27	18-8-97-4	18-8-97-5	18-8-97-7	18-8-97-8	SM0101	SM0102	SM0103	SM0103	SM0105	SM0107	SM0108
Location	1 km north of Cruz da Portela, Graciosa	Mosteiros, Sete Cidades, São Miguel	Mosteiros, Sete Cidades, São Miguel	Mosteiros, Sete Cidades, São Miguel	Mosteiros, Sete Cidades, São Miguel	Beira Mar de Beixo, Sete Cidades, São Miguel	Ponta dos Mosteiros, Sete Cidades, São Miguel	NW-flank, Lagoa Azul, Sete Cidades, São Miguel	NW-flank, Lagoa Azul, Sete Cidades, São Miguel	NNW-flank - rim, Sete Cidades, São Miguel	N - flank - rim, Sete Cidades, São Miguel	N - flank - rim, Sete Cidades, São Miguel
Chapter samples are used in	II	I-IV	I-IV	I-IV	I-IV	I-IV	I-IV	I-IV	I-IV	I-IV	I-IV	I-IV
Latitude [°N]	39°01.800	37°53.911	37°53.912	37°53.913	37°53.914	37°53.910	37°53.910	37°52.300	37°52.300	37°52.530	37°52.530	37°52.800
Longitude [°W]	27°57.900	25°49.131	25°49.132	25°49.133	25°49.134	25°49.130	25°49.162	25°47.400	25°47.400	25°47.400	25°47.400	25°46.800
	Subaeral	Subaeral	Subaeral	Subaeral	Subaeral	Subaeral	Subaeral	Subaeral	Subaeral	Subaeral	Subaeral	Subaeral
TAS classification	Basalt	Basalt	Gabbro	Gabbro	Gabbro	Basalt	Basalt	Trachyte	Trachyte	Trachybasalt	Trachybasalt	Basalt
WR/GL	WR	WR	WR	WR	WR	GL	GL	WR	GL	WR	WR	WR
[wt.%]												
SiO₂	48.26	46.14	37.12	45.00	51.54	46.73	47.26	61.36	64.93	48.13	46.40	46.12
TiO₂	2.38	2.71	5.05	2.28	5.29	4.22	3.62	0.60	0.59	3.31	3.34	3.44
Al₂O₃	16.21	10.09	16.82	8.08	19.45	15.17	13.75	16.19	17.69	15.92	16.08	13.99
Fe₂O₃	10.39	11.63	18.20	10.57	16.75			3.21		11.06	11.34	11.93
FeO						11.41	10.57		2.88			
MnO	0.16	0.17	0.14	0.14	0.22	0.17	0.18	0.21	0.21	0.18	0.18	0.17
MgO	7.36	14.43	8.37	15.97	2.83	5.42	6.46	0.39	0.33	4.30	4.35	7.07
CaO	9.25	12.04	13.94	18.22	7.02	11.85	12.91	0.68	0.62	8.74	8.91	10.63
Na₂O	3.48	1.71	0.93	0.65	4.30	2.72	2.35	7.41	6.78	3.53	3.24	2.80
K₂O	1.15	1.08	0.05	0.04	0.65	1.95	1.75	5.48	5.71	2.36	2.02	1.61
P₂O₅	0.53	0.39	0.05	0.02	0.95	0.84	0.68	0.07	0.08	0.81	0.79	0.51
SO₃						0.03	0.01		0.01			
Cl						0.05	0.05		0.23			
LOI	0.00	0.00	0.00	0.00	0.00	0.00	0.00	0.86	0.00	0.72	1.57	1.44
Total	99.17	100.39	100.67	100.97	109.00	100.56	99.59	96.46	100.06	99.06	98.22	99.71
[ppm]												
Sc			30.4		25.4			2.46				
Cr	156	1218	22.0	951	317			5.20		47.0	48.0	232
Co			49.9		33.3			0.74				
Ni	88.0	345	11.0	223	70.0			4.23		9.00	23.0	103
Cu			6.71		13.3			2.15				
Zn	91.0	88.0	103	47.0	177			122		114	116	108
Mo					0.14			7.99				
Rb	25.0	27.0	1.20	3.00	2.90			126		63.0	41.0	26.0
Sr	558	495	954	183	1319			2.85		819	827	673
Y			8.29		26.0			44.0				
Zr	207	254	30.9	78.0	99.3			865		391	393	309
Nb	36.0		4.87		73.7			200				
Cs								1.27				
Ba	337		44.2		906			42.3		763	740	693
La			3.66		59.4			93.0				
Ce	51.0		10.7		118			180				
Pr			1.94		14.8			20.3				
Nd			10.9		61.5			69.8				
Sm			3.26		12.1			12.2				
Eu			1.28		4.71			2.32				
Gd			3.27		10.2			9.72				
Tb			0.48		1.37			1.54				
Dy			2.54		7.15			8.86				
Ho			0.44		1.27			1.71				
Er			0.99		2.95			4.77				
Tm			0.11		0.34			0.69				
Yb			0.59		1.84			4.50				
Lu			0.08		0.25			0.65				
Hf			1.68		3.06			19.1				
Ta			0.55		5.38			11.4				
Pb			0.15		4.72			7.29				
Th			0.06		0.19			16.0				
U			0.02		0.10			4.26				

Table 1 continued

Sample	SM0110	SM0111	SM0112	SM0113	SM0115	SM0117	SM0118	SM0119	SM0123	SM0126	SM0127	SM0130
Location	Mosteiros coast, Sete Cidades, São Miguel	Mosteiros coast, Sete Cidades, São Miguel	N-caldera-wall, Sete Cidades, São Miguel	N-caldera-wall, Sete Cidades, São Miguel	Pico da Caramanihas, São Miguel	Ponta da Ferraria, Sete Cidades, São Miguel	Ponta da Ferraria, Sete Cidades, São Miguel	Ponta da Ferraria, Sete Cidades, São Miguel	Inner calderawall, Sete Cidades, São Miguel	Furnas volcano, São Miguel	Nordeste volcano, São Miguel	Mafra, Sete Cidades, São Miguel
Chapter samples are used in	I-IV	I-IV	I-IV	I-IV	I-IV	I-IV	I-IV	I-IV	I-IV	I-III	I-III	I-IV
Latitude [°N]	37°53.000	37°53.000	37°52.500	37°52.650	37°51.620	37°51.620	37°51.620	37°51.490	37°52.400	37°45.600	37°77.400	37°53.910
Longitude [°W]	25°49.500	25°49.500	25°47.400	25°46.700	25°51.570	25°51.570	25°51.570	25°51.310	25°48.610	25°19.760	25°14.700	25°49.130
	Subaeral	Subaeral	Subaeral	Subaeral	Subaeral	Subaeral	Subaeral	Subaeral	Subaeral	Subaeral	Subaeral	Subaeral
TAS classification	Trachybasalt	Trachybasalt	basalt. Trachyandesite	Trachybasalt	Basalt	Basalt	Basalt	Basalt	Trachyte	Trachyte	basalt. Trachyandesite	Basalt
WR/GL	WR	WR	WR	WR	WR	WR	WR	WR	GL	WR	WR	WR
[wt.%]												
SiO₂	50.61	50.36	53.48	49.80	45.93	46.33	46.54	46.48	61.20	62.95	52.84	44.84
TiO₂	2.60	2.57	1.97	2.90	3.45	3.53	3.46	2.98	0.77	0.50	2.59	3.64
Al₂O₃	17.09	17.00	17.37	16.15	15.07	14.39	15.14	13.62	17.72	17.29	16.57	12.86
Fe₂O₃	9.31	9.29	7.47	10.04	11.68	11.86	11.50	11.13		3.80	9.79	12.38
FeO									3.35			
MnO	0.18	0.18	0.17	0.18	0.18	0.17	0.18	0.18	0.15	0.23	0.17	0.18
MgO	3.33	3.34	2.61	2.94	6.53	7.20	6.40	8.39	0.60	0.34	2.88	8.75
CaO	7.32	7.30	5.53	7.15	9.85	10.18	9.79	9.90	1.49	0.83	6.29	10.98
Na₂O	3.92	4.94	5.04	4.04	3.21	3.09	3.38	2.92	5.65	7.03	4.04	2.55
K₂O	2.71	2.15	3.35	2.91	1.85	1.69	1.86	1.76	5.97	5.75	3.27	1.45
P₂O₅	0.94	0.93	0.67	0.89	0.76	0.58	0.75	0.66	0.19	0.07	0.88	0.67
SO₃									0.02			
Cl									0.27			
LOI	1.15	0.24	0.20	1.83	0.00	0.00	0.04	0.58	0.00	0.56	0.00	0.00
Total	99.16	98.30	97.86	98.83	98.51	99.02	99.04	98.60	97.37	99.35	99.32	98.30
[ppm]												
Sc		10.7			22.0	24.0		20.5				
Cr	18.0	7.44	10.0	8.00	141	190	148	363				451
Co		17.7			40.2	41.9		41.2				
Ni	12.0	4.48			56.8	62.9	54.0	140				121
Cu		10.5			47.8	34.5		64.7				
Zn	110	118	108	114	108	107	107	107				96.0
Mo		3.65			3.26	3.00		2.81				
Rb	68.0	35.2	85.0	86.0	49.0	37.4	46.0	43.7				37.0
Sr	877	932	797	814	896	807	845	802			756	718
Y		34.3			31.4	26.0		29.6				
Zr	440	432	492	450	387	324	380	330				270
Nb		103			78.9	71.4		74.6				
Cs		0.94			0.46	0.13		0.40				
Ba	819	783	946	950	561	497	800	581				728
La		71.9			58.3	47.7		51.2				
Ce		145			130	100		107				
Pr		16.9			14.2	12.1		13.0				
Nd		64.5			54.7	48.3		51.8				
Sm		12.1			10.4	9.57		10.2				
Eu		3.60			3.10	2.87		3.08				
Gd		9.94			8.47	7.97		8.69				
Tb		1.42			1.20	1.11		1.24				
Dy		7.45			6.07	5.86		6.53				
Ho		1.36			1.07	1.04		1.17				
Er		3.43			2.67	2.60		2.94				
Tm		0.45			0.34	0.33		0.38				
Yb		2.79			2.09	2.03		2.30				
Lu		0.39			0.29	0.28		0.32				
Hf		9.64			7.57	7.61		7.64				
Ta		6.28			4.64	4.53		4.60				
Pb		3.58			2.82	2.11		2.57				
Th		8.37			6.27	5.25		5.93				
U		2.27			1.70	1.46		1.56				

Table 1 continued

Sample	SM0131	SM0131	SM0132	SM0135	SM0137	SM0141	SM0142	SM0143	SM0147	SM0148	SM0149
Location	Mafra, Sete Cidades, São Miguel	Mafra, Sete Cidades, São Miguel	Mafra, Sete Cidades, São Miguel	Ponta da Ferraria, Sete Cidades, São Miguel	Ponta da Ferraria, Sete Cidades, São Miguel	Inner calderawall, Sete Cidades, São Miguel	Inner calderawall, Sete Cidades, São Miguel	Inner calderawall, Sete Cidades, São Miguel	Canada de Pilatos, Sete Cidades, São Miguel	Mosteiros coast, Sete Cidades, São Miguel	Relva Velha, Sete Cidades, São Miguel
Chapter samples are used in	I-IV	I-IV	I-IV	I-IV	I-IV	I-IV	I-IV	I-IV	I-IV	I-IV	I-IV
Latitude [°N]	37°53.910	37°53.910	37°53.910	37°51.652	37°51.652	37°52.400	37°52.400	37°52.400	37°53.760	37°53.000	37°52.620
Longitude [°W]	25°49.130	25°49.130	25°49.130	25°51.150	25°51.150	25°48.610	25°48.610	25°48.610	25°48.590	25°49.500	25°49.980
	Subaeral	Subaeral	Subaeral	Subaeral	Subaeral	Subaeral	Subaeral	Subaeral	Subaeral	Subaeral	Subaeral
TAS classification	Basalt	Trachyandesite	Basalt	Basalt	Basalt	basalt, Trachyandesite	basalt, Trachyandesite	Trachyte	basalt, Trachyandesite	basalt, Trachyandesite	Trachyte
WR/GL	WR	GL	WR	WR	WR	WR	WR	GL	WR	WR	WR
[wt.%]											
SiO₂	45.77	56.69	46.56	45.77	46.80	55.93	52.97	62.92	55.36	52.56	62.14
TiO₂	3.81	0.35	3.61	3.18	3.46	1.98	2.27	0.76	1.91	1.81	0.84
Al₂O₃	13.88	25.97	13.76	12.41	15.40	17.76	17.23	18.34	17.67	17.16	18.30
Fe₂O₃	12.77		12.26	11.65	11.71	7.26	8.54		6.92	7.00	4.11
FeO		0.97						3.11			
MnO	0.18	0.05	0.18	0.17	0.18	0.18	0.19	0.14	0.18	0.18	0.15
MgO	7.66	0.20	8.00	10.61	6.52	2.44	2.77	0.60	2.41	2.36	0.75
CaO	10.78	8.07	10.72	11.45	9.92	4.97	5.78	1.60	4.63	5.00	1.93
Na₂O	2.96	4.87	2.67	2.40	3.31	5.50	4.77	6.22	5.48	5.12	6.09
K₂O	1.52	2.70	1.58	1.27	1.85	3.76	3.22	5.71	3.84	3.52	5.39
P₂O₅	0.79	0.10	0.84	0.46	0.76	0.65	0.79	0.17	0.60	0.59	0.17
SO₃		0.01						0.02			
Cl		0.02						0.29			
LOI	0.00	0.00	0.00	0.27	0.00	0.59	0.50	0.00	0.10	0.40	0.79
Total	100.12	100.00	100.18	99.64	99.91	101.02	99.03	99.88	99.10	95.70	100.66
[ppm]											
Sc			26.1	30.4	21.7						
Cr	329		416	707	140	6.00	7.00		2.00	5.00	1.00
Co			53.8	52.1	38.2						
Ni	109		101	212	58.2	1.00			1.00	4.00	
Cu			44.5	77.2	48.5						
Zn	106		105	93.5	107	107	117		112	112	93.0
Mo			2.23	1.69	2.67						
Rb	35.0		39.9	31.4	48.0	88.0	70.0		90.0	84.0	143
Sr	825		856	684	887	765	835		732	783	358
Y			32.0	24.7	31.2						
Zr	284		289	246	382	568	519		566	527	670
Nb			58.8	58.1	78.5						
Cs			0.40	0.30	0.39						
Ba	766		619	466	559	1248	1024		1059	1013	998
La			47.7	40.4	57.9						
Ce			99.3	82.3	128						
Pr			12.7	10.0	14.1						
Nd			51.6	39.7	54.7						
Sm			10.2	7.77	10.3						
Eu			3.18	2.37	3.10						
Gd			8.74	6.64	8.42						
Tb			1.23	0.94	1.21						
Dy			6.30	4.85	6.09						
Ho			1.10	0.85	1.06						
Er			2.72	2.14	2.67						
Tm			0.34	0.27	0.34						
Yb			2.09	1.66	2.09						
Lu			0.29	0.23	0.29						
Hf			5.91	5.38	7.56						
Ta			3.61	3.48	4.65						
Pb			2.30	1.99	3.04						
Th			4.52	4.26	6.30						
U			1.19	1.16	1.66						

Table 1 continued

Sample	SM0151	SM0156	SM0163	SM0164	SM0165	SM0166	SM0167	SM0168	SM0172	SM0173
Location	NNE-inner caldera, Sete Cidades, São Miguel	Ponta da Escavaldo, Sete Cidades, São Miguel	Coast S of Mosteiros, Sete Cidades, São Miguel	Coast S of Mosteiros, Sete Cidades, São Miguel	Coast S of Mosteiros, Sete Cidades, São Miguel	Coast S of Mosteiros, Sete Cidades, São Miguel	Coast S of Mosteiros, Sete Cidades, São Miguel	Coast S of Mosteiros, Sete Cidades, São Miguel	Mosteiros coast, Sete Cidades, São Miguel	Mosteiros coast, Sete Cidades, São Miguel
Chapter samples are used in	I-IV	I-IV	I-IV	I-IV	I-IV	I-IV	I-IV	I-IV	I-IV	I-IV
Latitude [°N]	37°52.760	37°52.570	37°52.720	37°52.630	37°52.630	37°52.630	37°52.630	37°52.820	37°52.970	37°52.890
Longitude [°W]	25°46.620	25°49.960	25°49.970	25°49.95	25°49.950	25°49.950	25°49.950	25°49.710	25°49.640	25°49.740
	Subaeral	Subaeral	Subaeral	Subaeral	Subaeral	Subaeral	Subaeral	Subaeral	Subaeral	Subaeral
TAS classification	Trachyandesite	Basalt	Trachyandesite	Trachybasalt	basalt. Trachyandesite	basalt. Trachyandesite	basalt. Trachyandesite	basalt. Trachyandesite	Trachybasalt	Trachybasalt
WR/GL	WR	WR	WR	WR	WR	WR	WR	WR	WR	WR
[wt.%]										
SiO₂	54.90	45.06	57.49	53.00	51.31	51.59	52.37	56.45	50.15	50.17
TiO₂	2.03	3.18	1.47	2.23	2.37	2.40	2.24	1.55	2.49	2.58
Al₂O₃	17.46	12.28	18.05	17.95	16.95	17.26	17.76	17.97	17.38	16.90
Fe₂O₃	7.29	11.69	5.75	8.42	9.03	8.89	8.28	6.17	8.87	9.40
FeO										
MnO	0.19	0.16	0.17	0.17	0.17	0.18	0.17	0.16	0.16	0.18
MgO	2.55	9.63	1.46	2.99	3.73	3.57	2.97	1.99	3.70	3.47
CaO	5.15	12.39	3.82	6.72	6.87	6.95	6.63	4.49	7.83	7.37
Na₂O	5.62	2.45	5.75	4.68	4.40	4.49	4.74	5.56	3.94	4.35
K₂O	3.80	1.31	4.09	3.02	2.87	2.90	3.00	3.81	2.61	2.70
P₂O₅	0.67	0.47	0.41	0.86	0.84	0.85	0.82	0.50	0.83	0.94
SO₃										
Cl										
LOI	0.24	0.00	0.81	0.05	0.23	0.11	0.03	0.00	1.63	0.27
Total	99.90	98.62	99.27	100.09	98.77	99.19	99.01	98.65	99.59	98.33
[ppm]										
Sc						10.4			11.3	
Cr		505			27.0	23.6			30.1	13.0
Co						17.8			19.3	
Ni		175	1.00	6.00	11.0	10.8	8.00		12.2	
Cu						16.7			18.4	
Zn	117	86.0	97.0	106	111	110	110	99.0	99.7	109
Mo						3.14			2.24	
Rb	94.0	29.0	97.0	76.0	70.0	71.2	73.0	96.0	59.9	64.0
Sr	767	617	693	889	852	909	895	733	903	884
Y						34.1			31.8	
Zr	554	251	552	480	466	471	477	553	414	442
Nb						106			95.0	
Cs						0.58			0.38	
Ba	1076	613	1004	928	942	805	860	1061	716	924
La						73.5			66.1	
Ce						146			134	
Pr						16.9			15.4	
Nd						63.8			59.2	
Sm						11.8			10.8	
Eu						3.45			3.25	
Gd						9.60			9.00	
Tb						1.36			1.28	
Dy						7.16			6.81	
Ho						1.31			1.22	
Er						3.35			3.13	
Tm						0.44			0.41	
Yb						2.73			2.54	
Lu						0.39			0.36	
Hf						10.1			8.94	
Ta						6.31			5.66	
Pb						3.90			3.58	
Th						9.03			8.12	
U						2.45			2.15	

Table 1 continued

Sample	SM0175	SM0177	SM0178	SM0179	SM0201	SM160501-1	SM160501-2	SM160501-3	SM180501-1a	SM180501-1c
Location	Mosteiros coast, Sete Cidades, São Miguel	Mosteiros coast, Sete Cidades, São Miguel	Mosteiros coast, Sete Cidades, São Miguel	Mosteiros coast, Sete Cidades, São Miguel	Pico da Mariana, Waist Zone, São Miguel	N inner caldera wall, Sete Cidades, São Miguel	N inner caldera wall, Sete Cidades, São Miguel	N inner caldera wall, Sete Cidades, São Miguel	W inner caldera wall, Sete Cidades, São Miguel	W inner caldera wall, Sete Cidades, São Miguel
Chapter samples are used in	I-IV	I-IV	I-IV	I-IV	I-IV	I-IV	I-IV	I-IV	I-IV	I-IV
Latitude [°N]	37°83.180	37°53.180	37°53.180	37°52.920	37°47.950	37°52.500	37°52.550	37°52.550	37°51.950	37°51.950
Longitude [°W]	25°49.290 Subaeral	25°49.290 Subaeral	25°49.290 Subaeral	25°49.670 Subaeral	25°42.150 Subaeral	25°47.400 Subaeral	25°47.400 Subaeral	25°47.400 Subaeral	25°48.960 Subaeral	25°48.960 Subaeral
TAS classification	basalt. Trachyandesite	Trachybasalt	Trachybasalt	basalt. Trachyandesite	Basalt	basalt. Trachyandesite	basalt. Trachyandesite	Basalt	basalt. Trachyandesite	basalt. Trachyandesite
WR/GL	WR	WR	WR	WR	WR	WR	WR	WR	WR	WR
[wt.%]										
SiO₂	57.43	50.72	51.09	54.80	45.33	55.99	51.59	47.92	57.47	57.30
TiO₂	1.45	2.64	2.54	1.81	3.60	1.84	2.35	3.27	1.46	1.38
Al₂O₃	18.02	17.01	17.30	17.79	13.76	17.69	16.93	15.35	16.94	16.82
Fe₂O₃	5.73	9.44	9.21	6.97	12.15	6.40	8.66	11.17	6.57	6.28
FeO										
MnO	0.15	0.18	0.18	0.17	0.17	0.15	0.18	0.18	0.20	0.20
MgO	1.48	3.44	2.96	2.26	7.54	2.43	3.03	5.17	1.77	1.71
CaO	3.86	7.44	7.09	4.99	11.46	4.91	6.40	9.35	3.74	3.45
Na₂O	5.54	4.39	4.45	5.16	2.67	5.10	4.28	3.65	6.11	6.17
K₂O	4.10	2.69	2.78	3.60	1.45	3.93	3.16	2.13	4.11	4.16
P₂O₅	0.39	0.94	0.94	0.60	0.61	0.42	0.78	0.76	0.45	0.43
SO₃										
Cl										
LOI	0.78	0.27	0.32	0.58	0.52	1.50	1.50	0.51	0.57	0.31
Total	98.93	99.16	98.86	98.73	99.26	100.36	98.86	99.46	99.39	98.21
[ppm]										
Sc			9.59		26.7					
Cr			5.09	2.00	315	27.0	7.00	109	10.0	7.00
Co			16.6		44.8					
Ni			3.01		95.1	5.00	35.0	2.00		
Cu			10.1		72.7					
Zn	101	110	111	106	103	88.0	110	106	127	120
Mo			3.49		1.20					
Rb	95.0	65.0	64.2	82.0	36.6	95.0	78.0	54.0	86.0	89.0
Sr	705	885	932	778	763	618	836	779	452	411
Y			36.6		26.4					
Zr	572	435	463	517	269	564	489	370	540	542
Nb			107		57.8					
Cs			0.44		0.29					
Ba	1017	899	810	953	484	877	910	830	765	809
La			76.0		41.0					
Ce			149		84.1					
Pr			17.5		10.4					
Nd			66.7		41.4					
Sm			12.3		8.20					
Eu			3.61		2.52					
Gd			10.1		7.02					
Tb			1.44		1.01					
Dy			7.56		5.18					
Ho			1.39		0.91					
Er			3.56		2.27					
Tm			0.47		0.29					
Yb			2.89		1.76					
Lu			0.41		0.24					
Hf			9.84		5.55					
Ta			6.33		3.57					
Pb			3.65		1.97					
Th			9.00		4.47					
U			2.60		1.10					

Table 1 continued

Sample	SM190501-1	SM190501-2	SM190501-3	SM9701	SM9703	SM9704-b	SM9706	SM9708	SM9709	SM9711	SM9715
Location	W inner caldera wall, Sete Cidades, São Miguel	W inner caldera wall, Sete Cidades, São Miguel	SW inner caldera wall, Sete Cidades, São Miguel	Pico do Carvão, Sete Cidades, São Miguel	S of Relva, Aeroporto, São Miguel	S of Relva, Aeroporto, São Miguel	São Braz, São Miguel	Lagoa do Peixe, São Miguel	Serra Gorda, Waist Zone, São Miguel	Serra Gorda, Waist Zone, São Miguel	Agua Retorta, São Miguel
Chapter samples are used in	I-IV	I-IV	I-IV	I-IV	I-IV	I-IV	I-III	I-III	I-IV	I-IV	I-III
Latitude [°N]	37°51.890	37°51.890	37°52.689	37°49.300	37°45.310	37°45.311	37°49.200	37°47.150	37°47.380	37°47.380	37°45.900
Longitude [°W]	25°48.930	25°48.930	25°48.750	25°44.450	25°42.430	25°42.431	25°24.860	25°44.100	25°41.050	25°41.050	25°09.800
	Subaeral	Subaeral	Subaeral	Subaeral	Subaeral	Subaeral	Subaeral	Subaeral	Subaeral	Subaeral	Subaeral
TAS classification	basalt. Trachyandesite	basalt. Trachyandesite	basalt. Trachyandesite	Basalt	Basalt	Basalt	Trachyandesite	Basalt	Basalt	Basalt	Trachybasalt
WR/GL	WR	WR	WR	GL	WR	WR	WR	GL	WR	WR	WR
[wt.%]											
SiO₂	58.09	54.99	53.59	47.10	46.31	45.91	58.46	46.52	46.36	45.71	48.09
TiO₂	1.37	1.92	1.99	3.86	3.95	3.44	1.47	4.11	3.11	3.23	3.75
Al₂O₃	17.80	17.48	17.81	14.66	14.96	13.10	16.12	14.62	12.46	12.54	15.69
Fe₂O₃	5.25	6.96	7.52		13.04	12.83	5.73		12.39	12.26	13.46
FeO				10.66				11.33			
MnO	0.17	0.18	0.18	0.15	0.18	0.17	0.14	0.18	0.17	0.17	0.18
MgO	1.48	2.36	2.62	5.66	7.22	9.30	3.27	5.29	11.86	10.38	3.10
CaO	3.15	4.64	5.64	12.12	11.13	10.72	4.21	11.36	11.19	11.43	7.03
Na₂O	6.05	5.89	5.20	2.62	2.61	2.31	4.70	3.11	2.31	2.28	3.44
K₂O	4.51	3.83	3.42	1.57	1.48	1.39	5.21	1.78	1.21	1.17	2.43
P₂O₅	0.33	0.61	0.69	0.51	0.61	0.57	0.30	0.57	0.49	0.49	0.77
SO₃				0.05				0.07			
Cl				0.09				0.07			
LOI	0.41	0.12	0.15	0.00	0.00	0.00	0.00	0.00	0.00	0.00	0.00
Total	98.61	98.98	98.81	99.05	101.49	99.74	99.61	99.01	101.55	99.66	97.94
[ppm]											
Sc				26.4							
Cr	1.00		9.00	330	240	630	226		771	744	6.00
Co				43.4							
Ni			2.00	116	139	234	58.0		291	232	5.00
Cu				89.8							
Zn	107	112	106		106	106	92.0		94.0	97.0	139
Mo				2.00							
Rb	107	90.0	85.0	29.8	36.0	39.0	84.0		32.0	31.0	53.0
Sr	575	734	868	660	784	619	304		619	632	679
Y				21.6							
Zr	626	562	509	206	357	318	373		284	292	497
Nb				48.4							
Cs				0.35							
Ba	1098	1124	976	442							
La				38.6							
Ce				87.0							
Pr				10.2							
Nd				41.1							
Sm				8.73							
Eu				2.68							
Gd				7.44							
Tb				1.06							
Dy				5.72							
Ho				1.03							
Er				2.50							
Tm				0.32							
Yb				1.88							
Lu				0.27							
Hf				6.15							
Ta				3.28							
Pb				2.19							
Th				3.91							
U				1.19							

Table 1 continued

Sample	SM9717	AZT03-01	AZT03-02	AZT03-03	AZT03-04	AZT03-05	AZT03-06	AZT03-07	AZT03-08	AZT03-09	AZT03-10	AZT03-13
Location	Agua Retorta, São Miguel	W of Serreta, Terceira	W of Serreta, Terceira	W of Serreta, Terceira	S of Quarteiro, Terceira	S of Quarteiro, Terceira	Ponta do Queimado, Terceira	Ponta do Queimado, Terceira	Ponta do Queimado, Terceira	Coast at Cais dos Biscoitos, Terceira	Coast at Cais dos Biscoitos, Terceira	Road 502 at Malha Grande, Terceira
Chapter samples are used in	I-III	I & II	I & II	I & II	I & II	I & II	I & II	I & II	I & II	I & II	I & II	I & II
Latitude [°N]	37°45.900	38°44.800	38°44.800	38°44.800	38°44.800	38°44.800	38°46.000	38°46.000	38°46.000	38°47.98	38°47.98	38°53.830
Longitude [°W]	25°09.800	27°22.300	27°22.300	27°22.300	27°22.300	27°22.300	27°22.600	27°22.600	27°22.600	27°15.700	27°15.700	28°16.333
	Subaeral	Subaeral	Subaeral	Subaeral	Subaeral	Subaeral	Subaeral	Subaeral	Subaeral	Subaeral	Subaeral	Subaeral
TAS classification	Trachybasalt	Trachyte	Trachyte	Trachyte	Trachyte	Trachyte	Trachyte	Trachyte	Trachyte	Trachyte	Trachybasalt	Trachybasalt
WR/GL	WR	GL	WR	WR	WR	WR	WR	WR	WR	WR	WR	WR
[wt.%]												
SiO₂	48.77	69.22	67.57	66.71	66.46	67.65	68.34	67.84	67.76	49.77	49.81	49.32
TiO₂	3.86	0.35	0.33	0.32	0.31	0.32	0.35	0.33	0.34	3.23	3.41	3.06
Al₂O₃	15.25	12.74	13.74	13.63	13.30	13.68	12.88	12.71	12.86	15.28	15.22	14.98
Fe₂O₃	12.92		5.05	4.98	4.81	4.69	5.34	5.50	5.38	11.97	12.43	11.76
FeO		5.02										
MnO	0.16	0.22	0.18	0.18	0.18	0.18	0.20	0.20	0.20	0.19	0.19	0.21
MgO	4.71	0.09	0.08	0.09	0.19	0.12	0.26	0.09	0.10	3.85	3.87	4.31
CaO	8.50	0.50	0.55	0.57	0.59	0.60	0.53	0.48	0.51	8.29	8.35	8.18
Na₂O	3.02	6.45	6.28	6.25	6.37	6.53	6.08	6.41	6.61	4.10	4.02	4.29
K₂O	2.20	4.45	4.49	4.70	4.62	4.66	4.60	4.64	4.65	1.62	1.62	1.44
P₂O₅	0.57	0.02	0.02	0.02	0.02	0.02	0.02	0.03	0.02	0.72	0.74	1.25
SO₃		0.01										
Cl		0.38										
LOI	0.00	0.00	0.43	1.28	1.46	0.82	0.40	0.36	0.65	0.00	0.00	0.00
Total	99.96	99.44	98.72	98.73	98.31	99.27	99.00	98.59	99.08	99.02	99.66	98.80
[ppm]												
Sc	18.1								4.59	18.1		
Cr	59.3								1.63	19.5		27.0
Co	32.1								0.25	27.4		
Ni	41.7					52.0			0.13	16.7	6.00	83.0
Cu	23.2								3.00	22.1		
Zn	102		139	201	212	182	235	234	248	125	125	130
Mo	2.44								13.5	2.92		
Rb	59.7		103	132	133	132	129	139	177	36.2	39.0	32.0
Sr	621		9.00	11.0	12.0	8.00	8.00	8.00	2.04	663	614	659
Y	35.7								131	43.4		
Zr	363		1158	1154	1148	1077	1188	1241	1324	364	367	322
Nb	64.0		215	216	215			223	235	74.1		66.0
Cs	0.25								1.44	0.18		
Ba	515		188	217	206	182	186	151	166	437	710	746
La	59.6								157	56.6		
Ce	119		146	130	137			136	276	120		119
Pr	14.5								31.6	14.5		
Nd	56.1								112	58.4		
Sm	11.1								22.2	12.8		
Eu	3.24								3.30	4.02		
Gd	10.0								20.2	12.0		
Tb	1.50								3.23	1.76		
Dy	8.16								19.0	9.80		
Ho	1.50								3.62	1.77		
Er	3.87								10.1	4.55		
Tm	0.53								1.43	0.61		
Yb	3.29								9.30	3.83		
Lu	0.47								1.31	0.53		
Hf	9.92								29.0	9.09		
Ta	4.36								10.9	4.51		
Pb	3.84								9.10	2.40		
Th	7.37								19.4	5.76		
U	1.78								6.53	1.94		

Table 1 continued

Sample	AZT03-14	AZT03-15	AZT03-21	AZT03-23	AZT03-24	AZT03-25	AZT03-26	AZT03-27	AZT03-28	AZT03-29
Location	Road 502 at Malha Grande, Terceira	Road 502 to Gruta do Natal, Terceira	S flank of Santa Barbara, Terceira	S flank of Santa Barbara, Terceira	S flank of Santa Barbara, Terceira	S flank of Santa Barbara, Terceira	S flank of Santa Barbara, Terceira	S flank of Santa Barbara, Terceira	S flank of Santa Barbara, Terceira	S flank of Santa Barbara, Terceira
Chapter samples are used in	I & II	I & II	I & II	I & II	I & II	I & II	I & II	I & II	I & II	I & II
Latitude [°N]	38°44.001	38°44.300	38°43.800	38°43.800	38°43.800	38°43.800	38°43.800	38°43.500	38°43.600	38°43.500
Longitude [°W]	27°16.516	27°16.160	27°19.250	27°19.420	27°19.500	27°19.650	27°19.650	27°19.550	27°19.500	27°19.350
	Subaeral	Subaeral	Subaeral	Subaeral	Subaeral	Subaeral	Subaeral	Subaeral	Subaeral	Subaeral
TAS classification	Trachybasalt	Basalt	basalt. Trachyandesite	basalt. Trachyandesite	Basalt	Trachybasalt	basalt. Trachyandesite	Trachyte	basalt. Trachyandesite	basalt. Trachyandesite
WR/GL	WR	GL	WR	WR	WR	WR	WR	WR	WR	WR
[wt.%]										
SiO₂	48.89	47.05	54.32	53.55	47.87	50.88	52.40	63.94	52.75	52.96
TiO₂	3.17	2.85	2.10	2.54	3.61	2.82	2.57	0.74	2.49	2.51
Al₂O₃	15.00	14.02	16.04	16.03	16.22	16.52	15.49	16.15	15.70	15.62
Fe₂O₃	11.93	11.66	9.60	9.27	12.34	10.74	11.07	5.02	10.52	10.36
FeO										
MnO	0.21	0.17	0.20	0.18	0.19	0.18	0.21	0.13	0.21	0.21
MgO	4.57	9.04	2.63	2.51	3.96	3.30	3.04	0.54	3.03	3.14
CaO	8.47	10.30	5.58	6.49	8.94	8.18	6.58	1.67	6.35	6.42
Na₂O	4.16	2.40	4.96	4.86	3.70	4.17	4.62	6.11	4.64	4.93
K₂O	1.38	0.84	2.21	2.17	1.23	1.58	2.05	4.07	2.10	2.10
P₂O₅	1.26	0.69	0.77	0.95	0.65	0.81	0.98	0.15	0.96	0.99
SO₃										
Cl										
LOI	0.00	0.28	0.69	0.13	0.46	0.00	0.22	0.60	0.17	0.00
Total	99.04	99.30	99.10	98.68	99.17	99.18	99.23	99.12	98.92	99.24
[ppm]										
Sc										
Cr	36.0	361			6.00	6.00				
Co										
Ni	30.0	146	70.0		17.0	12.0	14.0			
Cu										
Zn	132	96.0	143	145	131	120	138	125	157	142
Mo										
Rb	30.0	17.0	52.0	35.0	21.0	32.0	31.0	109	39.0	43.0
Sr	678	513	570	599	622	681	597	246	578	602
Y										
Zr	323	191	511	531	346	398	508	750	520	487
Nb	67.0	37.0	104	104	65.0	77.0	101	131	100	101
Cs										
Ba	827	462	654	590	334	414	592	893	549	522
La										
Ce	123	62.0	119	122	53.0	85.0	118	191	116	113
Pr										
Nd										
Sm										
Eu										
Gd										
Tb										
Dy										
Ho										
Er										
Tm										
Yb										
Lu										
Hf										
Ta										
Pb										
Th										
U										

Table 1 continued

Sample	AZT03-30	AZT03-31	AZT03-32	AZT03-33	AZT03-34	AZT03-35	AZT03-36	AZT03-37	AZT03-38	AZT03-39	AZT03-40
Location	S flank of Santa Barbara, Terceira	S flank of Santa Barbara, Terceira	S flank of Santa Barbara, Terceira	S flank of Santa Barbara, Terceira	S of Cerrado das Sete, Terceira	W of Pico das Dez, Terceira	W of Doze Ribeiras, Terceira	NW of Doze Ribeiras, Terceira	S of Bagacinas, Terceira	N of Ponta da Serra, Terceira	N of Ponta da Serra, Terceira
Chapter samples are used in	I & II	I & II	I & II	I & II	I & II	I & II	I & II	I & II	I & II	I & II	I & II
Latitude [°N]	38°43.500	38°42.200	38°42.350	38°42.250	38°42.400	38°42.800	38°43.010	38°43.400	38°43.550	38°46.010	38°46.010
Longitude [°W]	27°19.350 Subaeral	27°19.400 Subaeral	27°19.650 Subaeral	27°19.600 Subaeral	27°18.900 Subaeral	27°20.800 Subaeral	27°21.100 Subaeral	27°21.300 Subaeral	27°21.800 Subaeral	27°19.500 Subaeral	27°19.500 Subaeral
TAS classification	basalt. Trachyandesite	basalt. Trachyandesite	Basalt	Trachybasalt	Trachybasalt	Basalt	Trachybasalt	Trachyandesite	Trachybasalt	Trachybasalt	Trachybasalt
WR/GL	WR	WR	WR	WR	WR	WR	WR	WR	GL	WR	WR
[wt.%]											
SiO₂	51.08	51.92	47.14	52.04	50.61	48.81	49.66	56.44	50.09	49.37	50.07
TiO₂	2.57	2.52	4.13	2.53	2.51	3.03	2.79	1.85	3.40	3.20	2.76
Al₂O₃	17.79	15.77	14.60	15.43	18.43	15.85	17.75	16.65	14.66	14.84	15.76
Fe₂O₃	9.85	10.51	13.59	10.45	9.25	11.55	10.13	7.86	12.29	12.37	11.15
FeO											
MnO	0.17	0.20	0.20	0.21	0.15	0.20	0.16	0.20	0.21	0.22	0.21
MgO	3.00	3.07	4.63	3.07	2.90	4.05	3.07	2.38	3.74	4.52	3.37
CaO	8.48	6.41	9.29	6.50	9.02	8.36	8.96	4.94	7.83	8.34	6.73
Na₂O	4.29	4.70	3.56	4.54	4.12	3.37	4.07	5.51	3.88	4.42	4.12
K₂O	1.47	2.01	1.19	2.00	1.32	1.28	1.36	2.61	1.76	1.41	1.74
P₂O₅	0.76	0.94	0.60	0.94	0.66	0.81	0.65	0.63	0.82	1.40	1.14
SO₃											
Cl											
LOI	0.00	0.78	0.00	0.16	0.00	2.16	0.00	0.00	0.10	0.00	2.25
Total	99.46	98.83	98.93	97.87	98.97	99.47	98.60	99.07	98.78	100.09	99.30
[ppm]											
Sc	13.8									18.3	
Cr	4.49		14.0		9.00	76.0				20.4	
Co	19.0									22.2	
Ni	7.50		13.0	108	7.00				64.0	12.6	
Cu	7.99									11.5	
Zn	112	138	117	146	108	134	119	144	136	128	145
Mo	2.28									2.79	
Rb	28.4	32.0	20.0	38.0	26.0	22.0	23.0	50.0	42.0	31.8	35.0
Sr	785	591	591	591	762	636	751	591	582	776	618
Y	42.7									50.4	
Zr	346	523	325	515	332	409	346	582	423	311	481
Nb	64.4	103	59.0	101	59.0	82.0	66.0	117	88.0	63.6	101
Cs	0.17									0.29	
Ba	413	547	396	550	401	455	360	666	474	719	518
La	56.0									62.2	
Ce	115	113	48.0	111	65.0	80.0	62.0	149	84.0	141	112
Pr	14.6									17.5	
Nd	59.6									74.8	
Sm	13.0									16.8	
Eu	4.16									5.98	
Gd	12.2									16.0	
Tb	1.78									2.25	
Dy	9.82									12.2	
Ho	1.77									2.17	
Er	4.52									5.40	
Tm	0.59									0.69	
Yb	3.68									4.26	
Lu	0.51									0.58	
Hf	8.90									7.97	
Ta	4.27									4.38	
Pb	2.39									2.19	
Th	5.21									4.32	
U	1.43									1.48	

Table 1 continued

Sample	AZT03-41	AZT03-42	AZT03-42	AZT03-43a)	AZT03-43b)	AZT03-44	AZT03-45	AZT03-46	AZT03-47	AZT03-48	AZT03-49	AZT03-50
Location	N of Pico Rachado Terceira	N of Pico Rachado Terceira	N of Pico Rachado Terceira	NNE of Pico Rachado, Terceira	NNE of Pico Rachado, Terceira	NNW of Ponte Velha, Terceira	Cal Pedra, Terceira	Cal Pedra, Terceira	W of Vigia, Terceira	W of Vigia, Terceira	W of Vigia, Terceira	W of Vigia, Terceira
Chapter samples are used in	I & II	I & II	I & II	I & II	I & II	I & II	I & II	I & II	I & II	I & II	I & II	I & II
Latitude [°N]	38°45.800	38°45.800	38°45.800	38°45.900	38°45.900	38°45.650	38°46.400	38°46.400	38°41.500	38°41.500	38°41.500	38°41.500
Longitude [°W]	27°18.700	27°18.700	27°18.700	27°18.400	27°18.400	27°17.200	27°17.700	27°17.700	27°21.300	27°21.300	27°21.300	27°21.300
	Subaeral	Subaeral	Subaeral	Subaeral	Subaeral	Subaeral	Subaeral	Subaeral	Subaeral	Subaeral	Subaeral	Subaeral
TAS classification	Trachyte	Trachyte	Trachyte	Trachyte	Trachyte	Trachybasalt	Trachybasalt	Trachybasalt	Basalt	Basalt	Basalt	Basalt
WR/GL	WR	GL	GL	WR	WR	WR	WR	WR	WR	WR	WR	WR
[wt.%]												
SiO₂	67.69	69.44	67.94	68.38	67.33	50.30	49.83	49.43	47.75	47.80	47.90	47.58
TiO₂	0.33	0.35	0.33	0.33	0.34	2.59	3.17	3.30	3.68	3.60	3.68	3.63
Al₂O₃	12.98	12.49	13.04	12.99	13.15	18.71	15.02	14.96	15.78	15.98	15.83	15.93
Fe₂O₃	5.17		5.05	5.44	5.72	9.41	11.69	12.06	12.47	11.95	12.01	11.77
FeO		5.21										
MnO	0.19	0.19	0.19	0.20	0.20	0.15	0.20	0.20	0.17	0.17	0.17	0.17
MgO	0.12	0.08	0.08	0.05	0.09	3.02	3.57	3.71	4.56	4.54	4.55	4.54
CaO	0.49	0.41	0.48	0.39	0.50	9.01	7.91	7.96	9.77	9.77	9.82	9.93
Na₂O	6.68	6.47	6.83	6.58	6.02	3.92	4.26	3.84	3.43	3.50	3.49	3.24
K₂O	4.68	4.55	4.64	4.66	4.65	1.31	1.74	1.65	1.20	1.21	1.23	1.08
P₂O₅	0.02	0.01	0.02	0.02	0.02	0.65	0.80	0.82	0.59	0.58	0.60	0.57
SO₃		0.01										
Cl		0.42										
LOI	0.49	0.00	0.56	0.22	0.00	0.00	0.87	0.12	0.00	0.00	0.00	0.14
Total	98.84	99.65	99.16	99.26	98.02	99.07	99.06	98.05	99.40	99.10	99.28	98.58
[ppm]												
Sc		3.77								20.0		
Cr		0.54				8.00			58.0	48.6	60.0	63.0
Co		4.77								33.7		
Ni	28.0	0.08							36.0	36.4	24.0	43.0
Cu		3.47								32.0		
Zn	226	214	225	217	257	114	140	142	119	111	117	117
Mo		12.4								2.20		
Rb	135	148	141	139	107	22.0	41.0	35.0	28.0	27.1	33.0	25.0
Sr	7.00	1.77	7.00	6.00	10.0	776	610	603	680	737	676	675
Y		115								32.9		
Zr	1126	1294	1128	1257	1250	341	399	409	327	270	308	314
Nb	213	213		229	234	61.0	80.0	84.0	60.0	55.9		56.0
Cs		1.40								0.21		
Ba	175	180	177	174	125	420	459	476	363	325	640	322
La		153								42.2		
Ce	127	288		124	148	70.0	80.0	83.0	45.0	91.2		51.0
Pr		32.3								11.2		
Nd		116								45.4		
Sm		24.3								10.0		
Eu		3.63								3.25		
Gd		22.1								9.33		
Tb		3.64								1.35		
Dy		21.7								7.46		
Ho		4.16								1.32		
Er		11.6								3.34		
Tm		1.65								0.44		
Yb		10.8								2.73		
Lu		1.52								0.37		
Hf		31.6								6.60		
Ta		12.2								3.56		
Pb		9.58								1.98		
Th		20.5								3.64		
U		7.21								1.26		

Table 1 continued

Sample	AZT03-51	AZT03-52	AZT03-53 a)	AZT03-53 b)	AZT03-54	AZT03-56	AZT03-57	AZT03-58	AZT03-59	AZT03-60	AZT03-61
Location	W of Vigia, Terceira	W of Vigia, Terceira	W of Vigia, Terceira	W of Vigia, Terceira	N of Macieira, Terceira	N of Malha Grande, Terceira	N of Malha Grande, Terceira	N of Práia da Vitoria, Ponta da Mã Merenda, Terceira	N of Práia da Vitoria, Ponta da Mã Merenda, Terceira	N of Práia da Vitoria, Ponta da Mã Merenda, Terceira	N of Práia da Vitoria, Ponta da Mã Merenda, Terceira
Chapter samples are used in	I & II	I & II	I & II	I & II	I & II	I & II	I & II	I & II	I & II	I & II	I & II
Latitude [°N]	38°41.500	38°41.500	38°41.500	38°41.500	38°45.900	38°45.550	38°45.550	38°43.960	38°43.910	38°43.920	38°43.930
Longitude [°W]	27°21.300	27°21.330	27°21.300	27°21.300	27°15.900	27°15.400	27°15.400	27°02.942	27°03.200	27°03.200	27°03.200
	Subaeral	Subaeral	Subaeral	Subaeral	Subaeral	Subaeral	Subaeral	Subaeral	Subaeral	Subaeral	Subaeral
TAS classification	Trachybasalt	Trachybasalt	Trachybasalt	basalt. Trachyandesite	Trachybasalt	Basalt	Trachybasalt	Trachybasalt	Trachybasalt	Trachybasalt	Basalt
WR/GL	WR	WR	WR	GL	WR	WR	WR	WR	WR	WR	WR
[wt.%]											
SiO₂	48.31	50.41	50.61	53.15	48.97	46.61	51.68	45.95	47.36	50.67	46.67
TiO₂	3.86	2.87	2.91	2.37	3.17	3.17	2.75	3.72	3.99	2.95	3.74
Al₂O₃	15.09	15.71	15.88	15.85	14.97	14.11	14.98	15.22	14.56	15.29	15.20
Fe₂O₃	12.77	11.13	11.16	9.51	12.23	11.92	11.54	13.47	13.60	11.22	13.31
FeO											
MnO	0.19	0.19	0.18	0.19	0.21	0.18	0.23	0.23	0.21	0.22	0.20
MgO	4.26	3.45	3.44	3.90	4.54	7.75	3.52	3.82	4.40	3.31	4.55
CaO	8.99	7.88	7.98	6.90	8.45	10.77	7.00	7.90	9.07	7.18	9.38
Na₂O	3.97	4.35	4.31	4.78	4.38	2.87	4.79	3.89	3.62	4.96	3.33
K₂O	1.43	1.76	1.72	2.00	1.39	0.88	1.73	1.43	1.41	1.89	1.39
P₂O₅	0.61	0.77	0.78	0.85	1.30	0.88	1.27	1.70	0.68	1.15	0.62
SO₃											
Cl											
LOI	0.00	0.00	0.00	0.00	0.00	0.00	0.00	1.45	0.00	0.00	0.00
Total	99.48	98.52	98.97	99.50	99.61	99.14	99.49	98.78	98.90	98.84	98.39
[ppm]											
Sc				16.1	18.9						
Cr	5.00	20.0		61.4	26.0	249	2.00	3.00	4.00		30.0
Co				18.6	23.9						
Ni	14.0			33.7	15.7	110		12.0	2.00		17.0
Cu				14.3	13.5						
Zn	130	129	136	133	126	101	155	135	133	137	115
Mo				4.29	2.37						
Rb	32.0	40.0	37.0	49.4	31.5	15.0	37.0	24.0	28.0	43.0	26.0
Sr	609	632	643	674	778	545	678	598	585	638	553
Y				51.4	48.8						
Zr	334	401	400	418	301	205	407	283	304	374	288
Nb	64.0	84.0	83.0	92.3	62.0	43.0		67.0	64.0	86.0	59.0
Cs				0.45	0.27						
Ba	408	453	437	515	791	442	707	705	401	632	463
La				68.5	58.4						
Ce	47.0	84.0	87.0	133	128	55.0		108	59.0	108	65.0
Pr				16.2	16.4						
Nd				63.7	69.7						
Sm				12.9	15.6						
Eu				3.99	5.48						
Gd				12.0	14.7						
Tb				1.70	2.06						
Dy				9.30	11.2						
Ho				1.66	1.99						
Er				4.30	4.94						
Tm				0.58	0.63						
Yb				3.55	3.86						
Lu				0.50	0.53						
Hf				9.50	7.34						
Ta				4.45	3.98						
Pb				3.03	2.07						
Th				6.20	4.09						
U				2.09	1.37						

Table 1 continued

Sample	AZT03-62	AZT03-63	AZT03-64	AZT03-65	AZT03-66	AZT03-67	AZT03-68	AZT03-69	AZT03-70	AZT03-71	AZT03-73
Location	N of Práia da Vitoria, Ponta da Má Merenda, Terceira	N of Práia da Vitoria, Ponta da Má Merenda, Terceira	N of Práia da Vitoria, Ponta da Má Merenda, Terceira	N of Práia da Vitoria, Ponta da Má Merenda, Terceira	N of Práia da Vitoria, Ponta da Má Merenda, Terceira	N of Gruta dos Balcoes, Terceira	NE of Antonio, Terceira	Biscoito Bravo, Terceira	East of Serreta, Terceira	East of Serreta, Terceira	SE of Rossa do Couto, Terceira
Chapter samples are used in	I & II	I & II	I & II	I & II	I & II	I & II	I & II	I & II	I & II	I & II	I & II
Latitude [°N]	38°43.940	38°43.950	38°43.960	38°43.970	38°43.980	38°45.500	38°48.010	38°47.800	38°44.900	38°44.900	38°45.400
Longitude [°W]	27°03.200 Subaeral	27°03.200 Subaeral	27°03.200 Subaeral	27°03.200 Subaeral	27°03.200 Subaeral	27°15.400 Subaeral	27°15.100 Subaeral	27°14.700 Subaeral	27°21.500 Subaeral	27°21.500 Subaeral	27°21.350 Subaeral
TAS classification	Basalt	Basalt	Basalt	Basalt	Trachybasalt	Trachybasalt	Basalt	Trachyte	Trachyte	basalt. Trachyandesite	Trachyte
WR/GL	WR	WR	WR	WR	WR	WR	WR	GL	GL	WR	WR
[wt.%]											
SiO₂	46.62	45.99	46.29	46.35	47.26	49.59	46.79	65.01	69.78	52.96	74.57
TiO₂	3.75	4.18	4.20	3.85	3.91	3.06	3.06	0.58	0.35	2.46	0.39
Al₂O₃	15.16	14.71	14.77	15.02	14.88	14.95	13.78	13.44	12.83	15.37	7.70
Fe₂O₃	13.51	13.19	13.20	13.30	13.25	12.54	11.91	6.26		10.46	3.45
FeO									5.04		
MnO	0.21	0.20	0.20	0.20	0.20	0.22	0.18	0.25	0.21	0.20	0.13
MgO	4.40	4.68	4.65	4.37	4.66	3.93	8.22	0.32	0.09	3.07	0.06
CaO	9.13	9.56	9.49	8.94	9.33	7.68	10.52	0.67	0.51	6.35	0.26
Na₂O	3.29	3.29	3.30	3.52	3.58	4.18	2.99	7.05	6.17	4.90	3.24
K₂O	1.45	1.34	1.37	1.38	1.39	1.46	0.94	4.87	4.46	2.08	2.72
P₂O₅	0.69	0.95	0.96	0.72	0.77	1.47	0.87	0.07	0.02	0.99	0.03
SO₃									0.01		
Cl									0.39		
LOI	0.00	0.00	0.10	0.71	0.00	0.40	0.00	0.51	0.00	0.00	6.69
Total	98.21	98.09	98.53	98.36	99.23	99.48	99.26	99.03	99.86	98.84	99.24
[ppm]											
Sc					24.8	16.6					
Cr	20.0	10.0	15.0	6.00	9.36	0.54	297				
Co					40.1	18.7					
Ni	28.0			14.0	20.0	0.64	121	15.0		8.00	
Cu					24.3	5.71					
Zn	130	123	125	130	128	148	101	201		141	159
Mo					1.55	2.92					
Rb	29.0	25.0	30.0	25.0	29.3	29.9	19.0	121		42.0	88.0
Sr	544	647	635	547	591	772	538	13.0		587	8.00
Y					42.8	58.7					
Zr	292	288	284	288	263	386	205	759		479	890
Nb	60.0	62.0	65.0	65.0	56.6	64.6	43.0	176		101	269
Cs					0.13	0.30					
Ba	466	453	462	434	403	474	514	160		528	101
La					40.6	69.6					
Ce	55.0	63.0	65.0	62.0	85.8	155	63.0	97.0		104	76.0
Pr					11.3	19.3					
Nd					46.4	81.0					
Sm					9.92	18.1					
Eu					3.08	5.87					
Gd					9.51	17.1					
Tb					1.37	2.45					
Dy					7.50	13.3					
Ho					1.39	2.38					
Er					3.58	5.93					
Tm					0.48	0.77					
Yb					2.99	4.66					
Lu					0.42	0.64					
Hf					5.78	9.42					
Ta					3.36	3.90					
Pb					2.10	2.63					
Th					3.31	5.36					
U					0.71	1.86					

Table 1 continued

Sample	AZT03-74	AZT03-75	AZT03-76	AZT03-78	AZT03-79	AZT03-80	AZT03-81	AZT03-82	AZT03-83	AZT03-84	AZT03-85	AZT03-86
Location	S of Faja do Pico Carneiro, Terceira	S of Faja do Pico Carneiro, Terceira	NW of Lagoinha, Terceira	SW of Ponta da Serra, Terceira	SE of Galhardo, Terceira	N inner caldeira wall Guilherme Moniz, Terceira	N inner caldeira wall Guilherme Moniz, Terceira	N of Penedinhos, Terceira	W of Penedinhos, Terceira	N of Quatro Canadas, Terceira	Cruzes in Cruz, Terceira	Cruzes in Cruz, Terceira
Chapter samples are used in	I & II	I & II	I & II	I & II	I & II	I & II	I & II	I & II	I & II	I & II	I & II	I & II
Latitude [°N]	38°45.600	38°45.600	38°45.500	38°45.500	38°43.600	38°42.800	38°42.750	38°41.600	38°41.400	38°40.700	38°40.300	38°40.300
Longitude [°W]	27°21.200	27°21.200	27°20.400	27°20.010	27°13.900	27°12.900	27°11.900	27°06.700	27°06.900	27°06.250	27°05.200	27°05.200
	Subaeral	Subaeral	Subaeral	Subaeral	Subaeral	Subaeral	Subaeral	Subaeral	Subaeral	Subaeral	Subaeral	Subaeral
TAS classification	Trachyte	Trachybasalt	Trachyte	Trachyte	Trachyte	Basalt	Basalt	Trachybasalt	Trachyte	Trachybasalt	Basalt	Basalt
WR/GL	GL	WR	GL	GL	WR	WR	WR	WR	WR	WR	WR	WR
[wt.%]												
SiO ₂	69.62	50.70	68.90	69.10	64.96	47.79	46.81	46.49	62.96	47.28	46.54	46.54
TiO ₂	0.34	2.87	0.38	0.36	0.52	3.42	3.66	3.78	0.71	3.44	2.85	3.29
Al ₂ O ₃	12.82	14.96	13.65	13.87	10.35	14.44	14.08	14.85	16.88	15.49	17.23	13.57
Fe ₂ O ₃		11.56			8.59	12.51	12.76	13.15	4.00	12.49	12.15	12.33
FeO	5.00		4.64	4.66								
MnO	0.21	0.21	0.22	0.21	0.30	0.18	0.19	0.21	0.18	0.23	0.17	0.18
MgO	0.09	3.45	0.10	0.12	0.26	6.53	6.57	3.85	0.52	3.46	4.66	8.45
CaO	0.47	7.24	0.61	0.63	0.59	10.39	10.32	8.02	0.82	7.24	8.98	10.89
Na ₂ O	6.16	4.54	6.36	6.55	6.08	3.25	3.15	3.97	7.24	4.19	3.28	2.58
K ₂ O	4.61	1.75	4.63	4.44	4.37	1.13	1.05	1.53	4.83	1.71	1.17	0.86
P ₂ O ₅	0.01	1.02	0.01	0.02	0.02	0.75	0.78	1.62	0.12	1.41	0.34	0.62
SO ₃	0.01		0.01	0.01								
Cl	0.41		0.32	0.32								
LOI	0.00	0.00	0.00	0.00	1.29	0.00	0.00	0.00	0.34	1.66	1.52	0.00
Total	99.74	98.30	99.83	100.29	97.33	100.39	99.37	97.47	98.60	98.60	98.89	99.31
[ppm]												
Sc						30.7			4.18			
Cr						251	183		1.18		149	375
Co						39.4			0.67			
Ni						70.8	63.0		0.14		40.0	143
Cu						40.3			2.88			
Zn		142			358	108	109	153	143	144	87.0	98.0
Mo						1.27			1.08			
Rb		26.0			190	26.1	24.0	34.0	134	37.0	25.0	16.0
Sr		613			19.0	553	529	613	44.9	558	512	500
Y						34.9			81.8			
Zr		414			1505	212	229	325	885	353	187	195
Nb		83.0			331	42.4	49.0	82.0	184	81.0	34.0	40.0
Cs						0.22			0.12			
Ba		451			86.0	445	478	545	524	547	327	350
La						33.2			96.5			
Ce		87.0			157	75.9	63.0	103	180	109	40.0	41.0
Pr						9.56			19.5			
Nd						40.3			67.1			
Sm						8.66			12.6			
Eu						2.99			2.31			
Gd						8.26			11.5			
Tb						1.18			1.88			
Dy						6.42			11.4			
Ho						1.16			2.30			
Er						2.92			6.69			
Tm						0.38			1.00			
Yb						2.35			6.65			
Lu						0.33			0.97			
Hf						4.90			18.8			
Ta						2.44			8.48			
Pb						1.34			7.45			
Th						2.54			13.0			
U						0.74			3.44			

Table 1 continued

Sample	AZT03-87	AZT03-88	AZT03-89	AZT03-90	AZT03-91	AZT03-92	AZT03-93	AZT03-94
Location	W of Ponta de José Vieira, terceira	W of Ponta de José Vieira, terceira	W of Ponta de José Vieira, terceira	Canada das Covas, Terceira	Ladeira da Pena, Terceira	Ladeira da Pena, Terceira	SE of Celeiro, Terceira	N of Casa da Ribeira, Terceira
Chapter samples are used in	I & II	I & II	I & II	I & II	I & II	I & II	I & II	I & II
Latitude [°N]	38°47.010	38°47.010	38°47.010	38°45.700	38°44.500	38°44.500	38°43.700	38°43.500
Longitude [°W]	27°06.850	27°06.850	27°06.850	27°07.400	27°06.700	27°06.700	27°06.100	27°04.800
	Subaeral	Subaeral	Subaeral	Subaeral	Subaeral	Subaeral	Subaeral	Subaeral
TAS classification	Basalt	Basalt	Basalt	Basalt	Basalt	Trachybasalt	Basalt	Basalt
WR/GL	WR	WR	WR	WR	WR	WR	WR	WR
[wt.%]								
SiO ₂	47.46	46.58	46.81	46.84	46.17	47.03	46.30	46.04
TiO ₂	3.56	3.53	3.44	2.98	4.34	4.02	3.90	3.85
Al ₂ O ₃	14.31	13.92	14.20	14.28	14.64	14.66	14.17	13.99
Fe ₂ O ₃	12.60	12.59	12.27	11.74	14.12	13.33	13.48	13.45
FeO								
MnO	0.20	0.20	0.19	0.17	0.21	0.22	0.20	0.20
MgO	5.98	6.30	6.32	7.38	4.25	4.00	5.70	5.78
CaO	9.95	9.84	10.07	11.12	8.70	8.86	9.86	9.89
Na ₂ O	3.46	3.44	3.31	2.85	3.55	3.69	3.11	3.41
K ₂ O	1.21	1.20	1.16	0.89	1.34	1.52	1.05	1.09
P ₂ O ₅	0.97	0.96	0.85	0.59	0.78	1.20	0.98	1.03
SO ₃								
Cl								
LOI	0.00	0.00	0.00	0.14	0.38	0.30	0.19	0.14
Total	99.70	98.56	98.62	98.98	98.48	98.83	98.94	98.87
[ppm]								
Sc	28.4			34.3			30.2	30.5
Cr	180	161	189	314			102	133
Co	37.7			46.6			46.4	41.5
Ni	56.2	49.0	64.0	112			45.9	58.2
Cu	40.0			60.2			31.7	46.6
Zn	122	116	111	105	132	139	123	123
Mo	1.63			1.37			1.74	1.38
Rb	26.6	25.0	26.0	20.1	29.0	34.0	26.0	23.9
Sr	548	526	529	561	577	582	616	595
Y	39.8			29.5			39.4	38.2
Zr	215	239	242	164	287	327	194	197
Nb	45.6	49.0	51.0	36.5	63.0	67.0	42.7	41.5
Cs	0.19			0.10			0.22	0.20
Ba	577	569	554	308	445	443	537	520
La	38.7			27.3			36.5	35.3
Ce	87.9	76.0	70.0	59.0	58.0	67.0	85.7	80.4
Pr	11.4			7.74			11.1	10.8
Nd	47.9			32.1			47.1	45.9
Sm	10.3			7.11			10.3	9.94
Eu	3.57			2.48			3.69	3.57
Gd	9.83			6.86			9.75	9.48
Tb	1.38			0.98			1.36	1.31
Dy	7.38			5.30			7.15	7.00
Ho	1.33			0.97			1.28	1.24
Er	3.36			2.41			3.12	3.07
Tm	0.43			0.32			0.40	0.39
Yb	2.62			1.94			2.41	2.35
Lu	0.36			0.27			0.33	0.33
Hf	4.94			3.94			4.47	4.52
Ta	2.68			2.03			2.42	2.35
Pb	1.61			1.37			1.56	1.82
Th	2.72			2.25			2.39	2.33
U	0.71			0.68			0.75	0.79

Table 1 continued

Sample	AZT03-95	AZT03-96	AZT03-97	AZT03-98	AZT03-99	AZT03-100	AZT03-101 a)	AZT03-101 b)	AZT03-102 a)	AZT03-102 b)	AZT03-103	AZT03-104
Location	Ribeira de Santo Antao, Terceira	NE of Capita, Terceira	Ponta da Baixa do Barreiro, Terceira	S of Ponta Negra at Porto de S. Fernando, Terceira	Porto Novo at Salgueiros, Terceira	Baía da Mina, Terceira	Faro das Contendas, Terceira	Faro das Contendas, Terceira	S of Contendas, Terceira	S of Contendas, Terceira	SW of Cavalas, Terceira	SW of Cavalas, Terceira
Chapter samples are used in	I & II	I & II	I & II	I & II	I & II	I & II	I & II	I & II	I & II	I & II	I & II	I & II
Latitude [°N]	38°43.250	38°41.650	38°41.300	38°40.650	38°40.300	38°38.900	38°38.600	38°38.600	38°37.800	38°37.800	38°37.800	38°37.800
Longitude [°W]	27°03.900	27°03.200	27°02.900	27°03.700	27°04.400	27°05.200	27°05.200	27°05.200	27°05.300	27°05.300	27°05.500	27°05.500
	Subaeral	Subaeral	Subaeral	Subaeral	Subaeral	Subaeral	Subaeral	Subaeral	Subaeral	Subaeral	Subaeral	Subaeral
TAS classification	Basalt	Basalt	Basalt	Basalt	Basalt	Basalt	Basalt	Basalt	Basalt	Basalt	Basalt	Basalt
WR/GL	WR	WR	WR	WR	WR	WR	GL	GL	WR	GL	WR	WR
[wt.%]												
SiO ₂	46.17	47.01	47.05	46.96	48.07	47.71	47.52	47.82	47.91	47.95	47.08	48.11
TiO ₂	3.88	2.86	2.85	2.62	2.28	3.34	3.03	2.65	1.97	1.95	1.91	1.92
Al ₂ O ₃	14.04	14.75	14.71	13.11	14.73	14.06	13.86	13.78	14.42	14.25	13.49	13.75
Fe ₂ O ₃	13.48	11.31	11.31	11.03	9.68	12.50	11.88	10.99	9.27	9.30	9.52	9.57
FeO												
MnO	0.20	0.17	0.17	0.16	0.16	0.19	0.18	0.17	0.15	0.14	0.15	0.15
MgO	5.67	6.95	7.23	10.88	7.81	6.80	7.40	8.51	10.61	10.40	11.14	11.19
CaO	9.90	10.10	10.19	11.14	10.05	10.41	10.76	11.55	11.13	11.26	11.40	11.48
Na ₂ O	3.33	3.13	3.10	2.45	2.91	3.06	2.87	2.67	2.54	2.56	2.27	2.56
K ₂ O	1.11	1.11	1.03	0.86	1.43	1.00	0.94	0.86	1.07	1.08	0.97	1.00
P ₂ O ₅	1.04	0.88	0.90	0.52	0.36	0.65	0.55	0.46	0.30	0.29	0.29	0.28
SO ₃												
Cl												
LOI	0.00	0.23	0.41	0.00	0.00	0.00	0.00	0.00	0.00	0.00	0.03	0.00
Total	98.82	98.50	98.95	99.73	97.48	99.72	98.99	99.46	99.37	99.18	98.25	100.01
[ppm]												
Sc				57.8					37.2			56.0
Cr	95.0	332	348	819	384	215	305	421	651	659	760	1074
Co				74.7					49.9			65.8
Ni	30.0	105	103	335	122	70.0	107	142	264	239	265	338
Cu				59.2					83.0			103
Zn	112	89.0	88.0	108	82.0	100	102	95.0	70.9	78.0	73.0	83.3
Mo				1.27					1.12			1.07
Rb	19.0	21.0	19.0	23.0	30.0	18.0	20.0	19.0	25.6	29.0	20.0	23.4
Sr	571	519	524	533	437	535	500	471	462	416	400	449
Y				26.3					19.9			20.3
Zr	229	201	199	175	231	217	203	184	136	152	150	148
Nb	45.0	43.0	38.0	33.8	46.0	42.0	39.0	33.0	30.8	32.0	30.0	32.6
Cs				0.17					0.13			0.20
Ba	528	523	506	350	400	365	324	275	325	298	305	271
La				23.3					20.4			18.5
Ce	71.0	65.0	68.0	52.8	55.0	43.0	41.0	28.0	41.7	38.0	30.0	39.8
Pr				6.81					5.17			4.84
Nd				29.8					20.4			19.9
Sm				6.64					4.39			4.33
Eu				2.43					1.38			1.43
Gd				6.51					4.27			4.23
Tb				0.98					0.62			0.65
Dy				5.32					3.52			3.67
Ho				1.00					0.66			0.71
Er				2.47					1.73			1.82
Tm				0.33					0.24			0.25
Yb				2.01					1.53			1.61
Lu				0.29					0.22			0.23
Hf				3.80					3.19			2.95
Ta				1.98					1.73			1.53
Pb				1.14					1.57			1.72
Th				2.37					2.07			2.33
U				0.71					0.53			0.64

Table 1 continued

Sample	AZT03-105	AZT03-106	AZT03-107	AZT03-108	AZT03-109	AZT03-110	AZT03-111	AZT03-112	AZT03-113	AZT03-114	AZT03-117
Location	NE of Baía da Salga, Terceira	NE of Baía da Salga, Terceira	NE of Baía da Salga, Terceira	S of Pico do Refugio, Terceira	S of Serretinha, Terceira	SW of Feteira, Terceira	Between Ladeira Grande and Amaro, Terceira	Baía de Vila Maria, Terceira	S of Bravio, Terceira	Ponta de S. Mateus, Terceira	N of Cal Pedra, Terceira
Chapter samples are used in	I & II	I & II	I & II	I & II	I & II	I & II	I & II	I & II	I & II	I & II	I & II
Latitude [°N]	38°38.900	38°38.900	38°38.900	38°38.650	38°38.800	38°39.200	38°39.500	38°39.400	38°39.300	38°39.200	38°46.400
Longitude [°W]	27°05.700	27°05.700	27°05.700	27°06.400	27°08.550	27°09.200	27°10.600	27°14.930	27°15.600	27°16.600	27°17.700
	Subaeral	Subaeral	Subaeral	Subaeral	Subaeral	Subaeral	Subaeral	Subaeral	Subaeral	Subaeral	Subaeral
TAS classification	Basalt	Basalt	Basalt	Basalt	Basalt	Trachyte	Trachybasalt	Trachybasalt	Trachybasalt	Trachyandesite	Trachybasalt
WR/GL	WR	WR	WR	WR	WR	WR	WR	WR	WR	WR	WR
[wt.%]											
SiO ₂	47.61	46.81	47.56	45.57	46.92	61.70	48.00	48.26	48.35	56.35	49.00
TiO ₂	1.95	1.94	1.92	2.21	3.54	0.88	3.67	3.44	3.47	1.78	3.30
Al ₂ O ₃	13.39	13.20	13.50	12.96	14.01	17.16	14.65	14.26	14.09	16.36	15.62
Fe ₂ O ₃	9.76	9.56	9.61	10.51	12.58	3.48	12.37	12.95	12.96	8.71	12.10
FeO											
MnO	0.15	0.15	0.15	0.16	0.20	0.11	0.21	0.22	0.23	0.22	0.20
MgO	11.49	11.21	11.29	11.54	6.21	0.76	4.01	4.33	4.21	2.29	3.64
CaO	11.47	11.42	11.40	10.99	9.87	1.82	8.38	8.55	8.26	4.93	8.16
Na ₂ O	2.27	2.37	2.26	2.35	3.38	7.08	3.89	4.08	3.83	5.44	3.97
K ₂ O	0.90	0.98	0.94	0.88	1.20	4.23	1.60	1.37	1.29	2.30	1.53
P ₂ O ₅	0.28	0.28	0.29	0.34	0.97	0.18	0.85	1.43	1.41	0.68	0.82
SO ₃											
Cl											
LOI	0.04	0.00	0.28	0.13	0.00	0.46	0.00	0.00	0.33	0.25	0.12
Total	99.31	97.92	99.20	97.64	98.88	97.86	97.63	98.89	98.43	99.31	98.46
[ppm]											
Sc	58.3							21.5		11.3	
Cr	1017	799	795	738	165			1.34		1.61	
Co	70.1							26.1		7.05	
Ni	367	261	279	314	66.0	6.00		2.25		0.52	12.0
Cu	80.8							8.54		3.12	
Zn	86.3	65.0	72.0	79.0	116	142	132	153	151	159	136
Mo	1.07							2.68		4.62	
Rb	19.9	24.0	23.0	22.0	27.0	93.0	31.0	31.0	25.0	56.1	21.0
Sr	460	400	399	414	524	173	581	748	660	712	623
Y	21.1							54.8		67.8	
Zr	151	154	151	165	241	703	352	314	348	485	415
Nb	30.4	33.0	31.0	34.0	46.0	148	76.0	67.0	74.0	109	83.0
Cs	0.17							0.27		0.49	
Ba	284	269	309	277	564	785	454	408	469	641	482
La	19.1							55.5		81.4	
Ce	37.8	30.0	32.0	33.0	79.0	190	90.0	127	84.0	153	86.0
Pr	4.96							16.4		19.2	
Nd	20.5							67.9		74.3	
Sm	4.50							14.7		15.1	
Eu	1.46							4.76		4.80	
Gd	4.43							13.8		13.8	
Tb	0.67							1.93		2.02	
Dy	3.81							10.3		11.0	
Ho	0.74							1.84		2.01	
Er	1.88							4.55		5.16	
Tm	0.27							0.58		0.70	
Yb	1.67							3.52		4.37	
Lu	0.24							0.48		0.61	
Hf	2.98							7.41		10.8	
Ta	1.57							3.75		5.46	
Pb	1.59							3.57		4.11	
Th	2.11							4.10		7.21	
U	0.57							1.41		2.43	

Table 1 continued

Sample	AZT03-118	AZT03-120	AZT03-121	AZT03-122	AZT03-123	AZT03-124	AZT03-125	AZT03-126	AZT03-127	AZT03-128	AZT03-129	AZT03-130
Location	N of Cal Pedra, Terceira	675m E of Pico Rachado	Lagoinha, Terceira	SW of River Ribeira da Lana, Terceira	S of Fontes, Terceira	Road Canada do Mato, Terceira	WSW of Pico Rachado, Terceira	WSW of Pico Rachado, Terceira	W of Pico Rachado, Terceira	Canada dos Morros, Terceira	Cabo do Raminho, Terceira	N of Alteres soccer place, Terceira
Chapter samples are used in	I & II	I & II	I & II	I & II	I & II	I & II	I & II	I & II	I & II	I & II	I & II	I & II
Latitude [°N]	38°46.400	38°45.400	38°45.300	38°45.700	38°44.750	38°45.550	38°45.260	38°45.260	38°45.250	38°47.200	38°46.800	38°47.800
Longitude [°W]	27°17.700	27°18.200	27°20.100	27°21.500	27°20.500	27°21.200	27°19.200	27°19.200	27°19.400	27°19.300	27°20.800	27°18.200
	Subaeral	Subaeral	Subaeral	Subaeral	Subaeral	Subaeral	Subaeral	Subaeral	Subaeral	Subaeral	Subaeral	Subaeral
TAS classification	Trachybasalt	Trachyte	Trachyte	Trachybasalt	Trachyte	Trachyte	Trachyte	Trachyte	Trachyte	Trachyte	Trachyte	Trachyandesite
WR/GL	WR	GL	WR	WR	GL	GL	GL	WR	WR	WR	WR	WR
[wt.%]												
SiO₂	49.78	68.30	67.55	50.83	69.32	70.08	69.48	63.30	62.32	64.58	56.64	48.15
TiO₂	3.27	0.28	0.38	2.64	0.35	0.34	0.37	0.65	0.64	0.60	1.55	3.49
Al₂O₃	15.60	13.19	13.70	16.42	12.74	12.94	13.84	16.02	16.15	14.91	16.22	14.61
Fe₂O₃	12.13	4.44	4.94	10.56				5.38	5.48	5.98	8.42	12.79
FeO					5.10	5.03	4.72					
MnO	0.20	0.17	0.20	0.17	0.24	0.21	0.22	0.18	0.18	0.24	0.20	0.21
MgO	3.68	0.07	0.12	3.51	0.09	0.08	0.11	0.52	0.48	0.29	1.82	3.94
CaO	7.88	0.52	0.60	8.05	0.51	0.51	0.62	1.70	1.16	1.16	4.39	8.17
Na₂O	4.04	6.53	6.62	3.76	6.19	6.03	6.11	6.61	6.45	6.81	5.57	3.87
K₂O	1.57	4.73	4.55	1.29	4.48	4.51	4.42	3.63	3.61	3.90	2.70	1.33
P₂O₅	0.82	0.02	0.03	0.82	0.03	0.02	0.01	0.13	0.14	0.09	0.52	0.86
SO₃					0.01	0.01	0.01					
Cl					0.39	0.37	0.32					
LOI	0.36	0.53	0.12	0.70	0.00	0.00	0.00	1.12	2.14	0.68	0.54	0.80
Total	99.33	98.78	98.81	98.75	99.46	100.13	100.24	99.24	99.26	99.24	98.57	98.22
[ppm]												
Sc	17.9											
Cr	1.14			60.0								
Co	24.5											
Ni	6.39	11.0		27.0					12.0			
Cu	16.8											
Zn	145	222	218	120				152	155	143	151	148
Mo	2.67											
Rb	26.6	157	117	20.0				87.0	79.0	58.0	61.0	30.0
Sr	651	9.00	9.00	665				202	198	51.0	506	631
Y	46.6											
Zr	394	1341	1002	414				757	794	422	596	389
Nb	79.3	253		76.0					147		116	82.0
Cs	0.12											
Ba	517	70.0	401	464				727	786	1504	663	426
La	58.9											
Ce	124	134		85.0					199		141	64.0
Pr	15.5											
Nd	62.8											
Sm	13.9											
Eu	4.36											
Gd	13.1											
Tb	1.92											
Dy	10.7											
Ho	1.93											
Er	4.96											
Tm	0.66											
Yb	4.15											
Lu	0.58											
Hf	10.0											
Ta	4.94											
Pb	2.74											
Th	6.02											
U	2.02											

Table 1 continued

Sample	AZT03-131	AZT03-132	AZT03-133	AZT03-134	AZT03-135	AZT03-136	AZT03-137	AZT03-140	AZT03-143	AZT03-144
Location	N of Alteres soccer place, Terceira	NW of Pico da Cancela, Terceira	Between Pico da Cancela and Pico do Gaspar, Terceira	N of Misterio dos Negros, Terceira	Lagoa das Patas, Terceira	WNW of Lagoa das Patas, Terceira	NNW of Misterio dos Negros, Terceira	SW of Pico Vermelho, Terceira	NW of Casa da Queimada de Baixo, Terceira	E of Pico das Faias, Terceira
Chapter samples are used in	I & II	I & II	I & II	I & II	I & II	I & II	I & II	I & II	I & II	I & II
Latitude [°N]	38°47.800	38°43.800	38°43.750	38°44.400	38°43.350	38°42.250	38°44.450	38°44.300	38°46.350	38°46.500
Longitude [°W]	27°18.200 Subaeral	27°16.930 Subaeral	27°16.550 Subaeral	27°16.850 Subaeral	27°17.750 Subaeral	27°17.760 Subaeral	27°17.010 Subaeral	27°14.800 Subaeral	27°16.500 Subaeral	27°19.700 Subaeral
TAS classification	Basalt	Trachyte	Trachyte	Trachyte	Trachyandesite	Trachyandesite	Trachyandesite	Trachybasalt	Basalt	Trachybasalt
WR/GL	WR	WR	WR	WR	WR	WR	WR	WR	WR	WR
[wt.%]										
SiO ₂	46.25	59.90	59.90	62.56	57.25	58.31	61.24	49.30	47.03	50.55
TiO ₂	3.07	1.14	1.31	0.58	1.46	1.38	1.13	3.23	2.96	2.74
Al ₂ O ₃	13.89	16.51	14.74	16.90	16.87	16.52	15.79	14.71	14.39	15.78
Fe ₂ O ₃	11.67	7.23	7.74	4.94	7.66	7.36	6.52	12.55	11.63	10.86
FeO										
MnO	0.16	0.19	0.22	0.16	0.19	0.18	0.18	0.22	0.17	0.20
MgO	9.45	1.28	1.38	0.43	1.71	1.62	1.27	4.29	8.03	3.29
CaO	11.05	3.29	3.14	1.39	4.00	3.78	2.86	8.19	11.06	7.07
Na ₂ O	2.46	6.22	6.14	6.55	5.82	6.00	5.89	4.39	2.86	4.24
K ₂ O	0.79	2.94	3.15	3.75	2.76	2.92	3.45	1.45	0.83	1.78
P ₂ O ₅	0.36	0.32	0.48	0.12	0.46	0.42	0.42	1.46	0.66	1.07
SO ₃										
Cl										
LOI	0.00	0.00	0.20	2.28	1.00	0.00	0.03	0.00	0.00	1.36
Total	99.15	99.02	98.40	99.66	99.18	98.49	98.78	99.79	99.62	98.94
[ppm]										
Sc		7.45					8.08	17.7	28.2	
Cr	449	0.65					0.66	12.2	269	
Co		3.46					4.67	21.8	40.5	
Ni	199	0.41					0.31	7.26	108	
Cu		4.01					3.38	8.84	46.4	
Zn	101	144	168	127	140	138	134	133	91.7	140
Mo		2.01					3.20	1.85	1.34	
Rb	14.0	58.5	70.0	83.0	58.0	63.0	77.5	31.1	16.9	39.0
Sr	516	440	312	159	477	464	292	779	529	631
Y		49.1					47.2	52.8	29.5	
Zr	210	623	637	828	566	578	762	317	179	443
Nb	39.0	113	129		113	116	132	52.0	35.0	88.0
Cs		0.07					0.23	0.28	0.16	
Ba	269	766	886	853	685	669	791	799	371	496
La		76.4					70.0	63.2	31.2	
Ce	32.0	158	185		136	132	161	140	66.5	104
Pr		17.6					17.5	17.8	8.99	
Nd		67.9					67.5	76.1	38.7	
Sm		14.3					14.4	17.1	8.92	
Eu		4.30					3.98	5.96	3.27	
Gd		12.8					12.8	16.1	8.74	
Tb		1.95					1.96	2.25	1.26	
Dy		11.1					11.0	12.2	6.98	
Ho		2.03					2.01	2.17	1.25	
Er		5.31					5.34	5.35	3.15	
Tm		0.75					0.75	0.68	0.41	
Yb		4.87					4.98	4.17	2.53	
Lu		0.69					0.71	0.57	0.35	
Hf		15.2					18.8	7.74	4.74	
Ta		6.38					7.53	3.01	2.41	
Pb		4.61					5.42	2.31	1.18	
Th		9.73					12.1	4.45	2.10	
U		2.36					3.42	1.50	0.68	

Table 1 continued

Sample	AZT03-145	AZT03-146	AZT03-147	AZT03-148
Location	SW of Ponte Velha, Terceira	Playa da Ribeira, Terceira	Playa da Ribeira, Terceira	Playa da Ribeira, Terceira
Chapter samples are used in	I & II	I & II	I & II	I & II
Latitude [°N]	38°44.800			
Longitude [°W]	27°17.800			
	Subaeral	Subaeral	Subaeral	Subaeral
TAS classification	basalt. Trachyandesite	Trachybasalt	Basalt	basalt. Trachyandesite
WR/GL	WR	WR	WR	WR
[wt.%]				
SiO₂	53.46	50.08	47.36	51.35
TiO₂	1.99	3.02	3.35	2.96
Al₂O₃	17.06	15.77	14.40	14.88
Fe₂O₃	9.52	11.35	11.76	11.52
FeO				
MnO	0.20	0.17	0.16	0.19
MgO	2.45	3.83	7.90	3.51
CaO	5.42	8.38	10.96	7.37
Na₂O	5.03	4.17	2.73	4.42
K₂O	2.21	1.58	0.89	1.91
P₂O₅	0.68	0.69	0.41	1.06
SO₃				
Cl				
LOI	1.10	0.00	0.00	0.00
Total	99.12	99.04	99.92	99.17
[ppm]				
Sc				
Cr		49.0	311	
Co				
Ni		19.0	116	
Cu				
Zn	154	134	98.0	141
Mo				
Rb	29.0	37.0	18.0	40.0
Sr	579	633	543	565
Y				
Zr	586	376	229	443
Nb	111	74.0	38.0	91.0
Cs				
Ba	700	430	281	495
La				
Ce	150	70.0	33.0	93.0
Pr				
Nd				
Sm				
Eu				
Gd				
Tb				
Dy				
Ho				
Er				
Tm				
Yb				
Lu				
Hf				
Ta				
Pb				
Th				
U				

Christoph Beier

Institut für Geowissenschaften
Christian-Albrechts-Universität zu Kiel

Ludewig-Meyn-Straße 10

D-24118 Kiel

Geburtsdatum und -ort:

11. Mai 1977 in Hamburg

Staatsangehörigkeit:

deutsch

Ausbildung:

- 30.06.1996: Abitur am Städtischen Gymnasium Köln-Rodenkirchen

- 01.07.1996 bis 01.08.1997: Zivildienst im Rettungsdienst/ Krankentransport des Arbeiter-Samariter-Bundes Köln.

- 01.10.1997 bis 22.09.2002: Studium der Geologie/Paläontologie an der Christian-Albrechts-Universität zu Kiel

Vordiplom Geologie/Paläontologie im
Dezember 1999

Diplomprüfung Geologie/Paläontologie im September 2002

- seit 15.02.2003 Doktorand am Institut für Geowissenschaften der Christian-Albrechts-Universität zu Kiel und am Max-Planck-Institut für Chemie in Mainz

Kiel, 24.04.2006

Christoph Beier